Novel Applications of Catalysis

for Green and Sustainable Chemistry

A thesis submitted in fulfilment of the

requirements for the degree of

Doctor of Philosophy (Cotutelle)

by

Jessica N. G. Stanley

THE UNIVERSITY OF SYDNEY

Università Ca'Foscari Venezia

Faculty of Science

The University of Sydney

2014

Scienze Chimiche

Università Ca' Foscari Venezia

Ciclo XXVI

Università
Ca'Foscari
Venezia

THE UNIVERSITY OF
SYDNEY

Scuola Dottorale
Graduate School

Dottorato di ricerca in Scienze Chimiche
Ciclo XXVI
Anno di discussione 2014

Novel Applications of Catalysis for Green and Sustainable Chemistry

SETTORE SCIENTIFICO DISCIPLINARE: CHIM/06

Tesi di Dottorato di Jessica N. G. Stanley
Matricola: 955965
In cotutela fra University of Sydney e Università Ca' Foscari Venezia

Coordinatore del Dottorato

Prof. Maurizio Selva

Tutors

Prof. Alvise Perosa
Prof. Thomas Maschmeyer

Co-tutors

Prof. Maurizio Selva
Prof. Anthony Masters

Preface

This thesis is a report of original research undertaken by the PhD Candidate and is submitted for admission to the degree of Doctor of Philosophy (Cotutelle) at the University of Sydney and the University of Ca' Foscari. The work and results presented in this thesis are those of the PhD Candidate, unless otherwise acknowledged.

The work presented in this thesis has been published, accepted for publication, or in preparation for publication:

Stanley, J.N.G.; Worthington, K.; Heinroth, F.; Masters, A.F.; Maschmeyer, T., *Catal. Today* **2011**, *178*, 164–171.

Stanley, J.N.G.; Heinroth, F.; Weber, C.C.; Masters, A.F.; Maschmeyer, T., *Appl. Catal., A* **2013**, *454*, 46–52.

Stanley, J.N.G.; Selva M.; Masters, A.F.; Maschmeyer, T.; Perosa, A., *Green Chem.* **2013**, *15*, 3195–3204.

Stanley, J.N.G., *J. Proc. Roy. Soc., New South Wales* **2014,** *147*, 64–76.

Stanley, J.N.G.; Benndorf, P.; Heinroth, F.; Masters, A.F.; Maschmeyer, T., *RSC Adv.* **2014**, *4*, 28062–28071.

Stanley, J.N.G.; Perosa, A.; Selva, M.; Masters, A.F.; Maschmeyer, T., manuscript in preparation.

Sections of this work have been presented by the PhD Candidate at scientific conferences:

Stanley, J.N.G.; Worthington, K.; Heinroth, F.; Masters, A.F.; Maschmeyer, T., **Designing nanoscopic, fluxional bimetallic Pt-Ru alloy hydrogenation catalysts**

for improved sulfur resistance *Inaugural One-day Student Symposium in Inorganic Chemistry*, Sydney, Australia, June 27, 2011. Oral Presentation.

Stanley, J.N.G.; Worthington, K.; Heinroth, F.; Masters, A.F.; Maschmeyer, T., **Reversible bimetallic Pt-Ru alloy hydrogenation catalysts with improved sulfur tolerance.** *Chemeca 2011: Engineering a Better World*, Sydney, Australia, September 18–21, 2011. Oral Presentation.

Stanley, J.N.G.; Selva, M.; Perosa, A., **Dimethyl carbonate as a green solvent for the synthesis of platform chemicals from renewable lignin feedstocks** *Green Solvents for Synthesis Conference 2012*, Boppard, Germany, October 8–10, 2012. Poster Presentation.

Stanley, J.N.G.; Selva, M.; Masters, A.F.; Maschmeyer, T.; Perosa, A., **DMC as a green reactive solvent for the upgrading of biomass**, *ARENA/SIEF Renewable Chemicals Symposium*, Sydney, Australia, May 23, 2013. Oral presentation.

Stanley, J.N.G.; Masters, A.F.; Maschmeyer, T., **Extended X-ray absorption fine structure study of catalytic bimetallic nanoparticles: probing structure-functionality relationships for improving sulfur resistance**, The 6th Asia-Pacific Congress on Catalysis (APCAT-6), Taipei, Taiwan, October 12–17, 2013. Poster presentation.

Stanley, J.N.G.; Benndorf, P.; Heinroth, F., Masters, A.F.; Maschmeyer, T., **Structure-Functionality Relationships of Catalytic Bimetallic Pt-Ru Nanoparticles. Towards an Improved Sulfur Resistance**. Australian Synchrotron User Meeting 2013, Melbourne, Australia, November 21–22, 2013. Oral presentation.

Abstract

Catalysts have a central role in chemistry and catalytic technology is expected to play an ever more crucial part in meeting society's technical challenges of the future. This thesis examines fundamental studies of catalysts for more sustainable processes, addressing three particular challenges:

(1) Developing sulfur resistant catalysts that have potential applications in the processing of biomass for the production of liquid transportation fuels.

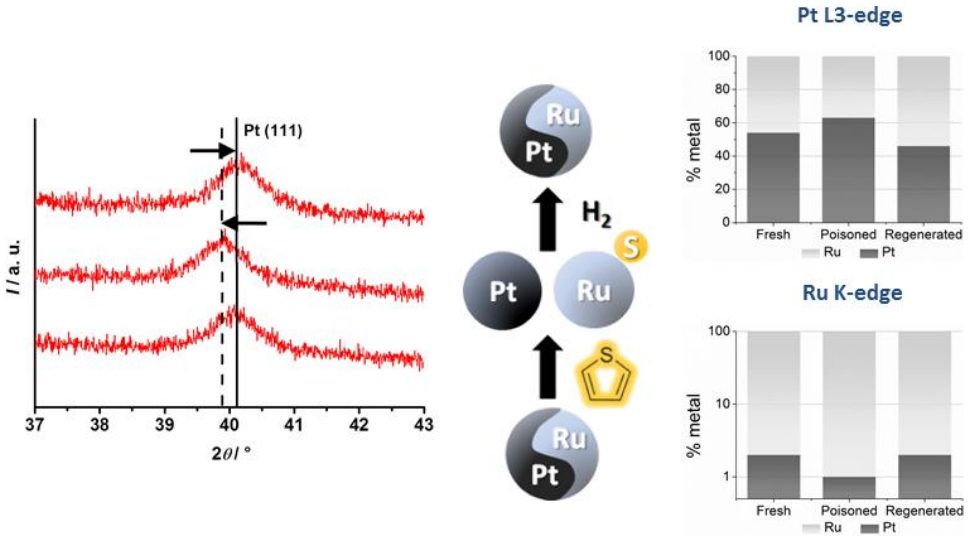

Supported Pt and Ru mono- and bimetallic alloy catalysts, with promising potential applications in biomass processing, were investigated for their tolerance to sulfur poisoning using the batch hydrogenation of cyclohexene to cyclohexane in the presence of thiophene as a screening reaction. Compared to their monometallic counterparts, the bimetallic catalysts exhibited higher turnover frequencies, both in the absence and presence of sulfur. XRD analysis of changes in the Pt unit cell size induced by sulfur poisoning suggest that the observed restructuring of the metal nanoparticles results from increasing amounts of sulfur species being coordinated to the ruthenium during poisoning, leading to at least a partial separation of the alloy. However, regeneration of the catalyst in

pure H_2 at 300 °C shows this to be a reversible process. Preliminary EXAFS investigations at the Pt L_{III} and Ru K-edges confirmed the alloyed character of the bimetallic catalysts, and further experiments allowed the clear determination of more detailed changes to the Pt/Ru bonding environments as induced by sulfur poisoning, *i.e.* partial particle dealloying. These results support the proposed sulfur and hydrogen spillover *in-situ* self regeneration mechanism.

(2) Reducing energy requirements and increasing the catalyst ease-of-use (especially water tolerance) for the hydrogenation of aromatics, particularly for the safe and feasible storage of hydrogen using the reversible toluene/methylcyclohexane couple.

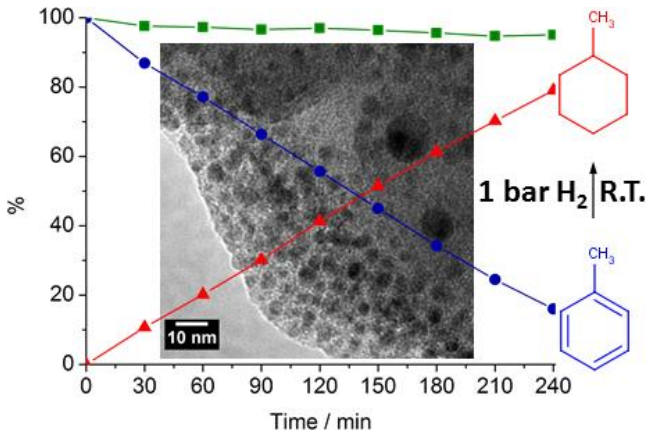

The second facet of this thesis fits as part of the drive towards ever lower energy, 'greener' processing. It was shown that a modified preparation of bimetallic aluminosilicate-supported Pt-Ru nanoparticles afforded catalysts that can, remarkably, operate under atmospheric conditions to catalyse the rapid room temperature hydrogenation of aromatics (toluene and tetralin) at 1 atm of hydrogen. The toluene/methylcyclohexane couple has the added interest of being a promising cyclic hydrocarbon combination for the storage of hydrogen. The easily handled, air-stable and water-stable catalysts were prepared using the incipient wetness method and characterised by ICP-AES, XRD, TEM as well as nitrogen sorption measurements. Compared to their monometallic counterparts, the bimetallic

catalysts displayed significantly higher turnover frequencies (TOFs), consistent with a synergistic relationship between platinum and ruthenium. These mild, high yielding hydrogenation catalysts are amongst the most active and easily handled catalysts for aromatic hydrogenations reported to date. Effecting the hydrogenation under mild conditions is an important challenge in terms of energy conservation and associated environmental considerations. Doing so in air and independent of moisture content, allows for a ready hydrogen stream to be generated in mobile applications, *e.g.* electric vehicles.

(3) Catalytically converting models of lignin building blocks as a source for renewable aromatic chemicals.

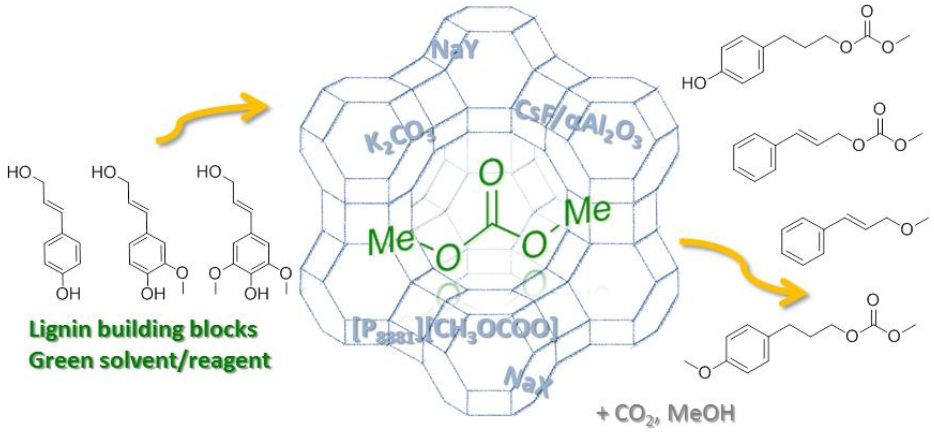

The final aspect of this research investigated the green catalytic processing of lignin. Cinnamyl alcohol and 4-(3-hydroxypropyl)phenol, two compounds resembling the lignin building block *p*-coumaryl alcohol, can be selectively transformed into different products by catalytic methodologies based on dimethyl carbonate (DMC) as a green solvent/reagent. Selectivity can be tuned as a function of the reaction temperature and of the nature of the catalyst. Basic catalysts such as K_2CO_3, trioctylmethylphosphonium methylcarbonate ($[P_{8881}][CH_3OCOO]$), and $CsF/\alpha Al_2O_3$ promote selective transesterification of the aliphatic hydroxyl group at 90 °C. However, amphoteric solids such as alkali metal-exchanged faujasites, NaX and NaY, selectively yield the corresponding alkyl ethers at higher temperatures (165–180 °C). The phenolic hydroxyl

group of 4-(3-hydroxypropyl)phenol can be methylated similarly with the faujasites at high temperatures. This preliminary screening for selectivity illustrates reactivity trends and delineates some of what might be among the most promising synthetic pathways to upgrade lignin-derived chemical building blocks.

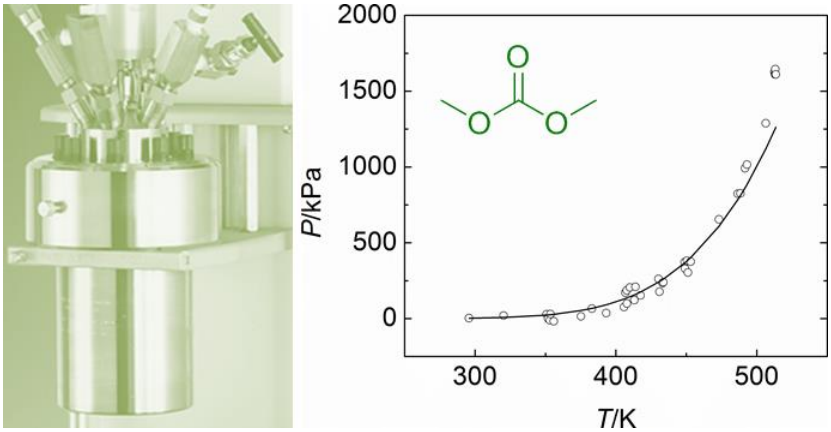

Additionally, the saturated vapour pressure of DMC was determined over a wide temperature range, T = (295.75 to 513.15) K. A batch reactor was used to perform the experiments, to replicate the conditions often used for batch alkylation reactions with DMC as reagent/solvent. The data could be fitted to the Clausius–Clapeyron equation, and the enthalpy of vaporisation (ΔH_{vap}) was calculated from the experimental data to verify the reliability of the results. DMC did not thermally decompose for the temperature range measured.

Estratto

I catalizzatori hanno un ruolo centrale nelle chimica, ed é previsto che la tecnologia della catalisi ne giochi uno ancor piú cruciale nell'affrontare le sfide tecnologiche future. Questa tesi prende in esame lo studio fondamentale di catalizzatori per processi più sostenibili. In particolare, affrontando tre sfide:

(1) *Lo sviluppo di catalizzatori resistenti allo zolfo, con potenziali applicazioni nel trattamento della biomassa per la produzione di carburanti liquidi per mezzi di trasporto.*

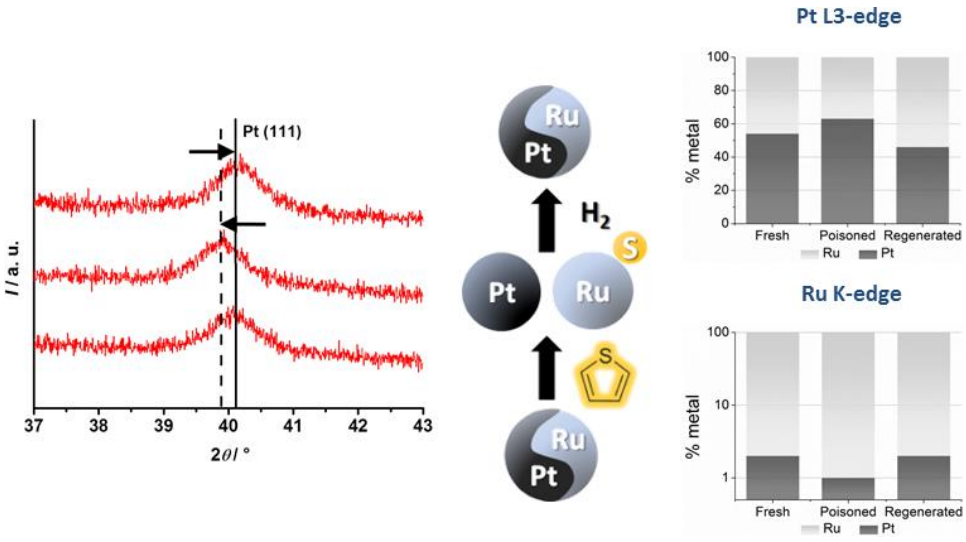

Sono stati studiati catalizzatori supportati, constituiti da leghe mono- e bimetalliche di Pt e Ru, per la loro tolleranza all'avvelenamento da zolfo, usando come reazione modello l'idrogenazione in batch del cicloesene a cicloesano, in presenza di tiofene. Paragonati alle loro controparti monometalliche, i catalizzatori bimetallici hanno frequenze di turnover (TOF) piú elevate, sia in assenza che in presenza di zolfo. Le analisi XRD delle variazioni in dimensione della cella unitaria di Pt, indotte dall'avvelenamento da zolfo, suggeriscono che la riorganizzazione delle nanoparticelle metalliche osservata, sia data dall'aumento di specie sulfuree coordinatesi al rutenio durante l'avvelenamento, portando ad almeno

parziale separazione della lega. Tuttavia la rigenerazione del catalizzatore in idrogeno puro a 300 °C dimostra come questo processo sia reversibile. Studi preliminiari di EXAFS alla soglia L_{III} del Pt e alla soglia K del Ru hanno confermato le caratteristiche di lega dei catalizzatori bimetallici, mentre ulteriori esperimenti hanno permesso di determinare in dettaglio i cambiamenti indotti dallo zolfo nei legami Pt/Ru, ovvero la parziale separazione della lega. Questi risultati supportano il meccanismo proposto di *spillover* di idrogeno e zolfo, con conseguente rigenerazione *in-situ* del catalizzatore.

(2) *La riduzione della domanda energetica ed il miglioramento della semplicità di utilizzo (in particolare riguardo alla tolleranza all'acqua) di catalizzatori per l'idrogenazione di aromatici. In particolare, per lo stoccaggio sicuro dell'idrogeno, attraverso la coppia reversibile toluene/metilcicloesano.*

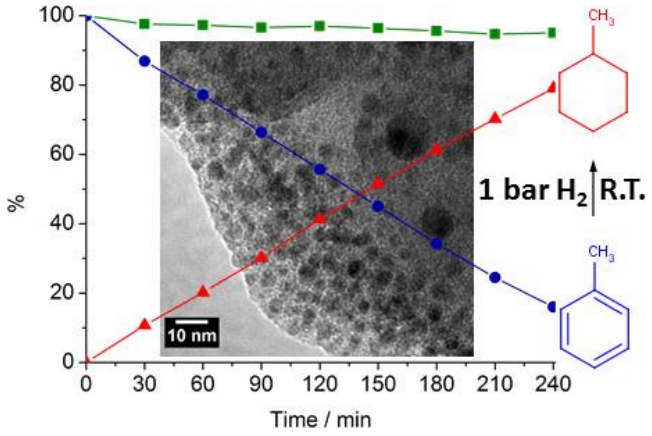

La seconda parte di questa tesi affronta il tema di nuovi processi meno "energivori", e quindi più verdi. Si dimostra che una preparazione alternativa di nanoparticelle bimetalliche Pt-Ru, supportate su alluminosilicati, ha generato catalizzatori in grado di promuovere la rapida idrogenazione di aromatici (toluene e tetralina) a temperatura ambiente e 1 atm d'idrogeno. La coppia toluene/metilcicloesano ha il valore aggiunto di essere una promettente combinazione di idrocarburi ciclici per lo stoccaggio d'idrogeno. I catalizzatori, facili da maneggiare, nonché stabili all'aria e all'acqua, sono stati preparati

per impregnazione e caratterizzati via ICP-AES, XRD, TEM e misure d'assorbimento d'azoto. In paragone alle loro controparti monometalliche, i catalizzatori bimetallici hanno dato TOF piú elevate, coerenti con una interazione sinergica tra platino e rutenio. Questi catalizzatori per l'idrogenazione di aromatici, che danno alte rese in condizioni blande, sono tra i piú attivi e di uso più semplice riportati ad oggi. L'idrogenazione in condizioni blande é un'importante sfida in termini di conservazione energetica e delle relative questioni ambientali. Potendo fare ciò in condizioni atmosferiche, indipendentemente dalla percentuale di umidità, potrebbe fornire accesso ad una fonte di idrogeno per applicazioni mobili (ad es. veicoli elettrici).

(3) *La conversione di molecole modello delle componenti della lignina come fonte di composti aromatici d'orgine rinnovabile.*

L'argomento finale di questa ricerca ha riguardato lo studio di processi catalitici "green" per la conversione della lignina. L'alcol cinnammico e il 4-(3-idrossipropil)fenolo, due composti modello del componente ligninico alcol *p*-cumarilico, possono essere trasformati selettivamente in diversi prodotti attraverso metodologie catalitiche basate sul dimetil carbonato (DMC) come solvente e reagente "green". La selettivitá puó essere indirizzata in funzione della temperatura e della natura del catalizzatore. Catalizzatori basici come K_2CO_3, triottilmetilfosfonio metilcarbonato ($[P_{8881}][CH_3OCOO]$) e $CsF/\alpha Al_2O_3$

promuovono selettivamente la transesterificazione del gruppo idrossile alifatico a 90 °C. D'altra parte solidi anfoteri come faujasiti scambiate con metalli alcalini, di tipo NaX e NaY, danno selettivamente, ad alte temperature (165–180 °C), i corrispondenti alchil eteri. Il gruppo idrossilico fenolico di 4-(3-idrossipropil)fenolo può altresì essere metilato in presenza di faujasiti ad alte temperature. Questo screening preliminare delle selettivitá ottenibili illustra degli interessanti profili di reattivitá e delinea alcune che potrebbero essere le strategie sintetiche piú promettenti per l'upgrade di molecole ottenute dalla lignina.

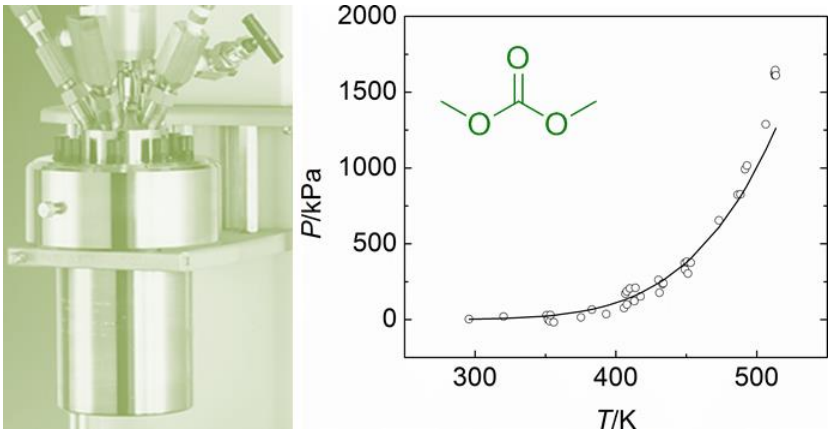

Infine la tensione di vapore saturo del DMC é stata determinata in un ampio intervallo di temperatura, T = (295.75–513.15) K. Gli esperimenti sono stati condotti in un reattore di tipo batch, per riprodurre le condizioni generalmente usate per le reazioni di alchilazione con DMC come reagente e solvente. I dati posso essere correlati con l'equazione di Clausius–Clapeyron e l'entalpia di vaporizzazione (ΔH_{vap}) é stata calcolata dai dati spreimentali per verificare la veridicitá dei risultati. Il DMC non decompone nell'intervallo di temperatura indagato.

Acknowledgements

For providing me with help and support throughout my PhD candidature, and for making the opportunities possible, there are many people I would like to thank.

Firstly I would like to thank my supervisors Prof Thomas Maschmeyer and A/Prof Tony Masters. You have provided me with experiences and opportunities that I could not have imagined when I started out. I sincerely thank you for everything you have taught me, for pushing me to do my best, and for all your support (especially through the tough times, of which there have been a few) and endless encouragement.

Secondly for enabling me to obliterate the "second year slump" I would like to thank my other two supervisors, (the newly titled) A/Prof Alvise Perosa and A/Prof Maurizio Selva. You made me welcome in your lab and you taught me some organic chemistry. Moreover, you helped me when I got locked into Ca' Foscari the night before the April 25 public holiday. Thanks to that experience, I learned not to work late hours while in Italy!

Thank you to all who have assisted with my work at the University of Sydney and at Ca' Foscari University of Venice: Dr Aviva Levina for help with my initial EXAFS analysis; Tom Savage for help with ICP-AES; Dr Hank de Bruyn for safe-guarding the XRD; Prof Vittorio Lucchini for safe-guarding the NMR; Marcel Kaegi and Andrew McVicar from the mechanical workshop for making my EXAFS sample holders; and Fernando Barasoain and Natalia Kislova from the level 4 service room for their patience in dealing with questions and requests.

At the Australian Synchrotron and the Australian National Beamline Facility, I would like to thank my beamline scientists Dr Bernt Johannessen and Dr Jade Aitken.

Particular thanks go to Bernt for all his guidance when I was preparing my synchrotron proposals.

I have often said that joining the Maschmeyer/Masters group was the best thing I've ever done, both professionally and personally. I remain extremely grateful that I landed amongst such a great group of individuals. Particular thanks go to: Dr Falk Heinroth for being a wonderful teacher and close friend; Dr Alex Yuen for leading the Biofuels Sub Group; Dr Antony Ward for keeping the lab running and for useful chats about my thesis over afternoon coffee; Dr Paul Benndorf for sharing your crystal structure expertise; Dr Lorenzo Costanzo for being there to chat about life and give me hugs; Dr Vincent Lau for your chauffeur skills; Dr Cameron Weber for helping me with maths and for continuing to be a "suppository of all wisdom"[i] from MIT; Dr Aaron Yap for leading the ordering of Thai for lunch; Alessio Caretto for helping me translate my Abstract to Estratto; and Max Easton for being my PhD buddy. Finally thanks to all the other past and present members of the Maschmeyer/Masters group: Beck, Bill, Donna, Eddy, François, Garreth, Ilona, John, Kaitlin, Kapil, Leo, Marina, Marion, Mel, Mike, Pete, Ramon, Son, Tomek, Wilm, Xiaobo, and Zoe.

I would like to sincerely thank the GOST group in Venice for accepting me into their lab. Particular thanks go to: Dr Marco Noè for assisting me in the lab and with NMR; Dr Giulia Fiorani for preparing my CsF/αAl_2O_3 and for all your wonderful tips for Rome; Manuela Facchin for making my $[P_{8881}][CH_3OCOO]$ and for finding a mobile phone carrier that let me call Australia for only 20 cents a minute; Alessio Caretto for your endless help from the moment you picked me up at Marco Polo airport; Sandro Guido for being my translator when talking to the glass blowers; Manuele Ganvin for laughing at my jokes; and Marta and Anna.

[i] Tony Abbott, August 2013.

Away from the lab in Venice, special thanks go to Isi Freris and Ale Loris. I am so fortunate that I met you, Isi, in my first week in Venice. I am not sure what I would have done without your friendship throughout the year. You and Ale are among the most generous, kind-hearted people I have ever met, and I was so happy to have you both just three bridges away.

I would also like to thank my other friends in the chemistry building in Sydney. There are just too many of you to name individually, but particular thanks go to Andrew Danos, Mitch Quinn, and everyone else in the laser lab (now at UNSW); Lisa Cameron, Michael Murphy, and the rest of the level four people; Andy West, Andrew Telford, and the KCPC; and everyone else with whom I've shared a jug (especially Tim Schmidt).

Finally, I thank my friends and family outside of chemistry. Particular thanks need to go to the girls, especially Sally Hatton who is always there for me, but also to Sian Myers, Amanda Siriwardana, Amy Bayliss, Emilia Lukeman, and Myee Gregory. Most importantly, I thank my parents John and Roselli and my brother Jamie; I don't see you very often these days, but it is comforting to know that I have your unwavering love and support. Thank you.

Table of Contents

List of Figures

List of Tables

List of Abbreviations

$[P_{8881}]$	-	**t**ri**o**ctyl**m**ethyl**p**hosphonium
APR	-	aqueous phase reforming
BET	-	Brunauer, Emmett and Teller
cf.	-	*confer*
CCD	-	charge-coupled device
CN	-	co-ordination number
DLS	-	dynamic light scattering
DMC	-	dimethyl carbonate
DME	-	dimethoxyethane
etc	-	*et cetera*
e.g.	-	*exempli gratia*
EXAFS	-	extended X-ray adsorption fine structure
fcc	-	face centred cubic
FCC	-	fluid catalytic cracking
GC	-	gas chromatography
GC-MS	-	gas chromatography – mass spectrometry
hcp	-	hexagonal closed packed
IL	-	ionic liquid
ICP-AES	-	inductively coupled plasma – atomic emission spectroscopy

i.e.	-	*id est*
JCPDS	-	Joint Committee on Powder Diffraction Standards
lit.	-	literature
m/z	-	mass/charge ratio (MS)
M	-	molar
MS	-	mass spectrometry
NMR	-	nuclear magnetic resonance
PMMA	-	poly(methyl methacrylate)
ppm	-	parts per million
RT	-	room temperature
TEA	-	triethanolamine
TEAOH	-	tetraethylammonium hydroxide
TEG	-	tetraethylene glycol
TEOS	-	tetraethylorthosilane
TMS	-	tetramethylsilane
TOF	-	turn over frequency
vs	-	*versus*
XANES	-	X-ray absorption near edge structure
XAS	-	X-ray absorption spectroscopy
XRD	-	X-ray diffraction

Chapter 1: Introduction

An extended version of this chapter was published in *The Journal and Proceedings of the Royal Society of New South Wales*. The complete manuscript can be found in Appendix A.

Stanley, J.N.G., *J. Proc. Roy. Soc., New South Wales,* **2014,** *147*, 64–76.

1.1 Introduction

Catalysts play a central role in chemistry, and are used in approximately 90% of all industrial chemical processes.[1–3,ii] In the last 250 years, especially during the 20th century, catalysts were involved in many technological developments that contributed to the lifestyle and standard of living that we enjoy today. Many of these developments emerged due to the convenience and abundance of fossil feedstocks. However, with global energy demands expected to double within the next forty years, peak oil being reached soon or even past, the growing concerns surrounding carbon dioxide emissions, and the political instability related to geographical restrictions of oil reserves, there is a growing need for 'greener' processing and to develop alternative resources. Just as catalysts played an important role in the 20th century, they are expected to have an ever more crucial role in the 21st century, as will be discussed in the subsequent sections.

1.2 Historical Perspective

The first use of catalysts can be traced back approximately 10 000 years, with depictions of brewing on archaeological remains.[4] Even back then, catalysts had an important role for humankind. However, it was not until the 19th century that the concept of catalysis was understood. Jöns Jacob Berzelius introduced the term *catalysis* in 1835 before Wilhelm Ostwald provided a scientific definition in 1895.[5] Over the next century, catalysts played a significant role in the development of industrial processes that have greatly influenced modern society. Arguably the most important catalytic development was the Haber–Bosch process, which is promoted by iron-based catalysts. Motivated by the need for fertiliser during the anticipated Chilean embargo on saltpetre, this process has had an enormous

[ii] References for Chapter 1 begin on page 16.

impact on the development of modern society. On the one hand, it was responsible for between 100 and 150 million deaths in the 20th century because of its role in the production of explosives and chemical weapons used in armed conflicts.[6] Indeed, the demand for explosives based upon nitric acid had a huge impact on the growth of the industrial production of bulk chemicals during World War One.[7] On the other hand, the Haber–Bosch process is responsible, through the production of agricultural fertiliser, for feeding approximately 48% of the world's population in 2008 (Figure 1.1).[6] As will be shown briefly in this section, major catalytic developments rarely occurred in isolation. Rather, they required societal, political, or environmental motivations as drivers. Equally important was the accessibility to raw materials, and in turn, new technology created new demands.

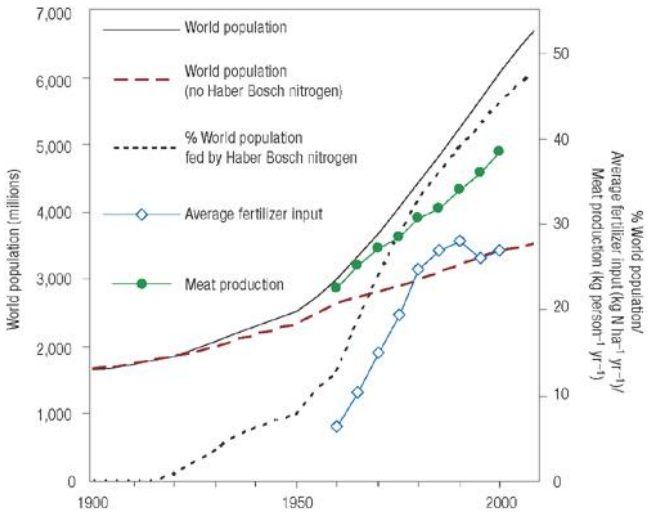

Figure 1.1 Trends in human population and nitrogen use in the 20th century. Reprinted by permission from Macmillan Publishers Ltd: NATURE GEOSCIENCE. Erisman *et al*. Nature Geoscience, 1, 10 (2008), copyright 2008.

Although the first crude oil was drilled in 1859, the main feedstock for chemicals at the onset of the 20th century was coal, based mainly on coal liquefaction, distillation of coal tar, acetylene, and coal gasification.[2] As the demands for explosives diminished, the focus after World War One moved to synthetic fuels. Among the most important catalytic developments in this period was the use of iron and copper catalysts for the synthesis of hydrocarbons from carbon monoxide and hydrogen (obtained from coal) by Franz Fischer and Hans Tropsch in 1923. The Fisher–Tropsch synthesis of fuels is just as relevant today as it was nearly a century ago. Nonetheless, the widespread use of crude oil as a feedstock began when Eugène Houdry developed the catalytic cracking of petroleum in 1936. Lewis and Gillian modified the process with the introduction of fluid catalytic cracking (FCC) in 1941, and this improvement enabled the supply of the vast quantities of high-octane aviation fuel needed to supply the Allied Forces in World War Two.

With the end of the war, needs again changed with society, and the automobile market accelerated in Europe. The increased demands for gasoline created the petrochemical industry, as petroleum refining enabled the production of plastics, pharmaceuticals, and specialty chemicals. Crude oil became entrenched as a convenient and accessible feedstock. The most important development during this period was the use of a modified X zeolite catalyst in the FCC of petroleum, and one of the most important concepts in zeolite catalysis was the discovery of shape-selective catalysis in zeolites.[8] With these advances, zeolites revolutionised the catalytic cracking and hydrocracking of the crude oil feedstocks, dramatically improving yield and process efficiencies. Indeed, the use of zeolite catalysts is estimated to save the petroleum industry 10 billion dollars a year.[9]

As the transportation industry and chemical processes expanded, research into new catalysts was required to meet the regulations regarding vehicle and stationary engine

emissions. Hydrodesulfurisation was developed in the 1960s for the removal of sulfur in fuels. In 1974, the first oxidation catalytic converter for automobiles was developed, followed by the three-way catalytic converter in 1978, and the Pd three-way converter in the 1990s. By 1990, the catalytic converter had reduced emissions from hydrocarbons, NO_x, and CO from vehicles by 90% compared to levels in 1965.[2]

Although emissions control catalysts are among the exceptions, the fundamental studies on catalysts in the 20th century were mostly focused on achieving high turnover rates. There is now a growing need to develop alternative resources and lower energy, 'greener' processing. Catalysts are expected to play a huge role as many of the challenges of the previous century will be revisited with changing feedstocks, as will be discussed in the subsequent sections.

1.3 Catalysts in the 21st Century

1.3.1 The Need for Green and Sustainable Processes

The U.S. Energy Information Administration anticipates that worldwide energy use will grow by 56% between 2010 and 2040, which is equivalent to global energy demand increasing by approximately 1.5% a year.[10] More than 85% of this increase occurs due to the strong economic growth and expanding populations in developing nations. However, this rapid increase in energy demand is problematic as finite fossil resources (coal, oil and gas) currently provide 85% of the world's energy.[11] Of the three, oil is the most concerning, as worldwide reserves of oil are sufficient for only another 55 years.[12] Indeed, a recent article in *Nature* argues that 'peak oil' (the time when global production of oil reaches a peak before declining) was passed in around 2005.[13] Access to the worldwide oil reserves is also compromised due to political instability (*e.g.* in the Middle East, an area

which accounts for almost 50% of proven oil reserves at the end of 2012),[14] causing problems of energy security to developed countries. Moreover, the level of carbon dioxide in the atmosphere has increased by approximately 40% compared to pre-industrial levels, largely because of the surge in fossil fuel consumption and land use changes.[15] This increased carbon dioxide has serious consequences for global warming, with the International Panel on Climate Change affirming human influence as "extremely likely" (*i.e.* 95–100% probability) to be the dominant cause of climate change.[16]

1.3.2 Green Chemistry and Catalysis

The last thirty years has seen a significant move towards green chemistry, as it is recognised that the challenges of sustainability will be met with new technologies that provide society with energy and materials in an environmentally responsible manner.[17] The Brundtland commission defined sustainable development in 1987 as "Meeting the needs of the present generation without compromising the ability of future generations to meet their own needs."[18] Four years later, Anastas defined green chemistry as "the utilisation of a set of principles that reduces or eliminates the use or generation of hazardous substances in the design, manufacture and application of chemical products".[19] These Twelve Principles of Green Chemistry, listed in Figure 1.2 are the means to achieving sustainable development.

The Twelve Principles of Green Chemistry

1. It is better to prevent waste than to treat or clean up waste after it is formed.
2. Synthetic methods should be designed to maximize the incorporation of all the materials used in the process into the final product.
3. Wherever practicable, synthetic methodologies should be designed to use and generate substances that possess little or no toxicity to human health and the environment.
4. Chemical products should be designed to preserve efficacy of function while reducing toxicity.
5. The use of auxiliary substances (*e.g.* solvents, separation agents, *etc.*) should be made unnecessary wherever possible, and innocuous when used.
6. Energy requirements should be recognized for their environmental and economic impacts and should be minimized. Synthetic methods should be conducted at ambient temperature and pressure.
7. A raw material of feedstock should be renewable rather than depleting wherever technically and economically practicable.
8. Unnecessary derivatization (blocking group, protection/deprotection, temporary modification of physical/chemical processes) should be avoided whenever possible.
9. Catalytic reagents (as selective as possible) are superior to stoichiometric reagents.
10. Chemical products should be designed so that at the end of their function they do not persist in the environment and break down into innocuous degradation products.
11. Analytical methodologies need to be further developed to allow for real-time, in-process monitoring and control prior to the formation of hazardous substances.
12. Substances and the form of a substance used in a chemical process should be chosen so as to minimize the potential for chemical accidents, including releases, explosions, and fires.

Figure 1.2 The Twelve Principles of Green Chemistry.[19]

The Twelve Principles comprise of three main aspects, identified by Sheldon. The first aspect aims to minimise waste through the efficient utilisation of raw materials.[20] Waste is defined as any material that is generated in a process that does not have realised value and includes the loss of unutilised energy.[21] With the need to double energy production within the next forty years (without increasing carbon dioxide emissions), the need to develop more energy efficient processes is essential. Secondly, avoiding the use of toxic and/or hazardous substances is important to circumvent health, safety and environmental issues. This aspect includes avoiding the use of solvents, which often account for the majority of mass wasted in syntheses and processes.[22] Finally, the third aspect identified by Sheldon is the use of renewable biomass feedstocks instead of non-renewable fossil feedstocks. Biomass conversion has become an important area of research due to the need for new technologies to obtain energy and chemical feedstocks in a sustainable manner,[23, 24] and it is a major aim of green chemistry.[22]

The motivations and drivers in the 21st century have changed. With the need for alternative resources, catalysts are expected to play an ever more crucial role in the technological developments for biomass conversion, enabling pathways previously unavailable in processing alternative feedstocks. Catalysts are also fundamental to improving the efficiency of reactions by lowering energy input, by avoiding the need for stoichiometric quantities of reagents, by decreasing the use of processing and separation agents, and by offering greater product selectivity.[21, 25] Over the next few decades, catalytic processes will be developed to convert biomass to fuels and chemicals, but no developments will be made that are not informed by the thinking of green chemistry and that do not fulfil their role in a sustainable manner.

In this research project, the key objective was to use catalysts, while guided by the thinking of green chemistry, to address these global energy challenges. Three different novel applications of catalysis were investigated and are outlined below.

1.3.3 Designing Sulfur Resistant Catalysts for Biomass Processing

With oil supplies diminishing significantly over the next few decades, there is an increasing need to develop liquid transport fuels from biomass. Due to the chemical, thermal, and functionality differences between biomass and petroleum feedstocks, new chemical pathways need to be developed for biomass processing.[26, 27] The current technologies for the conversion of biomass include gasification, pyrolysis, hydrothermal liquefaction, delignification followed by saccharification and fermentation, and aqueous phase reforming (APR). Many of these processes involve catalysts, such as APR, which is a promising technology that uses supported metal catalysts to convert biomass-derived feedstocks into either hydrogen or alkanes.[28, 29]

An important challenge in developing catalysts for biomass conversion, including APR, is operating the catalysts in the presence of sulfur in real biomass feedstocks (*e.g.*, wood: approx. 56 ppm), due to the presence of sulfur-containing amino acids and from the uptake of nutrients in the soil.[30] This sulfur is a problem because sulfur is known to poison noble metal catalysts.[31, 32] Although the sulfur tolerance of catalysts was widely investigated in the 20th century, both for the petrochemical and fine chemical industries,[31, 33, 34] there has been little research into improving the sulfur resistance of catalysts for use with biomass feedstocks. Thus, developing sulfur resistant catalysts for biomass processing is one of the catalytic challenges of the 20th century that is being

revisited in the 21st century as feedstocks change from fossil resources to biomass resources.

The design of supported Pt-Ru bimetallic catalysts with improved sulfur resistance for biomass processing was a major aim of the author for this thesis. The results are presented in Chapters 2 and 3.

1.3.4 Hydrogenation of Aromatics and Hydrogen Storage

The second catalytic challenge facing the 21st century fits in with the drive towards lower energy, 'greener' processing. In the previous century, the focus of fundamental studies was largely on achieving high turnover rates. Now, the main drivers for technological developments have changed, and a greater focus is on reducing energy requirements. The hydrogenation of aromatics is an important reaction both for small-scale synthesis and for industrial reactions, including the production of cyclohexane, which is an important precursor for the manufacturing of nylon-6,6.[35–37] These reactions are traditionally carried out using elevated temperatures and pressures, which often exceed 100 °C and 50 atm H_2.[38] Furthermore, aromatic compounds are responsible for undesired particle emissions in exhaust gas, leading to a tightening of fuel legislation.[39, 40] Thus, being able to perform the hydrogenations under mild conditions is an important challenge in terms of energy efficiency and environmental concerns.

Additionally, the reversible toluene/methylcyclohexane couple has the added interest of being a safe and feasible hydrocarbon combination for the storage of hydrogen.[41] Cyclic hydrocarbons have a relatively high hydrogen storage capacity, produce no carbon dioxide or carcinogenic products, and their volatility range makes them compatible with existing infrastructure such as refuelling stations and oil tankers for the

storage and transportation of the liquid hydrocarbons.[41–44] Thus, the cyclic hydrocarbon combinations have a distinct advantage over other solid hydrocarbons for hydrogen storage.

A modified method to that used in Chapters 2 and 3 for preparing supported Pt-Ru bimetallic catalysts was employed to develop robust catalysts for the low temperature and ambient pressure hydrogenation of toluene and tetralin. The results obtained are presented in Chapter 4.

1.3.5 Green Catalytic Processing of Lignin

Returning to renewable feedstocks, the third challenge is the need to develop the catalytic technologies to obtain chemicals from alternative resources. As already mentioned, biomass is the only renewable source for carbon-based materials. Lignin (which constitutes approx. 15–30% by weight and 40% by energy content of lignocellulosic biomass)[45] is particularly valuable, as its unique structure as an amorphous, highly substituted, aromatic polymer makes it the major renewable source of aromatics.[46] However, synthetic approaches for the conversion of lignin to chemicals are markedly less developed compared to the cellulosic components of biomass, partly due to the recalcitrant nature of lignin that provides plants with their strength.[47] Much effort is currently being devoted to the development of new technology to process low value lignin into higher value-added chemicals. Although aggressive depolymerisation of lignin yields chemicals such as benzene, toluene, and xylene, as well as phenols and aliphatic hydrocarbons used in conventional chemical processes, the selective depolymerisation of lignin could yield monomeric lignin aromatics which are not accessible by traditional petrochemical routes. For example, these monomeric lignin aromatics could be obtained from the pretreatment

streams of the pulp and paper industries, which alone produced 50 million tons of extracted lignin in 2004.[46] Extraordinarily, the vast majority of this type of lignin is burned as a low value fuel – only 2% is used commercially.[48]

Now, analogous to the petroleum refinery, a biorefinery could use biomass feedstocks to produce a range of products. As outlined earlier, the petroleum refinery developed over many decades in the 20th century, as crude oil emerged as a convenient and readily available feedstock. It began with only few products, but as the needs changed with those of society and new catalytic technology was developed, it expanded to produce plastics, pharmaceuticals, and speciality chemicals. With the growing need to obtain these products from renewable resources, the biorefinery is emerging. In the early stages, the biorefinery will need to produce large volumes of more chemically accessible, lower value fuels. Later, higher value chemicals produced in smaller quantities will be required to offset the costs.[49] Finally, it is expected that all components of biomass will need to be used for a biorefinery to be economically viable. Catalysts are critical to the development of the new technology for enabling the conversion of biomass. The catalytic challenges for performing the chemical transformations, which were overcome for crude oil over many decades in the 20th century in the petroleum refinery, are being revisited with biomass-derived feedstocks in the 21st century in the biorefinery.

Currently, there are two approaches for converting biomass-derived resources into higher-value added fuels. The first is a drop-in strategy, where the biomass feedstocks are transformed into existing platform chemicals, to directly replace well-established chemicals currently produced from fossil feedstocks.[50, 51] The other approach, which we favour, is a curiosity driven broad-based strategy that exploits the existing structure and functionality of biomass. In this approach, renewable platform chemicals based on the

structure of biomass could lead to the development of new chemistry and, in the longer term, a plethora of chemical products with as yet unknown applications.[46]

Fundamental to establishing the required catalytic technology for converting biomass-derived feedstocks into chemicals is an understanding of the reactivity trends and reaction pathways. The combination of the use of renewable feedstocks with innocuous solvents and auxiliaries is particularly favourable. The selectivity trends of screening models of lignin building blocks using different catalytic methodologies based on dimethyl carbonate (DMC) as a green solvent/reagent are reported in Chapter 5.

1.3.5.1 Saturated Vapour Pressure of Dimethyl Carbonate

Also reported in this thesis is the saturated vapour pressure data obtained for DMC. This data was collected as part of the investigation into the use of DMC as a green solvent and reagent for the catalytic upgrading of lignin model building blocks, as there is no experimental vapour pressure data of DMC available in the literature over a wide temperature range. The results are reported in Chapter 6.

1.4 Thesis Organisation

This thesis has been structured in the following way. After this introduction are five chapters. Each chapter is based on a published paper or a manuscript that is in preparation for publication. Each chapter contains work carried out entirely during the PhD candidature of Jessica N. G. Stanley, with the exception of Chapter 2, and presents original findings. The work is principally that of the PhD candidate under the supervision of Thomas Maschmeyer and Anthony F. Masters (Chapters 2–4, and 6), and Alvise Perosa

and Maurizio Selva (Chapter 5). The thesis finishes with a conclusion that summarises the key findings made during the course of this research project, and offers future research directions. Finally, contained in the Appendices is the extended version of the accepted paper contained in Chapter 1, and the Supplementary Information for published and accepted papers, where applicable.

The paper in Chapter 2 was published during the PhD candidature of the PhD candidate. The critical XRD results included in the paper were obtained during the PhD candidature. However, part of the catalytic results and preliminary XRD data were collected earlier. The paper is included herein because the higher level analysis was performed during the PhD candidature and because the work provides important background to research subsequently performed during the PhD candidature, presented in Chapter 3.

The title of each chapter and the relevant publication details are summarised as follows:

Chapter 1: Adapted from:

Past and Present Challenges in Catalysis: Towards Green and Sustainable Processes. Jessica N. G. Stanley, *J. Proc. Roy. Soc., New South Wales,* **2014,** *147*, 64–76.

Chapter 2: Designing Nanoscopic, Fluxional Bimetallic Pt-Ru Alloy Hydrogenation Catalysts for Improved Sulfur Tolerance. Jessica N. G. Stanley, Katy Worthington, Falk Heinroth, Anthony F. Masters, Thomas Maschmeyer. *Catal. Today* **2011**, 178, 164–171.

Chapter 3: Probing Structure-Functionality Relationships of Catalytic Bimetallic Pt Ru Nanoparticles Associated with Improved Sulfur Resistance. Jessica N. G.

Stanley, Paul Benndorf, Falk Heinroth, Anthony F. Masters, Thomas Maschmeyer. *RSC Adv.* **2014,** *4*, 28062–28071.

Chapter 4: Robust Bimetallic Pt-Ru Catalysts for the Rapid Hydrogenation of Toluene and Tetralin at Ambient Temperature and Pressure. Jessica N. G. Stanley, Falk Heinroth, Cameron C. Weber, Anthony F. Masters, Thomas Maschmeyer. *Appl. Cat., A* **2013,** 454, 46–52.

Chapter 5: Reactions of *p*-Coumaryl Alcohol Model Compounds with Dimethyl Carbonate. Towards the Upgrading of Lignin Building Blocks. Jessica N. G. Stanley, Maurizio Selva, Anthony F. Masters, Thomas Maschmeyer, Alvise Perosa. *Green Chem.* **2013**, 15, 3195–3204.

Chapter 6: Determination of Saturated Vapour Pressure of Dimethyl Carbonate over a Wide Temperature Range. Jessica N. G. Stanley, Alvise Perosa, Maurizio Selva, Anthony F. Masters, Thomas Maschmeyer. Manuscript in preparation.

Note on thesis format

Chapters 2–6 have been structured to match the published or prepared papers. Therefore, there are some variations in formatting between each chapter, which reflect the differing journals' publishing guidelines at the times of submission.

1.5 References

(1) Thomas, J. M.; Williams, R. J. P., Catalysis: principles, progress, prospects. *Philos. Trans. R. Soc. London, Ser. A* **2005,** *363*, 765–791.

(2) Armor, J. N., A history of industrial catalysis. *Catal. Today* **2011,** *163*, 3–9.

(3) Thomas, J. M., Turning Points in Catalysis. *Angew. Chem. Int. Ed. Engl*. **1994,** *33*, 913–937.

(4) Adams, C., Applied Catalysis: A Predictive Socioeconomic History. *Top. Catal.* **2009,** *52*, 924–934.

(5) Zaera, F., New Challenges in Heterogeneous Catalysis for the 21st Century. *Catal. Lett.* **2012,** *142*, 501–516.

(6) Erisman, J. W.; Sutton, M. A.; Galloway, J.; Klimont, Z.; Winiwarter, W., How a century of ammonia synthesis changed the world. *Nat. Geosci.* **2008,** *1*, 636–639.

(7) Lindstroem, B.; Pettersson, L. J., A brief history of catalysis. *CATTECH* **2003,** *7*, 130–138.

(8) Masters, A. F.; Maschmeyer, T., Zeolites - From curiosity to cornerstone. *Microporous Mesoporous Mater.* **2011,** *142*, 423–438.

(9) Weitkamp, J., Zeolites and catalysis. *Solid State Ionics* **2000,** *131*, 175–188.

(10) EIA International Energy Outlook 2013. http://www.eia.gov/forecasts/ieo/world.cfm (accessed March 2014).

(11) IPCC, *IPCC Special Report on Renewable Energy Sources and Climate Change Mitigation. Prepared by Working Group III of the Intergovernmental Panel on Climate Change.* Cambridge University Press: Cambridge, United Kingdom and New York, NY, USA, 2011.

(12) IEA World Energy Outlook 2012. http://www.worldenergyoutlook.org/publications/weo-2012 (accessed March 2014).

(13) Murray, J.; King, D., Climate policy: Oil's tipping point has passed. *Nature (London)* **2012,** *481*, 433–435.

(14) BP Statistical Review of World Energy 2013. http://www.bp.com/content/dam/bp/pdf/statistical-review/statistical_review_of_world_energy_2013.pdf (accessed March 2014).

(15) Edenhofer, O.; Pichs-Madruga, R.; Sokona, Y. Renewable Energy Sources and Climate Change Mitigation. http://srren.ipcc-wg3.de/report/IPCC_SRREN_Full_Report.pdf (accessed March 2014).

(16) IPCC, *Climate Change 2013 The Physical Science Basis. Contribution of Working Group I to the Fifth Asessment Report of the Intergovernmental Panel on Climate Change*. Cambridge University Press: Cambridge, United Kingdom and New York, NY, USA, 2013.

(17) Anastas, P. T.; Kirchhoff, M. M., Origins, current status, and future challenges of green chemistry. *Acc. Chem. Res.* **2002,** *35*, 686–694.

(18) Brundtland, C. G., *Our Common Future, The World Commission on Environmental Development*. Oxford University Press: Oxford, 1987.

(19) Anastas, P.; Warner, J. C., *Green Chemistry: Theory and Practice*. Oxford University Press: Oxford, 1998.

(20) Sheldon, R. A., Green and sustainable manufacture of chemicals from biomass: state of the art. *Green Chem.* **2014,** *16*, 950–963.

(21) Anastas, P.; Eghbali, N., Green Chemistry: Principles and Practice. *Chem. Soc. Rev.* **2010,** *39*, 301–312.

(22) Anastas, P. T.; Beach, E. S., Green chemistry: the emergence of a transformative framework. *Green Chem. Lett. Rev.* **2007,** *1*, 9–24.

(23) Huber, G. W.; Iborra, S.; Corma, A., Synthesis of transportation fuels from biomass: Chemistry, catalysts, and engineering. *Chem. Rev. (Washington, DC)* **2006,** *106*, 4044–4098.

(24) Corma, A.; Iborra, S.; Velty, A., Chemical Routes for the Transformation of Biomass into Chemicals. *Chem. Rev. (Washington, DC)* **2007,** *107*, 2411–2502.

(25) Anastas, P. T.; Kirchhoff, M. M.; Williamson, T. C., Catalysis as a foundational pillar of green chemistry. *Appl. Catal., A* **2001,** *221*, 3–13.

(26) Demirbas, A., Progress and recent trends in biofuels. *Prog. Energ. Combust.* **2007,** *33*, 1–18.

(27) Huber, G. W.; Dumesic, J. A., An overview of aqueous-phase catalytic processes for production of hydrogen and alkanes in a biorefinery. *Catal. Today* **2006,** *111*, 119–132.

(28) Cortright, R. D.; Davda, R. R.; Dumesic, J. A., Hydrogen from catalytic reforming of biomass-derived hydrocarbons in liquid water. *Nature (London)* **2002,** *418*, 964**–**967.

(29) Chheda, J. N.; Huber, G. W.; Dumesic, J. A., Liquid-phase catalytic processing of biomass-derived oxygenated hydrocarbons to fuels and chemicals. *Angew. Chem. Int. Ed.* **2007,** *46*, 7164–7183.

(30) Robinson, J. M.; Barrett, S. R.; Nhoy, K.; Pandey, R. K.; Phillips, J.; Ramirez, O. A.; Rodriguez, R. I., Energy Dispersive X-ray Fluorescence Analysis of Sulfur in Biomass. *Energ. Fuel.* **2009,** *23*, 2235–2241.

(31) Bartholomew, C. H.; Agrawal, P. K.; Katzer, J. R., Sulfur poisoning of metals. *Adv. Catal.* **1982,** *31*, 135–242.

(32) Rodriguez, J. A., The chemical properties of bimetallic surfaces: Importance of ensemble and electronic effects in the adsorption of sulfur and SO_2. *Prog. Surf. Sci.* **2006,** *81*, 141–189.

(33) Rodriguez, J. A.; Goodman, D. W., High-pressure catalytic reactions over single-crystal metal surfaces. *Surf. Sci. Rep.* **1991,** *14*, 1–107.

(34) Somorjai, G. A., *Introduction to Surface Chemistry and Catalysis*. Wiley: New York, 1994.

(35) Mevellec, V.; Nowicki, A.; Roucoux, A.; Dujardin, C.; Granger, P.; Payen, E.; Philippot, K., A simple and reproducible method for the synthesis of silica-supported rhodium nanoparticles and their investigation in the hydrogenation of aromatic compounds. *New J. Chem.* **2006,** *30*, 1214–1219.

(36) Park, I. S.; Kwon, M. S.; Kim, N.; Lee, J. S.; Kang, K. Y.; Park, J., Rhodium nanoparticles entrapped in boehmite nanofibers: recyclable catalyst for arene hydrogenation under mild conditions. *Chem. Commun. (Cambridge, U. K.)* **2005**, 5667–5669.

(37) Roucoux, A.; Schulz, J.; Patin, H., Arene hydrogenation with a stabilized aqueous rhodium(0) suspension: A major effect of the surfactant counter-anion. *Adv. Synth. Catal.* **2003,** *345*, 222–229.

(38) Augustine, R. L., *Heterogeneous Catalysis for the Synthetic Chemist*. Marcel Dekker: New York, 1995.

(39) Stanislaus, A.; Cooper, B. H., Aromatic hydrogenation catalysis: a review. *Catal. Rev. - Sci. Eng.* **1994,** *36*, 75–123.

(40) Cooper, B. H.; Donnis, B. B. L., Aromatic saturation of distillates: an overview. *Appl. Catal., A* **1996,** *137*, 203–23.

(41) Alhumaidan, F.; Cresswell, D.; Garforth, A., Hydrogen Storage in Liquid Organic Hydride: Producing Hydrogen Catalytically from Methylcyclohexane. *Energy Fuels* **2011,** *25*, 4217–4234.

(42) Kariya, N.; Fukuoka, A.; Ichikawa, M., Efficient evolution of hydrogen from liquid cycloalkanes over Pt-containing catalysts supported on active carbons under "wet-dry multiphase conditions". *Appl. Catal., A* **2002,** *233*, 91–102.

(43) Kariya, N.; Fukuoka, A.; Utagawa, T.; Sakuramoto, M.; Goto, Y.; Ichikawa, M., Efficient hydrogen production using cyclohexane and decalin by pulse-spray mode reactor with Pt catalysts. *Appl. Catal., A* **2003,** *247*, 247–259.

(44) Hodoshima, S.; Saito, Y. In *Hydrogen storage in organic chemical hydrides on the basis of superheated liquid-film concept*, 2009; CRC Press: 2009; pp 437–474.

(45) Perlack, R. D.; Wright, L. L.; Turhollow, A.; Graham, R. L.; Stokes, B.; Erbach, D. C., Biomass as a Feedstock for Bioenergy and Bioproducts Industry: The Technical Feasibility of a Billion-Ton Annual Supply. 2005. http://feedstockreview.ornl.gov/pdf/billion_ton_vision.pdf.

(46) Zakzeski, J.; Bruijnincx, P. C. A.; Jongerius, A. L.; Weckhuysen, B. M., The Catalytic Valorization of Lignin for the Production of Renewable Chemicals. *Chem. Rev. (Washington, DC)* **2010,** *110*, 3552–3599.

(47) Zakzeski, J.; Jongerius, A. L.; Bruijnincx, P. C. A.; Weckhuysen, B. M., Catalytic Lignin Valorization Process for the Production of Aromatic Chemicals and Hydrogen. *ChemSusChem* **2012,** *5*, 1602–1609.

(48) Gosselink, R. J. A.; de Jong, E.; Guran, B.; Abacherli, A., Co-ordination network for lignin-standardisation, production and applications adapted to market requirements (EUROLIGNIN). *Ind. Crops Prod.* **2004,** *20*, 121–129.

(49) Bozell, J. J.; Petersen, G. R., Technology development for the production of biobased products from biorefinery carbohydrates-the US Department of Energy's "Top 10" revisited. *Green Chem.* **2010,** *12*, 539–554.

(50) Vennestrom, P. N. R.; Osmundsen, C. M.; Christensen, C. H.; Taarning, E., Beyond Petrochemicals: The Renewable Chemicals Industry. *Angew. Chem. Int. Ed.* **2011,** *50*, 10502–10509.

(51) Dapsens, P. Y.; Mondelli, C.; Perez-Ramirez, J., Biobased Chemicals from Conception toward Industrial Reality: Lessons Learned and To Be Learned. *ACS Catal.* **2012,** *2*, 1487–1499.

Chapter 2: Designing Nanoscopic, Fluxional Bimetallic Pt-Ru Alloy Hydrogenation Catalysts for Improved Sulfur Tolerance

This chapter was published in *Catalysis Today*.

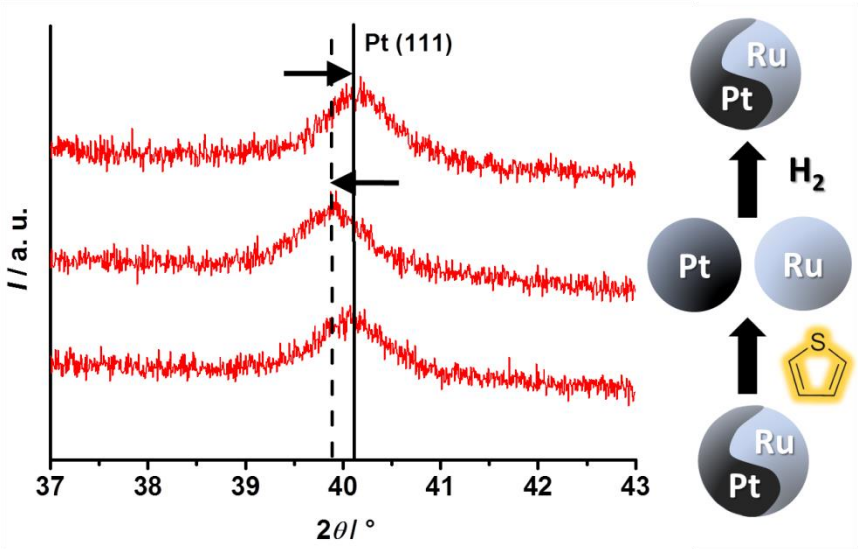

Stanley, J.N.G.; Worthington, K.; Heinroth, F.; Masters, A.F.; Maschmeyer, T., *Catal. Today* **2011**, *178*, 164–171.

2.1 Introduction

The finite nature of our fossil fuel reserves, combined with increasing environmental concerns related to emissions from fossil fuel combustion, make it ever more important to find sustainable and environmentally-friendly energy sources. In particular, supplies of liquid transport fuels (petrol, diesel, jet fuel) will be dwindling rapidly in the next forty years.[1,iii] Biomass is an attractive alternative source of liquid transport fuels, as it is the only foreseeable source of sustainable liquid fuels and chemicals,[1–5] and is more evenly distributed geographically than are fossil fuel reserves.[6] However, as biomass-based feedstocks have a high oxygen and moisture content, lower thermal stabilities, and higher degrees of functionality than do petroleum feedstocks, new chemical pathways and catalysts are required for biomass processing.[7] The current "in-principle" approaches for the conversion of lignocellulosic biomass to liquid fuels include gasification (followed by Fischer–Tropsch chemistry),[2, 8] pyrolysis,[9, 10] hydrothermal liquefaction,[11, 12] delignification (pulping) followed by saccharification and fermentation,[7, 13] and aqueous phase reforming (APR).[1, 14] Supported metal catalysts play an important role in many of these processes. For example, the gasification of biomass in supercritical water is improved by metal catalysts,[15–20] and Rioche *et al.*, continuing studies by Chornet *et al.* on the steam reforming of bio-oil over Ni-based catalysts,[21–26] found that ceria-zirconia supported noble metal catalysts were more efficient than alumina supported catalysts.[10] Recently, Dumesic *et al.* reported that biomass-derived feedstocks can be converted to hydrogen,[27–33] and to gaseous,[31, 34, 35] and liquid[36–41] alkanes using supported metal catalysts, and that the processes can be tailored to produce alkanes rather than hydrogen by tuning the catalyst and H_2/CO concentrations in the reactor.

[iii] References for Chapter 2 begin on page 47.

However, it is expected that the presence in real biomass feedstocks of sulfur (present in amino acids such as cysteine and methionine, and resulting from the uptake of soil nutrients) with values ranging from 10 ppm to 1000 ppm[42] will significantly impair catalytic performance, and thus there is a great need to develop sulfur-tolerant catalysts. For example, Elliot *et al.* claimed that the activity of ruthenium catalysts in supercritical water for the catalytic gasification of wet biomass is strongly decreased by the presence of sulfur,[43] and Osada *et al.* found that the adsorption of sulfur on the catalyst was at least partially responsible for the decrease in the process rate for the gasification of lignin.[44] Although sulfur tolerance has been widely investigated, both in the petrochemical and fine chemical industries,[45–47] there has been little research into improving sulfur tolerance for catalysts involved in the processing of biomass, such as when using the APR reaction.

Catalysts that combine two metals are common in industrial applications, and often show superior activity, selectivity, and sulfur tolerance compared with their monometallic counterparts.[29, 48–51] These improvements might be the result of electronic perturbations (produced by metal–metal bonding, or by changes in the number of available active sites on the surface of the catalyst) or structural changes leading to more edge-sites, kinks, defects, *etc*., or smaller particles.[51] Recently, Azad and Duran proposed a mechanism for sulfur poisoning on Pd-Re catalysts for steam reforming of sulfur-laden logistic fuels (diesel, gasoline, jet fuel).[52, 53] They proposed that palladium was able to transfer the sulfur onto the more readily sulfidable rhenium. This ‘spillover’ of sulfur onto rhenium allows palladium to remain active for longer. Similarly, hydrogen spillover can occur on bimetallic catalysts, and has been reviewed extensively.[54, 55] Based on these two spillover phenomena we envisaged the development of a bimetallic catalyst such that one metal would act preferentially as the hydrogenation catalyst and the other would interact preferentially with sulfur-containing compounds. Coupling these functions with hydrogen

spillover to the metal-coordinated sulfur species, may enable hydrogen to cleave the sulfur metal bond to effectively regenerate the catalyst.

In the work reported here, platinum was chosen as it displays high activity for the hydrogenation reaction, whereas ruthenium was selected as studies have shown that it possesses a higher affinity for sulfur than does platinum.[56] The acidic, mesoporous SiAlTUD-1 was used as the support material since it is well-established that noble metals immobilised on acidic supports are more sulfur-resistant than they are on other supports.[50, 57–63] The mesoporous TUD-1 structure family was chosen because of its characteristic large surface area, high thermostability, and tunable pore sizes.

Common techniques used to synthesise metal nanoparticles include vapour phase techniques,[64] sol-gel methods,[65] sputtering,[66] and co-precipitation.[67] The synthesis of bimetallic nanoparticles is complicated because of the challenges of controlling composition and size distribution.[68] The microemulsion method is an established alternative that can address these problems, and which has been used in the preparation of metal,[69, 70] metal sulfide,[71] and metal halide nanoparticles.[72] The final size of the nanoparticles is controlled by the size of the aqueous droplets, stabilised by the surfactant at the water/oil interface.[73] The sizes of the droplets are controlled by the water-to-surfactant ratio.[68, 74]

The hydrogenation of cyclohexene serves as a useful screening reaction because it is very sensitive to sulfur and because hydrogenation reactions are important steps in the conversion of biomass in various processes.[75] Herein, we report the results of studies probing the performance of bimetallic alloy Pt-Ru catalysts as compared to their monometallic counterparts during the hydrogenation of cyclohexene at room temperature in the presence of thiophene as a sulfur poisoning model.

2.2 Materials and Methods

2.2.1 Materials

The following reagents were used as received: tetraethylene glycol (TEG), polyethylene glycol dodecyl ether (Brij® 30, M_n ~362 amu), hydrogen hexachloroplatinate(IV) hydrate ($H_2PtCl_6 \cdot 5H_2O$), decane (all Adrich), aluminium isopropoxide, hydrazine hydrate ($N_2H_4 \cdot H_2O$) (both Ajax), ruthenium trichloride trihydrate ($RuCl_3 \cdot 3H_2O$) (Strem), *n*-heptane (APS), cyclohexene (Prolabo), and tetraethylorthosilane (TEOS) (Alfa Aesar). Absolute ethanol (Merck) and acetone (Redox) were analytical grade and were used as received. Deionised water was processed using a Milli-Q (Millipore) Ultrapure Water System. 2-Propanol, purchased from Ajax, was dried over calcium hydride (Aldrich) for 24 h, distilled under N_2, and stored under N_2 over dried 3 Å molecular sieves. Thiophene (Merck) was purified by passage through neutral alumina.

2.2.2 Catalyst Preparation

The SiAlTUD-1 support was prepared using an adaptation of the method described by Simons *et al.*[76] Aluminium isopropoxide (6.28 g, 30.7 mmol) was added to a mixture of ethanol (36 mL, 617 mmol), anhydrous 2-propanol (34 mL, 445 mmol), and TEOS (26 mL, 117 mmol) at 45 °C, and the mixture was stirred until all components dissolved. TEG (26 mL, 151 mmol) was added, followed by the dropwise addition of a solution containing ethanol (36 mL, 617 mmol), anhydrous 2-propanol (34 mL, 445 mmol) and water (6 mL, 333 mmol). This mixture was stirred at RT for 30 min, then aged without heating or stirring for 6 h. The resultant white gel was dried at 70 °C for 21 h, then at 98 °C for 2 h after which time the dry material was heated under autogeneous pressure at 165 °C in a Teflon-lined autoclave for 8 h. The template was removed by washing the

material in a Soxhlet extractor (Büchi Extraction System (B-811)) using warm ethanol for 3 h. The white solid obtained was dried at 60 °C before being calcined at 600 °C (ramp rate 5 °C min^{-1}) for 10 h.

The Pt-Ru, Pt, and Ru nanoparticles were prepared using the water-in-oil microemulsion method.[77, 78] Two microemulsions were prepared separately, each containing 80.5% v/v *n*-heptane, 16.5% v/v Brij® 30, and 3% v/v aqueous phase of either the metal salt precursor solution/s or the reducing agent solution. The aqueous phase of the first microemulsion consisted of either $H_2PtCl_6 \cdot 5H_2O$ solution (0.1 M) or $RuCl_3 \cdot 3H_2O$ solution (0.1 M) or both (each at 0.1 M). The aqueous phase of the second microemulsion consisted of $N_2H_4 \cdot H_2O$ solution (2.5 M). All the solutions were made using deionised water. The microemulsions were stirred separately for 15 min, before the hydrazine microemulsion was added to the metal salt microemulsion. The combined microemulsion was stirred until the metal cations of the precursors had been reduced to the metals, at which time a colour change occurred and the nanoparticles could be isolated by precipitation with acetone followed by centrifugation (72 h to 3 weeks).

The Pt-Ru and Pt on SiAlTUD-1 catalysts, denoted as $Pt_1Ru_{1.5}$ and Pt respectively (subscripts indicate the relative molar ratios), were prepared by stirring the SiAlTUD-1 with the appropriate nanoparticle suspension. In a typical example, the nanoparticle suspension (89 mL) was added to the support material (700 mg), and the mixture stirred for 24 h. The solid was isolated by centrifugation, washed with warm ethanol for 3 h using the Soxhlet extractor, and dried at 60 °C overnight. The powder was heat-treated at 450 °C (ramp rate 5 °C min^{-1}) for 2 h under N_2. A Pt/Ru on SiAlTUD-1 mixed monometallic catalyst, denoted as Pt_1/Ru_1, was also prepared in the same manner, by combining Pt and Ru nanoparticle suspensions with the support as described above.

The Ru (Ru), Ru-Pt (Pt_1Ru_3), and Pt-Ru ($Pt_{1.5}Ru_1$) catalysts could not be reduced as described. In these cases the combined microemulsion solutions were stirred with the support material before the metal salts were reduced. In a typical example, the combined microemulsions (89 mL) were added to the support material (700 mg), and the mixture was stirred for 24 h. The suspension was then centrifuged to isolate the solid, which was washed for 3 h with warm ethanol using the Soxhlet extractor, and dried at 60 °C overnight. The powder was calcined in air at 350 °C (ramp rate 5 °C min^{-1}) for 10 h, followed by heat-treatment for 0.5 h under H_2.

2.2.3 Characterisation

Powder X-ray diffraction (XRD) measurements were made using a PANalytical X-Pert PRO MRD X-ray diffractometer equipped with a PIXcel detector, and using Ni-filtered $Cu_{K\alpha}$ radiation (λ_{av} 1.5419 Å). Initial analyses were performed using the PANalytical HighScore software.[79] A Micromeritics ASAP 2020 Accelerated Surface Area and Porosity analyser was used to measure the N_2 adsorption/desorption isotherms of the samples at 77 K. Before analysis, samples were degassed at 200 °C. Transmission electron microscopy (TEM) images were recorded digitally with a Gatan slow-scan charge coupled device (CCD) camera on a Philips CM120 Biofilter electron microscope operating at 120 kV. A Varian Vista AX ICP-AES equipped with a CCD detector was used to measure elemental compositions.

2.2.4 Catalytic Activity

The hydrogenation reaction was performed in a two-necked, round bottom 50 mL glass Quickfit flask, fitted with Suba-Seal stoppers and equipped with a magnetic stirrer at RT.

Cyclohexene (160 µL, 1.58 mmol) and decane (200 µL, 1.03 mmol, internal standard) were added to ethanol (25 mL). The mixture was stirred at a rate of 400 rpm for 5 min in air and a sample (~0.10 mL) was taken. The catalyst (100 mg) was added to the reaction vessel, the mixture was stirred for 10 min, and a sample (~0.10 mL) was taken. The reactor was purged through a cannula with H_2 provided from a balloon, filled in-house, to replace the air in the reaction vessel, admitted through a septum cap fitted to one arm of the reactor, and the reaction was run under 1 bar H_2 with stirring at 400 rpm for 4 h. Samples (total 8–12, each ~0.10 mL) were taken at regular intervals using a syringe through a septum cap fitted to one arm of the reactor. During sulfur poisoning reactions, thiophene (0.02 µL or 0.20 µL, in 1.0 mL ethanol, equivalent to a thiophene content of 45 ppm or 450 ppm (v/v), or a sulfur content of 57 ppm or 560 ppm (mol/mol) in 160 µL cyclohexene) was added through a septum cap fitted to one arm of the reactor, after admitting H_2 to the reactor. All samples taken from the reactor were centrifuged to isolate the catalyst, the supernatant was diluted with ethanol, and the progress of the reaction was analysed using gas chromatography (Shimadzu GC-17A Gas Chromatograph equipped with a BP21 column – 30 m × 0.25 mm I.D.; 0.25 µm film thickness; J & W Scientific - and a flame ionization detector, using Ar as the carrier gas). For catalyst regeneration experiments, the catalyst was isolated from the reaction mixture by centrifugation, and dried in air for use in subsequent reactions. Additionally, for the regeneration reaction with heat treatment, the catalyst was heat-treated under H_2 for 1 h at 300 °C (ramp rate 5 °C min^{-1}).

2.2.5 Normalisation

As the TEM micrographs and bulk XRD patterns indicated similar metal particle sizes across the catalyst batches, it was assumed that the metal dispersion was relatively equal across all samples. Therefore, the catalytic results were calculated as turn-over-frequencies (TOF) from the number of moles of product (cyclohexane) at 10% conversion, and then normalised per mole of platinum (as determined by ICP-AES) per unit time (using the formula TOF = [mol cyclohexane]/[mol Pt] × time). It should be noted that in all cases the mass balance was >90%.

2.3 Results and Discussion

2.3.1 Characterisation

The acidic, mesoporous, aluminosilicate SiAlTUD-1 used as the catalyst support, was synthesised according to the literature.[76] Its BET surface area of 587 $m^2 g^{-1}$, total pore volume of 1.1 $cm^3 g^{-1}$, and maximum pore size of 15 nm are in close agreement with the literature values of ~600 $m^2 g^{-1}$, 1.1 $cm^3 g^{-1}$, and 15 nm, respectively.[76] Analysis of the product using ICP-AES gave the silicon to aluminium ratio (Si:Al) as 4.4:1, consistent with the 5:1 composition of the starting gel mixture.

The following six catalysts were prepared using this support material, *i.e.* in addition to a pure ruthenium (Ru) and a pure platinum (Pt) catalyst, a mixed monometallic catalyst (Pt_1/Ru_1) was prepared by first separately reducing the platinum and ruthenium monometallic precursor solutions and subsequently mixing the resulting suspensions in the immobilisation step. Three bimetallic alloyed catalysts (Pt_1Ru_3, $Pt_1Ru_{1.5}$, and $Pt_{1.5}Ru_1$) with different ruthenium and platinum ratios were also prepared. As outlined in the experimental section, not all catalysts could be directly reduced in the water-in-oil

microemulsion, therefore two different strategies were followed to reduce and immobilise the metal nanoparticles onto the support material. The first group of catalysts consists of $Pt_1Ru_{1.5}$, Pt, and Pt_1/Ru_1, which were directly reduced with hydrazine in the water-in-oil microemulsion and immobilised onto the support, followed by a heat treatment under nitrogen to remove all organic material. The second group consists of Ru, Pt_1Ru_3, and $Pt_{1.5}Ru_1$. For these catalysts it was necessary to immobilise the metal precursors in a first step by impregnation from solution, followed by calcination and subsequent hydrogenation. The physical properties of all catalysts are presented in Table 2.1.

Table 2.1 Physical properties of the unloaded support and all catalysts.

Catalyst	Metal / wt.%[a]	Pt / mol.%	Ru / mol.%	a / Å[b]	σ / Å[c]	S_{BET} / $m^2\ g^{-1}$	V_{Pore} / $cm^3\ g^{-1}$
SiAlTUD-1	0	–	–	–	–	587	1.10
Ru[e]	0.50	0	100	2.7098	0.0005	437	1.03
Pt_1Ru_3[e]	0.06	28	72	2.7133	0.0016	451	1.00
$Pt_1Ru_{1.5}$[d]	0.20	38	62	3.8905	0.0005	497	1.11
$Pt_{1.5}Ru_1$[d]	0.10	59	41	3.9178	0.0001	399	0.90
Pt[e]	1.79	100	0	3.9199	0.0001	455	0.91
Pt_1/Ru_1[e]	1.73	49	51	3.9153	0.0001	388	0.95

[a] Total metal loading determined by ICP-AES. [b] a is the lattice constant. [c] σ is the error of the lattice constant. [d] Immobilised followed by reduction with hydrogen. [e] Reduced with hydrazine followed by immobilisation.

The Pt to Ru ratios for the bimetallic alloyed catalysts, determined by ICP-AES (Table 2.1), cover a broad range from 1:1.6 for $Pt_1Ru_{1.5}$ to 1:2.6 for Pt_1Ru_3 to 1.4:1 for $Pt_{1.5}Ru_1$, and the mixed monometallic Pt_1/Ru_1 catalyst exhibits a metal ratio of 1:1. All metal ratios are in good agreement with those expected from the concentrations of the starting precursor solutions. Nitrogen sorption measurements of the catalysts, listed in Table 2.1, indicate a general decrease in surface areas and pore volumes compared with the unmodified support material. The surface areas and pore volumes were calculated to be between 390 to 500 $m^2\ g^{-1}$ and 0.9 to 1.1 $cm^3\ g^{-1}$, respectively. The decrease in the surface area of the material compared to that of the pure silica can be attributed to the heat treatment of the support material during the immobilisation step and to the immobilisation itself.[80] A general trend is not apparent between metal loading and surface areas. As expected, the pore size of silica is not affected by the immobilisation process.

As shown in Figure 2.1a, the XRD patterns of all samples display the typical reflections for platinum or ruthenium, indicating the presence of the metal nanoparticles, and in the case of the bimetallic samples, the formation of a Pt-Ru or Ru-Pt alloy. All supported nanoparticles have retained small particle sizes, generally below 15 nm, except $Pt_{1.5}Ru_1$, which has a particle size of 20 nm, as determined using the Scherrer equation. It can be deduced from the XRD pattern that the sample Pt_1Ru_3 exhibits the hcp crystal structure characteristic of ruthenium which is also observed in the pure catalyst Ru, which, for the Pt_1Ru_3 sample, is consistent with its high ruthenium content (Pt to Ru ratio of 1:2.6). However, extrapolating from the Pt-Ru equilibrium phase diagram of bulk ruthenium and platinum (reported only for $T \geq 500$ °C),[81] reflections attributable to the fcc phase of platinum might also be expected to be observed in the XRD pattern in the present case as in this range both metals are immiscible (at least at $T \geq 500$ °C).[82, 83] Although a second phase could not be detected in the XRD pattern, the intensities of the reflections

observed are relatively weak and broad due to the nature of the supported nanoparticles. In the literature different observations have been reported, for instance, Chu *et al*. could detect both phases in the XRD data of *ca*. 13 nm Pt-Ru nanoparticles with the same metal ratio.[84] In contrast, Pan *et al*. published results of alloyed Pt-Ru nanoparticles, again with the same metal ratio, where only a twinned fcc structure could be detected indicating the threshold between the fcc and hcp structures.[85]

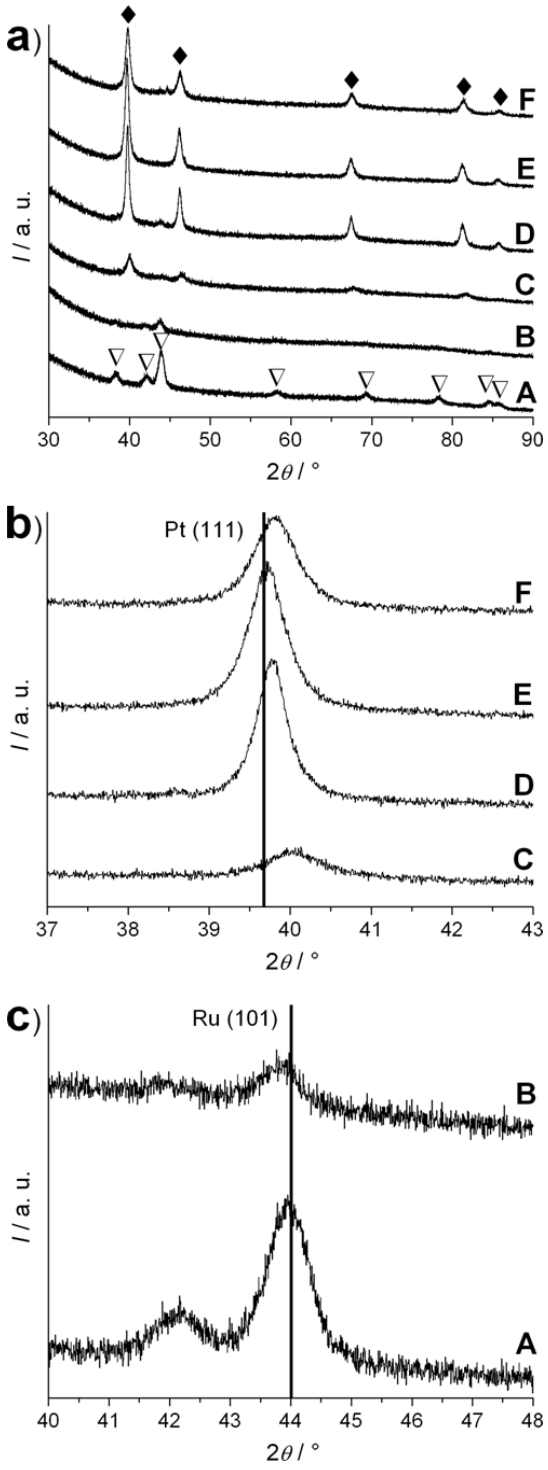

Figure 2.1 XRD patterns a) of all catalysts, b) in the range 37–43 2θ showing the (111) reflection of platinum and c) in the range of 40–48 2θ showing the (101) reflection of ruthenium with (A) Ru, (B) Pt_1Ru_3, (C) $Pt_1Ru_{1.5}$, (D) $Pt_{1.5}Ru_1$, (E) Pt and (F) Pt_1/Ru_1. Patterns of references are JCPDS 00-001-1190 for platinum (♦) and JCPDS 00-006-663 for ruthenium (▽).[86, 87]

When the platinum content is slightly increased as in catalyst $Pt_1Ru_{1.5}$, the catalyst exhibits the fcc crystal structure characteristic of platinum, rather than the hcp crystal structure of ruthenium, which is in good agreement with the literature.[82, 83, 88] The XRD patterns of catalyst $Pt_{1.5}Ru_1$ and the pure catalyst Pt show the typical platinum patterns, as expected due to their high platinum content. However, due to a small reflection at 44 degrees in 2θ in the XRD pattern of catalyst $Pt_{1.5}Ru_1$, the presence of an additional minor Ru phase cannot be completely excluded. In the case of the mixed monometallic catalyst Pt_1/Ru_1, in which the two separately reduced monometallic platinum and ruthenium suspensions were mixed prior to the immobilisation, the resulting XRD pattern reveals mainly the Pt reflections. Nevertheless, reflections of the ruthenium phase can also be found, indicating its presence.

To evaluate the bimetallic character of these catalysts, the (111) reflection of platinum (Figure 2.1b) and the (101) of ruthenium (Figure 2.1c) were analysed. In Figure 2.1b it is obvious that with increasing ruthenium content ($Pt < Pt_{1.5}Ru_1 < Pt_1Ru_{1.5}$) the (111) reflection shifts to higher 2θ values. Thus, the lattice constants for these catalysts decrease from 3.9199 Å for pure platinum in catalyst Pt to 3.9178 Å for $Pt_{1.5}Ru_1$ and down to 3.8905 Å for $Pt_1Ru_{1.5}$ (Table 2.1). This result reflects the fact that more ruthenium, which has a smaller atomic radius than platinum (r_{Ru} = 1.34 Å *vs* r_{Pt} = 1.38 Å), is being incorporated in the platinum lattice, and is consistent with alloy formation. Interestingly, catalyst Pt_1/Ru_1 also shows a small shift to higher 2θ values, displaying a lattice constant of 3.9153 Å. This smaller lattice constant indicates a volume fraction of alloy, which might arise during the final heat treatment. However, as the shift to lower 2θ is only slight, in spite of the relatively high ruthenium content, it is likely that most of the ruthenium does, indeed, exist in a separate phase. In the case of catalyst Pt_1Ru_3, a small but obvious shift towards smaller 2θ values is observed, which indicates the incorporation of the larger

platinum into the ruthenium lattice. The lattice constants were calculated to be 2.7098 Å for the pure Ru catalyst and to be 2.7133 Å for Pt_1Ru_3. This result, in combination with the lack of a second phase, indicates at least partial alloy formation, which is contrary to the phase diagram of the bulk materials but in agreement with the work of Pan *et al.* However, due to the nature of the XRD data set a second platinum phase cannot be completely excluded. All other XRD results of the bimetallic alloyed catalysts are in good agreement with the trends observed in studies of Pt-Ru and Ru-Pt alloys with various compositions.[82, 84, 89]

The TEM micrographs of the catalysts, presented in Figure 2.2, reveal a good dispersion of the nanoparticles on the surface of the supports. It is apparent that the nanoparticles have retained their spherical shape, dispersion and a narrow size distribution (12–15 nm). The main exception, $Pt_{1.5}Ru_1$ (Figure 2.2d), has a larger particle size of approximately 20 nm, which is in good agreement with the size obtained from the XRD analysis.

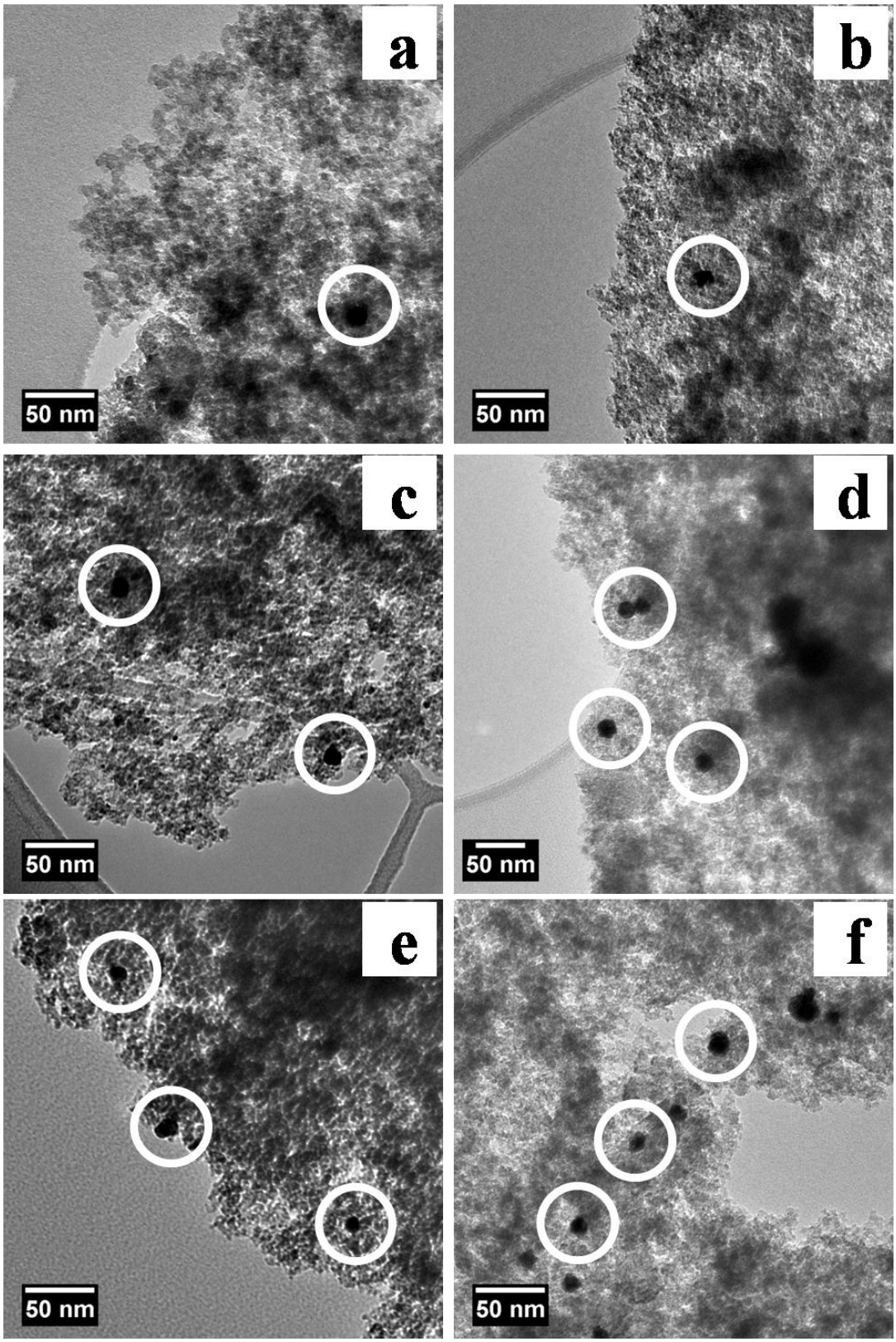

Figure 2.2 TEM micrographs of the catalysts prepared: a) Ru, b) Pt_1Ru_3, c) $Pt_1Ru_{1.5}$, d) $Pt_{1.5}Ru_1$, e) Pt and f) Pt_1/Ru_1. The nanoparticles are highlighted with white circles.

2.3.2 Catalytic activity

The turn-over-frequencies (TOF) were determined at 10% conversion to minimise distortions due to batch conditions and variance of metal loading between catalysts. They are summarized in Table 2.2. All alloy catalysts exhibit higher activity than the non-alloyed catalysts. Ruthenium alloys are more sulfur tolerant than pure platinum or a mixture of supported platinum/ruthenium nanoparticles. Ruthenium on its own is not active. At 57 ppm of added sulfur there appears to be a trend that shows the greater the ruthenium component of the alloy the greater its sulfur tolerance. However, at low activity in the presence of 560 ppm sulfur this trend becomes less clear.

Table 2.2 TOF results of the hydrogenation of cyclohexene in ethanol at RT under 1 bar H_2.

Catalyst	TOF / s^{-1}[c]		
	0 ppm S[g]	57 ppm S[g]	560 ppm S[g]
Ru[a, d]	0	0	0
Pt_1Ru_3[a]	63.3	9.8	1.8
$Pt_1Ru_{1.5}$[b]	23.0	8.9	3.3
$Pt_1Ru_{1.5}$[e]	24.9	–	–
$Pt_1Ru_{1.5}$[f]	4.7	–	–
$Pt_{1.5}Ru_1$[a]	34.7	6.4	2.3
Pt[b]	1.4	0.3	0
Pt_1/Ru_1[b]	1.9	0.4	0

[a] Immobilised followed by reduction with hydrogen. [b] Reduced with hydrazine followed by immobilisation. [c] At 10% conversion, TOF = [mol cyclohexane]/[mol Pt] × time. [d] Catalyst was completely inactive for the reaction studied. [e] After recycling and reduction under hydrogen. [f] After recycling and drying in air at RT. [g] Equals a proportion of 45 ppm or 450 ppm thiophene in 160 μL cyclohexene.

The close to linear conversion with time after the first 30 min (Figure 2.3a) for the alloys as compared to pure platinum are consistent with a hydrogen/sulfur spillover equilibrium having been established. The study of the alloyed catalysts reveals that the platinum to ruthenium ratio plays a crucial role for the catalytic performance and needs further investigations.

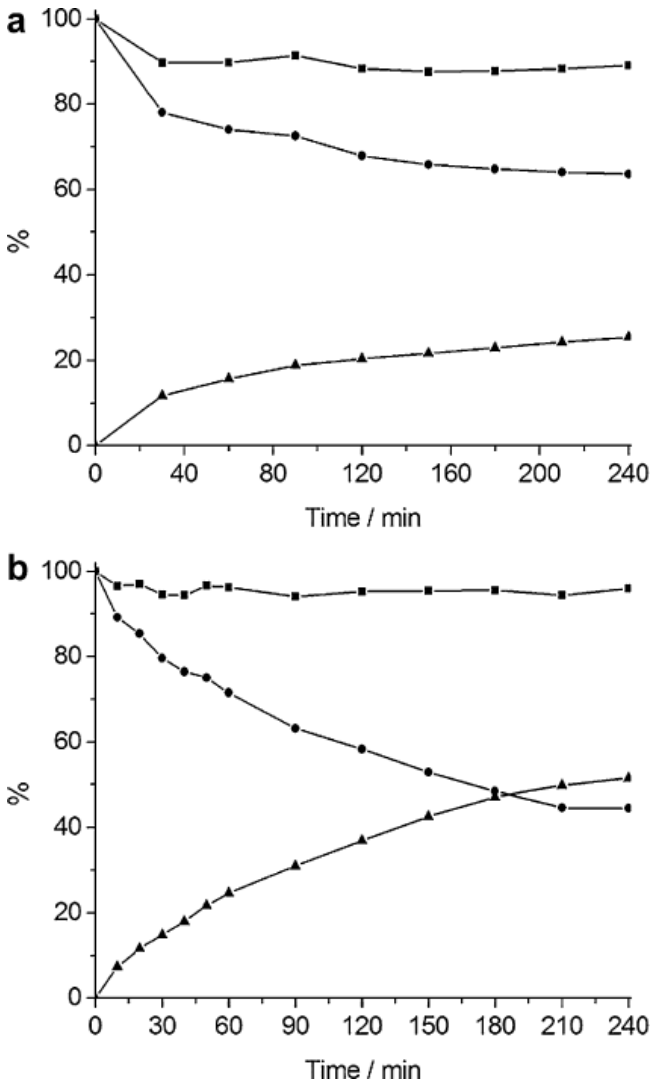

Figure 2.3 Plot of cyclohexene conversion (●), formation of cyclohexane (▲), and mass balance (■), a) in the presence of 560 ppm sulfur and b) in the presence of 0 ppm sulfur but after being exposed to 560 ppm sulfur, isolated and re-used (without being re-conditioned by heat treatment under hydrogen) for catalyst $Pt_1Ru_{1.5}$.

To determine the influence of sulfur poisoning on the alloy character of the bimetallic catalysts, the Pt(111) reflection in the case of $Pt_{1.5}Ru_1$ and $Pt_1Ru_{1.5}$ and the Ru(101) reflection for $Pt_{1.5}Ru_1$ of the XRD powder patterns were monitored before and after the catalytic reaction with 560 ppm sulfur (Figure 2.4 and Figure 2.5). This

comparison involves the catalyst having been isolated from the thiophene-containing solution after the flow of hydrogen was stopped. Figure 2.4 (A and B) illustrates that after poisoning $Pt_1Ru_{1.5}$ with 560 ppm sulfur the Pt(111) reflection shifts towards lower 2θ. This shift indicates that the catalyst loses some of its alloy character, partially separating into two metal domains, and the lattice constant increases accordingly to 3.9060 Å. This value is between the lattice constant of the catalyst before poisoning (3.8905 Å) and the lattice constant of pure platinum (3.9199 Å).[89] This result suggests that the ruthenium has been sequestered in the presence of thiophene, maybe in the form of ruthenium sulfide or a ruthenium-thiophene complex. The co-ordination of sulfur to ruthenium would lead to an internal restructuring of the particle, which suggests that ruthenium is acting as a sulfur trap. The observed shift of the reflections in the XRD patterns is consistent with studies by Menegazzo *et al.*, who observed similar shifts, in their investigations of sulfur poisoning on Pd-Au catalysts.[90] They attributed the shift to the formation of palladium sulfide, which could be confirmed by the presence of an additional palladium sulfide reflection, although no additional reflections could be observed in the present case. However, Menegazzo *et al.* used sodium sulfide (not thiophene) as sulfur source to poison the catalyst. It should be noted that this shift cannot be observed when 57 ppm sulfur is used to poison the catalyst.

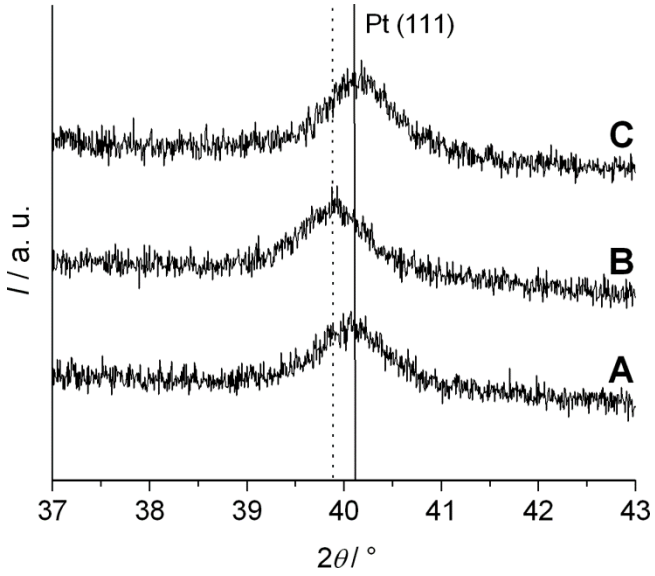

Figure 2.4 XRD patterns of $Pt_1Ru_{1.5}$ catalyst (A) before sulfur poisoning, (B) after sulfur poisoning with 560 ppm sulfur and (C) after regeneration with heat treatment under H_2. The solid line indicates the reflection position in the absence of sulfur and the dotted line, that in the presence of sulfur.

To test if the sulfur poisoning and Pt-Ru alloy internal restructuring is reversible, a $Pt_1Ru_{1.5}$ catalyst, previously operated in the presence of 560 ppm sulfur, was heat-treated under hydrogen for 1 h at 300 °C. Upon heat treatment, the XRD powder pattern (C in Figure 2.4) shows that the reflection has shifted back towards higher 2θ and the lattice constant (3.8891 Å) has almost reached its former value. This observation would be consistent with the catalyst returning to its original Pt-Ru alloy form, suggesting that the sulfur is no longer coordinated to the ruthenium, which has been incorporated back into the platinum lattice. Hence, there appears to be a dynamic alloy/de-alloying process occurring during the poisoning and regeneration processes. To verify that the catalyst was indeed regenerated, it was subsequently tested for its hydrogenation activity in the absence of sulfur, yielding a TOF of 24.9 s^{-1}, which is comparable to the TOF before poisoning (TOF

of 23.0 s^{-1}, Table 2.2). This reversibility is consistent with the suggestion made above as to the occurrence of hydrogen/sulfur spillover *in-situ* explaining the sulfur tolerance of the alloy catalyst to some degree. To underpin this suggestion, in an additional experiment the $Pt_1Ru_{1.5}$ catalyst, again exposed to 560 ppm sulfur, was isolated and re-used in a subsequent hydrogenation reaction in the absence of added thiophene, but this time without being re-conditioned by heat treatment under hydrogen. The catalyst yielded a TOF of 4.7 s^{-1} which is higher than the TOF achieved in the presence of 560 ppm sulfur (TOF of 3.3 s^{-1}, Table 2.2), as shown in Figure 2.3a and Figure 2.3b. If the sulfur species had been adsorbed irreversibly on the catalyst surface, no subsequent improvement in the activity of the catalyst would have been observable. However, as the catalyst did regain some activity, this result suggests that the sulfur poisoning is a dynamic and reversible process. The precise fate of the thiophene (simple equilibrium or conversion into eventually H_2S) will be elucidated with further experiments using very precise vibrational spectroscopic techniques that can deal with the very low surface coverages. However, under the relatively mild screening conditions used here, one would not assume full decomposition to H_2S, and we found no evidence of this gas being present.

In the case of Pt_1Ru_3 no observable shift could be found (Figure 2.5a), despite it being severely poisoned. This lack of shift could be attributed to the high content of ruthenium in Pt_1Ru_3 that results in the hcp crystal structure, making the segregation of ruthenium out of the alloy impossible to observe. Contrarily, in the XRD patterns of $Pt_{1.5}Ru_1$ (Figure 2.5b), a minor shift towards lower 2θ is observed. This XRD result indicates the internal restructuring of the Pt-Ru alloy, similar to the restructuring observed for $Pt_1Ru_{1.5}$, although the shift towards the (111) reflection of pure platinum is less pronounced for $Pt_{1.5}Ru_1$ than for $Pt_1Ru_{1.5}$. A reason can be that $Pt_{1.5}Ru_1$ had a much higher relative platinum content (Table 2.1) and therefore a smaller initial shift after the

incorporation of the ruthenium into the lattice than $Pt_1Ru_{1.5}$. Whereas the lattice constant of $Pt_1Ru_{1.5}$ after poisoning is 3.9060 Å, indicating a partial separation of the alloy into metal domains, the lattice constant of $Pt_{1.5}Ru_1$ after poisoning is 3.9214 Å (*cf.* the lattice constant of platinum of 3.9199 Å). Thus, the XRD pattern after poisoning suggests that $Pt_{1.5}Ru_1$ no longer displays any alloyed character, and the Pt-Ru appears to have completely separated into two metal domains, limiting the events of hydrogen and/or sulfur spillovers.

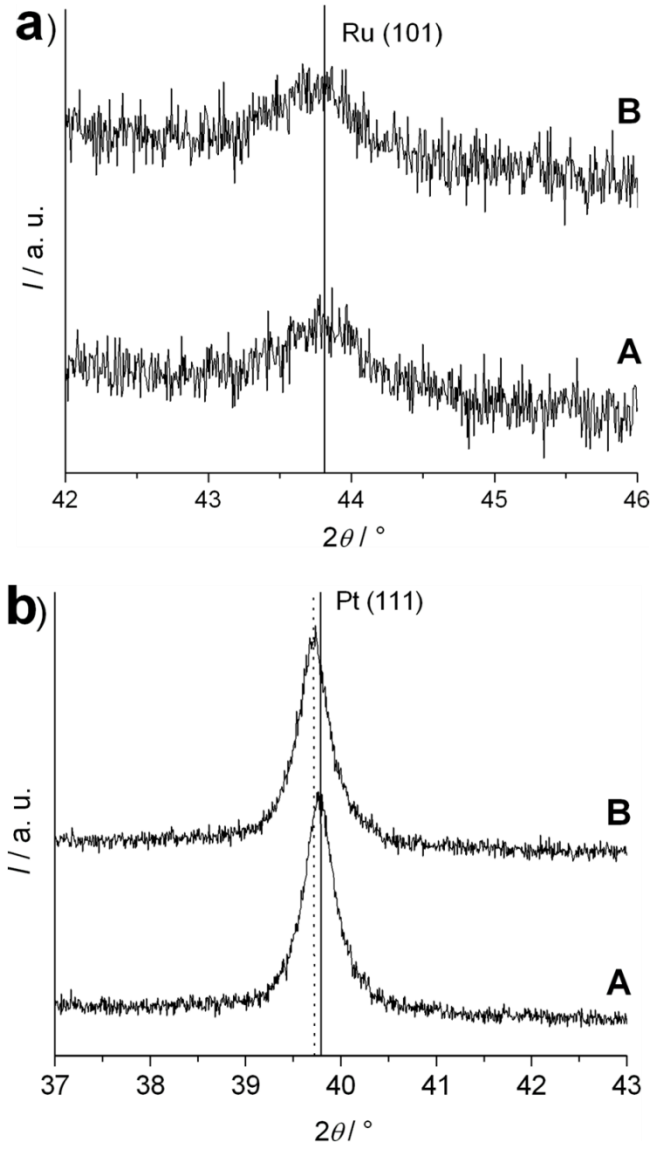

Figure 2.5 XRD patterns of a) Pt_1Ru_3 and b) $Pt_{1.5}Ru_1$, (A) before and (B) after sulfur poisoning with 560 ppm sulfur. The solid line indicates the reflection position in the absence of sulfur and the dotted line in the presence of sulfur.

In combination with the catalysis results there appears to be a correlation between the presence of an alloy character after poisoning with sulfur and the activity of the catalysts. The catalyst that is least poisoned ($Pt_1Ru_{1.5}$) exhibits only partial alloy separation, whereas the catalyst which displays greater overall poisoning ($Pt_{1.5}Ru_1$) exhibits complete alloy separation.

2.4 Conclusion

Improved sulfur tolerance in the catalysis of cyclohexene hydrogenation is observed for catalysts consisting of bimetallic Pt-Ru nanoparticles supported on a high surface area mesoporous Si/Al support of the TUD-1 type. This sulfur tolerance, observed for certain Ru to Pt ratios, might be due to sulfur and hydrogen intra-particle spillover. Regeneration of sulfur poisoned catalysts by heating in hydrogen after the reaction has been demonstrated. This is consistent with the operation of an *in-situ* self regeneration process during the reaction. To get a better understanding of the (self-) regeneration processes *in-situ* EXAFS studies are being pursued.

2.5 References

(1) Chheda, J. N.; Huber, G. W.; Dumesic, J. A., Liquid-phase catalytic processing of biomass-derived oxygenated hydrocarbons to fuels and chemicals. *Angew. Chem. Int. Ed.* **2007,** *46*, 7164–7183.

(2) Klass, D. L., *Biomass for Renewable Energy, Fuels, and Chemicals*. Academic Press: San Diego, 1998.

(3) Lynd, L. R.; Wyman, C. E.; Gerngross, T. U., Biocommodity Engineering. *Biotechnol. Prog.* **1999,** *15*, 777–793.

(4) Huber, G. W.; Iborra, S.; Corma, A., Synthesis of transportation fuels from biomass: Chemistry, catalysts, and engineering. *Chem. Rev. (Washington, DC)* **2006,** *106*, 4044–4098.

(5) Schmidt, L. D.; Dauenhauer, P. J., Chemical engineering: Hybrid routes to biofuels. *Nature* **2007,** *447*, 914–915.

(6) Demirbas, A., Progress and recent trends in biofuels. *Prog. Energ. Combust.* **2007,** *33*, 1–18.

(7) Huber, G. W.; Dumesic, J. A., An overview of aqueous-phase catalytic processes for production of hydrogen and alkanes in a biorefinery. *Catal. Today* **2006,** *111*, 119–132.

(8) Zwart, R. W. R.; Boerrigter, H., High Efficiency Co-production of Synthetic Natural Gas (SNG) and Fischer-Tropsch (FT) Transportation Fuels from Biomass. *Energ. Fuel.* **2005,** *19*, 591–597.

(9) Chen, N. Y.; Degnan Jr, T. F.; Koenig, L. R., Liquid Fuel from Carbohydrates. *Chemtech* **1986,** *16*, 506–511.

(10) Rioche, C.; Kulkarni, S.; Meunier, F. C.; Breen, J. P.; Burch, R., Steam reforming of model compounds and fast pyrolysis bio-oil on supported noble metal catalysts. *Appl. Catal., B* **2005,** *61*, 130–139.

(11) Elliott, D. C.; Beckman, D.; Bridgwater, A. V.; Diebold, J. P.; Gevert, S. B.; Solantausta, Y., Developments in direct thermochemical liquefaction of biomass: 1983-1990. *Energ. Fuel.* **1991,** *5*, 399–410.

(12) Elliott, D. C., Historical Developments in Hydroprocessing Bio-oils. *Energ. Fuel.* **2007,** *21*, 1792–1815.

(13) Katzen, R.; Tsao, G. T., A view of the history of biochemical engineering. *Adv. Biochem. Eng. Biot.* **2000,** *70*, 77–91.

(14) Davda, R. R.; Shabaker, J. W.; Huber, G. W.; Cortright, R. D.; Dumesic, J. A., A review of catalytic issues and process conditions for renewable hydrogen and alkanes by aqueous-phase reforming of oxygenated hydrocarbons over supported metal catalysts. *Appl. Catal,. B* **2005,** *56*, 171–186.

(15) Osada, M.; Sato, T.; Watanabe, M.; Shirai, M.; Arai, K., Catalytic gasification of wood biomass in subcritical and supercritical water. *Combust. Sci. Technol.* **2006,** *178*, 537–552.

(16) Matsumura, Y.; Sasaki, M.; Okuda, K.; Takami, S.; Ohara, S.; Umetsu, M.; Adschiri, T., Supercritical water treatment of biomass for energy and material recovery. *Combust. Sci. Technol.* **2006,** *178*, 509–536.

(17) Osada, M.; Sato, O.; Watanabe, M.; Arai, K.; Shirai, M., Water Density Effect on Lignin Gasification over Supported Noble Metal Catalysts in Supercritical Water. *Energ. Fuel.* **2006,** *20*, 930–935.

(18) Yoshida, T.; Oshima, Y., Partial Oxidative and Catalytic Biomass Gasification in Supercritical Water: A Promising Flow Reactor System. *Ind. Eng. Chem. Res.* **2004,** *43*, 4097–4104.

(19) Sato, T.; Osada, M.; Watanabe, M.; Shirai, M.; Arai, K., Gasification of Alkylphenols with Supported Noble Metal Catalysts in Supercritical Water. *Ind. Eng. Chem. Res.* **2003,** *42*, 4277–4282.

(20) Osada, M.; Sato, T.; Watanabe, M.; Adschiri, T.; Arai, K., Low-Temperature Catalytic Gasification of Lignin and Cellulose with a Ruthenium Catalyst in Supercritical Water. *Energ. Fuel.* **2004,** *18*, 327–333.

(21) Wang, D.; Montane, D.; Chornet, E., Catalytic steam reforming of biomass-derived oxygenates: acetic acid and hydroxyacetaldehyde. *Appl. Catal., A* **1996,** *143*, 245**–**270.

(22) Wang, D.; Czernik, S.; Montane, D.; Mann, M.; Chornet, E., Biomass to Hydrogen via Fast Pyrolysis and Catalytic Steam Re-Forming of the Pyrolysis Oil or Its Fractions. *Ind. Eng. Chem. Res.* **1997,** *36*, 1507–1518.

(23) Wang, D.; Czernik, S.; Chornet, E., Production of Hydrogen from Biomass by Catalytic Steam Reforming of Fast Pyrolysis Oils. *Energ. Fuel.* **1998,** *12*, 19–24.

(24) Marquevich, M.; Czernik, S.; Chornet, E.; Montane, D., Hydrogen from Biomass: Steam Reforming of Model Compounds of Fast-Pyrolysis Oil. *Energ. Fuel.* **1999,** *13*, 1160–1166.

(25) Garcia, L.; French, R.; Czernik, S.; Chornet, E., Catalytic steam reforming of bio-oils for the production of hydrogen: effects of catalyst composition. *Appl. Catal., A* **2000,** *201*, 225–239.

(26) Czernik, S.; French, R.; Feik, C.; Chornet, E., Hydrogen by Catalytic Steam Reforming of Liquid Byproducts from Biomass Thermoconversion Processes. *Ind. Eng. Chem. Res.* **2002,** *41*, 4209–4215.

(27) Shabaker, J. W.; Huber, G. W.; Dumesic, J. A., Aqueous-phase reforming of oxygenated hydrocarbons over Sn-modified Ni catalysts. *J. Catal.* **2004,** *222*, 180–191.

(28) Shabaker, J. W.; Davda, R. R.; Huber, G. W.; Cortright, R. D.; Dumesic, J. A., Aqueous-phase reforming of methanol and ethylene glycol over alumina-supported platinum catalysts. *J. Catal.* **2003,** *215*, 344–352.

(29) Huber, G. W.; Shabaker, J. W.; Evans, S. T.; Dumesic, J. A., Aqueous-phase reforming of ethylene glycol over supported Pt and Pd bimetallic catalysts. *Appl. Catal., B* **2006,** *62*, 226–235.

(30) Huber, G. W.; Shabaker, J. W.; Dumesic, J. A., Raney Ni-Sn Catalyst for H_2 Production from Biomass-Derived Hydrocarbons. *Science (Washington, DC)* **2003,** *300*, 2075–2078.

(31) Davda, R. R.; Shabaker, J. W.; Huber, G. W.; Cortright, R. D.; Dumesic, J. A., Aqueous-phase reforming of ethylene glycol on silica-supported metal catalysts. *Appl. Catal., B* **2003,** *43*, 13–26.

(32) Davda, R. R.; Dumesic, J. A., Renewable hydrogen by aqueous-phase reforming of glucose. *Chem. Commun. (Cambridge, U. K.)* **2004**, 36–37.

(33) Cortright, R. D.; Davda, R. R.; Dumesic, J. A., Hydrogen from catalytic reforming of biomass-derived hydrocarbons in liquid water. *Nature (London)* **2002,** *418*, 964–967.

(34) Lin, Y.-C.; Huber, G. W., The critical role of heterogeneous catalysis in lignocellulosic biomass conversion. *Energ. Environ. Sci.* **2009,** *2,* 68–80.

(35) Huber, G. W.; Cortright, R. D.; Dumesic, J. A., Renewable alkanes by aqueous-phase reforming of biomass-derived oxygenates. *Angew. Chem. Int. Ed.* **2004,** *43*, 1549–51.

(36) West, R. M.; Liu, Z. Y.; Peter, M.; Gartner, C. A.; Dumesic, J. A., Carbon-carbon bond formation for biomass-derived furfurals and ketones by aldol condensation in a biphasic system. *J. Mol. Catal. A: Chem.* **2008,** *296*, 18-27.

(37) West, R. M.; Liu, Z. Y.; Peter, M.; Dumesic, J. A., Liquid alkanes with targeted molecular weights from biomass-derived carbohydrates. *ChemSusChem* **2008,** *1*, 417–424.

(38) Huber, G. W.; Chheda, J. N.; Barrett, C. J.; Dumesic, J. A., Production of Liquid Alkanes by Aqueous-Phase Processing of Biomass-Derived Carbohydrates. *Science (Washington, DC)* **2005,** *308*, 1446–1450.

(39) Yan, N.; Zhao, C.; Dyson, P. J.; Wang, C.; Liu, L.-t.; Kou, Y., Selective degradation of wood lignin over noble-metal catalysts in a two-step process. *ChemSusChem* **2008,** *1,* 626–629.

(40) Kunkes, E. L.; Simonetti, D. A.; West, R. M.; Serrano-Ruiz, J. C.; Gaertner, C. A.; Dumesic, J. A., Catalytic conversion of biomass to monofunctional hydrocarbons and targeted liquid-fuel classes. *Science (Washington, DC)* **2008,** *322,* 417–421.

(41) Chheda, J. N.; Dumesic, J. A., An overview of dehydration, aldol-condensation and hydrogenation processes for production of liquid alkanes from biomass-derived carbohydrates. *Catal. Today* **2007,** *123,* 59–70.

(42) Robinson, J. M.; Barrett, S. R.; Nhoy, K.; Pandey, R. K.; Phillips, J.; Ramirez, O. A.; Rodriguez, R. I., Energy Dispersive X-ray Fluorescence Analysis of Sulfur in Biomass. *Energ. Fuel.* **2009,** *23*, 2235–2241.

(43) Elliott, D. C.; Neuenschwander, G. G.; Hart, T. R.; Butner, R. S.; Zacher, A. H.; Engelhard, M. H.; Young, J. S.; McCready, D. E., Chemical Processing in High-Pressure Aqueous Environments. 7. Process Development for Catalytic Gasification of Wet Biomass Feedstocks. *Ind. Eng. Chem. Res.* **2004,** *43*, 1999−2004.

(44) Osada, M.; Hiyoshi, N.; Sato, O.; Arai, K.; Shirai, M., Effect of Sulfur on Catalytic Gasification of Lignin in Supercritical Water. *Energ. Fuel.* **2007,** *21*, 1400–1405.

(45) Bartholomew, C. H.; Agrawal, P. K.; Katzer, J. R., Sulfur poisoning of metals. *Adv. Catal.* **1982,** *31*, 135–242.

(46) Rodriguez, J. A., The chemical properties of bimetallic surfaces: Importance of ensemble and electronic effects in the adsorption of sulfur and SO_2. *Prog. Surf. Sci.* **2006,** *81*, 141–189.

(47) Kullavanijaya, E.; Cant, N. W.; Trimm, D. L., Benzene formation during the oxidation of cyclohexene in the presence and absence of thiophene over a supported palladium catalyst. *Catal. Lett.* **2001,** *75*, 25–29.

(48) Rodriguez, J. A.; Goodman, D. W., High-pressure catalytic reactions over single-crystal metal surfaces. *Surf. Sci. Rep.* **1991,** *14*, 1–107.

(49) Somorjai, G. A., *Introduction to Surface Chemistry and Catalysis*. Wiley: New York, 1994.

(50) Yasuda, H.; Yoshimura, Y., Hydrogenation of Tetralin over zeolite-supported Pd-Pt catalysts in the presence of dibenzothiophene. *Catal. Lett.* **1997,** *46*, 43–48.

(51) Rodriguez, J. A.; Hrbek, J., Interaction of sulfur with well-defined metal and oxide surfaces: Unraveling the mysteries behind catalyst poisoning and desulfurization. *Acc. Chem. Res.* **1999,** *32*, 719–728.

(52) Azad, A.-M.; Duran, M. J., Development of ceria-supported sulfur tolerant nanocatalysts: Rh-based formulations. *Appl. Catal., A* **2007,** *330*, 77–88.

(53) Azad, A.-M.; Sundararajan, D., A phenomenological study on the synergistic role of precious metals in the steam reforming of logistic fuels on trimetal-supported catalysts. *Adv. Mater. Sci. Eng.* **2010**, 325683, 12 pp.

(54) Conner, W. C., Jr.; Falconer, J. L., Spillover in Heterogeneous Catalysis. *Chem. Rev. (Washington, DC)* **1995,** *95*, 759–88.

(55) Roessner, F., Spillover effects. In *Handbook of Heterogeneous Catalysis (2nd Edition)*, Wiley-VCH Verlag GmbH & Co. KGaA: 2008; Vol. 3, pp 1574–1585.

(56) Wise, H., Mechanisms of Catalyst Poisoning by Sulfur Species. In *Catalyst Deactivation Proceedings of the 5th International Symposium*, Bartholomew, C. H.; Butt, J. B., Eds. Elsevier Science Publishers: Amsterdam, 1991; Vol. 68, pp 497–503.

(57) Frety, R.; Da Silva, P. N.; Guenin, M., Iridium supported catalysts. variation of sulfur coverage with the nature of the carrier. *Catal. Lett.* **1989,** *3*, 9–16.

(58) Frety, R.; Da Silva, P. N.; Guenin, M., Supported iridium catalysts: Comparison between resistance to sulphur poisoning and hydrodesulphurization properties. *Appl. Catal.* **1990,** *57*, 99–103.

(59) Marécot, P.; Mahoungou, J. R.; Barbier, J., Benzene hydrogenation on platinum and iridium catalysts. Variation of the toxicity of sulfur with the nature of the support. *Appl. Catal., A* **1993,** *101*, 143–149.

(60) Hoyos, L. J.; Primet, M.; Praliaud, H., Sulfur poisoning and regeneration of palladium-based catalysts. 1. Dehydrogenation of cyclohexane on palladium/aluminum and palladium/silica-alumina catalysts. *J. Chem. Soc. Faraday T.* **1992,** *88*, 113–19.

(61) Stanislaus, A.; Cooper, B. H., Aromatic hydrogenation catalysis: a review. *Catal. Rev. - Sci. Eng.* **1994,** *36*, 75–123.

(62) Cooper, B. H.; Donnis, B. B. L., Aromatic saturation of distillates: an overview. *Appl. Catal., A* **1996,** *137*, 203–23.

(63) Sachtler, W. M. H.; Stakheev, A. Y., Electron-deficient palladium clusters and bifunctional sites in zeolites. *Catal. Today* **1992,** *12*, 283–295.

(64) Siegel, R. W.; Ramasamy, S.; Hahn, H.; Li, Z.; Lu, T.; Gronsky, R., Synthesis, characterization, and properties of nanophase titanium dioxide. *J. Mater. Res.* **1988,** *3*, 1367–72.

(65) Fegley, B., Jr.; White, P.; Bowen, H. K., Processing and characterization of zirconia and yttrium-doped zirconia powders. *Am. Ceram. Soc. Bull.* **1985,** *64*, 1115–20.

(66) Fayet, P.; Woeste, L., Experiments on size-selected metal cluster ions in a triple quadrupole arrangement. *Z. Phys. D. Atom. Mol. Cl.* **1986,** *3*, 177–82.

(67) Tang, Z. X.; Sorensen, C. M.; Klabunde, K. J.; Hadjipanayis, G. C., Preparation of manganese ferrite fine particles from aqueous solution. *J. Colloid Interface Sci.* **1991,** *146*, 38–52.

(68) Zhang, X.; Chan, K. Y., Water-in-oil microemulsion synthesis of platinum-ruthenium nanoparticles, their characterization and electrocatalytic properties. *Chem. Mater.* **2003,** *15*, 451–459.

(69) Boutonnet, M.; Kizling, J.; Stenius, P.; Maire, G., The preparation of monodisperse colloidal metal particles from microemulsions. *Colloids Surf.* **1982,** *5*, 209–25.

(70) Chen, D.-H.; Wu, S.-H., Synthesis of Nickel Nanoparticles in Water-in-Oil Microemulsions. *Chem. Mater.* **2000,** *12*, 1354–1360.

(71) Kortan, A. R.; Hull, R.; Opila, R. L.; Bawendi, M. G.; Steigerwald, M. L.; Carroll, P. J.; Brus, L. E., Nucleation and growth of cadmium selendie on zinc sulfide quantum crystallite seeds, and vice versa, in inverse micelle media. *J. Am. Chem. Soc.* **1990,** *112*, 1327–32.

(72) Pillai, V.; Kumar, P.; Multani, M. S.; Shah, D. O., Structure and magnetic properties of nanoparticles of barium ferrite synthesized using microemulsion processing. *Colloids Surf., A* **1993,** *80*, 69–75.

(73) Capek, I., Preparation of metal nanoparticles in water-in-oil (w/o) microemulsions. *Adv. Colloid Interface Sci.* **2004,** *110*, 49–74.

(74) Eriksson, S.; Nylén, U.; Rojas, S.; Boutonnet, M., Preparation of catalysts from microemulsions and their applications in heterogeneous catalysis. *Appl. Catal., A* **2004,** *265*, 207–219.

(75) Zhao, C.; Kou, Y.; Lemonidou, A. A.; Li, X. B.; Lercher, J. A., Highly Selective Catalytic Conversion of Phenolic Bio-Oil to Alkanes. *Angew. Chem. Int. Ed.* **2009,** *48*, 3987–3990.

(76) Simons, C.; Hanefeld, U.; Arends, I. W. C. E.; Sheldon, R. A.; Maschmeyer, T., Noncovalent Anchoring of Asymmetric Hydrogenation Catalysis on a New Mesoporous Aluminosilicate: Application and Solvent Effects. *Chem.--Eur. J.* **2004,** *10*, 5829–5835.

(77) Santos, L. G. R. A.; Oliveira, C. H. F.; Moraes, I. R.; Ticianelli, E. A., Oxygen reduction reaction in acid medium on Pt-Ni/C prepared by a microemulsion method. *J. Electroanal. Chem.* **2006,** *596*, 141–148.

(78) Siné, G.; Comninellis, C., Nafion®-assisted deposition of microemulsion-synthesized platinum nanoparticles on BDD: Activation by electrogenerated OH radicals. *Electrochim. Acta* **2005,** *50*, 2249–2254.

(79) PANalytical, PANalytical HighScore In Almelo, The Netherlands, 2010.

(80) Neves, I. C.; Botelho, G.; Machado, A. V.; Rebelo, P.; Ramoa, S.; Pereira, M. F. R.; Ramanathan, A.; Pescarmona, P., Feedstock recycling of polyethylene over AlTUD-1 mesoporous catalyst. *Polym. Degrad. Stab.* **2007,** *92*, 1513–1519.

(81) Okamoto, H., Pt-Ru (Platinum-Ruthenium). *J. Phase Equilib. Diffus.* **2008,** *29*, 471.

(82) Gasteiger, H. A.; Ross, P. N., Jr.; Cairns, E. J., LEIS and AES on sputtered and annealed polycrystalline Pt-Ru bulk alloys. *Surf. Sci.* **1993,** *293*, 67–80.

(83) Todi, R. M.; Warren, A. P.; Sundaram, K. B.; Barmak, K.; Coffey, K. R., Characterization of Pt-Ru binary alloy thin films for work function tuning. *IEEE Electron Device Lett.* **2006,** *27*, 542–545.

(84) Chu, D.; Gilman, S., Methanol electrooxidation on unsupported Pt-Ru alloys at different temperatures. *J. Electrochem. Soc.* **1996,** *143*, 1685–1690.

(85) Pan, C.; Dassenoy, F.; Casanove, M. J.; Philippot, K.; Amiens, C.; Lecante, P.; Mosset, A.; Chaudret, B., A new synthetic method toward bimetallic ruthenium platinum nanoparticles; composition induced structural changes. *J. Phys. Chem. B* **1999,** *103*, 10098–10101.

(86) Swanson, H. E.; Tatge, E., Standard x-ray diffraction powder patterns. *Natl. Bur. Stand. Circ. (U. S.)* **1953,** *539*, 95 pp.

(87) Swanson, H. E.; Gilfrich, N. T.; Ugrinic, G. M., Standard X-ray diffraction powder patterns. *Natl. Bur. Stand. Circ. (U. S.)* **1955,** *5*, 75 pp.

(88) Hamel, C.; Garbarino, S.; Irissou, E.; Bichat, M.-P.; Guay, D., Structural and Electrochemical Properties of Nanocrystalline PtRu Alloys Prepared by Crossed-Beam Pulsed Laser Deposition. *J. Phys. Chem. C* **2010,** *114*, 18931–18939.

(89) Antolini, E.; Cardellini, F., Formation of carbon supported PtRu alloys: an XRD analysis. *J. Alloys Compd.* **2001,** *315*, 118–122.

(90) Menegazzo, F.; Canton, P.; Pinna, F.; Pernicone, N., Bimetallic Pd-Au catalysts for benzaldehyde hydrogenation: Effects of preparation and of sulfur poisoning. *Catal. Commun. (Cambridge, U.K.)* **2008,** *9*, 2353–2356.

Chapter 3: Structure-Functionality Relationships of Catalytic Bimetallic Pt-Ru Nanoparticles Associated with Improved Sulfur Resistance

This chapter was published in *RSC Advances*.

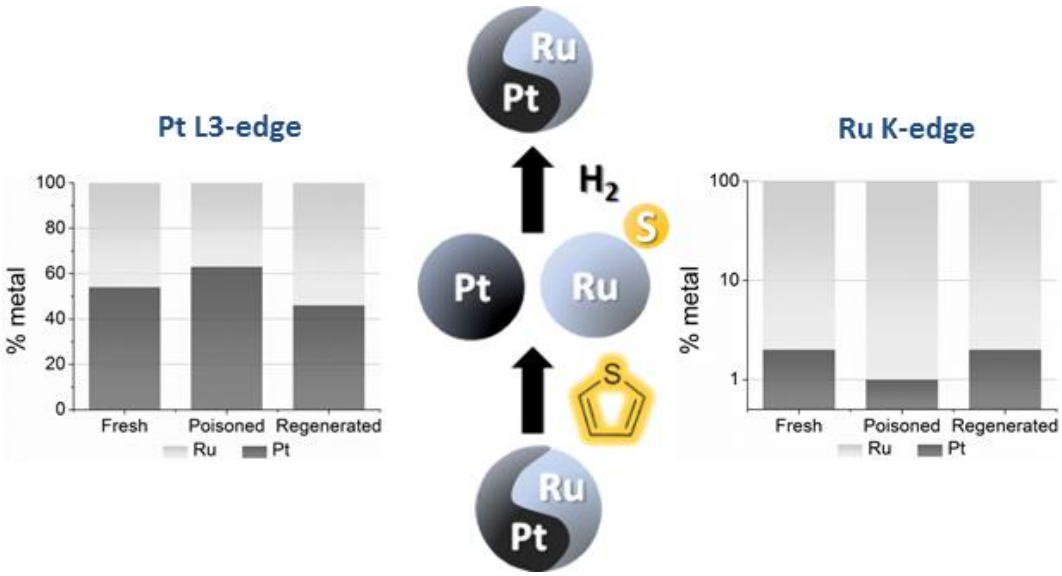

Stanley, J.N.G.; Benndorf, P.; Heinroth, F.; Masters, A.F.; Maschmeyer, T., *RSC Adv.* **2014,** *4*, 28062–28071.

3.1 Introduction

Biomass is one of the most promising renewable sources for liquid fuels and chemicals.[1–5,iv] Due to the differences in oxygen and moisture contents, thermal stabilities, and functionality between biomass and petroleum feedstocks, new chemical approaches are required for biomass processing, and catalysts are involved in many of the processes.[6, 7] A promising technology for biomass conversion is aqueous phase reforming (APR).[8] APR uses supported metal catalysts at relatively low temperatures and pressures for the conversion of biomass-derived feedstocks to hydrogen,[9–15] gaseous alkanes,[13, 16, 17] and liquid alkanes,[18–23] and the products can be tailored by altering the catalyst and H_2/CO concentrations in the reactor. However, it is expected that the performance of the catalysts will be impaired by the sulfur present in real biomass feedstocks (*e.g.*, already for wood it is approx. 56 ppm, significant protein content worsens this situation further, the sulfur substantially deriving from the amino acids cysteine and methionine and the uptake of soil nutrients),[24] as sulfur is well-known to poison noble metal catalysts.[25, 26] Thus, there is a great need to develop sulfur-resistant catalysts for biomass conversions.

We envisage the operation of a combined sulfur and hydrogen spillover mechanism on supported bimetallic catalysts to overcome these issues. Bimetallic catalysts are used in industrial applications as they often show improved activity, selectivity, and sulfur resistance compared to their monometallic counterparts.[11, 27–30] This improved performance could result from metal-metal bonding or changes to the number of available active sites on the surface of the catalyst leading to electronic perturbations, or edge-sites, kinks, or defects resulting in structural changes.[30] The concept of a sulfur 'spillover' was proposed by Azad and Duran for Pd-Re catalysts that have applications in the steam reforming of sulfur-laden logistic fuels (diesel, gasoline, jet fuel).[31, 32] They suggested that the catalyst

[iv] References for Chapter 3 begin on page 84.

could remain active for longer as palladium is able to transfer sulfur onto the more readily sulfidable rhenium. Although we acknowledge that 'sulfur spillover' is only loosely connected to the extensively studied conventional hydrogen spillover mechanism,[33, 34] given the literature precedent, we adopt the same terminology sulfur as well.

To facilitate these two spillover mechanisms on the same catalyst, we chose platinum for its hydrogenation ability and ruthenium, as it has a greater affinity for sulfur than does platinum.[35] Thus, any sulfur species that binds to platinum could spillover to ruthenium. Similarly, hydrogen could spillover from platinum to the sulfur species bound to ruthenium, and cleave a sulphur-containing derivative, effectively regenerating the catalyst. Note that these spillover mechanisms are most likely to occur if the platinum and ruthenium are separated only by atomic dimensions, *e.g.*, if they exist in the same lattice, perhaps as an alloy or a solid solution. A schematic of the proposed *in-situ* self regeneration pathway is shown in Figure 3.1.

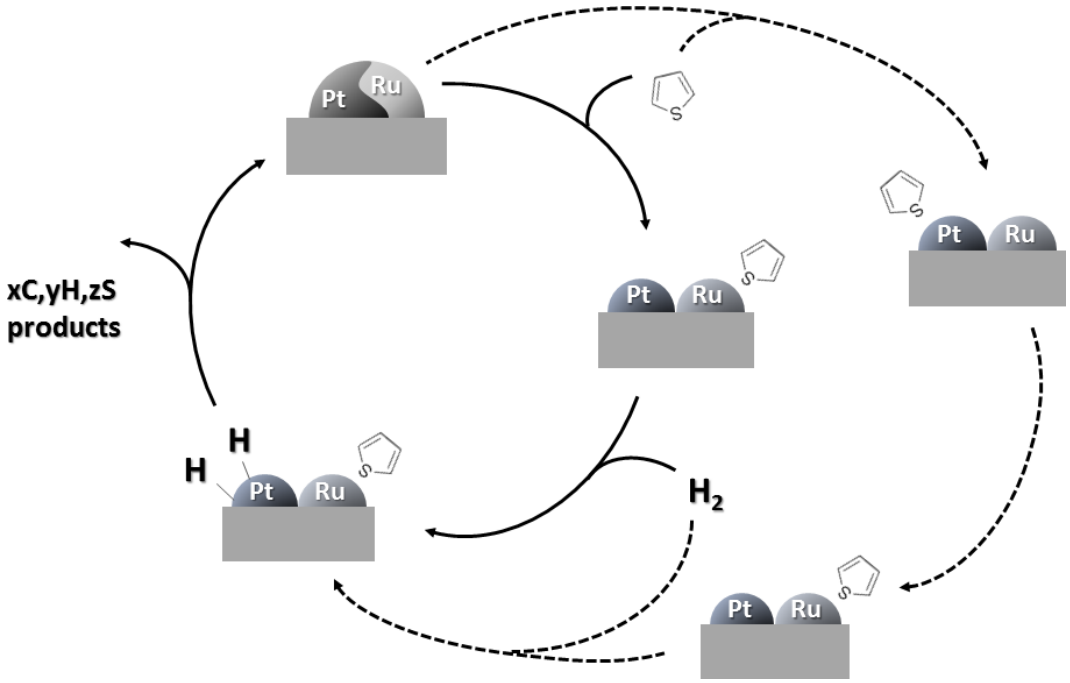

Figure 3.1 Schematic of the proposed *in-situ* self regeneration mechanism, showing thiophene as sulfur poisoning model compound.

Indeed, we have designed bimetallic Pt-Ru catalysts, supported on mesoporous SiAlTUD-1, that exhibit improved sulfur resistance and promising potential for the APR of model compounds, using the hydrogenation of cyclohexene to cyclohexane as a screening reaction.[36] These bimetallic catalysts achieve turnover frequencies higher than their monometallic counterparts in both the absence and presence of sulfur-containing species (as thiophene). What is more remarkable is that while the monometallic catalysts are completely poisoned, the bimetallic catalysts remain active even in the presence of sulfur concentrations that are ten times that expected in woody biomass feedstocks – a concentration that is equivalent to a sulfur:metal molar ratio of 17:1 for the bimetallic catalyst with the *highest* metal loading, $Pt_1Ru_{1.5}$ (of course, not all metal atoms are exposed, so the ratio of sulfur to active metal species is much higher). Thus, these catalytic

results are completely consistent with the operation of the proposed sulfur and hydrogen spillover mechanism on the bimetallic catalysts.

X-ray diffraction (XRD) characterisation of the bimetallic catalysts suggests that platinum and ruthenium atoms are incorporated in the same lattice, which is required for the operation of the regeneration mechanism. Further XRD studies of the used $Pt_1Ru_{1.5}$ catalyst suggest changes to the Pt unit cell size after poisoning, indicated by the shifting of the Pt reflections and changes to the Pt lattice constant. These changes are consistent with the catalyst losing some of its defined alloy character, partially separating into two amorphous and maybe somewhat elementally distinct domains. Thus, the XRD analyses suggest that the observed restructuring of the metal nanoparticles results from increasing amounts of sulfur-containing species being co-ordinated to the ruthenium atoms during poisoning, leading to change in alloy structure. Regeneration of the catalyst in pure hydrogen at 300 °C shows this to be a reversible process.

Although the catalytic results and the XRD analysis are consistent with the proposed regeneration pathway, extended X-ray absorption fine structure (EXAFS) was needed to probe the alloyed character of the bimetallic catalysts at the atomic level (in terms of nearest neighbour environments), and to provide further insights into the regeneration mechanism. Moreover, EXAFS was required to afford structural information on the bimetallic catalysts for which the peak shifts in the XRD was slight or not apparent, and to examine the possible contribution(s) of amorphous phases. The fingerprint of the X-ray absorption near edge structure (XANES) spectra is also useful in qualitatively determining the metallic character of the catalysts.

Herein, we report the XANES and EXAFS results of experiments confirming the alloyed character of $Pt_{1.5}Ru_1$, $Pt_1Ru_{1.5}$, and Pt_1Ru_3 bimetallic catalysts, and the EXAFS

results of experiments probing the sulfur poisoning and regeneration mechanism of $Pt_{1.5}Ru_1$ and Pt_1Ru_3 catalysts.

3.2 Results and Discussion

The synthesis, general characterisation, and catalytic activity of Pt, Ru, Pt/Ru, Pt_1Ru_3, $Pt_1Ru_{1.5}$, and $Pt_{1.5}Ru_1$ mono- and bimetallic catalysts have been described previously.[36]

3.2.1 XANES

The XANES spectra of the unused catalysts at the Pt L_{III}-edge and Ru K-edge are shown in Figure 3.2. The spectra of the reference materials (Pt foil, Ru foil, PtO_2, and RuO_2) are included for comparison with those of the catalysts. At the Pt L_{III}-edge (Figure 3.2a), the absorption positions of the catalysts were similar to the Pt foil, suggesting a highly metallic character. On the other hand, at the Ru K-edge (Figure 3.2b), some oxidation was suggested for the $Pt_1Ru_{1.5}$ catalyst, as shown by the flat top between the two characteristic absorptions of metallic ruthenium. The oxidation of ruthenium is not surprising, as ruthenium is oxophillic,[37] and no precautions to exclude air were taken when handling the catalysts. However, this contrasts with the Ru XANES spectra of other catalysts, which are similar to that of the Ru foil, suggesting that they have predominantly metallic character. The higher metal loading of the $Pt_1Ru_{1.5}$ catalyst compared to the other two bimetallic catalysts could account for why oxidation was only readily observed for this catalyst.[36]

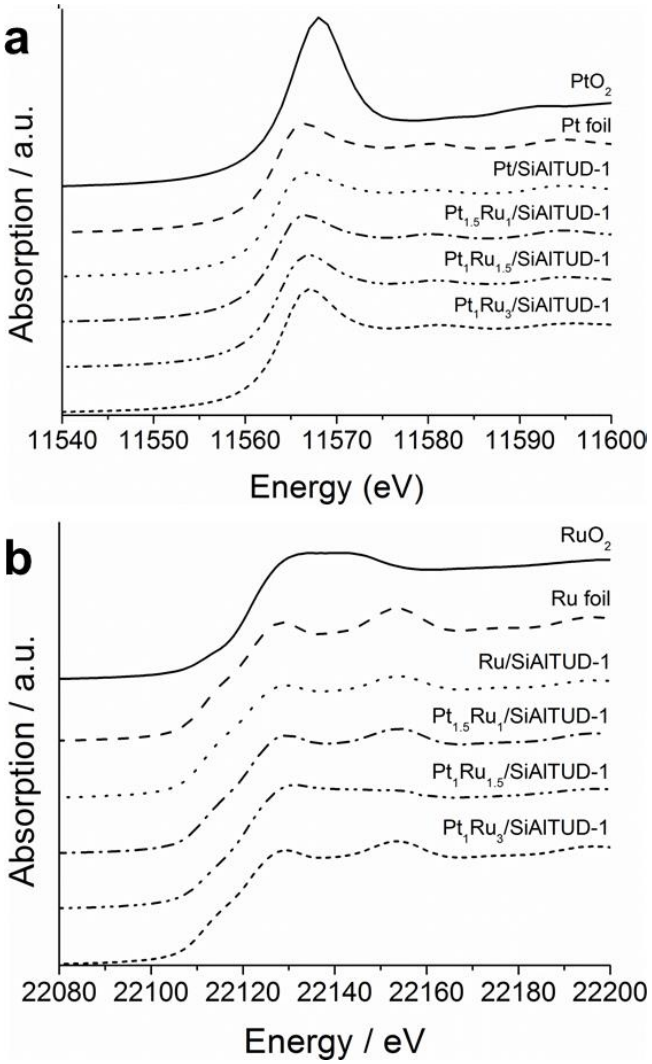

Figure 3.2 XANES spectra at the a) Pt L_{III}-edge and b) Ru K-edge for the unused catalysts compared with the reference samples.

3.2.2 EXAFS

3.2.2.1 Reference Foils and Monometallic Catalysts

To test the reliability of the EXAFS analysis procedure, the Pt and Ru foils (fits shown in Figure 3.3 and Figure 3.4, best-fit parameters reported in Table 3.1 and Table 3.2, for the Pt L_{III}-edge and Ru K-edge, respectively) were analysed first. The co-ordination numbers for the foils were fixed as determined by their respective crystal structures, *i.e.* fcc for

platinum and hcp for ruthenium. All other parameters, including co-ordination numbers, bond distances and Debye–Waller factors were free to vary. Using single scattering, only the first shell could be fitted due to strong back scattering at the higher shells. Thus, multiple scattering was used to analyse all samples. In fitting the monometallic Pt and Ru catalysts (best-fit parameters reported in Table 3.1 and Table 3.2, respectively), for the Ru catalyst it was necessary to restrain the co-ordination number for the fifth Ru shell to less than 12 to obtain a value that is physically meaningful, due to too strong a correlation between the Debye–Waller factor and the co-ordination number. In addition, it was necessary to fix the Debye–Waller factor in the second Ru shell to the value obtained for the first Ru shell Debye–Waller factor for the Ru catalyst.

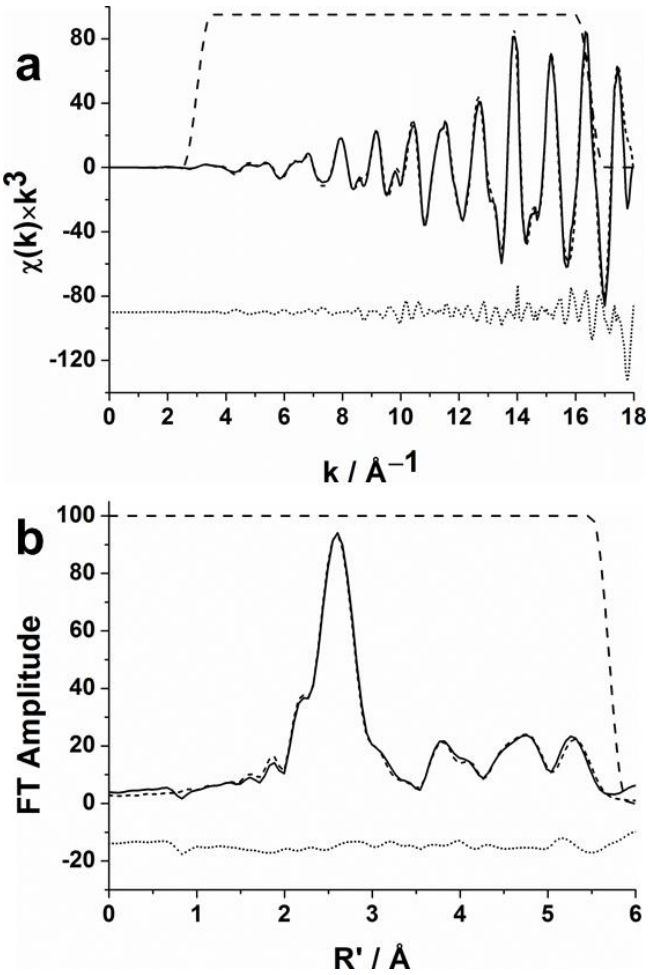

Figure 3.3 a) Raw $\chi(k)\times k^3$ EXAFS data and b) Fourier transformed EXAFS data from Pt foil measured at the Pt L_{III}-edge. Observed (solid line), calculated (short dashed line), residual (dotted line), and window (long dashed line).

Table 3.1 Best-fit parameters obtained by fitting EXAFS data measured from the Pt foil and monometallic Pt catalyst at the Pt L_{III}-edge, where *f* = fixed value.

Pt L_{III}-edge							
Pt foil				Monometallic Pt catalyst			
	R / Å	*N*	σ^2 / Å^2		*R* / Å	*N*	σ^2 / Å^2
Pt-Pt	2.76	12_f	0.001	Pt-Pt	2.76	8.9	0.003
Pt-Pt	3.91	6_f	0.002	Pt-Pt	3.91	4.4	0.004
Pt-Pt	4.80	24_f	0.002	Pt-Pt	4.80	15.9	0.004
Pt-Pt	5.53	12_f	0.003	Pt-Pt	5.53	8.9	0.006
R-factor = 5.81%		Chi^2 = 0.57		*R*-factor = 8.22%		Chi^2 = 0.53	

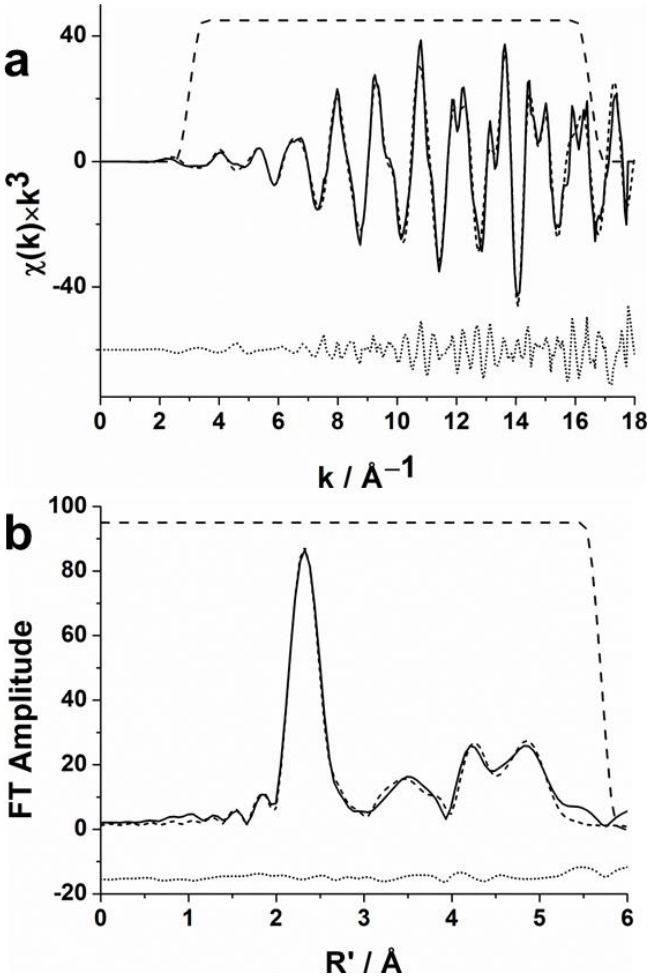

Figure 3.4 a) Raw $\chi(k)\times k^3$ EXAFS data and b) Fourier transformed EXAFS data from Ru foil measured at the Ru K-edge. Observed (solid line), calculated (short dashed line), residual (dotted line), and window (long dashed line).

Table 3.2 Best-fit parameters obtained by fitting EXAFS data measured from the Ru foil and monometallic Ru catalyst at the Ru K-edge, where *f* = fixed value.

Ru K-edge							
Ru foil				Monometallic Ru catalyst			
	R / Å	*N*	σ^2 /Å^2		*R* / Å	*N*	σ^2 / Å^2
Ru-Ru	2.67	12_f	0.002	Ru-Ru	2.67	8.3	0.002
Ru-Ru	3.79	6_f	0.002	Ru-Ru	3.79	4.4	0.002_f
Ru-Ru	4.25	2_f	0.001	Ru-Ru	4.26	0.5	0.0009
Ru-Ru	4.67	18_f	0.003	Ru-Ru	4.67	6.1	0.0004
Ru-Ru	5.08	12_f	0.001	Ru-Ru	5.08	12.5[a]	0.003
Ru-Ru	5.33	16_f	0.003	Ru-Ru	5.33	6.6	0.0008
R-factor = 11.0%		Chi^2 = 2.15		*R*-factor = 10.3%		Chi^2 = 1.41	

[a] Restrained where $N5 < 12$

Good fits were obtained for the Pt and Ru foils, as shown in Figure 3.3 and Figure 3.4, and as suggested by the low *R*-factors and chi^2 values reported for the best-fit parameters in Table 3.1 and Table 3.2, at the Pt L_{III}-edge and Ru K-edge, respectively. The refined bond distances were all consistent with the corresponding crystal structures.[38] It is worth noting that six shells were required to obtain a good fit for the Ru foil, as a model

using five shells previously reported in the literature for the same range was inadequate in fitting the present data.[37]

Similarly, good fits were obtained for the Pt and Ru monometallic catalysts (best-fit parameters reported in Table 3.1 and Table 3.2, respectively). For the Ru catalyst, it was necessary to fix the Debye–Waller factor in the second shell to 0.002 σ^2, which was the value obtained for the Debye–Waller factor in the first Ru shell, as a physically meaningful value could not be obtained when this parameter was free to vary. Fixing this parameter resulted in only a slight increase of the *R*-factor, from 8.69% to 10.3%, and the chi^2 value decreased, from 2.10 to 1.41. Thus, as the *R*-factor did not significantly change, the chi^2 value was low, and all the other parameters were sensible, the discrepancy of one Debye–Waller factor can be considered to be within the limitations of the model. The Pt L_{III}- and Ru K-edge models determined for these references samples were subsequently used as the basis for the models of the three bimetallic catalysts.

3.2.2.2 Particle Size Determined from EXAFS Results

In fitting the data from the Pt and Ru catalysts, the co-ordination numbers were found to be smaller than those of their respective foils, which could be due to the small particle size of the nanoparticles or due to a change in the particle morphology.[39-42] When calculating the particle sizes from the EXAFS data, substituting the first shell co-ordination numbers (CN) in the formula $\log_{10}(1000/d) = 2.5763 - 0.1319 \times (CN)$ and assuming hemispherical nanoparticles,[43, 44] the particle sizes were 4.0 nm for the Pt catalyst and 3.3 nm for the Ru catalyst. These particle sizes are smaller than the particle sizes of ~12–15 nm obtained by the XRD and TEM analyses for the supported nanoparticles that were reported previously.[36] Note that similarly to the monometallic Pt and Ru catalysts reported in the

present case, the weighted first shell co-ordination numbers for the three bimetallic catalysts (best-fit parameters discussed in the next section) suggested small particle sizes (< 10 nm).

The discrepancies between the small nanoparticle sizes calculated from the first shell co-ordination numbers obtained by EXAFS and the previous characterisation could arise as the values obtained from EXAFS represent an average of all the metal atoms present in the catalyst, *i.e.*, crystalline and non-crystalline domains, whereas the XRD results include only crystalline domains. Furthermore, at these very small sizes the Scherrer equation is edging towards its limits of applicability and as only the relatively larger nanoparticles are detected by XRD this biases the calculation of the particle sizes. Similarly, the three dimensional pore structure of the SiAlTUD-1 support also makes it very difficult to distinguish the smaller nanoparticles by TEM inspection.

3.2.2.3 Alloyed Character of Bimetallic Catalysts

To evaluate the alloy character of the catalysts, EXAFS data sets were collected at both the Pt L_{III}-edge and the Ru K-edge for fresh samples of each bimetallic catalyst: Pt_1Ru_3, $Pt_1Ru_{1.5}$, and $Pt_{1.5}Ru_1$. The data from each catalyst was initially fitted with the the best-fit parameters obtained for the foil at the edge at which the data were collected. For example, the data for the Pt_1Ru_3 catalyst measured at the Pt L_{III}-edge was fitted with the model for the Pt foil, then one Pt-Ru shell was added (*i.e.*, a Ru scatterer with a Pt-Ru bond length of 2.70 Å was added to the first co-ordination shell), which resulted in an improvement in the quality of the fit. All parameters were free to vary. Subsequent heteroatom scatterers were added to the second co-ordination shell, third co-ordination shell, *etc*., until the addition of further heteroatom shells did not result in an improvement in the quality of the fit. The fits

for all the bimetallic catalysts improved with the addition of one or more heteroatom shells at both the Pt L_{III}-edge and the Ru K-edge, which is consistent with alloy formation. The best-fit parameters are reported for the Pt L_{III}-edge and Ru K-edge in Table 3.3 and Table 3.4 respectively. Although there are a few occurances where the Debye–Waller factors are smaller than normal, as the *R*-factors and chi^2 values are low, and all the other parameters are sensible, these discrepancies can be considered to be within the limitations of the model.

The best fit for the $Pt_{1.5}Ru_1$ catalyst required the addition of one Pt-Ru shell at the Pt L_{III}-edge and one Ru-Pt shell at the Ru K-edge (Table 3.3 and Table 3.4, respectively). The first shell bond distance for the Pt-Ru and Ru-Pt shells were 2.72 Å at both edges, which is intermediate between the values for the bond distances of Pt-Pt (2.76 Å) and Ru-Ru (2.68 Å). The value for the heteroatom bond distance suggests the contracting of the Pt host lattice by the smaller Ru atoms, which provides further evidence for alloy formation.

The best fit for the Pt_1Ru_3 catalyst required four Pt-Ru shells at the Pt L_{III}-edge and one Ru-Pt shell at the Ru K-edge (Table 3.3 and Table 3.4, respectively). The first shell bond distance for the Pt-Ru and Ru-Pt shells in this case was 2.70 Å at both edges, suggesting the expansion of the Ru host lattice by the larger Pt atoms. At the Pt L_{III}-edge, the bond distances obtained for the second to fourth Pt-Ru shells also suggested an expansion of the Ru host lattice. The bond distances obtained for all Pt-Ru shells were consistent with those reported by Nashner *et al.* for simultaneously fitted Pt L_{III}-edge and Ru K-edge EXAFS data obtained for carbon-supported $[PtRu_5]$/C nanoparticles.[45]

In the case of the $Pt_1Ru_{1.5}$ catalyst, the inclusion of an Ru-O shell (with a Ru-O bond distance of 2.0 Å) in addition to an Ru-Pt shell was required at the Ru K-edge (Table 3.4), consistent with the oxidation suggested in the XANES spectrum for this

catalyst (Figure 3.2b). At the Pt L_{III}-edge, one Pt-Ru shell was needed. The Pt-Ru and Ru Pt bond distances were 2.70 Å, which is smaller than the Pt-Ru and Ru-Pt bond distances obtained for the $Pt_{1.5}Ru_1$ catalyst, and is consistent with the incorporation of more Ru atoms into the Pt host lattice of $Pt_1Ru_{1.5}$ compared with the $Pt_{1.5}Ru_1$ catalyst.

Table 3.3 Best-fit parameters obtained by fitting EXAFS data measured from fresh samples of the Pt_1Ru_3, $Pt_1Ru_{1.5}$, and $Pt_{1.5}Ru_1$ catalysts at the Pt L_{III}-edge.

Pt L_{III}-edge										
$Pt_{1.5}Ru_1$				$Pt_1Ru_{1.5}$				Pt_1Ru_3		
	R / Å	*N*	σ^2 / Å^2		*R* / Å	*N*	σ^2 / Å^2		*R* / Å	*N*	σ^2 / Å^2
Pt-Pt	2.76	9.9	0.0008	Pt-Pt	2.76	5.9	0.001	Pt-Pt	2.75	3.1	0.001
Pt-Pt	3.91	4.9	0.001	Pt-Pt	3.91	2.5	0.001	Pt-Pt	3.90	1.7	0.003
Pt-Pt	4.80	16.6	0.001	Pt-Pt	4.79	7.8	0.002	Pt-Pt	4.78	3.0	0.0009
Pt-Pt	5.53	9.9	0.003	Pt-Pt	5.53	5.9	0.004	Pt-Pt	5.53	0.4	0.001
Pt-Ru	2.72	1.2	0.009	Pt-Ru	2.70	0.3	0.001	Pt-Ru	2.70	2.2	0.002
								Pt-Ru	3.79	0.3	0.0009
								Pt-Ru	4.70	3.9	0.007
								Pt-Ru	5.41	2.2	0.005
R-factor = 4.96%		Chi^2 = 1.45		*R*-factor = 5.78%		Chi^2 = 0.50		*R*-factor = 9.67%		Chi^2 = 2.41	

Table 3.4 Best-fit parameters obtained by fitting EXAFS data measured from fresh samples of the Pt_1Ru_3, $Pt_1Ru_{1.5}$, and $Pt_{1.5}Ru_1$ catalysts at the Ru K-edge.

Ru K-edge											
$Pt_{1.5}Ru_1$				$Pt_1Ru_{1.5}$				Pt_1Ru_3			
	R / Å	*N*	σ^2 / Å^2		*R* / Å	*N*	σ^2 / Å^2		*R* /Å	*N*	σ^2 / Å^2
Ru-Ru	2.68	7.8	0.003	Ru-Ru	2.68	2.7	0.002	Ru-Ru	2.67	8.5	0.003
Ru-Ru	3.79	2.4	0.0008	Ru-Ru	3.78	1.3	0.0003	Ru-Ru	3.79	2.8	0.0007
Ru-Ru	4.26	0.2	0.001	Ru-Ru	4.23	1.9	0.005	Ru-Ru	4.29	3.1	0.001
Ru-Ru	4.68	7.0	0.002	Ru-Ru	4.68	3.4	0.003	Ru-Ru	4.67	6.2	0.0009
Ru-Ru	5.05	4.1	0.0008	Ru-Ru	5.07	5.5	0.002	Ru-Ru	5.08	12.2	0.004
Ru-Ru	5.34	4.2	0.0006	Ru-Ru	5.34	2.6	0.01	Ru-Ru	5.34	9.4	0.002
Ru-Pt	2.72	2.3	0.005	Ru-Pt	2.70	3.4	0.006	Ru-Pt	2.70	0.2	0.001
				Ru-O	2.00	0.7	0.001				
R-factor = 5.84%		Chi^2 = 0.64		*R*-factor = 16.6%		Chi^2 = 1.41		*R*-factor = 6.17 %		Chi^2 = 1.74	

3.2.2.4 Dealloying During Sulfur Poisoning

Previously published XRD data for the $Pt_1Ru_{1.5}$ catalyst suggested that dealloying/re-alloying was occuring during sulfur poisoning.[36] This dealloying, which could occur if the sulfur species becomes preferentially co-ordinated to the ruthenium and the ruthenium separates out of the platinum lattice, is consistent with the occurance of a sulfur spillover mechansim. Likewise, the re-alloying after heat treatment with hydrogen is consistent with a hydrogen spillover mechanism to remove the sulfur. For these spillovers to occur *in-situ*,

platinum and ruthenium are required to be present in close proximity, *e.g.*, in the same lattice. As discussed in the treatment of the EXAFS results above, the improvement of the fit with the addition of the metal heteroatoms, and the agreement of the first shell Pt-Ru and Ru-Pt bond distances at both the Pt L_{III}-edge and Ru K-edge, suggested that this is indeed the case.

The EXAFS investigation into the sulfur poisoning and regeneration mechanism was continued for the $Pt_{1.5}Ru_1$ and Pt_1Ru_3 catalysts. As there are relatively fewer Ru atoms in $Pt_{1.5}Ru_1$ compared to $Pt_1Ru_{1.5}$, the shifting in lattice parameters observed by XRD is only slight, while in the case of the Pt_1Ru_3 catalyst, no shifting of peak positions in the XRD pattern is observed, likely because of the noisy data. For these two catalysts, EXAFS experiments were performed on fresh, poisoned and regenerated catalyst samples. 'Fresh' refers to unused catalyst. 'Poisoned' refers to the catalyst that was used in the model hydrogenation reaction in the presence of 450 ppm of sulfur and then dried at room temperature in air. 'Regenerated' refers to the catalyst that was used in the presence of 450 ppm of sulfur, dried at room temperature in air, and heated for 2 h under hydrogen at 400 °C.

The raw and Fourier transformed EXAFS data for Pt_1Ru_3 at the Pt L_{III}-edge are shown in Figure 3.5. Qualitative analysis of the Fourier transformed data suggested differences between the poisoned sample and the fresh and regenerated samples. The dominant peak at ~2.5 Å in the Fourier transform results from contributions of both Pt and Ru scatterers. In the poisoned sample, the shoulder to the right of the peak disappeared, but was present in the regenerated sample. Thus, changes to the sample during poisoning appear to take place and can be followed with atomic resolution (in terms of nearest neighbour), and these changes are reversed (in terms of what can be glean via EXAFS analysis and catalytic performance data) after the regeneration of the catalyst.

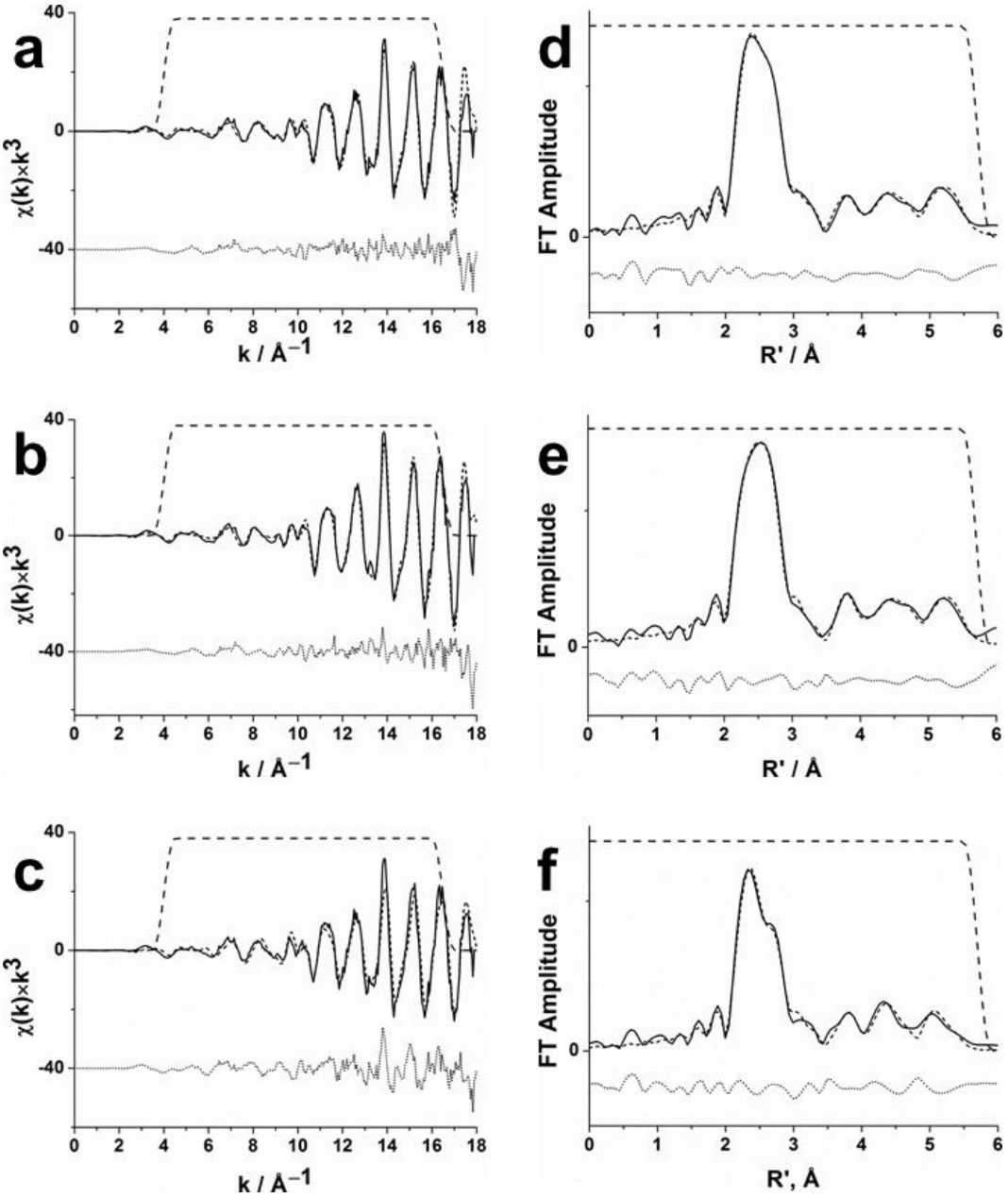

Figure 3.5 Raw $\chi(k)\times k^3$ EXAFS data for the a) fresh, b) poisoned, and c) regenerated sample and Fourier transformed EXAFS data for the d) fresh, e) poisoned, and f) regenerated sample of the Pt_1Ru_3 catalyst measured at the Pt L_{III}-edge. Observed (solid line), calculated (short dashed line), residual (dotted line), and window (long dashed line).

Quantitative analysis of the EXAFS data for both the Pt_1Ru_3 and $Pt_{1.5}Ru_1$ catalysts provided further insights into structural changes to the Pt and Ru bonding environments induced by sulfur poisoning and re-activation, and provided evidence at the atomic level that a dealloying/re-alloying mechanism was occurring. The poisoned and regenerated samples were fitted starting with the parameters obtained for the fresh Pt_1Ru_3 and $Pt_{1.5}Ru_1$ catalysts, reported in Table 3.3 and Table 3.4 (above). As the focus of the analysis was on changes to the co-ordination numbers between the different samples (*i.e.* fresh, poisoned, and regenerated samples) for each catalyst, the Debye–Waller factors and passive electron amplitude reduction factor (S_0^2) were fixed to the values obtained for the fresh samples, as the co-ordination numbers were found to be highly correlated with these parameters. All other parameters were free to vary. Tables with the complete best-fit parameter sets for both catalysts can be found in Appendix B. Note that as EXAFS shows the average of all the metal atoms, contributions from atoms not involved in the alloying are not discriminated against. This means that the overall effect is less pronounced compared to the clear changes in the Pt unit cell that could be observed for $Pt_1Ru_{1.5}$ by XRD.[36] Thus, while the overall effect is evident in EXAFS, it is diluted compared to the effect visible in XRD, since the XRD effectively filters out all amorphous particles.

The analyses of the results for the Pt_1Ru_3 and $Pt_{1.5}Ru_1$ catalysts are shown in Figure 3.6 and Figure 3.7, respectively. The graphs depict the relative percentage of Pt and Ru metal in the first shell for fresh, poisoned, and regenerated samples, at both the Pt L_{III}-edge (Figure 3.6a and Figure 3.7a) and Ru K-edge (Figure 3.6b and Figure 3.7b). The first shell co-ordination numbers only were used in the calculation as a single metal heteroatom shell was modelled in all but one case.

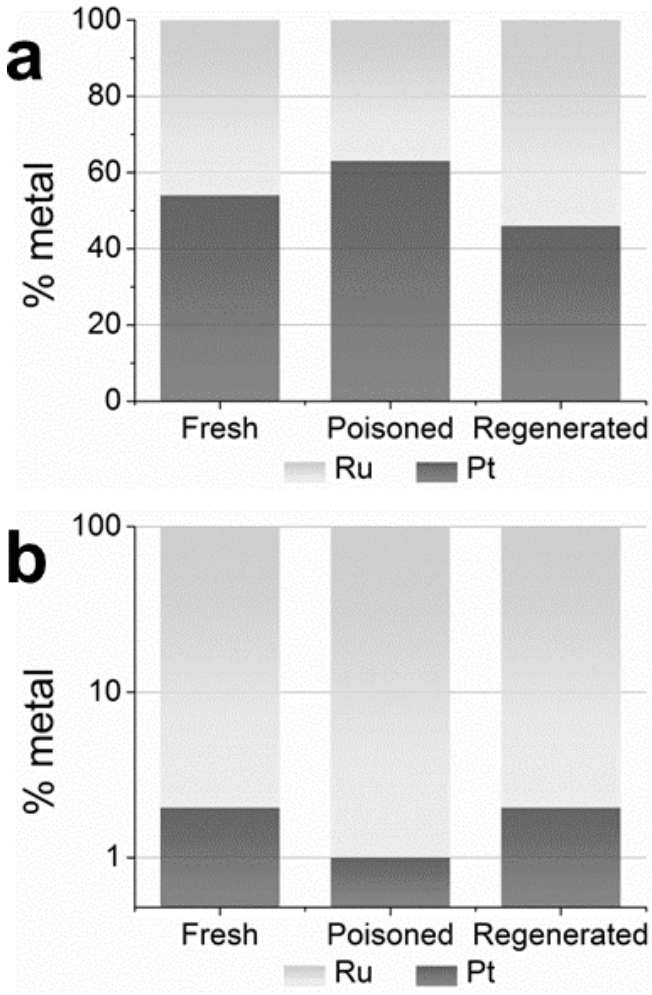

Figure 3.6 Relative percentages of Pt and Ru metal in the first shell of fresh, poisoned, and regenerated samples of the Pt_1Ru_3 catalyst, calculated for the a) Pt L_{III}-edge and b) Ru K-edge.

Examining the graph for the Pt_1Ru_3 catalyst at the Pt L_{III}-edge (Figure 3.6a), it is clear that the relative percentage of platinum increased after sulfur poisoning, while the relative percentage of ruthenium decreased. That is, after sulfur poisoning there were relatively more Pt-Pt bonding environments and relatively fewer Pt-Ru bonding environments. Conversely, at the Ru K-edge (Figure 3.6b), after sulfur poisoning there were relatively more Ru-Ru bonding environments and relatively fewer Ru-Pt bonding

environments. These results are consistent with the catalyst dealloying during poisoning, which could be due to the ruthenium being complexed to sulfur residues and the platinum separating out of the lattice. This situation was reversed when the catalyst was regenerated, which is consistent with the sulfur no longer being complexed to the ruthenium, and the platinum being reincorporated into the ruthenium host lattice.

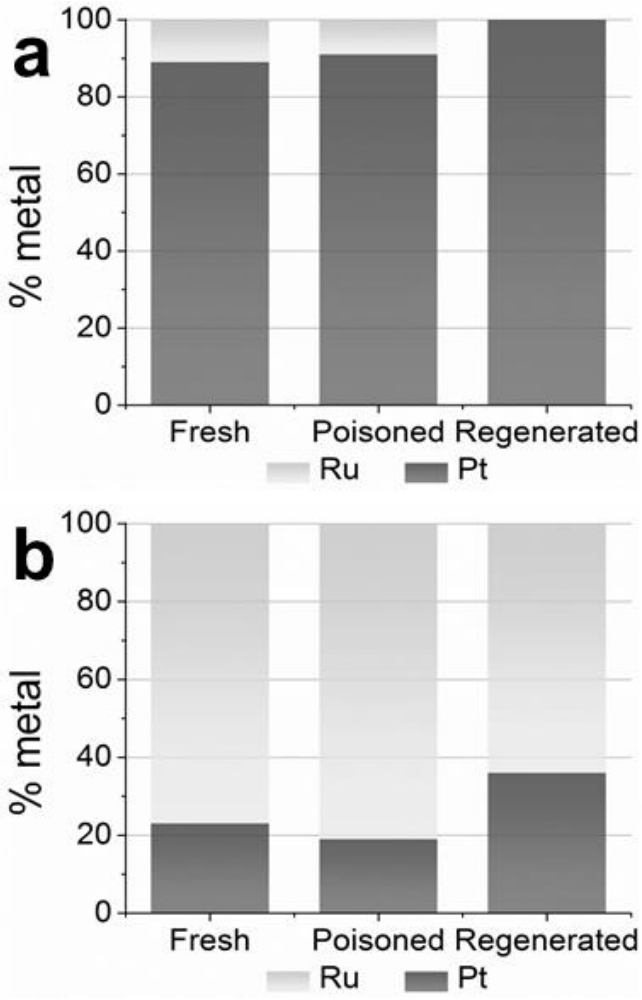

Figure 3.7 Relative percentages of Pt and Ru metal in the first shell of fresh, poisoned, and regenerated samples of the $Pt_{1.5}Ru_1$ catalyst, calculated for the a) Pt L_{III}-edge and b) Ru K-edge.

Although the effect is only subtle (see above), similar trends were seen in the poisoned samples for the $Pt_{1.5}Ru_1$ catalyst (Figure 3.7), suggesting that this catalyst was also partially dealloying during sulfur poisoning. At the Pt L_{III}-edge (Figure 3.7a), there were slightly more Pt-Pt bonding environments compared to Pt-Ru environments after sulfur poisoning, while the opposite was true at the Ru K-edge (Figure 3.7b). However, although it is clear at the Ru K-edge that the catalyst had re-alloyed after regeneration, this was not evident at the Pt L_{III}-edge. Indeed, the XRD data for the regenerated sample suggested the existence of an extra platinum phase. As platinum is a much stronger scatterer than ruthenium, this additional platinum phase could make it difficult to see the Pt-Ru bonding environments using EXAFS analysis, which appears to be the case with this sample.

While it was previously suggested that a correlation could exist between the presence of the alloy character after poisoning and the activity of the catalysts,[36] a similar trend could not be determined in the present case. Nonetheless, these results suggested that the sulfur resistance could be improved if, during poisoning, a catalyst was more readily able to retain its alloy character, which could be achieved through the more efficient operation of the spillover mechanism. If there is more ruthenium available to act as a sulfur trap, sulfur-resistance could be improved, but if the ruthenium ratio is too high compared with platinum, the spillover mechanism could be hindered.

3.3 Conclusion

We are able to confirm the alloyed character of three bimetallic catalysts that show improved sulfur tolerance in the presence of thiophene for a model APR reaction. Analyses of the first shell EXAFS best-fit parameters of the Pt_1Ru_3 and $Pt_{1.5}Ru_1$ catalysts

clearly shows that the metal partially dealloyed during poisoning, which we suggest is due to the ruthenium being sequestered by the sulfur species. However, after regenerating the poisoned catalysts under hydrogen, the sulfur is removed and the alloy is reformed. Evidence that this re-alloying could occur is suggested by the EXAFS analyses of the regenerated catalysts. Thus, these results provide evidence that the *in-situ* self regeneration mechanism, proposed earlier,[36] occurs indeed, *i.e.* during poisoning the metal partially dealloys, but a sulfur spillover and a hydrogen spillover take place to regenerate the catalyst *in-situ*, and the platinum and ruthenium are then re-alloyed, enabling the catalyst to remain active, and, significantly, sulfur-tolerant.

3.4 Experimental Section

3.4.1 Catalyst Preparation

The syntheses, general characterisation by ICP-AES, XRD, TEM, and nitrogen sorption measurements, and catalytic activity of the Pt, Ru, $Pt_{1.5}Ru_1$, $Pt_1Ru_{1.5}$, and Pt_1Ru_3 mono- and bimetallic catalysts have been described elsewhere.[36] The XAS studies described below were measured using the same samples to facilitate the continued investigation into the sulfur poisoning mechanism. In addition, a Pt foil, Ru foil (both EXAFS Materials), PtO sample (Johnson Matthey), and RuO_2 sample (Aldrich), were used as reference materials to inform and aid the modelling of the catalytic samples.

3.4.2 X-ray Absorption Spectroscopy

The XAS experiments were performed at the wiggler XAS beamline at the Australian Synchrotron, Victoria, Australia. Spectra of the catalytic samples, the PtO and RuO_2

samples, were recorded at the Pt L_{III}-edge (11580 eV) and at the Ru K-edge (22135 eV), at ~12 K in fluorescence mode with a 100-element solid-state Ge detector (Canberra). The scan range extended to k = 18 Å (EXAFS) with a step size of 0.01 Å at the pre-edge region, 0.00025 Å at the edge region, and 0.035 Å at the EXAFS region. Reference spectra of the Pt and Ru foils were measured in transmission mode at ~12 K at the Pt L_{III}-edge and Ru K-edge, respectively.

Samples measured at the Pt L_{III}-edge were pre-cooled in liquid nitrogen before being cooled and maintained at ~12 K using a closed-cycle He cryostat (Cryo Industries), whereas samples measured at the Ru K-edge were cooled directly in the cryostat. The total data acquisition time per scan was approximately 45–60 min., and repeat scans (up to a total of three scans per sample) were acquired to improve the signal-to-noise ratios of the scans. Thus, the data reported represent averages of up to three individual acquisitions, with a total collection time of up to 3 h per data set.

The effect of sulfur poisoning and regeneration on the Pt/Ru bonding environments was investigated by measuring fresh, poisoned, and regenerated catalyst samples. 'Fresh' refer to catalysts that have not been used in any catalytic reaction. 'Poisoned' samples were obtained by performing an hydrogenation reaction (described previously) in the presence of thiophene (0.20 μL, in 1.0 mL ethanol, equivalent to a thiophene content of 450 ppm (v/v), or a sulfur content of 560 ppm (mol/mol) in 160 μL cyclohexene.)[36] The poisoned samples were subsequently isolated from the reaction mixture by centrifugation, and dried at room temperature in air. 'Regenerated' samples were poisoned and isolated as described above, before being heat-treated under H_2 for 1 h at 300 °C (ramp rate 5 °C min^{-1}).

Catalytic samples were ground using an agate mortar and pestle to ensure homogeneity, before being packed into a PMMA multi-slit sample holder (slit size 2 ×

5 mm) sealed with Kapton tape. PtO and RuO_2 were diluted with cellulose (1 wt.%), similarly ground, and packed into the sample holder.

Calibration, averaging, and normalisation of XAS data were performed using the Average and Spline programs within the XFit software package.[46] Fittings of EXAFS data were performed using the XFit software based on the FEFF6 code.[47]

3.5 References

(1) Chheda, J. N.; Huber, G. W.; Dumesic, J. A., Liquid-phase catalytic processing of biomass-derived oxygenated hydrocarbons to fuels and chemicals. *Angew. Chem. Int. Ed.* **2007,** *46*, 7164–7183.

(2) Klass, D. L., *Biomass for Renewable Energy, Fuels, and Chemicals*. Academic Press: San Diego, 1998.

(3) Lynd, L. R.; Wyman, C. E.; Gerngross, T. U., Biocommodity Engineering. *Biotechnol. Prog.* **1999,** *15*, 777–793.

(4) Huber, G. W.; Iborra, S.; Corma, A., Synthesis of transportation fuels from biomass: Chemistry, catalysts, and engineering. *Chem. Rev. (Washington, DC)* **2006,** *106*, 4044–4098.

(5) Schmidt, L. D.; Dauenhauer, P. J., Chemical engineering: Hybrid routes to biofuels. *Nature (London)* **2007,** *447*, 914–915.

(6) Demirbas, A., Progress and recent trends in biofuels. *Prog. Energ. Combust.* **2007,** *33*, 1–18.

(7) Huber, G. W.; Dumesic, J. A., An overview of aqueous-phase catalytic processes for production of hydrogen and alkanes in a biorefinery. *Catal. Today* **2006,** *111*, 119–132.

(8) Cortright, R. D.; Davda, R. R.; Dumesic, J. A., Hydrogen from catalytic reforming of biomass-derived hydrocarbons in liquid water. *Nature (London)* **2002,** *418*, 964**–**967.

(9) Shabaker, J. W.; Huber, G. W.; Dumesic, J. A., Aqueous-phase reforming of oxygenated hydrocarbons over Sn-modified Ni catalysts. *J. Catal.* **2004,** *222*, 180−191.

(10) Shabaker, J. W.; Davda, R. R.; Huber, G. W.; Cortright, R. D.; Dumesic, J. A., Aqueous-phase reforming of methanol and ethylene glycol over alumina-supported platinum catalysts. *J. Catal.* **2003,** *215*, 344–352.

(11) Huber, G. W.; Shabaker, J. W.; Evans, S. T.; Dumesic, J. A., Aqueous-phase reforming of ethylene glycol over supported Pt and Pd bimetallic catalysts. *Appl. Catal., B* **2006,** *62*, 226–235.

(12) Huber, G. W.; Shabaker, J. W.; Dumesic, J. A., Raney Ni-Sn Catalyst for H_2 Production from Biomass-Derived Hydrocarbons. *Science (Washington, DC)* **2003,** *300*, 2075–2078.

(13) Davda, R. R.; Shabaker, J. W.; Huber, G. W.; Cortright, R. D.; Dumesic, J. A., Aqueous-phase reforming of ethylene glycol on silica-supported metal catalysts. *Appl. Catal., B* **2003,** *43*, 13–26.

(14) Davda, R. R.; Dumesic, J. A., Renewable hydrogen by aqueous-phase reforming of glucose. *Chem. Commun. (Cambridge, U.K.)* **2004**, 36–37.

(15) Cortright, R. D.; Davda, R. R.; Dumesic, J. A., Hydrogen from catalytic reforming of biomass-derived hydrocarbons in liquid water. *Nature (London)* **2002,** *418*, 964−967.

(16) Lin, Y.-C.; Huber, G. W., The critical role of heterogeneous catalysis in lignocellulosic biomass conversion. *Energ. Environ. Sci.* **2009,** *2*, 68–80.

(17) Huber, G. W.; Cortright, R. D.; Dumesic, J. A., Renewable alkanes by aqueous-phase reforming of biomass-derived oxygenates. *Angew. Chem. Int. Ed.* **2004,** *43*, 1549–51.

(18) West, R. M.; Liu, Z. Y.; Peter, M.; Gartner, C. A.; Dumesic, J. A., Carbon-carbon bond formation for biomass-derived furfurals and ketones by aldol condensation in a biphasic system. *J. Mol. Catal. A: Chem.* **2008,** *296*, 18–27.

(19) West, R. M.; Liu, Z. Y.; Peter, M.; Dumesic, J. A., Liquid alkanes with targeted molecular weights from biomass-derived carbohydrates. *ChemSusChem* **2008,** *1*, 417–424.

(20) Huber, G. W.; Chheda, J. N.; Barrett, C. J.; Dumesic, J. A., Production of Liquid Alkanes by Aqueous-Phase Processing of Biomass-Derived Carbohydrates. *Science (Washington, DC)* **2005,** *308*, 1446–1450.

(21) Yan, N.; Zhao, C.; Dyson, P. J.; Wang, C.; Liu, L.-t.; Kou, Y., Selective degradation of wood lignin over noble-metal catalysts in a two-step process. *ChemSusChem* **2008,** *1*, 626–629.

(22) Kunkes, E. L.; Simonetti, D. A.; West, R. M.; Serrano-Ruiz, J. C.; Gaertner, C. A.; Dumesic, J. A., Catalytic conversion of biomass to monofunctional hydrocarbons and targeted liquid-fuel classes. *Science (Washington, DC)* **2008,** *322*, 417–421.

(23) Chheda, J. N.; Dumesic, J. A., An overview of dehydration, aldol-condensation and hydrogenation processes for production of liquid alkanes from biomass-derived carbohydrates. *Catal. Today* **2007,** *123*, 59–70.

(24) Robinson, J. M.; Barrett, S. R.; Nhoy, K.; Pandey, R. K.; Phillips, J.; Ramirez, O. A.; Rodriguez, R. I., Energy Dispersive X-ray Fluorescence Analysis of Sulfur in Biomass. *Energ. Fuel.* **2009,** *23*, 2235–2241.

(25) Bartholomew, C. H.; Agrawal, P. K.; Katzer, J. R., Sulfur poisoning of metals. *Adv. Catal.* **1982,** *31*, 135–242.

(26) Rodriguez, J. A., The chemical properties of bimetallic surfaces: Importance of ensemble and electronic effects in the adsorption of sulfur and SO_2. *Prog. Surf. Sci.* **2006,** *81*, 141–189.

(27) Rodriguez, J. A.; Goodman, D. W., High-pressure catalytic reactions over single-crystal metal surfaces. *Surf. Sci. Rep.* **1991,** *14*, 1–107.

(28) Somorjai, G. A., *Introduction to Surface Chemistry and Catalysis*. Wiley: New York, 1994.

(29) Yasuda, H.; Yoshimura, Y., Hydrogenation of Tetralin over zeolite-supported Pd-Pt catalysts in the presence of dibenzothiophene. *Catal. Lett.* **1997,** *46*, 43–48.

(30) Rodriguez, J. A.; Hrbek, J., Interaction of sulfur with well-defined metal and oxide surfaces: Unraveling the mysteries behind catalyst poisoning and desulfurization. *Acc. Chem. Res.* **1999,** *32*, 719–728.

(31) Azad, A.-M.; Duran, M. J., Development of ceria-supported sulfur tolerant nanocatalysts: Rh-based formulations. *Appl. Catal., A* **2007,** *330*, 77–88.

(32) Azad, A.-M.; Sundararajan, D., A phenomenological study on the synergistic role of precious metals in the steam reforming of logistic fuels on trimetal-supported catalysts. *Adv. Mater. Sci. Eng.* **2010**, 325683, 12 pp.

(33) Conner, W. C., Jr.; Falconer, J. L., Spillover in Heterogeneous Catalysis. *Chem. Rev. (Washington, DC)* **1995,** *95*, 759–88.

(34) Roessner, F., Spillover effects. In *Handbook of Heterogeneous Catalysis (2nd Edition)*, Wiley-VCH Verlag GmbH & Co. KGaA: 2008; Vol. 3, pp 1574–1585.

(35) Wise, H., Mechanisms of Catalyst Poisoning by Sulfur Species. In *Catalyst Deactivation Proceedings of the 5th International Symposium*, Bartholomew, C. H.; Butt, J. B., Eds. Elsevier Science Publishers: Amsterdam, 1991; Vol. 68, pp 497–503.

(36) Stanley, J. N. G.; Worthington, K.; Heinroth, F.; Masters, A. F.; Maschmeyer, T., Designing nanoscopic, fluxional bimetallic Pt-Ru alloy hydrogenation catalysts for improved sulfur tolerance. *Catal. Today* **2011,** *178*, 164–171.

(37) Teddy, J.; Falqui, A.; Corrias, A.; Carta, D.; Lecante, P.; Gerber, I.; Serp, P., Influence of particles alloying on the performances of Pt-Ru/CNT catalysts for selective hydrogenation. *J. Catal.* **2011,** *278*, 59–70.

(38) Hull, A. W., X-Ray Crystal Analysis of Thirteen Common Metals. *Phys. Rev.* **1921,** *17*, 571–588.

(39) Benfield, R. E., Mean coordination numbers and the non-metal-metal transition in clusters. *J. Chem. Soc., Faraday Trans.* **1992,** *88*, 1107–10.

(40) Van, Z. J. B. A. D.; Koningsberger, D. C.; Van't, B. H. F. J.; Sayers, D. E., An EXAFS study of the structure of the metal-support interface in highly dispersed rhodium/alumina catalysts. *J. Chem. Phys.* **1985,** *82*, 5742–54.

(41) Gallezot, P.; Bienenstock, A. I.; Boudart, M., The atomic structure of platinum clusters. *Nouv. J. Chim.* **1978,** *2*, 263–6.

(42) Vaarkamp, M.; Miller, J. T.; Modica, F. S.; Koningsberger, D. C., On the relation between particle morphology, structure of the metal-support interface, and catalytic properties of Pt/γ-Al_2O_3. *J. Catal.* **1996,** *163*, 294–305.

(43) Lei, Y.; Jelic, J.; Nitsche, L. C.; Meyer, R.; Miller, J., Effect of particle size and adsorbates on the L3, L2 and L1 X-ray absorption near edge structure of supported Pt nanoparticles. *Top. Catal.* **2011,** *54*, 334–348.

(44) Miller, J. T.; Kropf, A. J.; Zha, Y.; Regalbuto, J. R.; Delannoy, L.; Louis, C.; Bus, E.; van Bokhoven, J. A., The effect of gold particle size on AuAu bond length and reactivity toward oxygen in supported catalysts. *J. Catal.* **2006,** *240*, 222–234.

(45) Nashner, M. S.; Frenkel, A. I.; Adler, D. L.; Shapley, J. R.; Nuzzo, R. G., Structural Characterization of Carbon-Supported Platinum-Ruthenium Nanoparticles from the Molecular Cluster Precursor PtRu5C(Co)16. *J. Am. Chem. Soc.* **1997,** *119*, 7760–7771.

(46) *XFit for Windows*, Australian Synchrotron Research Program: Sydney, 2004.

(47) Rehr, J. J.; Albers, R. C.; Zabinsky, S. I., High-order multiple-scattering calculations of x-ray-absorption fine structure. *Phys. Rev. Lett.* **1992,** *69*, 3397**–**400.

Chapter 4: Robust Bimetallic Pt-Ru Catalysts for the Rapid Hydrogenation of Toluene and Tetralin at Ambient Temperature and Pressure

This chapter was published in *Applied Catalysis A: General*.

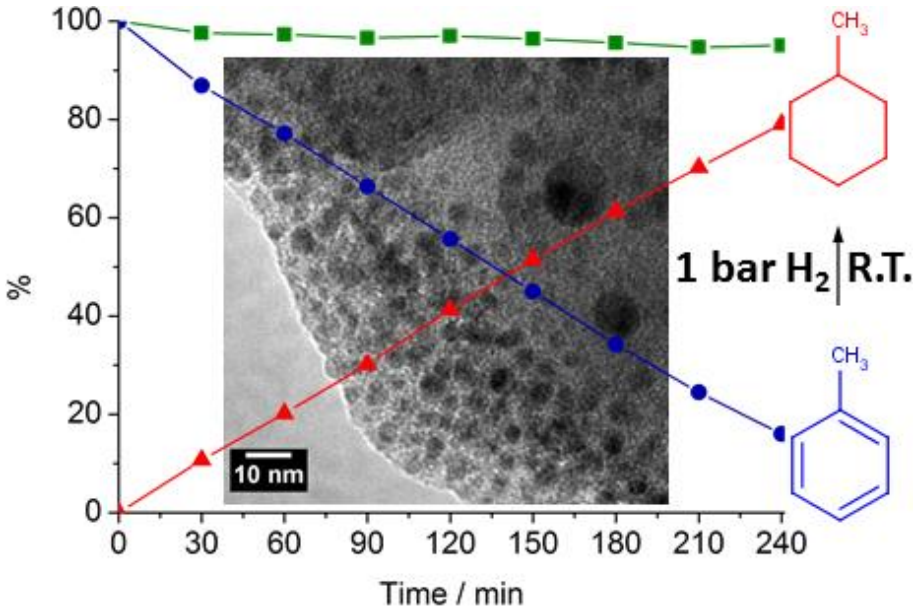

Stanley, J.N.G.; Heinroth, F.; Weber, C.C.; Masters, A.F.; Maschmeyer, T., *Appl. Cat., A* **2013**, 454, 46–52.

4.1 Introduction

The hydrogenation of aromatics is an important reaction, both for small-scale synthesis, and for industrial processes such as the production of cyclohexane − an important precursor in the manufacturing of nylon-6,6.[1–3,v] In particular, the toluene/methylcyclohexane couple is a promising cyclic hydrocarbon combination for the safe and feasible storage of hydrogen.[4] Not only is the toluene/methylcyclohexane couple reversible and highly selective, but it is free from carcinogenic products. Furthermore, it has a relatively high hydrogen storage capacity (6.2 wt.%, 46.5 kg-H_2/m^3), and the volatility range of the constituents makes the couple compatible with existing transportation infrastructure, such as storage tanks and refuelling stations, giving it an advantage over other solid hydrocarbons for hydrogen storage and transport.[4–7]

However, the hydrogenation of aromatics, including toluene, is traditionally performed using elevated temperatures and pressures, which often exceed 100 °C and 50 atm H_2.[8] Thus, effecting the reduction under mild conditions is an important challenge in terms of energy conservation and associated environmental considerations. This is of particular concern when examining the suitability of the toluene/methylcyclohexane couple for the reversible storage of hydrogen, *i.e.* the system's usability in a decentralised transport infrastructure.

Despite much research on the model hydrogenation of toluene (particularly over the last decade) at room temperature, elevated pressures are still required. Additionally, the catalyst preparations are often challenging, and yield catalysts with low activity and/or low stability.[2] Furthermore, many of these catalyst preparations and/or hydrogenation reactions require an inert atmosphere, resulting in additional difficulties in catalyst preparations and manipulations.

[v] References for Chapter 4 begin on page 111.

In Table 4.1, the most competitive literature results for the hydrogenation of toluene under mild conditions are summarised. A number of groups have demonstrated that metal nanoparticles can perform aromatic hydrogenation under mild conditions, and have undertaken considerable work in developing highly water-soluble surfactants to stabilise these particles in aqueous solution (entries 1–3, 6, 8, 13, 19, 20).[3, 9–15] In these cases the hydrogenation reactions are then performed in biphasic conditions, with the nanoparticles suspended in the aqueous phase. Similarly, other groups have investigated the use of ionic liquids for nanoparticle stabilisation (entries 5, 7).[12, 16–18] A further approach to overcome the problems of stability has been to immobilise the nanoparticles on a solid support, such as silica (entries 4, 11, 17, 18, 24, 29), boehmite nanofibers (entry 10), multi-walled carbon nanotubes (entries 21 and 25), titanium dioxide (entry 29), and others (entries 14–16, 23, 27).[1, 2, 19–31] Recently, Özkar *et al*. reported the hydrogenation of aromatics at room temperature under 3 atm H_2 using colloidal nanozeolite framework-stabilized ruthenium(0) nanoclusters (entry 26), and obtained a turnover-frequency (TOF) of 1800 h^{-1} for the hydrogenation of toluene. However, their reaction preparation and catalyst manipulations still required air-free conditions and thus the careful handling of the catalyst.[32] Where no inert conditions or special precautions are required and competitive TOFs are obtained (entries 8, 15, 21, 23, 24, 29), it appears elevated hydrogen pressures are necessary, presumably to achieve higher rates and/or to stabilise the catalytic surfaces.

Here, we introduce a system that combines the desirable aspects of simple preparation, stability and high activity under atmospheric conditions.

Table 4.1 Literature overview of catalysts, conditions, and reported TOFs for the batch hydrogenation of toluene.

Entry	Catalyst	Conditions	Notes / Remarks	TOF[a]	Ref
1	Rh(0)	20 °C / 1 atm / water	Stirred 1500 min^{-1}. Stabiliser: hydroxyalkylammonium salt.	53	10
2	Rh(0)	20 °C / 1 atm / water	Stirred 1500 min^{-1}. Inert conditions. TOF determined for 100% conversion. Stabiliser: N-alkyl-N-(2-hydroxyethyl)ammonium (HEA-C_{16}).	92	11
3	Rh(0)	20 °C / 1 atm / water	Stirred 1500 min^{-1}. Inert conditions. TOF determined for 100% conversion. Stabiliser: N-alkyl-N-(2-hydroxyethyl)ammonium (HEA-C_{16}).	256	9
4	Ru(0)/SiO_2	100 °C / 30 atm / *n*-octane	Stirred 1500 rpm. Inert conditions. TOFs average of at least 3 runs.	360	19
5	Ir(0)	75 °C / 4 atm / neat	Inert conditions. Stabiliser: 1-nbutyl-3-methylimidazolium hexafluorophosphate (BMI•PF6).	44 (78)[d]	12
6	Rh(0)	20 °C / 1 atm / water	Stirred 1500 min^{-1}. Inert conditions. TOF determined for 100% conversion. Stabiliser: N,N-dimethyl-N-cetyl-N-(2-hydroxyethyl)ammonium chloride (HEA16Cl).	83	3
7	Pt(0)	75 °C / 4 atm / neat	Inert conditions. Stabiliser: 1-*n*-butyl-3-methylimidazolium hexafluorophosphate (BMI•PF6).	17	16
8	Ir(0)	20 °C / 40 atm / water	Stirred 1000 min^{-1}. TOF determined for 100% conversion. Stabiliser: N,N-dimethyl-N-cetyl-N-(2-hydroxyethyl)ammonium chloride.	375	13
9	Ru(0)	75 °C / 4 atm / neat	Inert conditions. No stabiliser.	45	17

10	Rh/AlO(OH)	22 °C / 1 atm / hexane		300	2
11	Rh_{coll}/SiO_2	20 °C / 1 atm / water	Stirred 1500 min^{-1}. TOF determined for 100% conversion.	107	1
12	Ru(0)	20 °C / 1 atm / water	Stirred 1500 min^{-1}. Stabiliser: methylated cyclodextrin (Me-b-CD).	17	33
13	Ru(0)	20 °C / 30 atm / water	Using stirrer bar. TOF determined for 100% conversion. Inert conditions. Surfactant: N,N-dimethyl-N-cetyl-N-(2-hydroxyethyl) ammonium chloride (HEA16Cl).	150	34
14	Rh/C	RT / 1 atm / methanol		600	20
15	Rh/AlO(OH)	75 °C / 4 atm / neat	Stirred 800–900 min^{-1}.	500	21
16	Ru/CNF-P	100 °C / 30 atm / neat	Inert conditions.	14200	22
17	Rh-Si120	RT / 1 atm / hexane	Stirred 1500 min^{-1}. TOF determined for 100% conversion.	452	23
18	Rh-SiO_2	20 °C / 1 atm / hexane	Stirred 1500 min^{-1}. Inert conditions.	282	24
19	Rh(0)	RT / 1 atm / water	Stirred 1500 min^{-1}. Inert conditions. TOF determined for 100% conversion. Surfactant: *N*-hexadecyl-*N*-tris-(2-hydroxyethyl) ammonium chloride (THEA16Cl).	100	14
20	Ru(0)	20 °C / 1 atm / water	Stirred 1500 rpm. Surfactant: N,N-dimethyl,N-hexadecyl,N-(2-hydroxyethyl)-ammonium (HEA16Cl) and randomly methylated cyclodextrins (RAME-b-CD).	10.1	15
21	Rh/MWNTs	25 °C / 10 atm / neat	Stirred ~600 rpm.	838 (1949)[b,d]	25
22	$RuO_2 \cdot 3H_2O$	75 °C / 4 atm / neat	Inert conditions.	556 (1635)[d]	18
23	Ru/FDU-15-H_2	60 °C / 40 atm / water/ethanol	Stirred 1200 rpm.	1213	27
24	Ru/silica-PVP	110 °C / 40 atm / neat		28500[c]	28
25	RuL-	50 °C / 40 atm /	Inert conditions.	100 (192)[c,d]	29

	MWCNT	ethanol			
26	NFS-Ru(0)	25 °C / 2.8 atm / neat	Initial TOF. Inert conditions.	1800	32
27	Ru/PVPy	120 °C / 10 atm / THF	Inert conditions.	69	30
28	$Rh@TiO_2$	RT / 1 atm / water	Stirred 1700 min^{-1}. TOF determined for 100% conversion.	222	31
29	$Fe_3O_4@SiO_2$-Rh(0) NPs	RT / 10 atm / neat		16000	26

[a] All TOFs are reported as calculated in the respective references by taking the moles of hydrogen consumed per moles of catalyst per hour, unless otherwise indicated. [b] TOF calculated by taking the number of molecules reacted per unit "weight of catalyst per unit time".[25] [c] TOF calculated by taking the moles of substrate transformed per moles of catalyst.[29] [d] TOF in parentheses is corrected for exposed metal as reported in the respective references.[12, 18, 25, 29]

Thus, we report the hydrogenation of toluene at room temperature under 1 atm H_2 using a mesoporous aluminosilicate-supported, air-stable Pt-Ru bimetallic catalyst. The ratio of $Pt_1Ru_{1.5}$ was chosen as this ratio displays improved sulfur tolerance in the model hydrogenation of cyclohexene in the presence of sulfur-species,[35] which is an important feature for the catalyst's application to the hydrogenation of aromatics in real refinery streams, as sulfur is well-known to poison noble metal catalysts.[36, 37] Similarly, the acidic, mesoporous SiAlTUD-1 was chosen as support material as it is well-established that noble metals immobilised on acidic supports are more sulfur-resistant than they are on other supports.[38–45] The mesoporous TUD-1 structure family was chosen because of its characteristic large surface area, high thermostability, and tunable pore sizes. Toluene was chosen as substrate because the toluene/methylcyclohexane couple is a promising hydrocarbon combination for hydrogen storage.[4] Additionally, tetralin was chosen as a model compound for aromatic hydrogenation, as there is an increasing need for an ever lower aromatic content in petroleum fuels as such compounds are responsible for

undesirable particulate emissions, leading to environmental concerns and the subsequent tightening of fuel legislation.[42, 43] By analogy with the examples given above for toluene, tetralin hydrogenation is accomplished with high turnover frequencies typically only at elevated temperatures and pressures, hence the ability to hydrogenate this substrate under ambient temperatures and pressures would be desirable.[46]

4.2 Methods and Materials

4.2.1 Materials

The following reagents were used as received: tetraethylene glycol (TEG), polyethylene glycol dodecyl ether (Brij® 30, M_n ~362 amu), hydrogen hexachloroplatinate(IV) hydrate ($H_2PtCl_6 \cdot 5H_2O$), decane (all Adrich), aluminium isopropoxide, hydrazine hydrate ($N_2H_4 \cdot H_2O$), toluene (all Ajax), ruthenium trichloride trihydrate ($RuCl_3 \cdot 3H_2O$) (Strem), *n*-heptane (APS), tetralin (BDH), and tetraethylorthosilane (TEOS) (Alfa Aesar). Absolute ethanol (Merck) was analytical grade and was used as received. De-ionised water was processed using a Milli-Q (Millipore) Ultrapure Water System.

4.2.2 Catalyst Preparation

The SiAlTUD-1 support was prepared using an adaptation of the method described by Simons *et al.*[47] Aluminium isopropoxide (6.28 g, 30.7 mmol) was added to a mixture of ethanol (36 mL, 617 mmol), anhydrous 2-propanol (34 mL, 445 mmol), and TEOS (26 mL, 117 mmol) at 45 °C, and the mixture was stirred until all components dissolved. TEG (26 mL, 151 mmol) was then added, followed by the drop-wise addition of a solution containing ethanol (36 mL, 617 mmol), anhydrous 2-propanol (34 mL, 445 mmol) and

water (6 mL, 333 mmol). The mixture produced was stirred at RT for 30 min, then aged without heating or stirring for 6 h. The resultant white gel was dried at 70 °C for 21 h, then at 98 °C for 2 h after which time the dry material was heated under autogenous pressure at 165 °C in a 50 mL Teflon-lined autoclave for 8 h. The template was removed by washing the material in a Soxhlet extractor (Büchi Extraction System (B-811)) using warm ethanol for 3 h. The white solid obtained was dried at 60 °C before being calcined at 600 °C (ramp rate 5 °C min^{-1}) for 10 h.

The catalysts were prepared following the incipient wetness method. Platinum and ruthenium precursor solutions were made by adding the necessary volume of deionized water to the $H_2PtCl_4 \cdot 5H_2O$ and $RuCl_3 \cdot 3H_2O$ precursor salts. The nanoparticle precursor solution (0.84 mL) was added drop-wise to SiAlTUD-1 (800 mg, pore volume 1.05 cm^3g^{-1}) whilst stirring. The sticky solid obtained was dried at 100 °C for 12 h then heat treated under H_2 for 2 h at 400 °C (ramp rate 5 °C min^{-1}).

4.2.3 Characterisation

Powder X-ray diffraction (XRD) measurements were made using a PANalytical X-Pert PRO MRD X-ray diffractometer equipped with a PIXcel detector, using Ni-filtered $Cu_{K\alpha}$ radiation (λ_{av} 1.5419 Å). A Micromeritics ASAP 2020 Accelerated Surface Area and Porosity analyser was used to measure the N_2 adsorption/desorption isotherms of the samples at 77 K. Before analysis, samples were degassed at 200 °C. Transmission electron microscopy (TEM) images were recorded digitally with a Gatan slow-scan charge coupled device camera on a Philips CM120 Biofilter electron microscope operating at 120 kV. A Varian Vista AX ICP-AES equipped with a CCD detector was used to measure elemental compositions.

4.2.4 Catalytic Activity

The hydrogenation reactions were performed at room temperature (RT) in a two-necked, round bottom 50 mL glass Quickfit flask, fitted with Suba-Seal stoppers and equipped with a magnetic stirrer. In general, toluene or tetralin (200 mg) and decane (200 µL, 1.03 mmol, internal standard) were added to ethanol (25 mL). The mixture was stirred at a rate of 400 rpm for 5 min in air and a sample (~0.10 mL) was taken. The catalyst (200 mg) was added to the reaction vessel, the mixture was placed in an ultra-sonic bath for 30 s, and a sample (~0.10 mL) was taken. Prior to reaction, the reactor was purged through a needle with H_2 provided from a balloon, filled in-house, with the H_2 admitted through a septum cap fitted to one arm of the reactor. The reaction was carried out under 1 bar H_2 with stirring at 400 rpm for 4 h. In the case of tetralin, the reaction time was extended to 19 h. Samples (total 10, each ~0.10 mL) were taken at regular intervals using a syringe through a septum cap fitted to one arm of the reactor. All samples taken from the reactor were centrifuged to isolate the catalyst, the supernatant was diluted with ethanol, and the progress of the reaction was analysed using gas chromatography (Shimadzu GC-17A Gas Chromatograph equipped with a BP21 column – 30 m × 0.25 mm I.D.; 0.25 µm film thickness; J & W Scientific - and a flame ionization detector, using Ar as the carrier gas). The formation of the products was confirmed by analysing the reaction mixture at the end of the reaction by GC-MS (Shimadzu GCMS-QP2010 Gas Chromatograph equipped with a Rtx-5Sil MS column – 30 m × 0.25 mm I.D.; 0.25 µm film thickness; Restek).

4.2.5 Turn-Over-Frequencies

The catalytic results were recorded as uncorrected TOFs, defined as the number of moles of hydrogen consumed per moles of metal (total moles metal, determined by ICP-AES) per

unit time. Due to experimental limitations that prevented the amount of hydrogen consumed being measured directly, and the fact that three moles of hydrogen were required to react with one mole of substrate, the uncorrected TOFs were obtained by dividing three times the number of moles of substrate consumed by the number of moles of catalyst per unit time. Corrected TOFs were calculated by applying a model of surface exposed metal atoms (assuming that on average half of the surface atoms are accessible), based on the ICP metal loadings, an average particle size of 10 nm, and assuming a single element (Ru) with spherical shape (see Appendix C).[48] In all cases, the TOFs were calculated using the slope of conversion, as the reactions appear to be zero-order (see 4.3 Results and Discussion).

4.3 Results and Discussion

4.3.1 Characterisation

The acidic, mesoporous, aluminosilicate SiAlTUD-1 used as the support material, was synthesised following a literature protocol.[47] Its BET surface area of 567 $m^2 g^{-1}$, total pore volume of 1.1 $cm^3 g^{-1}$, and maximum pore size of 15 nm are in good agreement with the literature values of ~600 $m^2 g^{-1}$, 1.1 $cm^3 g^{-1}$, and 15 nm, respectively.[47] The ICP analysis gives a silicon to aluminium ratio (Si:Al) of 4.1:1, which is consistent with the 5:1 composition of the starting gel mixture.

Four catalysts were prepared with this support material using the incipient wetness method. In addition to a pure platinum (Pt), a pure ruthenium (Ru), and a bimetallic platinum-ruthenium ($Pt_1Ru_{1.5}$) catalyst, with theoretical total metal loadings of 5.0 wt.%, a bimetallic platinum-ruthenium ($Pt_1Ru_{1.5}$) catalyst was prepared with a theoretical metal

loading of 0.5 wt.%. The physical properties and molar compositions of the catalysts prepared are presented in Table 4.2.

Table 4.2 Physical properties and molar compositions of all catalysts.

Catalyst	Total Metal load. / wt.%	Pt / mol.%	Ru / mol.%	S_{BET} / $m^2\ g^{-1}$	V_{Pore} / $cm^3\ g^{-1}$
$Pt_1Ru_{1.5}$	0.4	40	60	419	1.01
$Pt_1Ru_{1.5}$	4.0	41	59	370	0.85
Pt	3.5	100	0	396	0.98
Ru	4.2	0	100	371	0.85

All metal loadings, determined by ICP-AES (Table 4.2), are in good agreement with the theoretical metal loadings of 5.0 wt.% and 0.5 wt.%, ranging from 3.5 to 4.2 wt.% for the higher loading catalysts, and 0.4 wt.% for the lower loading catalyst. The Pt to Ru ratios for the bimetallic catalysts are in good agreement with the concentrations of the starting precursor solutions. Henceforth, the bimetallic catalysts will be referred to as $Pt_1Ru_{1.5}$ (4.0 wt.%) and $Pt_1Ru_{1.5}$ (0.4 wt.%). Nitrogen sorption measurements of the catalysts, listed in Table 4.2, indicate a general decrease in surface areas and pore volumes compared with the unmodified support material. The surface areas and pore volumes were calculated to be between 370 to 419 $m^2\ g^{-1}$ and 0.85 to 1.01 $cm^3\ g^{-1}$, respectively. The decrease in the surface area of the catalysts compared to that of the unmodified support can be attributed to the impregnation of metal sites due to the incipient wetness method.[49]

As shown in Figure 4.1, the TEM micrographs of the catalysts reveal particle sizes below 10 nm and a good dispersion of the nanoparticles on the surface of the support. XRD patterns of the Pt and Ru catalysts (C and D in Figure 4.2) show the typical reflections of platinum and ruthenium, respectively. The particle sizes for the Pt catalyst and Ru catalyst are 8 nm and 11 nm, respectively, as determined by the Scherrer equation. However, pronounced crystalline peaks are not observed for the bimetallic catalysts (A and B in Figure 4.2). Nevertheless, for the more highly loaded catalyst (B in Figure 4.2), broad low intensity reflections in the range of the platinum (111) reflection and the ruthenium (101) reflection can be seen. The lack of observable crystallinity could be attributed to the small particle size of the catalysts, consistent with the TEM micrographs, and/or the metal loadings in the case of $Pt_1Ru_{1.5}$/SiAlTUD-1 (0.4 wt.%) (determined by ICP-AES) being just below the threshold for detection by XRD. Moreover, it has been reported that a loss of crystallinity is observed with increasing ruthenium content of bimetallic Pt-Ru nanoparticles.[50]

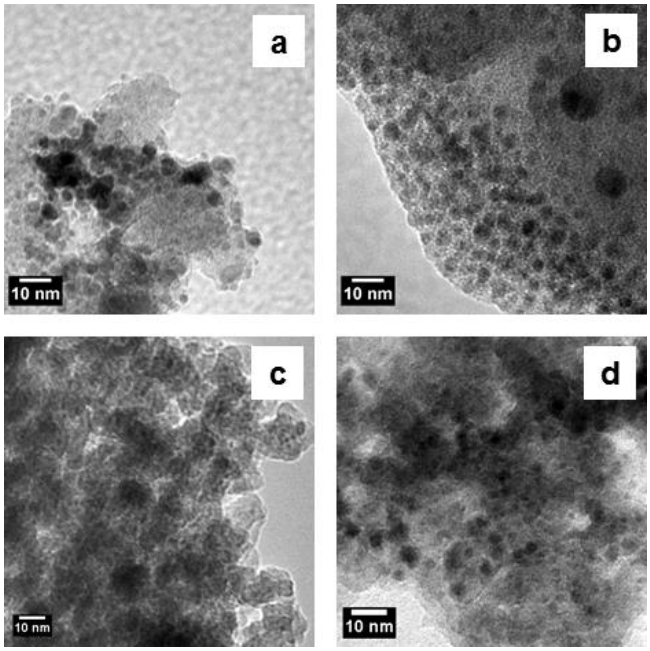

Figure 4.1 Representative TEM micrographs of the catalysts prepared: a) $Pt_1Ru_{1.5}$/SiAlTUD-1 (0.4 wt.%), b) $Pt_1Ru_{1.5}$/SiAlTUD-1 (4.0 wt.%), c) Pt/SiAlTUD-1 (3.5 wt.%), and d) Ru/SiAlTUD-1 (4.2 wt.%).

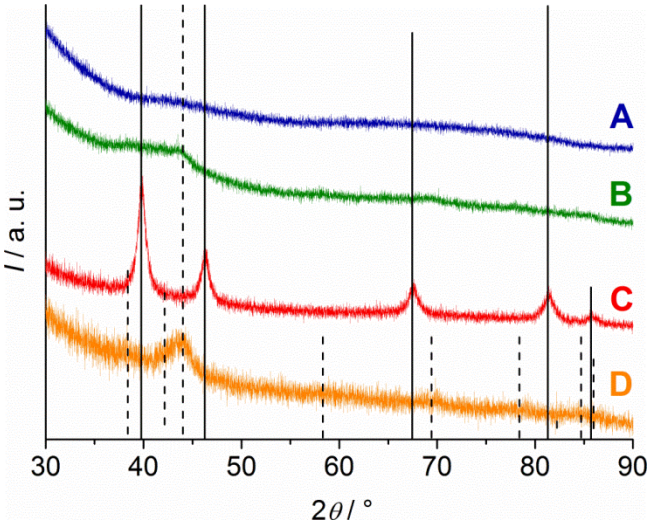

Figure 4.2 XRD patterns of the catalysts prepared with by incipient wetness impregnation: a) $Pt_1Ru_{1.5}$/SiAlTUD-1 (0.4 wt.%), b) $Pt_1Ru_{1.5}$/SiAlTUD-1 (4.0 wt.%), c) Pt/SiAlTUD-1 (3.5 wt.%), and d) Ru/SiAlTUD-1 (4.2 wt.%). Patterns for references: JCPDS 00-001-1190 reference for platinum (solid line) and JCPDS 00-006-663 for ruthenium (dashed line).[51, 52]

4.3.2 Catalytic Activity

4.3.2.1 Catalytic Hydrogenation of Toluene

The catalytic activity of all catalysts prepared was tested in the hydrogenation of toluene in ethanol at room temperature under 1 atm of hydrogen. Toluene is selectively hydrogenated to methylcyclohexane with high conversion. Moreover, it should be noted that no by-products were observed by GC analysis and excellent mass balances obtained. It is apparent in the graphs of conversion as a function of time (Figure 4.3) that the bimetallic catalyst (4.0 wt.%) exhibits a higher activity compared with the monometallic catalysts (metal loadings of 3.5 and 4.2 wt.%). The conversion increases linearly with time for all catalysts suggesting the reaction is zero-order in toluene, which means that the calculated activity is independent of conversion. Even at the low metal loading, the bimetallic catalyst

$Pt_1Ru_{1.5}$ (0.4 wt.%) is active for the hydrogenation of toluene (Figure 4.3b). Interestingly, an induction period of approximately two hours can be observed for the pure ruthenium catalyst (Figure 4.3d) after which an apparently zero-order reaction occurs.

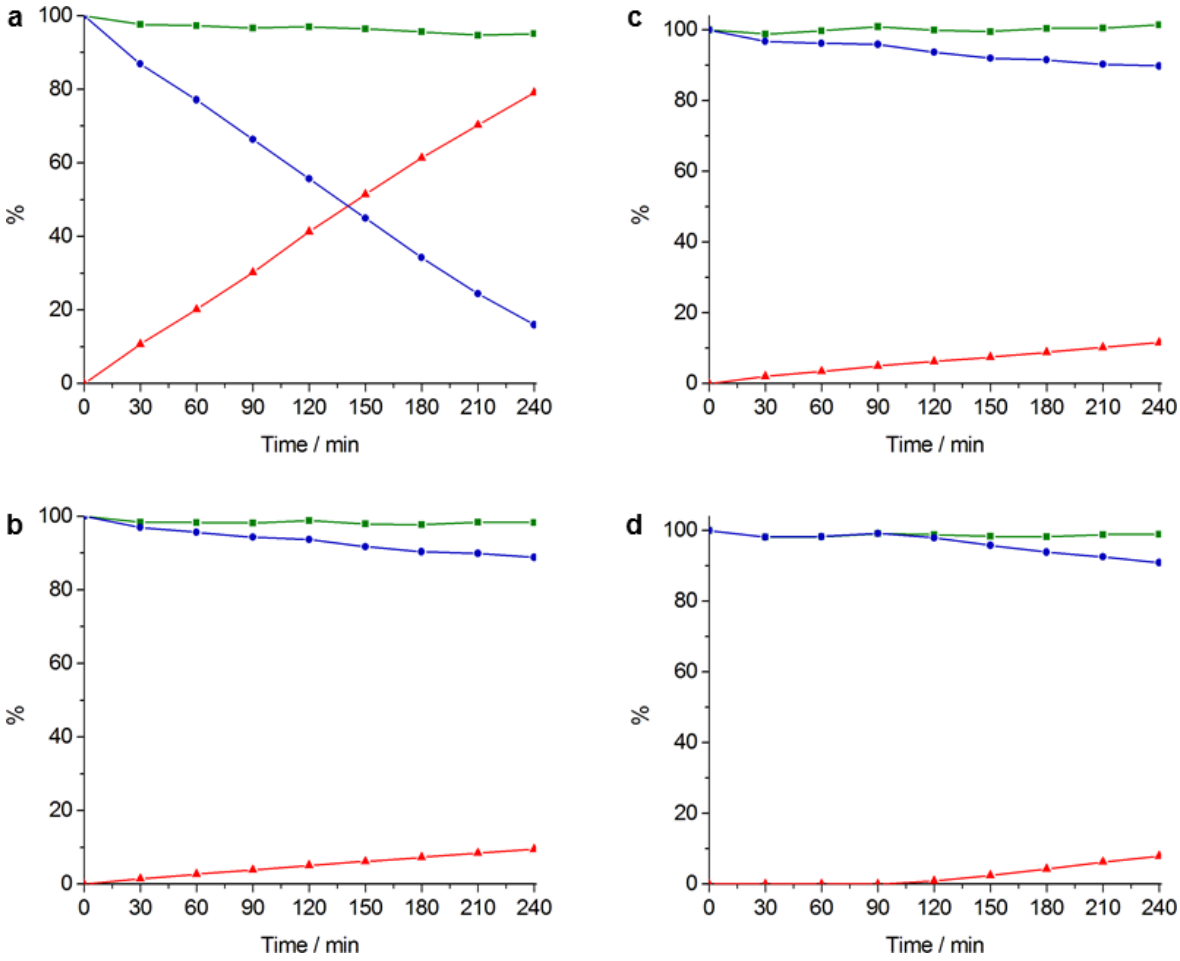

Figure 4.3 Plot of loss of toluene (●), formation methylcyclohexane (▲), and mass balance (■) for the hydrogenation of toluene as a function of time for a) $Pt_1Ru_{1.5}$ (4.0 wt.%), b) $Pt_1Ru_{1.5}$ (0.4 wt.%), c) Pt (3.5 wt.%), and d) Ru (4.2 wt.%), in ethanol at RT under 1 atm H_2.

The uncorrected turn-over-frequencies for toluene conversion (TOFs, moles H_2/moles total metal/hour) were calculated by dividing three times the number of moles of toluene consumed by the number of moles of catalyst (total moles metal) per unit time. Note that these TOFs were not corrected for the number of active surface sites, leading to a significant underestimation of the TOFs. When applying a model of surface exposed metal atoms, based on the average particle size, assuming a single element (Ru) with spherical shape, and the cross-sectional area of each sphere, the TOF per mole surface metal increased by a factor of 15 (see Appendix C).[48] Unless otherwise indicated, the TOFs presented in the literature are calculated for total moles of metal, and no attempts to correct these TOFs for exposed metal have been attempted due to the unavailability of the necessary ancillary data. Furthermore, Redel *et al.* point out that estimating TOFs based on exposed surface atoms can be problematic, *e.g.* due to effects such as rearrangement of the surface atoms of the nanoparticle during catalysis, and the influence of the precise details of surface topology, *etc*.[53] Nonetheless, we believe that this correction is justified in the present case because (a) the correction is modest, (b) because it is modest, it is likely an underestimate of the correction for effects such as the influence of surface topology, and (c) our experiments are at RT and 1 atm, under which conditions, catalyst rearrangements are likely to be less significant than at the higher temperatures of many studies summarised in Table 4.1. Finally, many of the catalysts in the literature are present as aqueous colloidal suspensions (and thus have a higher percentage of exposed metal atoms), making it more reasonable in those instances to calculate the TOFs based on total moles of metal.

In all cases, the TOFs were calculated using the slope of the conversion/time plots, as the reactions appear to be zero-order in toluene. The catalytic results are summarised in Table 4.3 showing the uncorrected and the corrected TOFs.

Table 4.3 TOF results of the hydrogenation of toluene in ethanol at RT under 1 bar H_2.

Catalyst	Metal loading / wt.%	TOF / h^{-1}[a]	Corrected TOF / h^{-1}[b]
$Pt_1Ru_{1.5}$	0.4	32.1	483
$Pt_1Ru_{1.5}$	4.0	22.0	331
Pt	3.5	3.7	55
Ru	4.2	2.2	34

[a] TOF defined as moles of hydrogen consumed per moles of catalyst (total moles metal) per hour.

[b] TOF corrected for moles exposed metal.

As listed in Table 4.3 and indicated in the discussion of the conversion *vs* time graphs, the TOFs are significantly higher for the bimetallic catalysts compared with the monometallic catalysts. Hence, a synergistic relationship between the platinum and ruthenium is suggested, which might be the result of electronic perturbations (produced by metal–metal bonding, or by changes in the number of available active sites on the surface of the catalyst) or structural changes leading to more edge-sites, kinks, defects, *etc*., in agreement with literature reports.[35, 54–56] These electronic perturbations or structural changes could explain the high activity of the bimetallic catalysts compared to their monometallic counterparts.

The TOFs calculated for the bimetallic catalysts of 32.1/483 h^{-1} (uncorrected/corrected) for $Pt_1Ru_{1.5}$ (0.4 wt.%) and 22.9/331 h^{-1} for $Pt_1Ru_{1.5}$ (4.0 wt.%) are very competitive when compared with the literature (Table 4.1) and taking into account the mild reaction conditions employed here, including the solvent ethanol (which enhances

operational ease, but does not dissolve hydrogen as readily as water or neat toluene). Indeed, half the catalysts in Table 4.1 needed inert conditions and only five that did not require inert conditions were tested at RT and ambient pressure, achieving TOFs of 300, 107, 600, 452, and 222 h^{-1} (entries 10, 11, 14, 17, and 28). However, they were all based on pure rhodium, rather than the less expensive ruthenium/platinum alloy presented here.

4.3.2.2 Catalytic Hydrogenation of Tetralin

To explore the capability of the bimetallic catalysts, $Pt_1Ru_{1.5}$ (4.0 wt.%) and $Pt_1Ru_{1.5}$ (0.4 wt.%), the catalytic study was extended to the hydrogenation of tetralin, under the same mild conditions. The results for tetralin hydrogenation are presented in Figure 4.4 and Table 4.4.

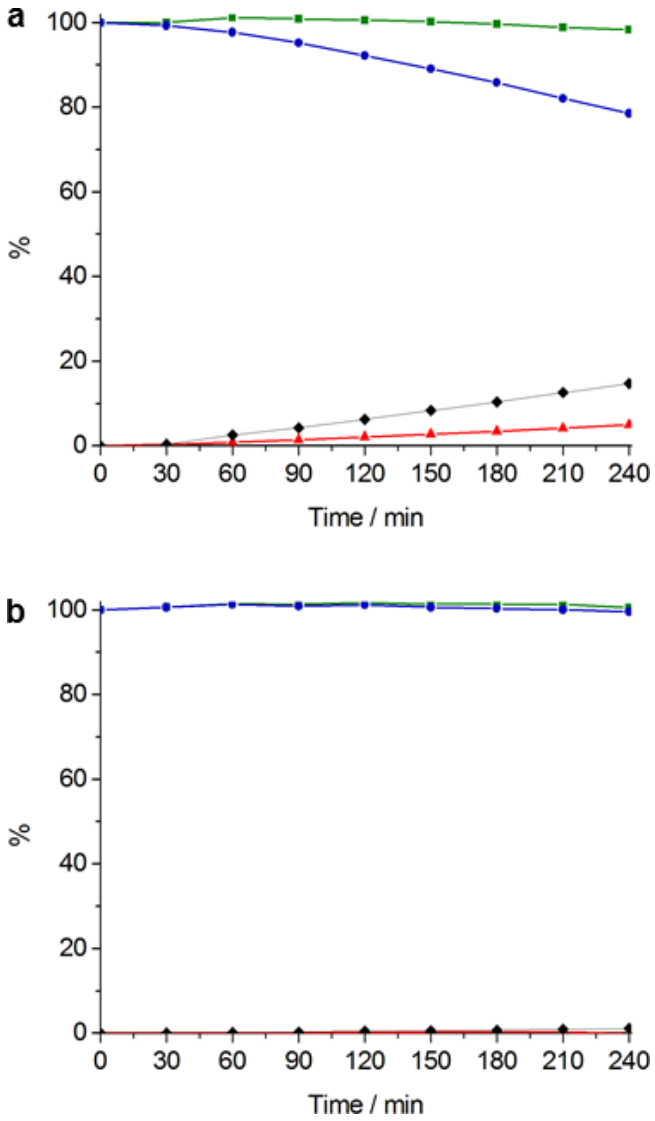

Figure 4.4 Plot of loss of tetralin (●), formation of *trans*-decalin (▲), formation of *cis*-decalin (♦) and mass balance (■) for the hydrogenation of tetralin as a function of time for a) $Pt_1Ru_{1.5}$ (4.0 wt.%), and b) $Pt_1Ru_{1.5}$ (0.4 wt.%) in ethanol at RT under 1 atm H_2.

Table 4.4 Summary of hydrogenation results for $Pt_1Ru_{1.5}$/SiAlTUD-1 for toluene and tetralin in ethanol at RT under 1 bar H_2.

Substrate	Cat. Loading / wt.%	Time / h	Conv. / %[a]	TOF / h^{-1}[c]	Corrected TOF / h^{-1}[d]
Toluene	0.4	4	9.5	32.1	443
Toluene	4.0	4	79	22.9	331
Tetralin	0.4	4	1.1 (100:1)[b]	-	-
Tetralin	4.0	4	19.7 (75:25)[b]	-	-
Tetralin	0.4	19	12.8 (75:25)[b]	4.4	66
Tetralin	4.0	19	90.7 (73:27)[b]	4.1	62

[a] Conversions determined by GC analysis. [b] Ratios in parentheses indicate the selectivity towards the *cis*- and *trans*-decalin products, respectively. [c] TOF defined as moles of hydrogen consumed per moles of catalyst (total moles metal) per hour. [d] TOF corrected for moles exposed metal.

As shown in Figure 4.4a and Table 4.4, the hydrogenation of tetralin in ethanol using $Pt_1Ru_{1.5}$ (4.0 wt.%) at room temperature under 1 atm H_2 achieved a conversion of 19.7%, with selectivities of 75% and 25% to *cis*-decalin and *trans*-decalin, respectively. The bimetallic catalyst with the lower metal loading, $Pt_1Ru_{1.5}$ (0.4 wt.%), was also tested for this reaction. At a conversion of 1.1% after 4 h (Figure 4.4b and Table 4.4) only *cis*-decalin product could be observed. The catalysts were then further tested by leaving the tetralin hydrogenation reaction to run overnight. The conversions increased linearly, as expected for zero-order reactions and after 19 h, $Pt_1Ru_{1.5}$ (4.0 wt.%) achieved a conversion of 90.7%, with a selectivity to *cis*-decalin of 75% and to *trans*-decalin of 25%. Similarly, $Pt_1Ru_{1.5}$ (0.4 wt.%) showed an increased yield at the longer reaction time, with a conversion of 12.8% and selectivities of 73% and 27% for *cis*- and *trans*-decalin, respectively. Remarkably, corrected TOFs of up to 66 h^{-1} were achieved, calculated for the 19 h reaction (Table 4.4).

4.4 Conclusions

The incipient wetness method, requiring no inert conditions, for the preparation of the bimetallic catalysts, $Pt_1Ru_{1.5}$ (4.0 wt.%) and $Pt_1Ru_{1.5}$ (0.4 wt.%), proved to be an effective and simple route to highly active catalysts for the hydrogenation of toluene at room temperature and 1 bar hydrogen. The advantages of this system over the few similarly active pure rhodium catalysts reported in the literature are that these catalysts are robust under atmospheric conditions, *i.e.* air-free conditions are not required for their handling, and that the alloys discussed are less expensive.

The synergistic effect within the Ru and Pt alloy is subject of further investigations at the atomic level by *in-situ* EXAFS.

4.5 References

(1) Mevellec, V.; Nowicki, A.; Roucoux, A.; Dujardin, C.; Granger, P.; Payen, E.; Philippot, K., A simple and reproducible method for the synthesis of silica-supported rhodium nanoparticles and their investigation in the hydrogenation of aromatic compounds. *New J. Chem.* **2006,** *30*, 1214–1219.

(2) Park, I. S.; Kwon, M. S.; Kim, N.; Lee, J. S.; Kang, K. Y.; Park, J., Rhodium nanoparticles entrapped in boehmite nanofibers: recyclable catalyst for arene hydrogenation under mild conditions. *Chem. Commun. (Cambridge, U. K.)* **2005**, 5667–5669.

(3) Roucoux, A.; Schulz, J.; Patin, H., Arene hydrogenation with a stabilized aqueous rhodium(0) suspension: A major effect of the surfactant counter-anion. *Adv. Synth. Catal.* **2003,** *345*, 222–229.

(4) Alhumaidan, F.; Cresswell, D.; Garforth, A., Hydrogen Storage in Liquid Organic Hydride: Producing Hydrogen Catalytically from Methylcyclohexane. *Energy Fuels* **2011,** *25*, 4217–4234.

(5) Kariya, N.; Fukuoka, A.; Ichikawa, M., Efficient evolution of hydrogen from liquid cycloalkanes over Pt-containing catalysts supported on active carbons under "wet-dry multiphase conditions". *Appl. Catal., A* **2002,** *233*, 91–102.

(6) Kariya, N.; Fukuoka, A.; Utagawa, T.; Sakuramoto, M.; Goto, Y.; Ichikawa, M., Efficient hydrogen production using cyclohexane and decalin by pulse-spray mode reactor with Pt catalysts. *Appl. Catal., A* **2003,** *247*, 247–259.

(7) Hodoshima, S.; Saito, Y. In *Hydrogen storage in organic chemical hydrides on the basis of superheated liquid-film concept*, 2009; CRC Press: 2009; pp 437–474.

(8) Augustine, R. L., *Heterogeneous Catalysis for the Synthetic Chemist*. Marcel Dekker: New York, 1995.

(9) Schulz, J.; Levigne, S.; Roucoux, A.; Patin, H., Aqueous rhodium colloidal suspension in reduction of arene derivatives in biphasic system: a significant physico-chemical role of surfactant concentration on catalytic activity. *Adv. Synth. Catal.* **2002,** *344*, 266–269.

(10) Schulz, J.; Roucoux, A.; Patin, H., Unprecedented efficient hydrogenation of arenes in biphasic liquid-liquid catalysis by re-usable aqueous colloidal suspensions of rhodium. *Chem. Commun. (Cambridge, U. K.)***1999**, 535–536.

(11) Schulz, J.; Roucoux, A.; Patin, H., Stabilized rhodium(0) nanoparticles: a reusable hydrogenation catalyst for arene derivatives in a biphasic water-liquid system. *Chem.--Eur. J.* **2000,** *6*, 618–624.

(12) Fonseca, G. S.; Umpierre, A. P.; Fichtner, P. F. P.; Teixeira, S. R.; Dupont, J., The Use of Imidazolium Ionic Liquids for the Formation and Stabilization of Ir0 and Rh0 Nanoparticles: Efficient Catalysts for the Hydrogenation of Arenes. *Chem.--Eur. J.* **2003,** *9*, 3263–3269.

(13) Mevellec, V.; Roucoux, A.; Ramirez, E.; Philippot, K.; Chaudret, B., Surfactant-stabilized aqueous iridium(0) colloidal suspension: An efficient reusable catalyst for hydrogenation of arenes in biphasic media. *Adv. Synth. Catal.* **2004,** *346*, 72–76.

(14) Hubert, C.; Denicourt-Nowicki, A.; Guegan, J.-P.; Roucoux, A., Polyhydroxylated ammonium chloride salt: a new efficient surfactant for nanoparticle stabilization in aqueous media. Characterization and application in catalysis. *Dalton Trans.* **2009**, 7356–7358.

(15) Hubert, C.; Denicourt-Nowicki, A.; Roucoux, A.; Landy, D.; Leger, B.; Crowyn, G.; Monflier, E., Catalytically active nanoparticles stabilized by host-guest inclusion complexes in water. *Chem. Commun. (Cambridge, U. K.)* **2009**, 1228–1230.

(16) Scheeren, C. W.; Machado, G.; Dupont, J.; Fichtner, P. F. P.; Texeira, S. R., Nanoscale Pt(0) Particles Prepared in Imidazolium Room Temperature Ionic Liquids: Synthesis from an Organometallic Precursor, Characterization, and Catalytic Properties in Hydrogenation Reactions. *Inorg. Chem.* **2003,** *42*, 4738–4742.

(17) Silveira, E. T.; Umpierre, A. P.; Rossi, L. M.; Machado, G.; Morais, J.; Soares, G. V.; Baumvol, I. J. R.; Teixeira, S. R.; Fichtner, P. F. P.; Dupont, J., The Partial Hydrogenation of Benzene to Cyclohexene by Nanoscale Ruthenium Catalysts in Imidazolium Ionic Liquids. *Chem.--Eur. J.* **2004,** *10*, 3734–3740.

(18) Rossi, L. M.; Machado, G., Ruthenium nanoparticles prepared from ruthenium dioxide precursor: Highly active catalyst for hydrogenation of arenes under mild conditions. *J. Mol. Catal. A: Chem.* **2009,** *298*, 69–73.

(19) Bianchini, C.; Dal, S. V.; Meli, A.; Moneti, S.; Moreno, M.; Oberhauser, W.; Psaro, R.; Sordelli, L.; Vizza, F., A comparison between silica-immobilized ruthenium(II) single sites and silica-supported ruthenium nanoparticles in the catalytic hydrogenation of model hetero- and polyaromatics contained in raw oil materials. *J. Catal.* **2003,** *213*, 47–62.

(20) Park, K. H.; Jang, K.; Kim, H. J.; Son, S. U., Near-monodisperse tetrahedral rhodium nanoparticles on charcoal: the shape-dependent catalytic hydrogenation of arenes. *Angew. Chem. Int. Ed.* **2007,** *46*, 1152–1155.

(21) Park, I. S.; Kwon, M. S.; Kang, K. Y.; Lee, J. S.; Park, J., Rhodium and iridium nanoparticles entrapped in aluminum oxyhydroxide nanofibers: catalysts for hydrogenations of arenes and ketones at room temperature with hydrogen balloon. *Adv. Synth. Catal.* **2007,** *349*, 2039–2047.

(22) Takasaki, M.; Motoyama, Y.; Higashi, K.; Yoon, S.-H.; Mochida, I.; Nagashima, H., Ruthenium nanoparticles on nano-level-controlled carbon supports as highly effective catalysts for arene hydrogenation. *Asian J. Chem.* **2007,** *2*, 1524–1533.

(23) Barthe, L.; Denicourt-Nowicki, A.; Roucoux, A.; Philippot, K.; Chaudret, B.; Hemati, M., Model arenes hydrogenation with silica-supported rhodium nanoparticles: The role of the silica grains and of the solvent on catalytic activities. *Catal. Commun.* **2009,** *10*, 1235–1239.

(24) Barthe, L.; Hemati, M.; Philippot, K.; Chaudret, B.; Denicourt-nowicki, A.; Roucoux, A., Rhodium colloidal suspension deposition on porous silica particles by dry impregnation: Study of the influence of the reaction conditions on nanoparticles location and dispersion and catalytic reactivity. *Chem. Eng. J.* **2009,** *151*, 372–379.

(25) Pan, H.-B.; Wai, C. M., Sonochemical One-Pot Synthesis of Carbon Nanotube-Supported Rhodium Nanoparticles for Room-Temperature Hydrogenation of Arenes. *J. Phys. Chem. C* **2009,** *113*, 19782–19788.

(26) Pélisson, C.-H.; Vono, L. L. R.; Hubert, C.; Denicourt-Nowicki, A.; Rossi, L. M.; Roucoux, A., Moving from surfactant-stabilized aqueous rhodium (0) colloidal suspension to heterogeneous magnetite-supported rhodium nanocatalysts: Synthesis, characterization and catalytic performance in hydrogenation reactions. *Catal. Today* **2012,** *1*, 124–129.

(27) Song, L.; Li, X.; Wang, H.; Wu, H.; Wu, P., Ru Nanoparticles Entrapped in Mesopolymers for Efficient Liquid-phase Hydrogenation of Unsaturated Compounds. *Catal. Lett.* **2009,** *133*, 63–69.

(28) Zhou, X.; Wu, T.; Hu, B.; Jiang, T.; Han, B., Ru nanoparticles stabilized by poly(N-vinyl-2-pyrrolidone) grafted onto silica: Very active and stable catalysts for hydrogenation of aromatics. *J. Mol. Catal. A: Chem.* **2009,** *306*, 143–148.

(29) Jahjah, M.; Kihn, Y.; Teuma, E.; Gomez, M., Ruthenium nanoparticles supported on multi-walled carbon nanotubes: Highly effective catalytic system for hydrogenation processes. *J. Mol. Catal. A: Chem.* **2010,** *332*, 106–112.

(30) Fang, M.; Machalaba, N.; Sanchez-Delgado, R. A., Hydrogenation of arenes and N-heteroaromatic compounds over ruthenium nanoparticles on poly(4-vinylpyridine): a versatile catalyst operating by a substrate-dependent dual site mechanism. *Dalton Trans.* **2011,** *40*, 10621–10632.

(31) Hubert, C.; Bile, E. G.; Denicourt-Nowicki, A.; Roucoux, A., Rh(0) colloids supported on TiO2: a highly active and pertinent tandem in neat water for the hydrogenation of aromatics. *Green Chem.* **2011,** *13*, 1766–1771.

(32) Zahmakiran, M.; Tonbul, Y.; Ozkar, S., Ruthenium(0) Nanoclusters Stabilized by a Nanozeolite Framework: Isolable, Reusable, and Green Catalyst for the Hydrogenation of Neat Aromatics under Mild Conditions with the Unprecedented Catalytic Activity and Lifetime. *J. Am. Chem. Soc.* **2010,** *132*, 6541–6549.

(33) Nowicki, A.; Zhang, Y.; Leger, B.; Rolland, J.-P.; Bricout, H.; Monflier, E.; Roucoux, A., Supramolecular shuttle and protective agent: a multiple role of methylated cyclodextrins in the chemoselective hydrogenation of benzene

derivatives with ruthenium nanoparticles. *Chem. Commun. (Cambridge, U. K.)* **2006**, 296–298.

(34) Nowicki, A.; Le Boulaire, V.; Roucoux, A., Nanoheterogeneous Catalytic Hydrogenation of Arenes: Evaluation of the Surfactant-Stabilized Aqueous Ruthenium(0) Colloidal Suspension. *Adv. Synth. Catal.* **2007,** *349,* 2326–2330.

(35) Stanley, J. N. G.; Worthington, K.; Heinroth, F.; Masters, A. F.; Maschmeyer, T., Designing nanoscopic, fluxional bimetallic Pt-Ru alloy hydrogenation catalysts for improved sulfur tolerance. *Catal. Today* **2011,** *178,* 164–171.

(36) Bartholomew, C. H.; Agrawal, P. K.; Katzer, J. R., Sulfur poisoning of metals. *Adv. Catal.* **1982,** *31*, 135–242.

(37) Rodriguez, J. A., The chemical properties of bimetallic surfaces: Importance of ensemble and electronic effects in the adsorption of sulfur and SO_2. *Prog. Surf. Sci.* **2006,** *81*, 141–189.

(38) Frety, R.; Da Silva, P. N.; Guenin, M., Iridium supported catalysts. variation of sulfur coverage with the nature of the carrier. *Catal. Lett.* **1989,** *3*, 9–16.

(39) Frety, R.; Da Silva, P. N.; Guenin, M., Supported iridium catalysts: Comparison between resistance to sulphur poisoning and hydrodesulphurization properties. *Appl. Catal.* **1990,** *57*, 99–103.

(40) Marécot, P.; Mahoungou, J. R.; Barbier, J., Benzene hydrogenation on platinum and iridium catalysts. Variation of the toxicity of sulfur with the nature of the support. *Appl. Catal., A* **1993,** *101,* 143–149.

(41) Hoyos, L. J.; Primet, M.; Praliaud, H., Sulfur poisoning and regeneration of palladium-based catalysts. 1. Dehydrogenation of cyclohexane on

palladium/aluminum and palladium/silica-alumina catalysts. *J. Chem. Soc. Faraday T.* **1992,** *88*, 113–19.

(42) Stanislaus, A.; Cooper, B. H., Aromatic hydrogenation catalysis: a review. *Catal. Rev. - Sci. Eng.* **1994,** *36*, 75–123.

(43) Cooper, B. H.; Donnis, B. B. L., Aromatic saturation of distillates: an overview. *Appl. Catal., A* **1996,** *137*, 203–23.

(44) Yasuda, H.; Yoshimura, Y., Hydrogenation of Tetralin over zeolite-supported Pd-Pt catalysts in the presence of dibenzothiophene. *Catal. Lett.* **1997,** *46*, 43–48.

(45) Sachtler, W. M. H.; Stakheev, A. Y., Electron-deficient palladium clusters and bifunctional sites in zeolites. *Catal. Today* **1992,** *12*, 283–295.

(46) Kong, H.; Zhou, M.; Lin, G.-D.; Zhang, H.-B., Pt Catalyst Supported on Multi-Walled Carbon Nanotubes for Hydrogenation-Dearomatization of Toluene and Tetralin. *Catal. Lett.* **2010,** *135*, 83–90.

(47) Simons, C.; Hanefeld, U.; Arends, I. W. C. E.; Sheldon, R. A.; Maschmeyer, T., Noncovalent Anchoring of Asymmetric Hydrogenation Catalysis on a New Mesoporous Aluminosilicate: Application and Solvent Effects. *Chem.--Eur. J.* **2004,** *10*, 5829–5835.

(48) Lewis, D. J.; Day, T. M.; MacPherson, J. V.; Pikramenou, Z., Luminescent nanobeads: attachment of surface reactive Eu(III) complexes to gold nanoparticles. *Chem. Commun. (Cambridge, U. K.)* **2006**, 1433–1435.

(49) Neves, I. C.; Botelho, G.; Machado, A. V.; Rebelo, P.; Ramoa, S.; Pereira, M. F. R.; Ramanathan, A.; Pescarmona, P., Feedstock recycling of polyethylene over AlTUD-1 mesoporous catalyst. *Polym. Degrad. Stab.* **2007,** *92*, 1513–1519.

(50) Sine, G.; Duo, I.; El, R. B.; Foti, G.; Comninellis, C., Deposition of clusters and nanoparticles onto boron-doped diamond electrodes for electrocatalysis. *J. Appl. Electrochem.* **2006,** *36*, 847–862.

(51) Swanson, H. E.; Tatge, E., Standard X-ray diffraction powder patterns. *Natl. Bur. Stand. Circ. (U. S.)* **1953,** *539*, 95 pp.

(52) Swanson, H. E.; Gilfrich, N. T.; Ugrinic, G. M., Standard X-ray diffraction powder patterns. *Natl. Bur. Stand. Circ. (U. S.)* **1955,** *5*, 75 pp.

(53) Redel, E.; Kraemer, J.; Thomann, R.; Janiak, C., Synthesis of Co, Rh and Ir nanoparticles from metal carbonyls in ionic liquids and their use as biphasic liquid-liquid hydrogenation nanocatalysts for cyclohexene. *J. Organomet. Chem.* **2009,** *694*, 1069–1075.

(54) Somorjai, G. A., *Introduction to Surface Chemistry and Catalysis*. Wiley: New York, 1994.

(55) Rodriguez, J. A.; Goodman, D. W., High-pressure catalytic reactions over single-crystal metal surfaces. *Surf. Sci. Rep.* **1991,** *14*, 1–107.

(56) Rodriguez, J. A.; Hrbek, J., Interaction of sulfur with well-defined metal and oxide surfaces: Unraveling the mysteries behind catalyst poisoning and desulfurization. *Acc. Chem. Res.* **1999,** *32*, 719–728.

Chapter 5: Reactions of *p*-Coumaryl Alcohol Model Compounds with Dimethyl Carbonate. Towards the Upgrading of Lignin Building Blocks.

This chapter was published in *Green Chemistry*.

Stanley, J.N.G.; Selva M.; Masters, A.F.; Maschmeyer, T.; Perosa, A., *Green Chem.* **2013**, *15*, 3195–3204.

5.1 Introduction

As the availability and security of organic fossil resources dwindle, and environmental concerns regarding emissions from the combustion of fossil fuels continue to grow, the percentage of chemicals and fuels obtained from renewable sources, such as lignocellulosic biomass, can be expected to rise. Lignocellulose, which is more evenly distributed geographically than fossil resources,[1,vi] is comprised mainly of cellulose, hemicellulose, and lignin, with lignin generally comprising 15–30% by weight and 40% by energy content. Synthetic approaches for the conversion of lignin to chemicals are not as well developed as for the cellulosic components, which is partly due to the recalcitrant nature of lignin that gives plants some of their strength.[2] However, the unique structure of lignin as an amorphous, highly substituted, aromatic polymer, makes it particularly valuable as a potential source for a variety of chemicals, especially as it is the major bio-based source of aromatics.[3] Much effort is devoted to the development of new chemical technology to process lignin streams into higher value-added compounds. Aggressive depolymerisation of lignin yields BTX (benzene, toluene, xylene) chemicals, plus phenol and aliphatics that can all be used in conventional chemical processes. Selective depolymerisation could instead yield monomeric lignin aromatics, not accessible by traditional petrochemistry. Sources of this kind of monomeric lignin include pretreatment streams, such as those from the pulp and paper industries (Kraft and Sulfite pulping), as well as new feedstock streams from biorefinery schemes (*e.g.* organosolv, steam explosion, pyrolysis, ammonia fibre explosion, hot water, and dilute acid, *etc*.).[3, 4] The products consist of lignin with a molecular weight that ranges from 50,000–20,000 for lignosulfonate from sulfite pulping, to 2,000–3,000 in Kraft liquors, to under 1,000 for organosolv. These fractions consist of monomeric lignin molecules based on C9

[vi] References for Chapter 5 begin on page 152.

phenylpropenyl units with an average number of C, H and O atoms of approximately 9, 6–9, and 2.5, respectively. The molecular complexity of these monomeric streams has prompted the use of simpler low molecular weight lignin model compounds to aid their investigation. It has been recognised that many of the products derived from the disruption of various lignin linkages resemble *p*-coumaryl-, coniferyl-, and sinapyl alcohol (Figure 5.1), and effort has been placed on the conversion of these models to other target chemicals by exploiting their functionality.

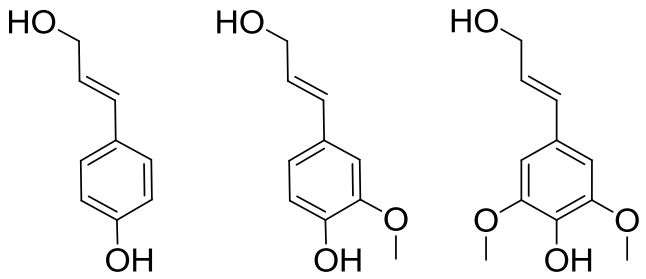

Figure 5.1 *p*-Coumaryl alcohol, coniferyl alcohol, and sinapyl alcohol.

Such an approach, however, poses the issue of the overabundance of targets that can potentially be produced. The experience of the chemical industry shows that this complexity is best handled by using broad-based technologies (selective reductions and oxidations, bond making/breaking processes, catalysis, *etc*.) to produce multiple outputs,[5] as opposed to a 'like-for-like' target-based approach aimed at replacing well-established chemicals produced from fossil feedstocks.[6, 7]

A curiosity driven broad-based strategy was, therefore, in our opinion a constructive approach towards the development of new chemistry and, in the longer term, a plethora of new chemicals. Some products are already in commercial use by the chemical

industry, making them interesting in the short term, while others might be structural building blocks that enable new products/applications.[3]

For the present study we focused our attention on two compounds resembling *p*-coumaryl alcohol: cinnamyl alcohol **1**, and 4-(3-hydroxypropyl)phenol **2**. These compounds were chosen because they not only have -OH groups that closely resemble the ones present in *p*-coumaryl alcohol, but they are also readily available in the pure form, and their derivatives are easily identifiable by standard analytical techniques.

Dimethylcarbonate (DMC) is an excellent reagent and solvent for the upgrading of these compounds with lignin chemical functionalities, especially when viewed from a 'green' perspective. DMC is a good alternative to traditional methylating agents such as harmful dimethylsulfate and methyl halides,[8] while the only by-products obtained during methylation reactions are carbon dioxide and methanol. The latter can, in principle, be recycled to form DMC.[9, 10] Furthermore, DMC is one of six organic carbonates that have been identified as especially useful green solvents.[11] Thus, we propose to develop chemistry with compounds that model lignin functional groups by combining their use with a green methylating agent and solvent.

A further advantage of DMC is that its reactivity can be tuned for a variety of nucleophiles.[12–19] Of particular relevance to the reactivity of *p*-coumaryl model compounds investigated in the present case, is the tuneable selectivity of DMC towards aromatic and aliphatic OH groups, depending on the catalyst and reaction conditions.[13, 18–21] For example, basic catalysts can be used to promote a transesterification process, that is an equilibrium reaction, to form methyl alkyl carbonates, while weak bases or alkali metal-exchanged faujasites can be used to form methyl ethers irreversibly (Scheme 5.1). Furthermore, the methoxycarbonylating *vs* methylating selectivity of DMC can also be

tuned by changing the reaction conditions,[22] while basic catalysed methylation could also occur on aromatic OH groups.

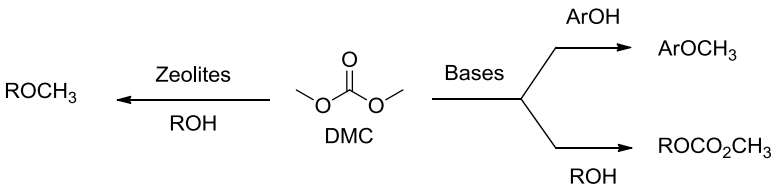

Scheme 5.1

The main focus of this work was to assess greener and easily accessible synthetic procedures for the transformation of cinnamyl alcohol **1**, and 4-(3-hydroxypropyl)phenol **2**, with DMC. This was performed by investigating range of catalysts, including solid K_2CO_3, $CsF/\alpha Al_2O_3$, NaX, NaY and an ionic liquid (IL) $[P_{8881}][CH_3OCOO]$, for the methylation and transesterification of the target compounds used as models of *p*-coumaryl alcohol. Cinnamyl alcohol, **1**, was chosen as it contains a propylene side chain with a terminal OH, which is a common feature in many lignin streams.[23] Likewise, 4-(3-hydroxypropyl)phenol **2,** was chosen as a compound to model lignin functionalities as it has both an aliphatic OH on a propyl side chain, as well as a phenolic OH in the *para* position. The focus of this study lies on screening the product selectivity associated with different catalyst types and reaction conditions. Our interest was therefore focused on understanding the reactivity trends of DMC with the different OH groups, the relevant reaction equilibria, and the reaction pathways. A thorough understanding of these types of reactivities is of fundamental importance for the development of new greener processes aimed at transforming phenolic streams derived from lignin into higher value bio-based chemicals. Thus, we report that the selectivity of methylation/decarboxylation on the

aliphatic and phenolic OH sites of these compounds in the presence of DMC can be tuned by changing the catalyst and/or reaction temperature. A range of products was observed of which four are highlighted, as they could be obtained selectively and isolated in good yields: cinnamyl methyl carbonate (**1a**, Scheme 5.2), cinnamyl methyl ether (**1b**, Scheme 5.2), 3-(4-hydroxyphenyl)propyl methyl carbonate (**2c**, Scheme 5.4), and 3-(4-methoxyphenyl)propyl methyl carbonate (**2d**, Scheme 5.4).

5.2 Results

5.2.1 Cinnamyl Alcohol, 1

The reaction of DMC with cinnamyl alcohol, **1**, was investigated first at 90 °C and then at 165 and 180 °C. In both cases a solution of **1** (0.3 g, 1.9 mmol) in DMC (0.36 mol, 30 mL; DMC serving both as a reagent and solvent) was set to react in the presence of different catalysts: K_2CO_3, $CsF/\alpha Al_2O_3$, NaX, NaY, or $[P_{8881}][CH_3OCOO]$ (the weight ratio (*Q*) of solid catalyst: substrate was 3:1; the molar ratio $[P_{8881}][CH_3OCOO]$:**1** was 0.05:1). The reaction conditions for the solid catalysts in particular were chosen based on previously reported experimental conditions.[18, 24] The weight ratios were not optimised. The progress of the reactions was followed by GC-MS. When operating at 90 °C all reactions were carried out in glassware under atmospheric conditions. When operating at 165 and 180 °C a stainless steel autoclave was used and the mixture was flushed with N_2.

The study was aimed at understanding the effect of different catalysts and temperatures on the conversion of **1**, in terms of its extent and the relative selectivities achievable.

Three main compounds were observed, isolated, and characterised by GC-MS and ^{1}H NMR (**1a**, **1b**, and **1c**, Scheme 5.2). Unidentified by-products amounted to ≤ 17%. The results are listed in Table 5.1 (90 °C) and Table 5.2 (165–180 °C).

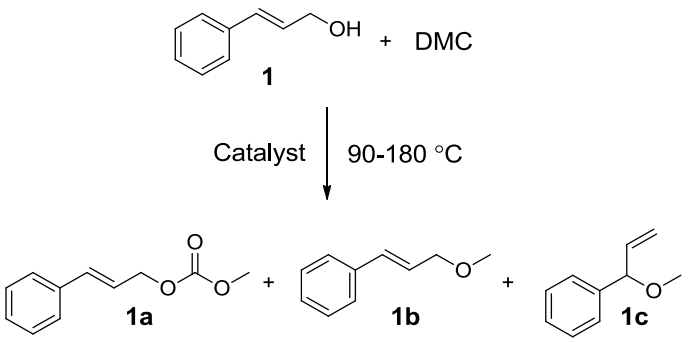

Scheme 5.2

Table 5.1 The reaction of DMC with **1** at 90 °C in the presence of K_2CO_3, $[P_{8881}][CH_3OCOO]$, NaX and NaY

Entry	Catalyst	Q^a (wt : wt) or mol:mol (IL)	Time^b / h	Conv. / %	GC-MS Selectivity / %		
					1a	**1b**	Others^d
1	K_2CO_3	3	96	91	90	2	8
2	$[P_{8881}][CH_3OCOO]$	0.05	5.5	89	90	4	6
3	$CsF/\alpha Al_2O_3$	3	50	94	81	3	17
4	NaX	3	24^c	0	-	-	-
5	NaY	3	24^c	0	-	-	-

^{a} *Q* is the weight (or molar) ratio between catalyst and substrate. ^{b} Time to reach equilibrium. ^{c} Time reaction stopped. ^{d} Others: unidentified by-products detected by GC-MS analyses.

Table 5.2 The reaction of DMC with **1** at 165–180 °C in the presence of K_2CO_3, $[P_{8881}][CH_3OCOO]$, NaX and NaY[a]

Entry	Catalyst	Q^b (wt : wt) or mol:mol (IL)	Temp / °C	Conv. / %	GC-MS Selectivity / %			
					1a	**1b**	**1c**	Others[c]
1	K_2CO_3	3	165	98	82	10	3	4
2	$[P_{8881}][CH_3OCOO]$	0.05	165	71	86	5	1	8
3	NaY	3	165	51	4	70	21	5
4	NaX	3	165	85	29	45	21	6
5	NaY	3	180	100	-	91	8	2
6	NaX	3	180	100	-	56	39	5

[a] All reactions lasted 3 h. [b] *Q* is the weight (or molar) ratio between catalyst and substrate. [c] Others: unidentified by-products detected by GC-MS analyses.

For the reaction catalysed by $CsF/\alpha Al_2O_3$ at 90 °C, a typical plot of the conversion of **1** as a function of time is shown in Figure 5.2. In the case of K_2CO_3, $[P_{8881}][CH_3OCOO]$, and $CsF/\alpha Al_2O_3$ (Table 5.1, entries 1–3; Figure 5.2), the reaction proceeded with high conversion (89–94%) and good selectivity (81–90%) towards the transesterification product, cinnamyl methyl carbonate (**1a**), with only traces of cinnamyl methyl ether (**1b**). The transesterification equilibrium was achieved in 5.5 h to 96 h, for $[P_{8881}][CH_3OCOO]$ and K_2CO_3, respectively. As shown in Figure 5.2 for $CsF/\alpha Al_2O_3$, equilibrium was achieved in 50 h. Isolated yields of 80–81% were reached for product **1a**. In the case of the reaction with K_2CO_3 (entry 1, Table 5.1), **1a** could be isolated in 95% purity (^{1}H NMR) simply by the removal of the solid catalyst by filtration, and of excess DMC by rotary evaporation. In the case of the reaction with $[P_{8881}][CH_3OCOO]$, **1a** was isolated by flash column chromatography on silica gel eluting with a mixture of petroleum ether / diethyl ether (50:50 v/v) as the eluant. No attempts to optimise product isolation were performed as this was beyond the scope of the work. No conversion of **1** was observed after 24 h for either of the NaX or NaY catalysts at 90 °C.

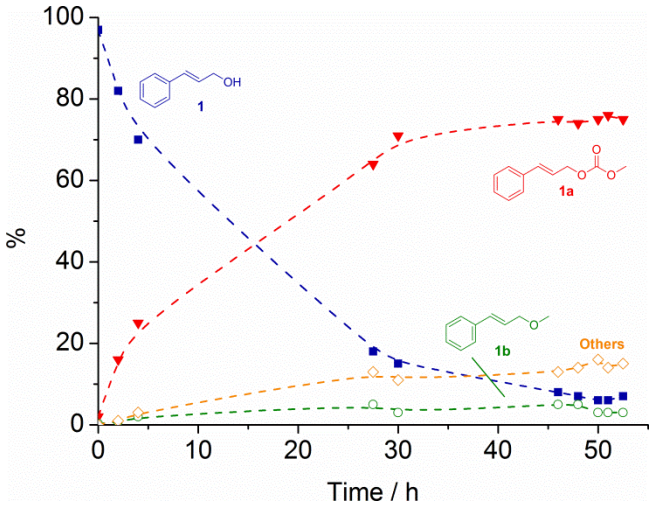

Figure 5.2 Plot of the conversion of **1** (■), and formation of **1a** (▼), **1b** (○), and unidentified by-products (◊) at 90 °C in the presence of $CsF/\alpha Al_2O_3$. Broken lines as visual guide only.

The higher temperature regime of 165–180 °C was also investigated using K_2CO_3, $[P_{8881}][CH_3OCOO]$, NaX and NaY as catalysts in an autoclave. The reaction time was 3 h. In addition to products **1a** and **1b**, 3-methoxy-3-phenylpropene, **1c**, was observed (Scheme 5.1). The results are listed in Table 5.2.

Just as was observed at 90 °C, **1a** was the major product in the presence of K_2CO_3 and $[P_{8881}][CH_3OCOO]$ at 165 °C. However, bearing in mind the different reaction times: i) the selectivity to **1a** decreased from 90% (90 °C), to 82–86% at 165 °C; ii) in the presence of K_2CO_3, the conversion increased to 98% at 165 °C, compared to 91% at 90 °C; iii) instead, at the same temperatures, in the presence of $[P_{8881}][CH_3OCOO]$, the conversion decreased from 89% to 71%.

At 165 °C NaY and NaX prompted conversion (51% and 85% for NaY and NaX, respectively) mainly to **1b** with 70% selectivity in the presence of NaY and with 45% selectivity in the presence of NaX. A minor product, 3-methoxy-3-phenylpropene, **1c**, was

also observed. The transesterification product, **1a**, was only obtained with 4% and 29% selectivity with NaY and NaX, respectively.

To reach quantitative conversion in the presence of both NaY and NaX it was sufficient to increase the temperature to 180 °C. In the presence of NaY, the major product, **1b**, could be obtained with 91% selectivity and 64% isolated yield (by flash column chromatography). The minor product, **1c**, was also observed with 8% selectivity. In the presence of NaX, the selectivity towards the major product, **1b**, decreased to 56% due to the sizable amounts of the co-product, **1c**, (38%). The different selectivities of the two zeolites towards **1a** prompted us to consider as a cause an *in-situ* decarboxylation reaction of **1a** to **1b**. To corroborate such an hypothesis, cinnamyl methyl carbonate, **1a**, (entry 1, Table 5.1) was heated in the presence of NaY under conditions identical to those reported in entry 5, Table 5.2, with the solvent changed from DMC to dimethoxyethane (DME). In this case, **1b** was the sole observed product (Scheme 5.3).

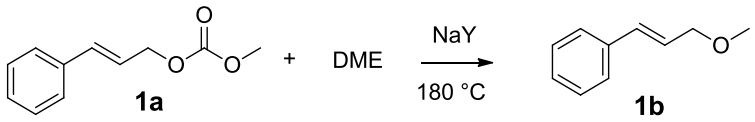

Scheme 5.3

In consideration of the relatively large quantity of zeolites used it is desirable that the catalyst be recyclable. Thus, a series of zeolite recycling experiments was carried out. Once the experiment of entry 3 in Table 5.2 completed, the solid NaY zeolite was filtered, washed with diethyl ether, and dried at 70 °C under vacuum overnight. The recovered NaY was then used to repeat the reaction, under identical conditions to those reported above

(entry 3, Table 5.2), and the results are reported in Figure 5.3 (Run 1). The recovery/reaction cycle was repeated once more. Both runs 1 and 2 showed a significant drop in the catalyst performance: after 2 runs the conversion of **1** and the selectivity to **1b** decreased to 26 and 61%, respectively. However, if the used zeolite was re-calcined (400 °C, ramp rate 5 °C min^{-1}) and used in another reaction, the catalytic activity was restored (Run 3). To probe the recyclability of the zeolite further, an additional recovery/reaction cycle was performed, followed by another re-calcination/reaction sequence. As expected, the conversion dropped in the reaction where the catalyst was simply dried under vacuum (Run 4, Figure 5.3), while the activity was restored after the second re-calcination (Run 5).

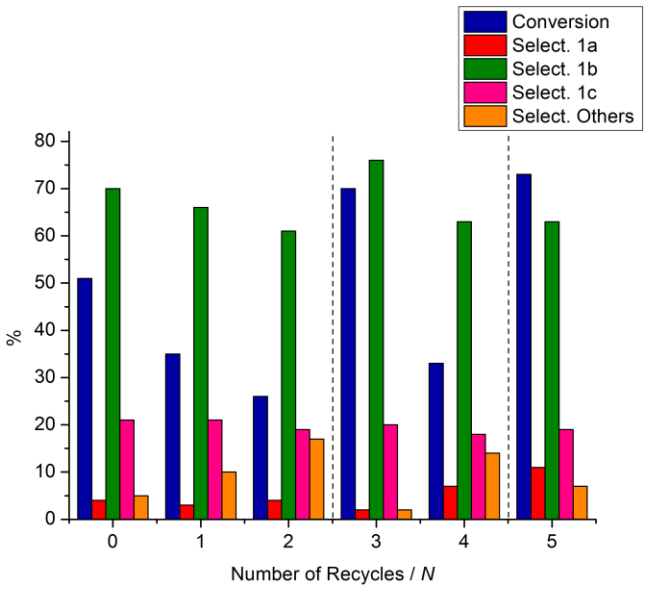

Figure 5.3 The recycling of NaY. All reactions are carried out at 165 °C for 3 h.

5.2.2 4-(3-Hydroxypropyl)phenol, 2

The reaction of 4-(3-hydroxypropyl)phenol, **2**, with DMC was tested under reaction conditions analogous to those described above, first at 90 °C at atmospheric pressure, and then at 165 and 180 °C in an autoclave under N_2. A solution of **2** (0.3 g, 1.9 mmol) in DMC (0.36 mol, 30 mL) was prepared to react in the presence of different catalysts: K_2CO_3, CsF/αAl_2O_3, NaX, NaY or $[P_{8881}][CH_3OCOO]$ (the weight ratio (*Q*) of solid catalyst : substrate was 3:1; the molar ratio $[P_{8881}][CH_3OCOO]$:**2** was 0.05:1). Here, too, the reaction conditions were chosen based on previous experience,[13, 19] and the weight ratios were not optimised.[18, 19] As with cinnamyl alcohol, **1**, the study was aimed at understanding the effect on the conversion of **2** of different catalysts at different temperatures, and on controlling product selectivity. Five main products were observed, isolated, and characterised by GC-MS and ^{1}H NMR (**2a**, **2b**, **2c**, **2d**, and **2e**, Scheme 5.4). The new product, **2d**, and the product, **2b**, for which there was no previously reported NMR data, were also characterised by ^{13}C NMR. Other unidentified by-products (≤ 8% total yield, by GC-MS) were also detected. The results are listed in Table 5.3 and Table 5.4, and in Figure 5.4.

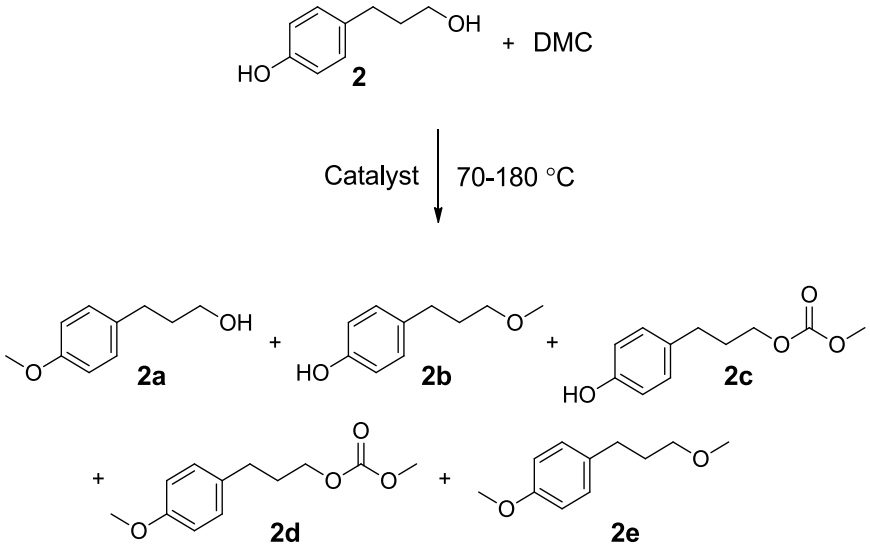

Scheme 5.4

Table 5.3 The reaction of DMC with **2** at 70–90 °C in the presence of different catalysts.

Entry	Catalyst	Q^a (wt : wt) or mol:mol (IL)	Temp / °C	Time[b] / h	Conv. / %	GC-MS Selectivity / %			
						2a	**2c**	**2d**	Others[f]
1	K_2CO_3	3	90	74	97	-	89	4	7
2	$[P_{8881}][CH_3OCOO]$	0.05	90	150[e]	97	-	72	23	4
3	$CsF/\alpha Al_2O_3$	3	90	18[c]	96	-	83	13	4
4	NaY	3	90	240[e]	14	5	95	0	0
5	NaX	3	90	240[e]	53	42	36	13	8
6	$CsF/\alpha Al_2O_3$	3	70	119[d]	95	-	94	5	1

[a] *Q* is the weight(or molar) ratio between catalyst and substrate. [b] Time to reach equilibrium. [c] Non-optimised time. Equilibrium reached between 3–18 h.

[d] Non-optimised time. Equilibrium reached between 55–119 h. [e] Time reaction stopped. [f] Others: unidentified by-products detected by GC-MS analyses.

Table 5.4 The reaction of DMC with **2** at 165–180 °C in the presence of K_2CO_3, $[P_{8881}][CH_3OCOO]$, NaX and NaY[a.]

Entry	Catalyst	Q^b (wt:wt)or mol:mol (IL)	Temp / °C	Conv. / %	GC-MS Selectivity / %					
					2a	**2b**	**2c**	**2d**	**2e**	Others [c]
1	K_2CO_3	3	165	99	0	-	60	38	-	2
2	$[P_{8881}][CH_3OCOO]$	0.05	165	95	2	-	62	32	-	4
3	NaY	3	165	48	8	11	77	3	-	0
4	NaX	3	165	100	3	4	5	78	10	0
5	NaY	3	180	80	2	14	76	6	-	1
6	NaX	3	180	100	1	17	2	65	12	3

[a] All reactions lasted 3 h. [b] *Q* is the weight(or molar) ratio between catalyst and substrate. [c] Others: unidentified by-products detected by GC-MS analyses.

At 90 °C, in the presence of K_2CO_3, $[P_{8881}][CH_3OCOO]$, and $CsF/\alpha Al_2O_3$, the main reaction was the transesterification of the aliphatic OH of **2** with DMC, which yielded 3-(4-hydroxyphenyl)propyl methyl carbonate, **2c**, (entries 1–3, Table 5.3). With K_2CO_3 and $CsF/\alpha Al_2O_3$ as catalysts conversions of **2** and selectivities to **2c** were 96–97% and 83–89%, achieved after 74 h or 18 h, respectively (entries 1 and 3, Table 5.3). An experiment to improve selectivity using $CsF/\alpha Al_2O_3$ was conducted at lower temperature (70 °C, entry 6, Table 5.3). In this case, notwithstanding a longer reaction time (119 h *vs* 18 h @ 90 °C), the selectivity to product **2c** increased up to 94% (by GC-MS). The product **2c** could be isolated with yields up to 72%.

Different behaviour was observed in the case of $[P_{8881}][CH_3OCOO]$. Initially, the conversion to **2c** reached a maximum of 74% at 49 h, and then dropped to 67% after 150 h due to the formation of **2d** that increased from 16% to 26%, as shown in Figure 5.4.

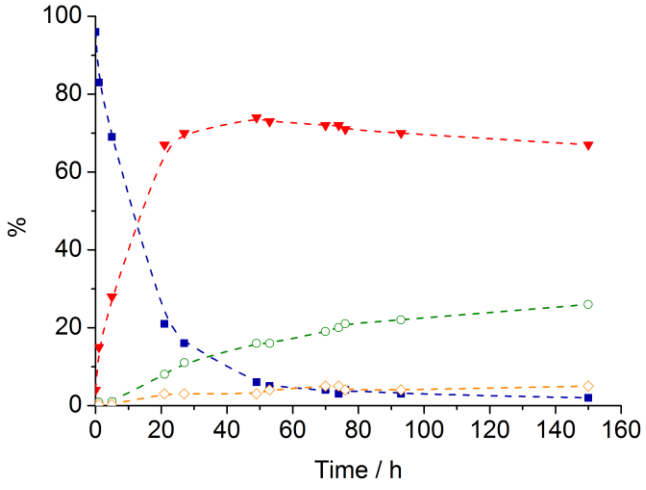

Figure 5.4 Plot of the conversion of **2** (■), and formation of **2c** (▼), **2d** (○), and unidentified by-products (◊) at 90 °C in the presence of $[P_{8881}][CH_3OCOO]$. Broken lines as visual guide only.

In the presence of NaY and NaX (entries 4–5, Table 5.3), low conversions (14 and 53% respectively) were obtained even after extended reaction times. The transesterification compound, **2c**, was again the major product of the reaction catalysed by NaY. In contrast, in the presence of NaX methylation occurred predominantly on the aromatic OH group to form **2a**, while low conversion to the transesterification products **2c** and **2d** was observed after longer reaction times.

The investigation was then performed at 165–180 °C, conditions as per above. In addition to **2a**, **2c** and **2d**, methyl ethers **2b** and **2e** were also observed (Scheme 5.4). The results are listed in Table 5.4.

At 165 °C, in the presence of K_2CO_3 and $[P_{8881}][CH_3OCOO]$, conversion was similar to that at 90 °C (again, bearing in mind the different reaction times); however, the product distributions were remarkably different: the selectivity towards **2c** dropped because of the formation of **2d**. The ratio **2c**:**2d** was in the range of 1.5–1.8 (entries 1 and 2, Table 5.4). It should be noted that product **2d** had not been previously reported in the literature.

With NaY and NaX as catalysts two distinct product distributions were observed. NaY yielded **2c** both at 165 °C and at 180 °C, with 48% and 80% conversion and with selectivities of 77% and 76%, respectively. On the other hand, NaX achieved 100% conversion with **2d** the major product both at 165 and 180 °C. The fully methylated product **2e**, was also present with yields of 10–12% after 3 h. To shed light on the reaction pathway of **2** with DMC in the presence of NaX at 180 °C, a preliminary kinetic profile was collected (Figure 5.5), with samples taken at different reaction times between 10 min and 5 h.

The profile of Figure 5.5 indicated that: i) the proportion of product **2a** reached a maximum of 50% in 30 min, and then dropped to less than 1% within 4 h; ii) similarly, the proportion of product **2c** went up to a maximum of 12% in 1 h, and then decreased as the reaction proceeded further; iii) the proportion of product **2d** reached 80% after 120 min, and remained steady for the next 3 hours; iv) the proportion of product **2b** remained low, reaching a maximum of 3% within 3 h and then decreasing as the reaction proceeded; and v) the proportion of product **2e** increased with time, and reached a selectivity of 16% in 5 h.

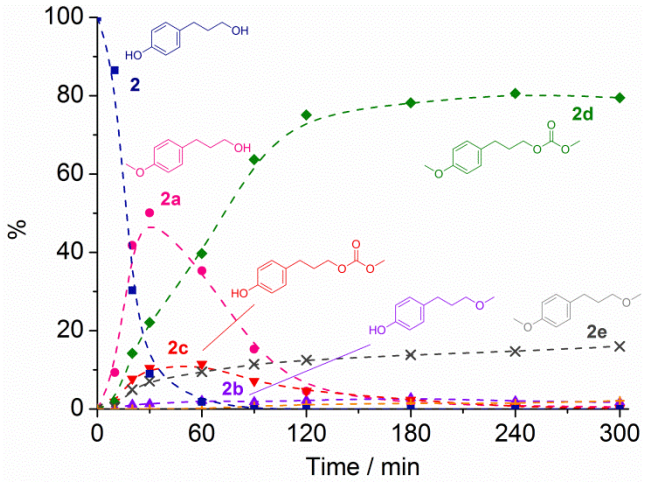

Figure 5.5 Plot of the conversion of **2** (■) and formation of **2a** (●), **2b** (▲), **2c** (▼), **2d** (♦), **2e** (×), and unidentified by-products (+) at 180 °C in the presence of NaX. Broken lines as visual guide only.

Although the concentration of **2d** appeared to plateau, as shown in Figure 5.5, an additional experiment was performed to determine whether **2d** could react further to give **2e** via an *in-situ* decarboxylation, by analogy to the conversion of **1a** to **1b**. The reaction was performed at 180 °C for 3 h. Pure **2d** was used as a starting material, NaX as a

catalyst, and DME as a solvent in place of DMC. However, in this case **2e** was not formed (Scheme 5.5). Instead, **2a** was obtained as the major product. When an identical reaction was performed with NaX replaced with NaY, no conversion was attained at all.

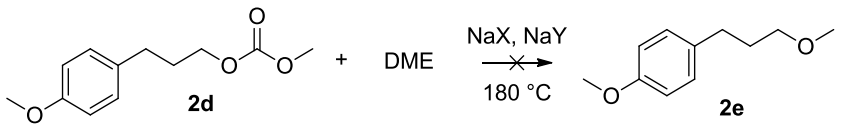

Scheme 5.5

5.3 Discussion

5.3.1 Effect of the different catalysts at 90 °C: selective formation of the carbonates 1a and 2c by transesterification.

The five catalysts tested at 90 °C showed that the reactivity of **1** and **2** with DMC followed trends that could be rationalised based on the previous knowledge of base-catalysed reactions of DMC with hydroxyl-containing substrates. In particular, basic catalysts such as K_2CO_3, $CsF/\alpha Al_2O_3$, and $[P_{8881}][CH_3OCOO]$ at this lower temperature, prompted a selective equilibrium reaction of **1** and **2** to yield the transesterification products at the aliphatic OH: **1a** and **2c**. Selectivity towards the transesterification product **2c** with $CsF/\alpha Al_2O_3$ could be improved by lowering the temperature and increasing reaction times. This was consistent with previous investigations of reactions of dialkyl carbonates with alcohols in the presence of basic catalysts.[24–26] The aromatic hydroxyl group of **2** remained relatively inert, except with $[P_{8881}][CH_3OCOO]$. In this case, after reaching a maximum of 74% selectivity towards **2c**, the reaction progressed further in favour of the product **2d** showing that this catalyst promoted the methylation of the phenolic OH. This higher

reactivity of $[P_{8881}][CH_3OCOO]$ for methylation on the phenolic OH occurred notwithstanding the lower catalyst loadings (5% mol), compared to the other solid catalysts used in up to 3 weight excess over the substrate. This behaviour was in analogy to our recently reported results on the IL-catalysed transesterification of alcohols with dialkylcarbonates.[24] No attempts were made here to recycle K_2CO_3, as this is an already established option.[7]

The NaX and NaY solid zeolite catalysts are also basic, but less so than K_2CO_3, $CsF/\alpha Al_2O_3$ and $[P_{8881}][CH_3OCOO]$, and this probably accounts for the observation that at 90 °C no conversion was observed in 24 h for the reaction of DMC with **1**, and that low conversion was observed for the reaction with **2** after extended reaction periods. Albeit with low conversion, in the presence of NaX, **2a** was formed, followed by a separate transesterification step to form **2c**. This result was opposite to that observed previously by us in the reaction of DMC with hydroxybenzyl alcohols catalysed by X and Y-faujasites.[18] In that case, the benzyl OH group was more prone to methylation than the aromatic OH one. When the reaction of **2** in the presence of NaX at 90 °C was allowed to proceed further, **2d** was also observed. While selectivity in this case was low, these results were in agreement with the mechanistic study undertaken at 180 °C, as described below.

In the presence of NaY at 90 °C, only **2c** was observed at low conversion indicating preferential reaction at the aliphatic OH.

5.3.2 Effect of temperature on catalysis by K_2CO_3 and $[P_{8881}][CH_3OCOO]$.

For the reaction of DMC with cinnamyl alcohol, **1**, there was no benefit with increasing the temperature from 90 °C to 165 °C. While conversion increased in the presence of K_2CO_3 despite the shorter reaction time (entry 1, Table 5.1 and entry 1, Table 5.2),

selectivity to the transesterification product **1a** decreased with temperature in favour of the methyl derivative **1b** and of compound **1c**. This selectivity was in agreement with the occurrence of a decarboxylation process as reported for high temperature reactions of dialkyl carbonates over faujasite catalysts (see also the next paragraph).[20] Conversion decreased in the presence of $[P_{8881}][CH_3OCOO]$ (entry 2, Table 5.1 and entry 2, Table 5.2).

In the reaction of DMC with **2**, there was negligible change in conversion between 90 and 165 °C (although the reactions were performed over different reaction times); however, the selectivity dropped from the sole transesterification reaction product **2c** at 90 °C, to a mixture of **2c** and **2d** at 165 °C, the latter deriving from *O*-methylation competing with transesterification at the higher temperature (entries 1 and 2, Table 5.3 and entries 1 and 2, Table 5.4). Hardly any conversion to the products **2a**, **2b**, and **2e** was observed after 3 h.

5.3.3 Effect of the type of zeolite on the reaction of DMC with cinnamyl alcohol 1 at 165–180 °C: selective formation of the methyl ether 1b.

The data reported in Table 5.2 suggest that NaX and NaY exhibit different activities for the reaction of DMC with **1**. Although both zeolites have the same framework, their Si/Al ratio is 1.2 and 2.4 for X and Y zeolites, respectively.[vii] This difference results in a higher abundance of active sites and a higher basicity of NaX compared to NaY, and in our case, the greater abundance of sites may be directly correlated to the higher conversion achieved with NaX.

[vii] For morphological details and other properties of NaY and NaX faujasites, see (*a*) F. Schwochow and L. Puppe, *Angew. Chem., Int. Ed. Engl.*, 1975, **14**, 620; (*b*) G. C. Bond, in *Heterogeneous Catalysis Principles and Applications*, Oxford University Press, New York, USA, 2nd edn, 1987, pp. 104–110; and ref. 27.

As for the selectivity, it also appears to be dependent on the nature of the site: the less basic sites in NaY favour formation of **1b**, while the stronger basic sites of NaX favour **1a**. The product **1c** is also formed preferentially with the more basic NaX catalyst. The result is consistent with the position of NaX in the acid-base scale proposed by Barthomeuf for faujasites,[27, 28] and with our previous findings on the reactivity of indolyl carboxylic acids with DMC in the presence of zeolites.[17] Plausible reaction pathways that account for the formation of **1a**, **1b**, and **1c** are shown in Scheme 5.6.

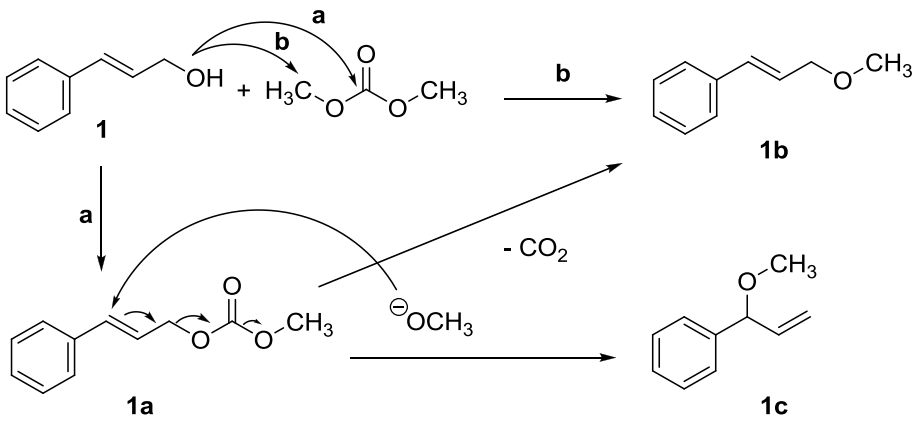

Scheme 5.6

Formation of **1a** can occur only by a carboxymethylation pathway (**a**). The methyl ether **1b**, instead, can be formed either by direct methylation of **1** (path **b**), or by decarboxylation of **1a**.

The lack of **1a** at incomplete conversion in the presence of NaY suggested that pathway (**b**) in Scheme 5.6 could be favoured over pathway (**a**).

The product **1c** could be formed from **1a** by an allyl rearrangement catalysed by methoxide, followed by decarboxylation as indicated in Scheme 5.6. Indirect evidence for

this hypothesis was collected by heating **1a** under the same experimental conditions, but in the absence of DMC as source of methanol, and observing **1b** as the sole product. The lack of **1c** indicated that it was formed only when DMC was present and able to generate methoxide. As **1a** is required for the formation of **1c**, this explanation could also account for the lack of conversion to **1c** in the presence of NaY compared to NaX. We considered it was unnecessary to run a full kinetic profile of the reaction of **1** in the presence of zeolite NaX as this pathway is less complex than the one that applies for **2** (see later), making identification of the intermediates easier.

5.3.4 Recycling Experiments of NaY at 165 °C

Figure 5.3 clearly shows that NaY can be reused for the reaction with **1** with no loss in activity after re-calcination at 400 °C in dry air, or with some loss in conversion after mild thermal treatment (70 °C, under vacuum). Recyclability is desirable as the catalyst is used in quite high amounts (although it is conceivable that the weight ratio could be dropped from $Q = 3$ to $Q = 1.518$). Nonetheless, the drop in conversion in the recycling runs 1, 2, and 4 (Figure 5.3) could be explained by the absorption of water by the zeolite, which could occur during the handling of the catalyst between runs (water is not efficiently removed during the mild thermal treatment), causing hydrolysis of the cinnamyl methyl carbonate intermediate **1a**, back to the starting cinnamyl alcohol. This is consistent with the restoration of the catalytic activity (Runs 3 and 5, Figure 5.3) after the used zeolite was re-calcined (400 °C, ramp rate 5 °C min^{-1}), although some fouling by organic compounds cannot be ruled out. This hydration/fouling of the zeolite could also account for the poorer selectivity after each recycle, particularly as the water could promote other reactions such as hydrolysis. The formation of coke from the initial fouling components could in principle

cause loss of activity after recycle runs, and the subsequent improvement in activity after calcination is also consistent with the removal of any coke. Nonetheless, the zeolite remained white throughout the experiments and the reaction solutions were clear and colourless. Thus, although the formation of undetectable white coke on the catalyst[29] cannot be ruled out, we deem it unlikely that any was formed in the present case. It is interesting to note that the selectivity towards products **1a** and **1c** was otherwise relatively unchanged between the recycling/regeneration runs.

5.3.5 The reaction pathway of 2 in the presence of NaX: formation of carbonate 2d.

Based on the results reported in Table 5.3 and Table 5.4, and Figure 5.5, the sequence for the reaction of DMC with **2** in the presence of NaX could involve three different pathways with two final products, as shown in Scheme 5.7. Methylation could occur first on the phenolic OH, forming **2a**, followed by transesterification at the aliphatic OH to form **2d**. At the same time, transesterification could occur on the aliphatic OH to form **2c**, which then undergoes methylation at the phenolic OH to also form **2d**. These pathways are consistent with the results obtained in the presence of NaX at 90 °C. Simultaneously, at the higher temperature, **2b** could be formed from the methylation of the aliphatic OH, and then undergo methylation at the phenolic OH to form **2e** as the final product.

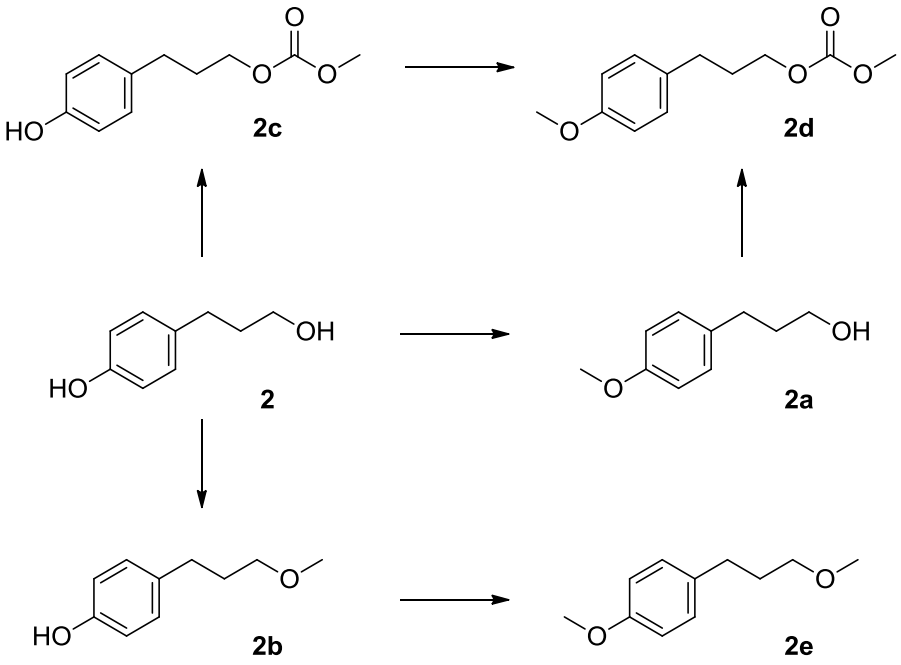

Scheme 5.7

5.3.6 The Formation of 2e

In contrast with the observed formation of **1b** from the *in-situ* decarboxylation of **1a** with NaY (Scheme 5.3), the reaction of **2d** with NaX using DME as solvent (Scheme 5.5) indicates that an *in-situ* decarboxylation of **2d** (or indeed of **2c**) does not occur. The data of Table 5.2 show that at *e.g.* 165 °C (compare entries 3-4) NaY is less active than NaX, but shows a much greater selectivity towards the decarboxylation of **1a** to yield **1b**. Likewise, in the reaction of **2** (Table 5.4), NaY is also less active than NaX. The lower basicity of NaY as compared to NaX originates from a higher Si:Al ratio. This means that fewer active sites are present and that these active sites will be able to interact more strongly with the various electron-rich species during the reaction. Both of these phenomena might lead to lower conversions. The difference in selectivity, however, is most likely due to the less basic sites as they promote decarboxylation over hydrolysis. In the case of **2b** this is even more extreme due to the additional electron-donating methoxy group, which further

strengthens the interactions of the substrates with the zeolite, leading to complete deactivation with NaY.

5.4 Experimental[viii]

5.4.1 General

The following reagents were used as received: 4-(3-hydroxypropyl)phenol, **2**, dimethyl carbonate (DMC), potassium carbonate (K_2CO_3), diethyl ether, and petroleum ether (all Aldrich). Cinnamyl alcohol, **1** (Sigma), was purified by vacuum distillation. Dimethoxyethane (DME, Aldrich) was dried by distillation over sodium and stored under nitrogen. The zeolites NaX and NaY (both Aldrich) were calcined at 400 °C (ramp rate 5 °C min^{-1}) under dry air for 8–14 h immediately before use. $[P_{8881}][CH_3OCOO]$ was prepared according to a method recently reported by us.[19] $CsF/\alpha Al_2O_3$ was also prepared according to the literature.[26]

MS (EI, 70 eV) analyses were run using a HP5/MS capillary column (30 m). ^{1}H NMR spectra were recorded on a 300 MHz spectrometer. ^{13}C NMR spectra were recorded on a 100 MHz spectrometer. $CDCl_3$ was used as solvent. Chemical shifts were reported in δ values downfield from TMS.

5.4.2 General Procedure for Reactions Carried Out in Glassware

A two-necked, 50 mL round bottom glass Quickfit flask, was fitted with a Sura-Seal stopper and condenser, and equipped with a magnetic stirrer. The substrate (cinnamyl

[viii] ^{1}H NMR and MS spectra of all reported compounds and ^{13}C NMR spectra of new compounds can be found in the Supplementary Information contained in Appendix D.

alcohol, **1**, or 4-(3-hydroxypropyl)phenol, **2**, 1.9 mmol), and dimethyl carbonate (0.36 mol, 30 mL) were added to the flask. The mixture was allowed to stir at RT for ~5 min and a sample was taken (~0.1 mL). The catalyst (K_2CO_3, $CsF/\alpha Al_2O_3$, NaX, NaY or $[P_{8881}][CH_3OCOO]$) [the weight ratio (*Q*) of solid catalyst : substrate was 3:1; the molar ratio $[P_{8881}][CH_3OCOO]$: substrate was 0.05:1]) was then added, and the reaction run at 90 °C with stirring at 800 rpm. Samples (~0.1 mL) were taken at regular intervals using a syringe through one arm of the reactor. All samples taken from the reactor were diluted with diethyl ether, either centrifuged to remove the solid catalyst (K_2CO_3, $CsF/\alpha Al_2O_3$, NaX, NaY) or passed over silica gel F60 to remove the ionic liquid catalyst ($[P_{8881}][CH_3OCOO]$), and the progress of the reaction was followed by GC-MS. The reaction was generally run until equilibrium was established (5.5–119 h), as determined by GC-MS.

5.4.3 General Procedure for Reactions Carried out in an Autoclave

A stainless-steel autoclave (120 mL internal volume) was charged with the substrate (cinnamyl alcohol, **1**, or 4-(3-hydroxypropyl)phenol, **2**, 1.9 mmol), dimethyl carbonate (0.36 mol, 30 mL) and the catalyst (K_2CO_3, $[P_{8881}][CH_3OCOO]$, NaX and NaY) [the weight ratio (*Q*) of solid catalyst : substrate was 3:1; the molar ratio $[P_{8881}][CH_3OCOO]$: substrate was 0.05:1]). Before the reaction, the autoclave was purged at RT with N_2 to remove air. The autoclave was then electrically heated to the desired temperature (165–180 °C), with the reaction mixture kept under magnetic stirring throughout the reaction. After 3 h, the autoclave was cooled to RT, purged to remove CO_2, and opened. A sample of the reaction mixture (~0.1 mL) was taken, diluted with diethyl ether, either centrifuged to remove the solid catalyst (K_2CO_3, NaX, NaY) or passed over silica gel F60

to remove the ionic liquid catalyst ([P_{8881}][CH_3OCOO]), and the progress of the reaction was followed by GC-MS.

5.4.4 Reaction Carried Out in an Autoclave with Sampling

A stainless-steel autoclave (240 mL internal volume), fitted with a Swagelok tap for sampling, was charged with the substrate (4-(3-hydroxypropyl)phenol, **2**, 3.8 mmol), dimethyl carbonate (0.72 mol, 60 mL) and NaX [the weight ratio (*Q*) of zeolite : substrate was 3:1]. Before the reaction, the autoclave was purged at RT with N_2 to remove air. The autoclave was then electrically heated to 180 °C, with the reaction mixture kept under magnetic stirring throughout the reaction. Samples (~0.3 mL) were taken by opening the Swagelok tap at 10, 20, 30, 60, 90, 120, 180, 240, and 300 min. All samples taken from the reactor were diluted with diethyl ether, the solid catalyst removed by centrifugation, and the progress of the reaction was analysed by GC-MS. After 5 h, the autoclave was cooled to RT, purged to remove CO_2, and opened.

5.4.5 Recycling of NaY

A series of recycling experiments was carried out for NaY for the reaction of DMC with cinnamyl alcohol **1**. Once the experiment of entry 3 in Table 5.2 was completed, the solid NaY zeolite was removed by filtration, washed with diethyl ether, and dried at 70 °C under vacuum overnight. The recovered NaY was then used in a subsequent reaction under identical conditions. The recovery/reaction cycle was repeated once more. After the second recycle, the solid NaY was re-calcined at 400 °C (ramp rate 5 °C min^{-1}) for 12 h, and used for a subsequent reaction. The recovery/reaction was then repeated another time, followed by another re-calcination and final re-use of the catalyst.

5.4.6 The isolation and characterisation of products obtained from cinnamyl alcohol, 1, using solid catalysts.

Cinnamyl methyl carbonate, **1a**, was isolated and purified by flash column chromatography on silica gel F60 (eluent: petroleum ether / diethyl ether in 50:50 v/v), and characterised by GC-MS and ^{1}H NMR.

5.4.7 The isolation and characterisation of products obtained from 4-(3-hydroxypropyl)phenol, 2.

3-(4-Hydroxyphenyl)propyl methyl carbonate **2c** was isolated and purified by flash column chromatography on silica gel F60 (eluent: petroleum ether / diethyl ether in 50:50 v/v). 4-(3-Methoxypropyl)phenol, **2b**, was isolated and purified by flash column chromatography on silica gel F60 (eluent: petroleum ether / diethyl ether in 30:70 v/v). 3-(4-Methoxyphenyl)-1-propanol, **2a**, 3-(4-methoxyphenyl)propyl methyl carbonate, **2d**, and 1-methoxy-4-(3-methoxypropyl)benzene, **2e**, were isolated and purified by flash column chromatography on silica gel F60 (gradient dilution, eluent: petroleum ether / diethyl ether in 30:70–50:50 v/v). All products were characterised by GC-MS and ^{1}H NMR. The new product, 3-(4-methoxyphenyl)propyl methyl carbonate, **2d**, and the product for which there was no previously reported NMR data in the literature, 4-(3-methoxypropyl)phenol, **2b**, were also characterised by ^{13}C NMR.

5.5 Conclusions

In order to establish synthetic procedures to upgrade phenolic streams derived from lignin processing, the easily accessible catalysts K_2CO_3, $CsF/\alpha Al_2O_3$, NaX, NaY and an ionic

liquid (IL) $[P_{8881}][CH_3OCOO]$ were studied for the methylation and transesterification of cinnamyl alcohol **1**, and 4-(3-hydroxypropyl)phenol **2**, selected as functional model compounds of *p*-coumaryl alcohol. The results indicated that a straightforward, efficient and selective catalytic upgrading was possible with DMC as solvent/reagent, and that derivatives with largely different chemical properties compared to the starting molecules (*e.g.* polarity, hydrogen-bonding ability, *etc*.) can be obtained, making them potentially interesting in their own right.

The basic catalysts K_2CO_3, $CsF/\alpha Al_2O_3$, and $[P_{8881}][CH_3OCOO]$ yielded the aliphatic carbonates **1a** and **2c** at 90 °C, by transesterification, with high conversions (>90%) and selectivity (>80%).

The corresponding methyl ethers were instead accessible at higher temperature in the presence of faujasites NaY or NaX as catalysts. For example, cinnamyl methyl ether **1b**, was formed with 100% conversion and 91% selectivity from **1** with NaY at 180 °C.

The zeolites displayed different reactivity for **1** and **2**. With cinnamyl alcohol **1**, the more basic NaX favoured reaction at the carbonyl carbon of DMC forming the methyl carbonate intermediate **1a**, followed by *in-situ* decarboxylation to the methyl ether **1b**. Instead, NaY promoted direct reaction towards **1b**, presumably because DMC reacts more favourably at the methyl carbon without passing through the methyl carbonate intermediate.

With 4-(3-hydroxypropyl)phenol **2**, NaX was also more active than NaY as catalyst. Two separate reaction sequences occurred: the fully methylated product **2e** was formed through the direct methylation of both the aliphatic and aromatic hydroxyls, while transesterification of the aliphatic hydroxyl and aromatic OH methylation with DMC yielded **2d**.

Several green aspects can be recognised: i) DMC is non-toxic and used both as a reagent and solvent; ii) NaY and NaX are safe catalysts that can be recovered, reactivated, and re-used, without any loss of conversion or selectivity; iii) methanol and CO_2 are the only by-products, and can be recycled to form DMC and iv) the model compounds themselves are an inherently renewable, environmentally friendly feedstock.

5.6 References

(1) Demirbas, A., Progress and recent trends in biofuels. *Prog. Energ. Combust.* **2007,** *33*, 1–18.

(2) Zakzeski, J.; Jongerius, A. L.; Bruijnincx, P. C. A.; Weckhuysen, B. M., Catalytic Lignin Valorization Process for the Production of Aromatic Chemicals and Hydrogen. *ChemSusChem* **2012,** *5*, 1602–1609.

(3) Zakzeski, J.; Bruijnincx, P. C. A.; Jongerius, A. L.; Weckhuysen, B. M., The Catalytic Valorization of Lignin for the Production of Renewable Chemicals. *Chem. Rev. (Washington, DC)* **2010,** *110*, 3552–3599.

(4) Bozell, J. J. H., J. E.; Johnson, D.; White, J. F. , *Top Value Added Candidates from Biomass, Volume II: Results of Screening fo Potential Candidates from Biorefinery Lignin*. Pacific Northwest Laboratory: Richland, WA, 2007.

(5) Bozell, J. J.; Petersen, G. R., Technology development for the production of biobased products from biorefinery carbohydrates-the US Department of Energy's "Top 10" revisited. *Green Chem* **2010,** *12*, 539–554.

(6) Vennestrom, P. N. R.; Osmundsen, C. M.; Christensen, C. H.; Taarning, E., Beyond Petrochemicals: The Renewable Chemicals Industry. *Angew. Chem., Int. Ed.* **2011,** *50*, 10502–10509.

(7) Dapsens, P. Y.; Mondelli, C.; Perez-Ramirez, J., Biobased Chemicals from Conception toward Industrial Reality: Lessons Learned and To Be Learned. *ACS Catal.* **2012,** *2*, 1487–1499.

(8) Selva, M.; Perosa, A., Green chemistry metrics: a comparative evaluation of dimethyl carbonate, methyl iodide, dimethyl sulfate and methanol as methylating agents. *Green Chem.* **2008,** *10*, 457–464.

(9) Delledonne, D.; Rivetti, F.; Romano, U., Oxidative carbonylation of methanol to dimethyl carbonate (DMC): a new catalytic system. *J. Organomet. Chem.* **1995,** *488*, C15–C19.

(10) Keller, N.; Rebmann, G.; Keller, V., Catalysts, mechanisms and industrial processes for the dimethylcarbonate synthesis. *J. Mol. Catal. A: Chem.* **2010,** *317*, 1–18.

(11) Schaffner, B.; Schaffner, F.; Verevkin, S. P.; Borner, A., Organic Carbonates as Solvents in Synthesis and Catalysis. *Chem. Rev. (Washington, DC)* **2010,** *110*, 4554–4581.

(12) Selva, M.; Marques, C. A.; Tundo, P., Selective monomethylation of arylacetonitriles and methyl arylacetates by dimethyl carbonate. *J. Chem. Soc., Perkin Trans. 1* **1994**, 1323–8.

(13) Bomben, A.; Selva, M.; Tundo, P.; Valli, L., A Continuous-Flow O-Methylation of Phenols with Dimethyl Carbonate in a Continuously Fed Stirred Tank Reactor. *Ind. Eng. Chem. Res.* **1999,** *38*, 2075–2079.

(14) Selva, M., The reaction of dialkyl carbonates with o-aminophenol catalyzed by K_2CO_3: A novel high-yield synthesis of N-alkylbenzoxazol-2-ones. *Synthesis* **2003**, 2872–2876.

(15) Selva, M.; Tundo, P.; Foccardi, T., Mono-N-methylation of functionalized anilines with alkyl methyl carbonates over NaY faujasites. 4. Kinetics and selectivity. *J Org Chem* **2005,** *70*, 2476–85.

(16) Selva, M.; Tundo, P., Highly Chemoselective Methylation and Esterification Reactions with Dimethyl Carbonate in the Presence of NaY Faujasite. The Case of Mercaptophenols, Mercaptobenzoic Acids, and Carboxylic Acids Bearing OH Substituents. *J. Org. Chem.* **2006,** *71*, 1464–1470.

(17) Selva, M.; Tundo, P.; Brunelli, D.; Perosa, A., Chemoselective reactions of dimethyl carbonate catalyzed by alkali metal exchanged faujasites: the case of indolylcarboxylic acids and indolyl-substituted alkylcarboxylic acids. *Green Chem.* **2007,** *9*, 463–468.

(18) Selva, M.; Militello, E.; Fabris, M., The methylation of benzyl-type alcohols with dimethyl carbonate in the presence of Y- and X-faujasites: selective synthesis of methyl ethers. *Green Chem.* **2008,** *10*, 73–79.

(19) Fabris, M.; Lucchini, V.; Noè, M.; Perosa, A.; Selva, M., Ionic Liquids Made with Dimethyl Carbonate: Solvents as well as Boosted Basic Catalysts for the Michael Reaction. *Chem.--Eur. J.* **2009,** *15*, 12273–12282.

(20) Selva, M.; Fabris, M.; Perosa, A., Decarboxylation of dialkyl carbonates to dialkyl ethers over alkali metal-exchanged faujasites. *Green Chem.* **2011,** *13*, 863–872.

(21) Selva, M.; Benedet, V.; Fabris, M., Selective catalytic etherification of glycerol formal and solketal with dialkyl carbonates and K_2CO_3. *Green Chem.* **2012,** *14*, 188–200.

(22) Tundo, P.; Selva, M., The Chemistry of Dimethyl Carbonate. *Acc. Chem. Res.* **2002,** *35*, 706–716.

(23) Zakzeski, J.; Jongerius, A. L.; Weckhuysen, B. M., Transition metal catalyzed oxidation of Alcell lignin, soda lignin, and lignin model compounds in ionic liquids. *Green Chem.* **2010,** *12*, 1225–1236.

(24) Selva, M.; Noè, M.; Perosa, A.; Gottardo, M., Carbonate, acetate and phenolate phosphonium salts as catalysts in transesterification reactions for the synthesis of non-symmetric dialkyl carbonates. *Org. Biomol. Chem.* **2012,** *10*, 6569–6578.

(25) Tundo, P.; Trotta, F.; Moraglio, G.; Ligorati, F., Continuous-flow processes under gas-liquid phase-transfer catalysis (GL-PTC) conditions: the reaction of dialkyl carbonates with phenols, alcohols, and mercaptans. *Ind. Eng. Chem. Res.* **1988,** *27*, 1565–71.

(26) Clacens, J.-M.; Genuit, D.; Veldurthy, B.; Bergeret, G.; Delmotte, L.; Garcia-Ruiz, A.; Figueras, F., CsF supported by α-alumina: an efficient basic catalyst. *Appl. Catal., B* **2004,** *53*, 95–100.

(27) Barthomeuf, D., Conjugate acid-base pairs in zeolites. *J. Phys. Chem.* **1984,** *88*, 42–5.

(28) Su, B.; Barthomeuf, D., Effect of reaction temperature on the alkylation of aniline by methanol over almost neutral zeolites LiY and NaY. *Stud. Surf. Sci. Catal.* **1995,** *94*, 598–605.

(29) Schlögl, R., Carbons. In *Preparation of Solid Catalysts*, Wiley-VCH Verlag GmbH: 1999; pp 150–240.

Chapter 6: Determination of Saturated Vapour Pressure of Dimethyl Carbonate in a Batch Reactor over a Wide Temperature Range.

This chapter is in preparation for publication.

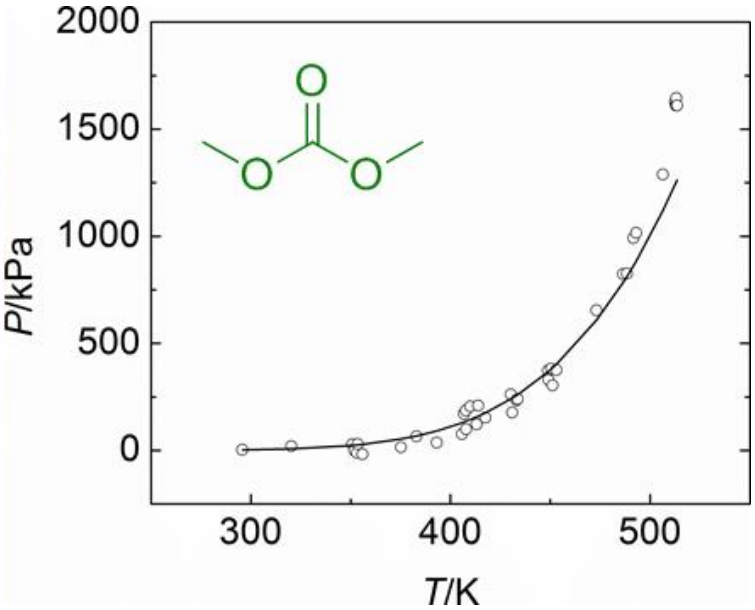

Stanley, J.N.G.; Perosa, A.; Selva, M.; Masters, A.F.; Maschmeyer, T., manuscript in preparation.

6.1 Introduction

Dimethyl carbonate (DMC) has been identified as a green substitute to replace toxic solvents and reagents.[1–3,ix] Indeed, DMC is one of six organic carbonates that has been identified as an especially useful green solvent, and its solvation properties have recently been reviewed by Börner *et al*.[4] Furthermore, as a reagent, DMC is a good alternative to traditional methylating agents such as potentially harmful dimethyl sulfate and methyl halides.[2] In many of these reactions, DMC not only acts as a methylating agent, but also serves as solvent. Alkylation reactions involving g DMC are typically performed at temperatures greater than 433 K.[3]

Vapour pressure is an important thermodynamic parameter and is crucial in the design and operation of high temperature reactions. However, there are few experimental vapour pressure data in the literature for DMC, and where the data do exist, they are reported only over a narrow temperature range.[5] For example, the widest temperature ranges that contain a significant amount of data are reported by Jiang and Zhang at T = (288 to 371) K,[5] Steele *et al*. at T = (311 to 397) K,[6, 7] Rodriguez *et al*. at T = (326 to 411) K,[8] and Kozlova *et al*. at T = (275 to 304) K.[9] Remarkably, there is no data reported above T = 428 K. With the increasing use of DMC, there is a need for isochoric data, to guide the planning of experiments. Although theoretical predictions are published, they do not cover the temperature range relevant to the practical chemist. Furthermore, whether or not DMC decomposition takes place needs to be established, as such thermally induced decomposition would give rise to pressures that significantly deviated from those calculated from literature extrapolations.

In the present work, the vapour pressure for DMC was determined in a batch reactor for the temperature range of T = (295.75 to 513.15) K. As highlighted in Figure 6.1

[ix] References for Chapter 6 begin on page 165.

and Figure 6.2 (see below), this temperature range encompasses temperatures significantly higher than those previously reported in the literature. These batch conditions were chosen because we believe that it is imperative that vapour pressure data, obtained using experimental conditions analogous to those under which DMC is commonly used, are available in the literature. Significantly, the results showed that DMC did not decompose within this temperature range. In addition, the vapour pressure data were fitted to the Clausius–Clapeyron equation, and, as a test of the validity of this fit and of the stability of the DMC over the temperature range, the enthalpy of vaporisation (ΔH_{vap}/kJ·mol^{-1}) was determined and compared with the literature data available.

6.2 Materials and Methods

Chemicals. Dimethyl carbonate (DMC, Aldrich) and nitrogen (BOC) were used as received (Table 6.1).

Table 6.1 Sample Information

Chemical Name	Source	Initial Mole Fraction Purity	Purification Method	Final Mole Fraction Purity	Analysis Method
dimethyl carbonate	Aldrich	0.99	none	-	-
nitrogen	BOC	>0.9999	none	-	-

Apparatus and Procedure. A batch reactor (245 mL internal volume, Parr Instrument Company, modified with the inclusion of a second external thermocouple) was charged

with DMC (60 mL, 64.2 g, 0.71 mol). The reactor was purged with N_2 and pressurised to 676 kPa with N_2. The reactor was heated stepwise in integral control mode under continuous stirring, holding the temperature at each of the chosen set-points (below) for 10 min, to allow for equilibration. The heating steps were: 295.75 K – hold – 353.15 K – hold – 413.15 K – hold – 433.15 K – hold – 453.15 K – hold – 493.15 K – hold – 503.15 K – hold – 513.15 K – hold. The reactor pressure was recorded approximately every 10 min. The measurement series was performed twice and the data sets combined.

6.3 Results and Discussion

The experimental total pressures, calculated N_2 pressures, and calculated DMC pressures, at T = (295.75 to 513.15) K, are reported in Table 6.2. After correcting for the partial pressure of N_2 by assuming N_2 to behave as an ideal gas, three negative vapour pressure values were obtained for DMC between T = (351.95 and 355.85) K, these are clearly not physically meaningful and indicate the error at these temperatures, where the vapour pressure of DMC is very low. These values were omitted in subsequent analysis. The vapour pressure of DMC as a function of temperature is also shown in Figure 6.1.

Table 6.2 Vapour Pressure for Dimethyl Carbonate[a]

T_{exp} / K		*P* / kPa	
	DMC, calc	N_2, calc	tot, exptl
295.75	2.70	672.99	675.69
320.25[c]	19.34	728.74	748.08
350.75	29.23	798.14	827.37
351.95	-1.08[b]	800.87	799.79
353.15	-10.70[b]	803.60	792.90
353.55	29.75	804.51	834.27
355.85	-16.85[b]	809.75	792.90
375.25	14.85	853.89	868.74
383.05	66.05	871.64	937.69
393.15	36.17	894.62	930.79
405.85	76.22	923.52	999.74
406.85	170.47	925.80	1096.27
407.75[c]	185.67	927.84	1113.51
407.85	99.25	928.07	1027.32
409.95	204.78	932.85	1137.63
413.15	121.66	940.13	1061.79
413.95	209.47	941.95	1151.42
417.45	153.24	949.92	1103.16
430.25	262.01	979.04	1241.06
430.95	177.68	980.64	1158.32

433.15	234.73	985.64	1220.37
433.75	240.26	987.01	1227.27
448.85	371.37	1021.37	1392.74
449.05	329.55	1021.82	1351.37
450.55	381.29	1025.24	1406.53
451.15	304.09	1026.60	1330.69
453.15	375.38	1031.15	1406.53
473.15	653.92	1076.66	1730.58
486.45	823.60	1106.93	1930.53
488.45	825.95	1111.48	1937.43
491.75	990.81	1118.99	2109.80
493.15	1015.20	1122.17	2137.37
506.45	1288.30	1152.44	2440.74
512.55	1626.06	1166.32	2792.38
513.05	1611.13	1167.46	2778.59
513.15	1645.38	1167.69	2813.06
513.55	1609.99	1168.60	2778.59

[a] The vapour pressure of DMC was calculated from the total reactor pressure measured, and the vapour pressure of N_2 (calculated using the ideal gas law), following Dalton's Law of partial pressures: $p_{tot} = p_{DMC} + p_{N2}$. [b] Negative vapour pressures were calculated for these temperatures. These values were omitted in subsequent analysis. [c] Two measurements were taken at these temperatures. Consequently, the values reported for the $p_{tot,\ exptl}$ at these temperatures are an average. Standard uncertainties (2σ) are 48.76 and 9.74 for the p_{tot} at 320.25 K and 407.75 K, respectively.

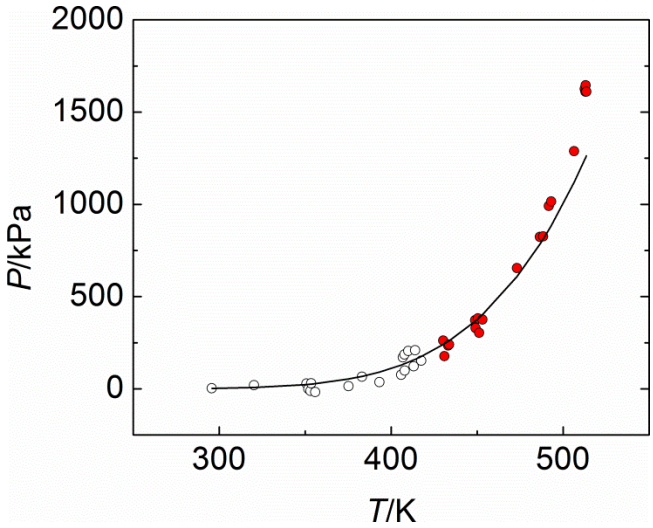

Figure 6.1 Vapour pressure of DMC as a function of temperature, combining data sets from the two measurements. Raw data shown as open and closed circles, solid line obtained from fit to Equation 6.1 and Figure 6.2, see text. The red fill indicates the raw data obtained in a temperature range previously unreported in the literature.

The data were fitted to the integrated form of the Clausius–Clapeyron equation (Equation 6.1):

$$\ln P = -\frac{-\Delta H_{\text{vap}}}{R}\left(\frac{1}{T}\right) + C \qquad 6.1$$

where P is the vapour pressure in kPa, T is the absolute temperature in Kelvin, ΔH_{vap} is the enthalpy of vaporisation in kJ·mol^{-1}, R is the gas constant (= 8.314 J·mol^{-1}·K^{-1}), and C is a constant.

The linear fit in Figure 6.1 was obtained by translating the fit from Figure 6.2 onto the original data. Equation 6.1 assumes that the enthalpy of vaporisation is constant across the entire temperature range. Furthermore, DMC is assumed to behave as an ideal gas. These assumptions are valid except at high pressures, which could account for the deviation of the fit (Figure 6.1). As shown in the plot of ln(P/kPa) *vs*

$10^3 T/K^{-1}$ (Figure 6.2), a straight line could be fitted with an R-Square value of 0.91. This linear fit suggests that, under these conditions, the DMC is stable.

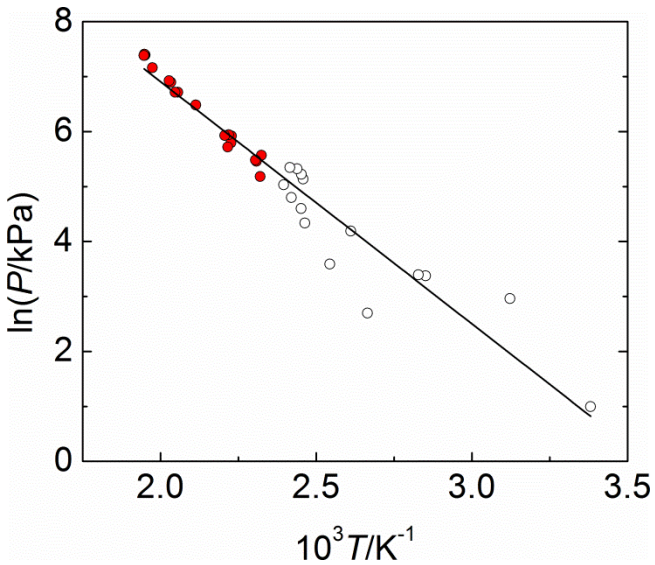

Figure 6.2 Graph of ln(P/kPa) versus $10^3 T/K^{-1}$, combining data sets from the two measurements. Raw data shown as open and closed circles, fitted data using Equation 6.1, see above, shown as solid line. The red fill indicates the raw data obtained in a temperature range previously unreported in the literature.

To verify the reliability of the measurements obtained in this work, and the appropriateness of assuming that the Clausius–Clapeyron relationship applies in this system, the enthalpy of vaporisation over the experimental temperature range was calculated from the value of the slope obtained from the plot in Figure 6.2. The experimental value of (36.6 ± 3.4) kJ·mol^{-1} (2σ error) for the enthalpy of vaporisation determined from our data is in excellent agreement with the literature values reported by Steele *et al.* and Walker, of 37.7 kJ·mol^{-1} at 298.15 K and 37.3 kJ·mol^{-1} at 293.15 K, respectively.[6, 10]

Thus, as the data fit the Clausius–Clapeyron equation, as confirmed by the value obtained for the enthalpy of vaporisation, we have shown that DMC is stable under these reaction conditions and that the behaviour of DMC is predictable. Although the data are not strictly obtained under complete equilibrium conditions, the system was left to equilibrate for intervals consistent with synthetic practice, rather than with the thermodynamically limiting case. The excellent fit with theory suggests the approximation to equilibrium conditions is good, and the data provide an empirical guide for the planning and assessment of reactions in DMC over an extended temperature range.

6.4 Conclusions

In this work, we report the vapour pressures of DMC over a large temperature range (T = (295.75 to 513.15) K) determined in a batch reactor under an inert atmosphere. The experimental data encompass a significantly wider temperature range than previously reported in the literature. From the DMC vapour pressures, the enthalpy of vaporisation was calculated as 36.6 $kJ \cdot mol^{-1}$.The comparison of this value with those of the literature confirmed the reliability of the present study. Finally, it is clear from the data obtained that DMC does not decompose under the present reaction conditions and that the behaviour of DMC is predictable.

6.5 References

(1) Shaikh, A.-A. G.; Sivaram, S., Organic Carbonates. *Chem. Rev. (Washington, DC)* **1996,** *96*, 951–76.

(2) Selva, M.; Perosa, A., Green chemistry metrics: a comparative evaluation of dimethyl carbonate, methyl iodide, dimethyl sulfate and methanol as methylating agents. *Green Chem.* **2008,** *10*, 457–464.

(3) Tundo, P.; Selva, M., The Chemistry of Dimethyl Carbonate. *Acc. Chem. Res.* **2002,** *35*, 706–716.

(4) Schaffner, B.; Schaffner, F.; Verevkin, S. P.; Borner, A., Organic Carbonates as Solvents in Synthesis and Catalysis. *Chem. Rev. (Washington, DC)* **2010,** *110*, 4554–4581.

(5) Zhou, Y.; Wu, J.; Lemmon, E. W., Thermodynamic Properties of Dimethyl Carbonate. *J. Phys. Chem. Ref. Data* **2011,** *40*, 043106/1–043106/11.

(6) Steele, W. V.; Chirico, R. D.; Knipmeyer, S. E.; Nguyen, A.; Smith, N. K., Thermodynamic Properties and Ideal-Gas Enthalpies of Formation for Dicyclohexyl Sulfide, Diethylenetriamine, Di-n-octyl Sulfide, Dimethyl Carbonate, Piperazine, Hexachloroprop-1-ene, Tetrakis(dimethylamino)ethylene, N,N'-Bis-(2-hydroxyethyl)ethylenediamine, and 1,2,4-Triazolo[1,5-a]pyrimidine. *J. Chem. Eng. Data* **1997,** *42*, 1037–1052.

(7) Steele, W. V.; Chirico, R. D.; Knipmeyer, S. E.; Nguyen, A., Vapor Pressure, Heat Capacity, and Density along the Saturation Line.. Measurements for Dimethyl Isophthalate, Dimethyl Carbonate, 1,3,5-Triethylbenzene, Pentafluorophenol, 4-tert-Butylcatechol, α-Methylstyrene, and N,N'-Bis(2hydroxyethyl)ethylenediamine. *J. Chem. Eng. Data* **1997,** *42*, 1008–1020.

(8) Rodriguez, A.; Canosa, J.; Dominguez, A.; Tojo, J., Isobaric vapour-liquid equilibria of dimethyl carbonate with alkanes and cyclohexane at 101.3 kPa. *Fluid Phase Equilib.* **2002,** *198,* 95–109.

(9) Kozlova, S. A.; Emel'yanenko, V. N.; Georgieva, M.; Verevkin, S. P.; Chernyak, Y.; Schaeffner, B.; Boerner, A., Vapour pressure and enthalpy of vaporization of aliphatic dialkyl carbonates. *J. Chem. Thermodyn.* **2008,** *40,* 1136–1140.

(10) Walker, E. E., Solvent action of organic substances on polyacrylonitrile. *J. Appl. Chem.* **1952,** *2,* 470–81.

Appendix A

This appendix contains the complete version of the published paper, *Past and Present Challenges in Catalysis: Developing Green and Sustainable Processes*, found in Chapter 1.

Stanley, J.N.G., *J. Proc. Roy. Soc., New South Wales* **2014,** *147*, 64–76.

Journal and Proceedings of the Royal Society of New South Wales, vol. 147, nos. 451 & 452, pp. 64-76.
ISSN 0035-9173/14/0100064-13

Past and Present Challenges in Catalysis: Developing Green and Sustainable Processes

Jessica N. G. Stanley*
RSNSW Scholarship Winner, 2013

Laboratory of Advanced Catalysis for Sustainability
School of Chemistry, F11 The University of Sydney, Sydney, NSW 2006 Australia

* Corresponding author.
E-mail: jessica.stanley@sydney.edu.au

Abstract

This article is based on a lecture by one of the four recipients of the Royal Society of New South Wales Scholarships for 2013, delivered at the Union, University and Schools Club, on Wednesday, 5 February 2014. It briefly discusses the role of societal, political, and environmental drivers on the development of catalysts in the 20th century, which led to the technological advances that enabled the modern lifestyle we enjoy today. Three challenges of catalysis in the 21st century will then discussed in more detail, with a focus on changing feedstocks from fossil resources to biomass resources, and the growing emphasis on lower energy, 'greener' processing.

Keywords: Catalysis, biomass, green chemistry, sustainability.

Introduction

Catalysts play a central role in chemistry, and are used in approximately 90% of all industrial chemical processes (Thomas and Williams 2005, Armor 2011, Thomas 1994). In the last 250 years, especially during the 20th century, catalysts were involved in many technological developments that contributed to the lifestyle and standard of living that we enjoy today. Many of these developments emerged due to the convenience and abundance of fossil feedstocks. However, with global energy demands expected to double within the next forty years, peak oil being reached soon or even past, the growing concerns surrounding carbon dioxide emissions, and the political instability related to geographical restrictions of oil reserves, there is a growing need for greener processing and to develop alternative resources. Just as catalysts played an important role in the 20th century, they are expected to have an ever more crucial role in the 21st century, as will be discussed in the subsequent sections.

Historical Perspective

The first use of catalysts can be traced back approximately 10 000 years, with depictions of brewing on archaeological remains (Adams 2009). Even back then, catalysts had an important role for humankind! However, it was not until the 19th century that the concept of catalysis was understood. Jöns Jacob Berzelius introduced the term *catalysis* in 1835 before Wilhelm Ostwald provided a scientific definition in 1895 (Zaera 2012). Over the next century, catalysts played a significant role in the development of industrial processes that have greatly influenced modern society. Arguably the most important catalytic

development was the Haber–Bosch process, which is promoted by iron-based catalysts. Motivated by the need for fertiliser during the anticipated Chilean embargo on saltpetre, this process has had an enormous impact on the development of modern society. On the one hand, it was responsible for between 100 and 150 million deaths in the 20th century because of its role in the production of explosives and chemical weapons used in armed conflicts (Erisman et al. 2008). Indeed, the demand for explosives based upon nitric acid had a huge impact on the growth of the industrial production of bulk chemicals during World War One (Lindstroem and Pettersson 2003). On the other hand, the Haber–Bosch process is responsible, through the production of agricultural fertiliser, for feeding approximately 48% of the world's population in 2008 (Fig. 1) (Erisman et al. 2008). As will be shown briefly in this section, major catalytic developments rarely occurred in isolation. Rather, they required societal, political, or environmental motivations as drivers. Equally important was the accessibility to raw materials, and in turn, new technology created new demands.

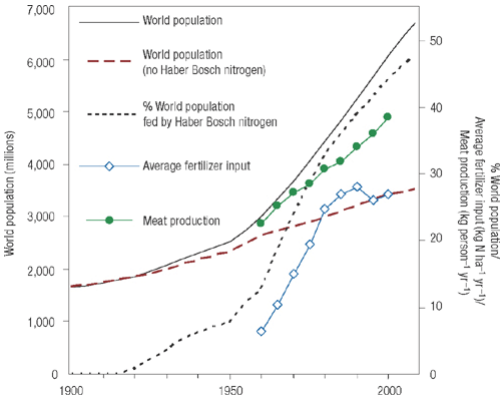

Figure 1: Trends in human population and nitrogen use in the 20th century. Reprinted by permission from Macmillan Publishers Ltd: NATURE GEOSCIENCE. Erisman et al. Nature Geoscience, 1, 10 (2008), copyright 2008.

Although the first crude oil was drilled in 1859, the main feedstock for chemicals at the onset of the 20th century was coal, based mainly on coal liquefaction, distillation of coal tar, acetylene, and coal gasification (Armor 2011). As the demands for explosives diminished, the focus after World War One moved to synthetic fuels. Among the most important catalytic developments in this period was the use of iron and copper catalysts for the synthesis of hydrocarbons from carbon monoxide and hydrogen (obtained from coal) by Franz Fischer and Hans Tropsch in 1923. The Fisher–Tropsch synthesis of fuels is just as relevant today as it was nearly a century ago. Nonetheless, the widespread use of crude oil as a feedstock began when Eugène Houdry developed the catalytic cracking of petroleum in 1936. Lewis and Gillian modified the process with the introduction of fluid catalytic cracking (FCC) in 1941, and this improvement enabled the supply of the vast quantities of high-octane aviation fuel needed to supply the Allied Forces in World War Two.

With the end of the war, needs again changed with society, and the automobile market accelerated in Europe. The increased demands for gasoline created the petrochemical industry, as petroleum refining enabled the production of plastics, pharmaceuticals, and specialty chemicals. Crude oil became entrenched as a convenient and accessible feedstock. The most important development during this period was the use of a modified X zeolite catalyst in the FCC of petroleum, and one of the most important concepts in zeolite catalysis was the discovery of shape-selective catalysis in zeolites (Masters and Maschmeyer 2011). With these advances, zeolites revolutionised the catalytic cracking and hydrocracking of the crude oil feedstocks, dramatically improving yield and process efficiencies.

Indeed, the use of zeolite catalysts is estimated to save the petroleum industry 10 billion dollars a year (Weitkamp 2000).

As the transportation industry and chemical processes expanded, research into new catalysts was required to meet the regulations regarding vehicle and stationary engine emissions. Hydrodesulfurisation was developed in the 1960s for the removal of sulfur in fuels. In 1974, the first oxidation catalytic converter for automobiles was developed, followed by the three-way catalytic converter in 1978, and the Pd three-way converter in the 1990s. By 1990, the catalytic converter had reduced emissions from hydrocarbons, NO_x, and CO from vehicles by 90% compared to levels in 1965 (Armor 2011).

Although emissions control catalysts are among the exceptions, the fundamental studies on catalysts in the 20th century were mostly focused on achieving high turnover rates. There is now a growing need to develop alternative resources and lower energy, 'greener' processing. Catalysts are expected to play a huge role as many of the challenges of the previous century will be revisited with changing feedstocks, as will be discussed in the subsequent sections.

Catalysts in the 21st Century

The Need for Green and Sustainable Processes

The U.S. Energy Information Administration anticipates that worldwide energy use will grow by 56% between 2010 and 2040, which is equivalent to global energy demand increasing by approximately 1.5% a year (EIA 2013). More than 85% of this increase occurs due to the strong economic growth and expanding populations in developing nations. However, this rapid increase in energy demand is problematic as finite fossil resources (coal, oil and gas) currently provide 85% of the world's energy (IPCC 2011). Of the three, oil is the most concerning, as worldwide reserves of oil are sufficient for only another 55 years (IEA 2012). Indeed, a recent article in *Nature* argues that 'peak oil' (the time when global production of oil reaches a peak before declining) was passed in around 2005 (Murray and King 2012). Access to the worldwide oil reserves is also compromised due to political instability (*e.g.* in the Middle East, an area which accounts for almost 50% of proven oil reserves at the end of 2012) (BP 2013), causing problems of energy security to developed countries. Moreover, the level of carbon dioxide in the atmosphere has increased by approximately 40% compared to pre-industrial levels, largely because of the surge in fossil fuel consumption and land use changes (Edenhofer et al. 2012). This increased carbon dioxide has serious consequences for global warming, with the International Panel on Climate Change affirming human influence as "extremely likely" (i.e. 95–100% probability) to be the dominant cause of climate change (IPCC 2013).

Green Chemistry and Catalysis

The last thirty years has seen a significant move towards green chemistry, as it is recognised that the challenges of sustainability will be met with new technologies that provide society with energy and materials in an environmentally responsible manner (Anastas and Kirchhoff 2002). The Brundtland commission defined sustainable development in 1987 as "Meeting the needs of the present generation without compromising the ability of future generations to meet their own needs" (Brundtland 1987). Four years later, Anastas defined green chemistry as "the utilisation of a set of principles that reduces or eliminates

the use or generation of hazardous substances in the design, manufacture and application of chemical products" (Anastas and Warner 1998). These Twelve Principles of Green Chemistry, listed in Figure 2, are the means to achieving sustainable development.

The Twelve Principles of Green Chemistry

1. It is better to prevent waste than to treat or clean up waste after it is formed.
2. Synthetic methods should be designed to maximize the incorporation of all the materials used in the process into the final product.
3. Wherever practicable, synthetic methodologies should be designed to use and generate substances that possess little or no toxicity to human health and the environment.
4. Chemical products should be designed to preserve efficacy of function while reducing toxicity.
5. The use of auxiliary substances (e.g. solvents, separation agents, etc.) should be made unnecessary wherever possible, and innocuous when used.
6. Energy requirements should be recognized for their environmental and economic impacts and should be minimized. Synthetic methods should be conducted at ambient temperature and pressure.
7. A raw material of feedstock should be renewable rather than depleting wherever technically and economically practicable.
8. Unnecessary derivization (blocking group, protection/deprotection, temporary modification of physical/chemical processes) should be avoided whenever possible.
9. Catalytic reagents (as selective as possible) are superior to stoichiometric reagents.
10. Chemical products should be designed so that at the end of their function they do not persist in the environment and break down into innocuous degradation products.
11. Analytical methodologies need to be further developed to allow for real-time, in-process monitoring and control prior to the formation of hazardous substances.
12. Substances and the form of a substance used in a chemical process should be chosen so as to minimize the potential for chemical accidents, including releases, explosions, and fires.

Figure 2: The Twelve Principles of Green Chemistry (Anastas and Warner 1998).

The Twelve Principles comprise of three main aspects, identified by Sheldon. The first aspect aims to minimise waste through the efficient utilisation of raw materials (Sheldon 2014). Waste is defined as any material that is generated in a process that does not have realised value and includes the loss of unutilised energy (Anastas and Eghbali 2010). With the need to double energy production within the next forty years (without increasing carbon dioxide emissions), the need to develop more energy efficient processes is essential. Secondly, avoiding the use of toxic and/or hazardous substances is important to circumvent health, safety and environmental issues. This aspect includes avoiding the use of solvents, which often account for the majority of mass wasted in syntheses and processes (Anastas and Beach 2007). Finally, the third aspect identified by Sheldon is the use of renewable biomass feedstocks instead of non-renewable fossil feedstocks. Biomass conversion has become an important area of research due to the need for new technologies to obtain energy and chemical feedstocks in a sustainable manner (Huber et al. 2006, Corma et al. 2007), and it is a major aim of green chemistry (Anastas and Beach 2007).

The motivations and drivers in the 21st century have changed. With the need for alternative resources, catalysts are expected to play an ever more crucial role in the technological developments for biomass conversion, enabling pathways previously unavailable in processing alternative feedstocks. Catalysts are also fundamental to improving the efficiency of reactions by lowering energy input, by avoiding the need for stoichiometric quantities of reagents, by decreasing the use of processing and separation agents, and by offering greater product selectivity (Anastas and Eghbali 2010, Anastas et al. 2001). Over the next few decades, catalytic processes will be developed to convert biomass to fuels and chemicals, but no developments will be made that are not informed by the thinking of green chemistry and that do not fulfil their role in a sustainable manner.

Current Challenges in Catalysis

For the remainder of this paper, three different but related novel applications of

catalysis to address the challenges of the 21st century will be discussed. This paper will focus on biomass as a renewable feedstock for fuels and chemicals, and the move towards lower energy, 'greener' processing. It is by no means a comprehensive investigation of all the challenges facing catalysis, but comprises of three niche areas of particular interest to the author. A brief context will be given highlighting the current challenges in each area, and an example of how these problems can be met based on the PhD research of the author will be provided.

Designing Sulfur Resistant Catalysts for Biomass Processing

With oil supplies diminishing significantly over the next few decades, there is an increasing need to develop liquid transport fuels from biomass. Due to the chemical, thermal and functionality differences between biomass and petroleum feedstocks, new chemical pathways need to be developed for biomass processing (Demirbas 2007, Huber and Dumesic 2006). The current technologies for the conversion of biomass include gasification, pyrolysis, hydrothermal liquefaction, delignification followed by saccharification and fermentation, and aqueous phase reforming (APR). Many of these processes involve catalysts, such as APR, which is a promising technology that uses supported metal catalysts to convert biomass-derived feedstocks into either hydrogen or alkanes (Cortright et al. 2002, Chheda et al. 2007).

An important challenge in developing catalysts for biomass conversion, including APR, is operating the catalysts in the presence of sulfur in real biomass feedstocks (e.g., wood: approx. 56 ppm), due to the presence of sulfur-containing amino acids and from the uptake of nutrients in the soil (Robinson et al. 2009). This sulfur is a problem because sulfur is known to poison noble metal catalysts (Bartholomew et al. 1982, Rodriguez 2006.(Bartholomew et al. 1982, Rodriguez 2006) Although the sulfur tolerance of catalysts was widely investigated in the 20th century, both for the petrochemical and fine chemical industries (Bartholomew et al. 1982, Rodriguez and Goodman 1991, Somorjai 1994), there has been little research into improving the sulfur resistance of catalysts for use with biomass feedstocks. Thus, developing sulfur resistant catalysts for biomass processing is one of the catalytic challenges of the 20th century that is being revisited in the 21st century as feedstocks change from fossil resources to biomass resources.

We have recently designed supported bimetallic Pt-Ru catalysts that exhibit improved sulfur resistance and show promising potential for APR of model compounds, using the hydrogenation of cyclohexane as a screening reaction (Stanley et al. 2011). Thiophene was used as the model sulfur source. In all cases, the bimetallic catalysts achieved higher turnover frequencies than their monometallic counterparts in both the absence and presence of the sulfur-containing species. Indeed, the bimetallic catalysts remained active even in reactions having *ten times* the concentration of sulfur expected in woody biomass feedstocks, suggesting the operation of a sulfur/hydrogen spillover equilibrium. In contrast, the monometallic catalysts were completely poisoned.

Powder X-ray diffraction (XRD) and extended X-ray absorption fine structure (EXAFS) experiments were used to probe changes to the Pt unit cell and Pt/Ru bonding environments induced by sulfur poisoning for the bimetallic catalysts (Stanley et al. 2011, Stanley et al. 2014). The results

from these investigations are consistent with increasing concentrations of sulfur-containing species coordinating to the ruthenium atoms during sulfur poisoning, leading to a partial separation of the alloy. However, after regenerating the poisoned catalysts under pure hydrogen to remove the sulfur species, the alloy is reformed, showing that this process is reversible. Thus, these results are consistent with an *in-situ* self-regeneration mechanism, which we propose is occurring to enable the bimetallic catalysts to remain active. That is, during poisoning the catalyst partially dealloys, but a sulfur spillover and a hydrogen spillover take place to regenerate the catalyst *in-situ*, and the metals are then re-alloyed. The catalysts are sulfur-resistant.

Hydrogenation of Aromatics and Hydrogen Storage

The second catalytic challenge facing the 21st century fits in with the drive towards lower energy, 'greener' processing. In the previous century, the focus of fundamental studies was largely on achieving high turnover rates. Now, the main drivers for technological developments have changed, and a greater focus is on reducing energy requirements. The hydrogenation of aromatics is an important reaction both for small-scale synthesis and for industrial reactions, including the production of cyclohexane, which is an important precursor for the manufacturing of nylon-6,6 (Mevellec et al. 2006, Park et al. 2005, Roucoux et al. 2003). These reactions are traditionally carried out using elevated temperatures and pressures, which often exceed 100 °C and 50 atm H_2 (Augustine 1995). Furthermore, aromatic compounds are responsible for undesired particle emissions in exhaust gas, leading to a tightening of fuel legislation (Stanislaus and Cooper 1994, Cooper and Donnis 1996). Thus, being able to perform the hydrogenations under mild conditions is an important challenge in terms of energy efficiency and environmental concerns.

Additionally, the reversible toluene/methylcyclohexane couple has the added interest of being a safe and feasible hydrocarbon combination for the storage of hydrogen (Alhumaidan et al. 2011). Cyclic hydrocarbons have a relatively high hydrogen storage capacity, produce no carbon dioxide or carcinogenic products, and their volatility range makes them compatible with existing infrastructure such as refuelling stations and oil tankers for the storage and transportation of the liquid hydrocarbons (Kariya et al. 2002, Kariya et al. 2003, Hodoshima and Saito 2009, Alhumaidan et al. 2011). Thus, the cyclic hydrocarbon combinations have a distinct advantage over other solid hydrocarbons for hydrogen storage.

Over the last ten years, there has been an increased focus on effecting the hydrogenation of toluene under mild conditions, particularly at room temperature. However, the catalyst preparations are often challenging, and the resulting catalysts often have poor activity and/or poor stability (Park et al. 2005). Several groups have demonstrated that metal nanoparticles can perform the reactions with highly water-soluble surfactants used to stabilise these particles in aqueous solution (Schulz et al. 2002, Schulz et al. 1999, Schulz et al. 2000, Fonseca et al. 2003, Mevellec et al. 2004, Hubert et al. 2009a, Hubert et al. 2009b, Roucoux et al. 2003), while others have investigated the use of ionic liquids for nanoparticle stabilisation (Fonseca et al. 2003, Scheeren et al. 2003, Silveira et al. 2004, Rossi and Machado 2009). Further still, a range of solid supports has been used in an attempt overcome the problems of stability (Bianchini et al. 2003, Park et al. 2005, Mevellec et al. 2006, Park et al. 2007b, Park et al. 2007a,

Takasaki et al. 2007, Barthe et al. 2009a, Barthe et al. 2009b, Pan and Wai 2009, Pélisson et al. 2012, Song et al. 2009, Zhou et al. 2009, Jahjah et al. 2010, Fang et al. 2011, Hubert et al. 2011, Zahmakiran et al. 2010). However, in many cases the reaction and/or catalyst manipulations required air-free conditions and, where special precautions were not required, elevated hydrogen pressures were again used.

To overcome these challenges, we have developed robust bimetallic supported Pt-Ru catalysts that, remarkably, operate under one atmosphere to rapidly catalyse the room temperature hydrogenation of toluene (and tetralin) at 1 atm H_2 (Stanley et al. 2013a). Higher turnover frequencies were achieved with the bimetallic catalysts compared to their monometallic counterparts, suggesting a synergistic effect between platinum and ruthenium. These easily handled, air-stable catalysts are amongst the most active catalysts for aromatic hydrogenations under ambient conditions reported to date.

Green Catalytic Processing of Lignin

Returning to renewable feedstocks, the third challenge is the need to develop the catalytic technologies to obtain chemicals from alternative resources. As already mentioned, biomass is the only renewable source for carbon-based materials. Lignin (which constitutes approx. 15–30% by weight and 40% by energy content of lignocellulosic biomass (Perlack et al. 2005)) is particularly valuable, as its unique structure as an amorphous, highly substituted, aromatic polymer makes it the major renewable source of aromatics (Zakzeski et al. 2010). However, synthetic approaches for the conversion of lignin to chemicals are markedly less developed compared to the cellulosic components of biomass, partly due to the recalcitrant nature of lignin that provides plants with their strength (Zakzeski et al. 2012). Much effort is currently being devoted to the development of new technology to process low value lignin into higher value-added chemicals. Although aggressive depolymerisation of lignin yields chemicals such as benzene, toluene, and xylene, as well as phenols and aliphatic hydrocarbons used in conventional chemical processes, the selective depolymerisation of lignin could yield monomeric lignin aromatics which are not accessible by traditional petrochemical routes. For example, these monomeric lignin aromatics could be obtained from the pretreatment streams of the pulp and paper industries, which alone produced 50 million tons of extracted lignin in 2004 (Zakzeski et al. 2010). Extraordinarily, the vast majority of this type of lignin is burned as a low value fuel – only 2% is used commercially (Gosselink et al. 2004).

Now, analogous to the petroleum refinery, a biorefinery could use biomass feedstocks to produce a range of products. As outlined earlier, the petroleum refinery developed over many decades in the 20th century, as crude oil emerged as a convenient and readily available feedstock. It began with only few products, but as the needs changed with those of society and new catalytic technology was developed, it expanded to produce plastics, pharmaceuticals, and speciality chemicals. With the growing need to obtain these products from renewable resources, the biorefinery is emerging. In the early stages, the biorefinery will need to produce large volumes of more chemically accessible, lower value fuels. Later, higher value chemicals produced in smaller quantities will be required to offset the costs (Bozell and Petersen 2010). Finally, it is expected that all components of biomass will need to be used for a biorefinery to be economically viable. Catalysts are critical to the development of the new

technology for enabling the conversion of biomass. The catalytic challenges for performing the chemical transformations, which were overcome for crude oil over many decades in the 20th century in the petroleum refinery, are being revisited with biomass-derived feedstocks in the 21st century in the biorefinery.

Currently, there are two approaches for converting biomass-derived resources into higher-value added fuels. The first is a drop-in strategy, where the biomass feedstocks are transformed into existing platform chemicals, to directly replace well-established chemicals currently produced from fossil feedstocks (Vennestrom et al. 2011, Dapsens et al. 2012). The other approach, which we favour, is a curiosity driven broad-based strategy that exploits the existing structure and functionality of biomass. In this approach, renewable platform chemicals based on the structure of biomass could lead to the development of new chemistry and, in the longer term, a plethora of chemical products with as yet unknown applications (Zakzeski et al. 2010).

Fundamental to establishing the required catalytic technology for converting biomass-derived feedstocks into chemicals is an understanding of the reactivity trends and reaction pathways. It has been recognised that many of the building blocks obtained from the disruption of lignin into monomeric aromatics resemble *p*-coumaryl, coniferyl, and sinapyl alcohol. We have recently shown that model compounds based on the *p*-coumaryl structure, specifically cinnamyl alcohol and 4-(3-hydroxypropyl)phenol, can be selectively transformed into different products by catalytic methodologies based on dimethyl carbonate (DMC) as a green solvent/reagent (Stanley et al. 2013b). This selectivity can be tuned by varying the reaction temperature and the nature of the catalyst. In general, basic catalysts promote selective transesterification of the aliphatic hydroxyl group at 90 °C. On the other hand, amphoteric solids such as alkali metal-exchanged faujasites selectivity produce the corresponding alkyl ethers at higher temperatures (165–180 °C). Phenolic hydroxyl groups can be similarly methylated with the faujasites at high temperatures. Thus, these results indicate that efficient and selective catalytic upgrading of lignin-derived chemical building blocks is possible with DMC, and the preliminary screening for selectivity illustrates the reactivity trends and the most promising synthetic pathways.

Conclusions

Catalysts will play a crucial role in the 21st century in moving away from fossil resources. Although oil will still be the main source of fuels and chemicals in the earlier part of this century, there is a great need to improve our current processes to make them more energy efficient. The development of robust catalysts that perform reactions at lower temperatures and pressures is one way to achieve this aim. However, biomass is the only sustainable source of liquid transportation fuels and aromatic chemicals, and the development of new catalytic technology and chemical pathways for use in the biorefinery is essential. Nonetheless, there is no one solution to addressing the challenges of sustainable development. The 21st century will require a combination of solar, geothermal, wind, biomass, hydrogen, and nuclear to meet our energy needs.

Acknowledgements

I gratefully acknowledge the RSNSW for the 2013 Royal Society of New South Wales Scholarship, the University of Sydney for an

Australian Postgraduate Award, and my PhD supervisors Anthony F. Masters and Thomas Maschmeyer (in Sydney, Australia) and Maurizio Selva and Alvise Perosa (in Venice, Italy) for fruitful discussions.

References

Adams, C. (2009) Applied Catalysis: A Predictive Socioeconomic History, *Top. Catal.*, 52, 8, 924-934.

Alhumaidan, F., Cresswell, D. & Garforth, A. (2011) Hydrogen Storage in Liquid Organic Hydride: Producing Hydrogen Catalytically from Methylcyclohexane, *Energy Fuels*, 25, 10, 4217-4234.

Anastas, P. & Eghbali, N. (2010) Green Chemistry: Principles and Practice, *Chem. Soc. Rev.*, 39, 1, 301-312.

Anastas, P. & Warner, J. C. (1998) *Green Chemistry: Theory and Practice*, (Eds.), Oxford University Press, Oxford, 135.

Anastas, P. T. & Beach, E. S. (2007) Green chemistry: the emergence of a transformative framework, *Green Chem. Lett. Rev.*, 1, 1, 9-24.

Anastas, P. T. & Kirchhoff, M. M. (2002) Origins, current status, and future challenges of green chemistry, *Acc. Chem. Res.*, 35, 9, 686-694.

Anastas, P. T., Kirchhoff, M. M. & Williamson, T. C. (2001) Catalysis as a foundational pillar of green chemistry, *Applied Catalysis A: General*, 221, 1–2, 3-13.

Armor, J. N. (2011) A history of industrial catalysis, *Catal. Today*, 163, 1, 3-9.

Augustine, R. L. (1995) *Heterogeneous Catalysis for the Synthetic Chemist*, (Eds.), Marcel Dekker, New York.

Barthe, L., Denicourt-Nowicki, A., Roucoux, A., Philippot, K., Chaudret, B. & Hemati, M. (2009a) Model arenes hydrogenation with silica-supported rhodium nanoparticles: The role of the silica grains and of the solvent on catalytic activities, *Catal. Commun.*, 10, Copyright (C) 2011 American Chemical Society (ACS). All Rights Reserved., 1235-1239.

Barthe, L., Hemati, M., Philippot, K., Chaudret, B., Denicourt-nowicki, A. & Roucoux, A. (2009b) Rhodium colloidal suspension deposition on porous silica particles by dry impregnation: Study of the influence of the reaction conditions on nanoparticles location and dispersion and catalytic reactivity, *Chem. Eng. J. (Amsterdam, Neth.)*, 151, Copyright (C) 2011 American Chemical Society (ACS). All Rights Reserved., 372-379.

Bartholomew, C. H., Agrawal, P. K. & Katzer, J. R. (1982) Sulfur poisoning of metals, *Adv. Catal.*, 31, Copyright (C) 2010 American Chemical Society (ACS). All Rights Reserved., 135-242.

Bianchini, C., Dal, S. V., Meli, A., Moneti, S., Moreno, M., Oberhauser, W., Psaro, R., Sordelli, L. & Vizza, F. (2003) A comparison between silica-immobilized ruthenium(II) single sites and silica-supported ruthenium nanoparticles in the catalytic hydrogenation of model hetero- and polyaromatics contained in raw oil materials, *J. Catal.*, 213, Copyright (C) 2012 American Chemical Society (ACS). All Rights Reserved., 47-62.

Bozell, J. J. & Petersen, G. R. (2010) Technology development for the production of biobased products from biorefinery carbohydrates-the US Department of Energy's "Top 10" revisited, *Green Chem.*, 12, Copyright (C) 2013 American Chemical Society (ACS). All Rights Reserved., 539-554.

BP, *BP Statistical Review of World Energy June 2013*, http://www.bp.com/content/dam/bp/pdf/statistical-review/statistical_review_of_world_energy_2013.pdf, (Accessed March 2014).

Brundtland, C. G. (1987) *Our Common Future, The World Commission on Environmental Development*, (Eds.), Oxford University Press, Oxford, 400.

Chheda, J. N., Huber, G. W. & Dumesic, J. A. (2007) Liquid-phase catalytic processing of biomass-derived oxygenated hydrocarbons to fuels and chemicals, *Angew. Chem. Int. Edit.*, 46, Copyright (C) 2010 American Chemical Society (ACS). All Rights Reserved., 7164-7183.

Cooper, B. H. & Donnis, B. B. L. (1996) Aromatic saturation of distillates: an overview, *Appl. Catal. A-Gen.*, 137, Copyright (C) 2010 American Chemical Society (ACS). All Rights Reserved., 203-23.

Corma, A., Iborra, S. & Velty, A. (2007) Chemical Routes for the Transformation of Biomass into Chemicals, *Chem. Rev.* , 107, Copyright (C) 2010 American Chemical Society (ACS). All Rights Reserved., 2411-2502.

Cortright, R. D., Davda, R. R. & Dumesic, J. A. (2002) Hydrogen from catalytic reforming of biomass-derived hydrocarbons in liquid water, *Nature*, 418, 964-967.

Dapsens, P. Y., Mondelli, C. & Perez-Ramirez, J. (2012) Biobased Chemicals from Conception toward Industrial Reality: Lessons Learned and To Be Learned, *ACS Catal.*, 2, 7, 1487-1499.

Demirbas, A. (2007) Progress and recent trends in biofuels, *Prog. Energ. Combust.*, 33, Copyright (C) 2010 American Chemical Society (ACS). All Rights Reserved., 1-18.

Edenhofer, O., Pichs-Madruga, R. & Sokona, Y., *Renewable Energy Sources and Climate Change Mitigation*, http://srren.ipcc-wg3.de/report/IPCC_SRREN_Full_Report.pdf, (Accessed March 2014).

EIA, *International Energy Outlook 2013*, http://www.eia.gov/forecasts/ieo/world.cfm, (Accessed March 2014).

Erisman, J. W., Sutton, M. A., Galloway, J., Klimont, Z. & Winiwarter, W. (2008) How a century of ammonia synthesis changed the world, *Nat. Geosci.*, 1, 10, 636-639.

Fang, M., Machalaba, N. & Sanchez-Delgado, R. A. (2011) Hydrogenation of arenes and N-heteroaromatic compounds over ruthenium nanoparticles on poly(4-vinylpyridine): a versatile catalyst operating by a substrate-dependent dual site mechanism, *Dalton Trans.*, 40, Copyright (C) 2011 American Chemical Society (ACS). All Rights Reserved., 10621-10632.

Fonseca, G. S., Umpierre, A. P., Fichtner, P. F. P., Teixeira, S. R. & Dupont, J. (2003) The Use of Imidazolium Ionic Liquids for the Formation and Stabilization of Ir0 and Rh0 Nanoparticles: Efficient Catalysts for the Hydrogenation of Arenes, *Chemistry – A European Journal*, 9, 14, 3263-3269.

Gosselink, R. J. A., de Jong, E., Guran, B. & Abacherli, A. (2004) Co-ordination network for lignin-standardisation, production and applications adapted to market requirements (EUROLIGNIN), *Ind. Crops Prod.*, 20, 2, 121-129.

Hodoshima, S. & Saito, Y. (2009) *Hydrogen storage in organic chemical hydrides on the basis of superheated liquid-film concept*, 437-474.

Huber, G. W. & Dumesic, J. A. (2006) An overview of aqueous-phase catalytic processes for production of hydrogen and alkanes in a biorefinery, *Catal. Today*, 111, 1-2, 119-132.

Huber, G. W., Iborra, S. & Corma, A. (2006) Synthesis of transportation fuels from biomass: Chemistry, catalysts, and engineering, *Chem. Rev.*, 106, 9, 4044-4098.

Hubert, C., Bile, E. G., Denicourt-Nowicki, A. & Roucoux, A. (2011) Rh(0) colloids supported on TiO2: a highly active and pertinent tandem in neat water for the hydrogenation of aromatics, *Green Chem.*, 13, Copyright (C) 2011 American Chemical Society (ACS). All Rights Reserved., 1766-1771.

Hubert, C., Denicourt-Nowicki, A., Guegan, J.-P. & Roucoux, A. (2009a) Polyhydroxylated ammonium chloride salt: a new efficient surfactant for nanoparticle stabilization in aqueous media. Characterization and application in catalysis, *Dalton Trans.*, Copyright (C) 2011 American Chemical Society (ACS). All Rights Reserved., 7356-7358.

Hubert, C., Denicourt-Nowicki, A., Roucoux, A., Landy, D., Leger, B., Crowyn, G. & Monflier, E. (2009b) Catalytically active nanoparticles stabilized by host-guest inclusion complexes in water, *Chemical Communications*, 10, 1228-1230.

IEA, *World Energy Outlook 2012*, http://wwww.worldenergyoutlook.org/publications/weo-2012, (Accessed March 2014).

IPCC (2011) *IPCC Special Report on Renewable Energy Sources and Climate Change Mitigation. Prepared by Working Group III of the Intergovernmental Panel on Climate Chnage.*, Edenhofer, O., Pichs-Madruga, R., Sokona, Y., Seyboth, K., Matschoss, P., Kadner, S., Zwickel, T., Eickemeier, P., Hansen, G., Schlömer, S. & vonStechow, C.s (Eds.), Cambridge University Press, Cambridge, United Kingdom and New York, NY, USA, 1075.

IPCC (2013) *Climate Change 2013 The Physical Science Basis. Contribution of Working Group I to the Fifth Asessment Report of the Intergovernmental Panel on Climate Change*, Stocker, T. F., Qin, D., Plattner,

G.-K., Tignor, M. M. B., Allen, S. K., Boschung, J., Nauels, A., Xia, Y., Bex, V. & Midgeley, P. M.s (Eds.), Cambridge University Press, Cambridge, United Kingdom and New York, NY, USA, 1535.

Jahjah, M., Kihn, Y., Teuma, E. & Gomez, M. (2010) Ruthenium nanoparticles supported on multi-walled carbon nanotubes: Highly effective catalytic system for hydrogenation processes, *J. Mol. Catal. A: Chem.*, 332, Copyright (C) 2011 American Chemical Society (ACS). All Rights Reserved., 106-112.

Kariya, N., Fukuoka, A. & Ichikawa, M. (2002) Efficient evolution of hydrogen from liquid cycloalkanes over Pt-containing catalysts supported on active carbons under "wet-dry multiphase conditions", *Appl. Catal., A*, 233, Copyright (C) 2012 American Chemical Society (ACS). All Rights Reserved., 91-102.

Kariya, N., Fukuoka, A., Utagawa, T., Sakuramoto, M., Goto, Y. & Ichikawa, M. (2003) Efficient hydrogen production using cyclohexane and decalin by pulse-spray mode reactor with Pt catalysts, *Appl. Catal., A*, 247, Copyright (C) 2012 American Chemical Society (ACS). All Rights Reserved., 247-259.

Lindstroem, B. & Pettersson, L. J. (2003) A brief history of catalysis, *CATTECH*, 7, 4, 130-138.

Masters, A. F. & Maschmeyer, T. (2011) Zeolites - From curiosity to cornerstone, *Microporous Mesoporous Mater.*, 142, 2-3, 423-438.

Mevellec, V., Nowicki, A., Roucoux, A., Dujardin, C., Granger, P., Payen, E. & Philippot, K. (2006) A simple and reproducible method for the synthesis of silica-supported rhodium nanoparticles and their investigation in the hydrogenation of aromatic compounds, *New J. Chem.*, 30, Copyright (C) 2011 American Chemical Society (ACS). All Rights Reserved., 1214-1219.

Mevellec, V., Roucoux, A., Ramirez, E., Philippot, K. & Chaudret, B. (2004) Surfactant-stabilized aqueous iridium(0) colloidal suspension: An efficient reusable catalyst for hydrogenation of arenes in biphasic media, *Adv. Synth. Catal.*, 346, Copyright (C) 2011 American Chemical Society (ACS). All Rights Reserved., 72-76.

Murray, J. & King, D. (2012) Climate policy: Oil's tipping point has passed, *Nature (London, U. K.)*, 481, 7382, 433-435.

Pan, H.-B. & Wai, C. M. (2009) Sonochemical One-Pot Synthesis of Carbon Nanotube-Supported Rhodium Nanoparticles for Room-Temperature Hydrogenation of Arenes, *J. Phys. Chem. C*, 113, Copyright (C) 2011 American Chemical Society (ACS). All Rights Reserved., 19782-19788.

Park, I. S., Kwon, M. S., Kang, K. Y., Lee, J. S. & Park, J. (2007a) Rhodium and iridium nanoparticles entrapped in aluminum oxyhydroxide nanofibers: catalysts for hydrogenations of arenes and ketones at room temperature with hydrogen balloon, *Adv. Synth. Catal.*, 349, Copyright (C) 2011 American Chemical Society (ACS). All Rights Reserved., 2039-2047.

Park, I. S., Kwon, M. S., Kim, N., Lee, J. S., Kang, K. Y. & Park, J. (2005) Rhodium nanoparticles entrapped in boehmite nanofibers: recyclable catalyst for arene hydrogenation under mild conditions, *Chem. Commun. (Cambridge, U. K.)*, Copyright (C) 2011 American Chemical Society (ACS). All Rights Reserved., 5667-5669.

Park, K. H., Jang, K., Kim, H. J. & Son, S. U. (2007b) Near-monodisperse tetrahedral rhodium nanoparticles on charcoal: the shape-dependent catalytic hydrogenation of arenes, *Angew. Chem., Int. Ed.*, 46, Copyright (C) 2011 American Chemical Society (ACS). All Rights Reserved., 1152-1155.

Pélisson, C.-H., Vono, L. L. R., Hubert, C., Denicourt-Nowicki, A., Rossi, L. M. & Roucoux, A. (2012) Moving from surfactant-stabilized aqueous rhodium (0) colloidal suspension to heterogeneous magnetite-supported rhodium nanocatalysts: Synthesis, characterization and catalytic performance in hydrogenation reactions, *Catalysis Today*, 0.

Biomass as a Feedstock for Bioenergy and Bioproducts Industry: The Technical Feasibility of a Billion-Ton Annual Supply (2005), Perlack, R. D., Wright, L. L., Turhollow, A., Graham, R. L., Stokes, B. & Erbach, D. C.

Robinson, J. M., Barrett, S. R., Nhoy, K., Pandey, R. K., Phillips, J., Ramirez, O. A. & Rodriguez, R. I. (2009) Energy Dispersive X-ray Fluorescence Analysis of Sulfur in Biomass, *Energ. Fuel.*, 23, 2235-2241.

Rodriguez, J. A. (2006) The chemical properties of bimetallic surfaces: Importance of ensemble and electronic effects in the adsorption of sulfur and SO2, *Prog. Surf. Sci.*, 81, Copyright (C) 2010 American Chemical Society (ACS). All Rights Reserved., 141-189.

Rodriguez, J. A. & Goodman, D. W. (1991) High-pressure catalytic reactions over single-crystal metal surfaces, *Surf. Sci. Rep.*, 14, Copyright (C) 2010 American Chemical Society (ACS). All Rights Reserved., 1-107.

Rossi, L. M. & Machado, G. (2009) Ruthenium nanoparticles prepared from ruthenium dioxide precursor: Highly active catalyst for hydrogenation of arenes under mild conditions, *J. Mol. Catal. A: Chem.*, 298, Copyright (C) 2012 American Chemical Society (ACS). All Rights Reserved., 69-73.

Roucoux, A., Schulz, J. & Patin, H. (2003) Arene hydrogenation with a stabilized aqueous rhodium(0) suspension: A major effect of the surfactant counter-anion, *Adv. Synth. Catal.*, 345, Copyright (C) 2011 American Chemical Society (ACS). All Rights Reserved., 222-229.

Scheeren, C. W., Machado, G., Dupont, J., Fichtner, P. F. P. & Texeira, S. R. (2003) Nanoscale Pt(0) Particles Prepared in Imidazolium Room Temperature Ionic Liquids: Synthesis from an Organometallic Precursor, Characterization, and Catalytic Properties in Hydrogenation Reactions, *Inorganic Chemistry*, 42, 15, 4738-4742.

Schulz, J., Levigne, S., Roucoux, A. & Patin, H. (2002) Aqueous rhodium colloidal suspension in reduction of arene derivatives in biphasic system: a significant physico-chemical role of surfactant concentration on catalytic activity, *Adv. Synth. Catal.*, 344, Copyright (C) 2011 American Chemical Society (ACS). All Rights Reserved., 266-269.

Schulz, J., Roucoux, A. & Patin, H. (1999) Unprecedented efficient hydrogenation of arenes in biphasic liquid-liquid catalysis by re-usable aqueous colloidal suspensions of rhodium, *Chem. Commun. (Cambridge)*, Copyright (C) 2011 American Chemical Society (ACS). All Rights Reserved., 535-536.

Schulz, J., Roucoux, A. & Patin, H. (2000) Stabilized rhodium(0) nanoparticles: a reusable hydrogenation catalyst for arene derivatives in a biphasic water-liquid system, *Chem.--Eur. J.*, 6, Copyright (C) 2011 American Chemical Society (ACS). All Rights Reserved., 618-624.

Sheldon, R. A. (2014) Green and sustainable manufacture of chemicals from biomass: state of the art, *Green Chemistry*.

Silveira, E. T., Umpierre, A. P., Rossi, L. M., Machado, G., Morais, J., Soares, G. V., Baumvol, I. J. R., Teixeira, S. R., Fichtner, P. F. P. & Dupont, J. (2004) The Partial Hydrogenation of Benzene to Cyclohexene by Nanoscale Ruthenium Catalysts in Imidazolium Ionic Liquids, *Chemistry – A European Journal*, 10, 15, 3734-3740.

Somorjai, G. A. (1994) *Introduction to Surface Chemistry and Catalysis*, (Eds.), Wiley, New York.

Song, L., Li, X., Wang, H., Wu, H. & Wu, P. (2009) Ru Nanoparticles Entrapped in Mesopolymers for Efficient Liquid-phase Hydrogenation of Unsaturated Compounds, *Catal. Lett.*, 133, Copyright (C) 2012 American Chemical Society (ACS). All Rights Reserved., 63-69.

Stanislaus, A. & Cooper, B. H. (1994) Aromatic hydrogenation catalysis: a review, *Catal. Rev.* , 36, Copyright (C) 2010 American Chemical Society (ACS). All Rights Reserved., 75-123.

Stanley, J. N. G., Benndorf, P., Heinroth, F., Masters, A. F. & Maschmeyer, T. (2014) Probing Structure-Functionality Relationships of Catalytic Bimetallic Pt-Ru Nanoparticles Associated with Improved Sulfur Resistance, *Unpublished*.

Stanley, J. N. G., Heinroth, F., Weber, C. C., Masters, A. F. & Maschmeyer, T. (2013a) Robust bimetallic Pt–Ru catalysts for the rapid hydrogenation of toluene and tetralin at ambient temperature and pressure, *Applied Catalysis A: General*, 454, 46-52.

Stanley, J. N. G., Selva, M., Masters, A. F., Maschmeyer, T. & Perosa, A. (2013b) Reactions of p-coumaryl alcohol model compounds with dimethyl carbonate. Towards the upgrading of lignin building blocks, *Green Chemistry,* 15, 11, 3195-3204.

Stanley, J. N. G., Worthington, K., Heinroth, F., Masters, A. F. & Maschmeyer, T. (2011) Designing nanoscopic, fluxional bimetallic Pt-Ru alloy hydrogenation catalysts for improved

sulfur tolerance, *Catal. Today*, 178, Copyright (C) 2012 American Chemical Society (ACS). All Rights Reserved., 164-171.

Takasaki, M., Motoyama, Y., Higashi, K., Yoon, S.-H., Mochida, I. & Nagashima, H. (2007) Ruthenium nanoparticles on nano-level-controlled carbon supports as highly effective catalysts for arene hydrogenation, *Chem.--Asian J.*, 2, Copyright (C) 2011 American Chemical Society (ACS). All Rights Reserved., 1524-1533.

Thomas, J. M. (1994) Turning Points in Catalysis, *Angewandte Chemie International Edition in English*, 33, 9, 913-937.

Thomas, J. M. & Williams, R. J. P. (2005) Catalysis: principles, progress, prospects, *Philos. Trans. R. Soc. London, Ser. A*, 363, 1829, 765-791.

Vennestrom, P. N. R., Osmundsen, C. M., Christensen, C. H. & Taarning, E. (2011) Beyond Petrochemicals: The Renewable Chemicals Industry, *Angew. Chem., Int. Ed.*, 50, 45, 10502-10509, S10502/1-S10502/2.

Weitkamp, J. (2000) Zeolites and catalysis, *Solid State Ionics*, 131, 1,2, 175-188.

Zaera, F. (2012) New Challenges in Heterogeneous Catalysis for the 21st Century, *Catal. Lett.*, 142, 5, 501-516.

Zahmakiran, M., Tonbul, Y. & Ozkar, S. (2010) Ruthenium(0) Nanoclusters Stabilized by a Nanozeolite Framework: Isolable, Reusable, and Green Catalyst for the Hydrogenation of Neat Aromatics under Mild Conditions with the Unprecedented Catalytic Activity and Lifetime, *J. Am. Chem. Soc.*, 132, Copyright (C) 2011 American Chemical Society (ACS). All Rights Reserved., 6541-6549.

Zakzeski, J., Bruijnincx, P. C. A., Jongerius, A. L. & Weckhuysen, B. M. (2010) The Catalytic Valorization of Lignin for the Production of Renewable Chemicals, *Chem. Rev. (Washington, DC, U. S.)*, 110, Copyright (C) 2012 American Chemical Society (ACS). All Rights Reserved., 3552-3599.

Zakzeski, J., Jongerius, A. L., Bruijnincx, P. C. A. & Weckhuysen, B. M. (2012) Catalytic Lignin Valorization Process for the Production of Aromatic Chemicals and Hydrogen, *ChemSusChem*, 5, Copyright (C) 2012 American Chemical Society (ACS). All Rights Reserved., 1602-1609.

Zhou, X., Wu, T., Hu, B., Jiang, T. & Han, B. (2009) Ru nanoparticles stabilized by poly(N-vinyl-2-pyrrolidone) grafted onto silica: Very active and stable catalysts for hydrogenation of aromatics, *J. Mol. Catal. A: Chem.*, 306, Copyright (C) 2012 American Chemical Society (ACS). All Rights Reserved., 143-148.

Appendix B

This appendix contains the Supplementary Information of the accepted paper, *Probing Structure-Functionality Relationships of Catalytic Bimetallic Pt-Ru Nanoparticles Associated with Improved Sulfur Resistance*, found in Chapter 3.

Supplementary Information of Stanley, J.N.G.; Benndorf, P.; Heinroth, F.; Masters, A.F.; Maschmeyer, T., *RSC Adv*. **2014**, DOI: 10.1039/C4RA03474K.

B.1 Models

B.1.1 Pt Foil

Based on fcc structure.

N(1) = 12

x(1) = (1/2 × 3.909) = 1.9545

y(1) = (1/2 × 3.909) = 1.9545

z(1) = 0

N(2) = 6

x(2) = 3.909

y(2) = 0

z(2) = 0

N(3) = 24

x(3) = 3.909

y(3) = (1/2 × 3.909) = 1.9545

z(3) = -(1/2 × 3.909) = -1.9545

N(4) = 12

x(4) = 3.909

y(4) = 3.909

z(4) = 0

B.1.2 Ru Foil

Based on hcp structure.

N(1) = 12
x(1) = (1/3 × 2.31) = 0.77
y(1) = (2.67 / 2) = 1.335
z(1) = (4.27 / 2) = 2.135

N(2) = 6
x(2) = (2.31 + (1/3 × 2.31)) = 3.08
y(2) = 0
z(2) = 2.135

N(3) = 2
x(3) = 0
y(3) = 0
z(3) = 4.27

N(4) = 18
x(4) = 4.67
y(4) = 0
z(4) = 0

N(5) = 12
x(5) = (2.67 / 2) = 2.31
y(5) = (2.67 / 2) = 1.335
z(5) = 4.27

N(6) = 16
x(6) = 4.67
y(6) = 2.67
z(6) = 0

B.2 Best-Fit Parameters for Fresh, Poisoned, and Regenerated Samples

B.2.1 Pt_1Ru_3

Table B.2.1 Best-fit parameters for fresh, poisoned, and regenerated samples of Pt_1Ru_3 at the Pt L_{III}-edge.

Pt L_{III}-edge											
Pt_1Ru_3 fresh				Pt_1Ru_3 poisoned				Pt_1Ru_3 regenerated			
	R / Å	*N*	σ^2 / Å^2		*R* / Å	*N*	σ^2 / Å^2		*R* / Å	*N*	σ^2 / Å^2
Pt-Pt	2.75	3.1	0.001	Pt-Pt	2.76	3.8	0.001_f	Pt-Pt	2.75	2.4	0.001_f
Pt-Pt	3.90	1.7	0.003	Pt-Pt	3.91	2.8	0.003_f	Pt-Pt	3.91	1.5	0.003_f
Pt-Pt	4.78	3.0	0.0009	Pt-Pt	4.79	3.8	0.0009_f	Pt-Pt	4.77	2.1	0.0009_f
Pt-Pt	5.53	0.4	0.001	Pt-Pt	5.54	0.4	0.001_f	Pt-Pt	5.53	0.2	0.001_f
Pt-Ru	2.70	2.6	0.002	Pt-Ru	2.70	2.2	0.002_f	Pt-Ru	2.71	2.8	0.002_f
Pt-Ru	3.79	0.7	0.0009	Pt-Ru	3.79	0.3	0.0009_f	Pt-Ru	3.79	0.3	0.0009_f
Pt-Ru	4.70	4.7	0.007	Pt-Ru	4.70	3.9	0.007_f	Pt-Ru	4.70	6.6	0.007_f
Pt-Ru	5.41	2.6	0.005	Pt-Ru	5.40	2.2	0.005_f	Pt-Ru	5.40	2.8	0.005_f
R-factor = 9.67%		Chi^2 = 2.41		*R*-factor = 9.56%		Chi^2 = 1.73		*R*-factor = 13.2%		Chi^2 = 5.09	

Table B.2.2 Best-fit parameters for fresh, poisoned, and regenerated samples of Pt_1Ru_3 at the Ru K-edge.

Ru K-edge											
Pt_1Ru_3 fresh				Pt_1Ru_3 poisoned				Pt_1Ru_3 regenerated			
	R / Å	*N*	σ^2 / Å^2		*R* / Å	*N*	σ^2 / Å^2		*R* / Å	*N*	σ^2 / Å^2
Ru-Ru	2.67	8.5	0.003	Ru-Ru	2.67	8.5	0.003_f	Ru-Ru	2.68	8.5	0.003_f
Ru-Ru	2.79	2.8	0.0007	Ru-Ru	2.79	2.4	0.0007_f	Ru-Ru	3.79	2.8	0.0007_f
Ru-Ru	4.29	3.1	0.001	Ru-Ru	4.29	2.6	0.001_f	Ru-Ru	4.30	2.3	0.001_f
Ru-Ru	4.67	6.2	0.0009	Ru-Ru	4.67	5.6	0.0009_f	Ru-Ru	4.67	5.5	0.0009_f
Ru-Ru	5.08	12.2	0.004	Ru-Ru	5.08	12.3	0.004_f	Ru-Ru	5.08	12.5	0.004_f
Ru-Ru	5.34	9.4	0.002	Ru-Ru	5.34	8.0	0.002_f	Ru-Ru	5.33	7.9	0.002_f
Ru-Pt	2.70	0.2	0.001	Ru-Pt	2.70	0.1	0.001_f	Ru-Pt	2.72	0.2	0.001_f
R-factor = 6.17 %		Chi^2 = 1.74		*R*-factor = 6.59%		Chi^2 = 2.09		*R*-factor = 7.46%		Chi^2 = 1.30	

B.2.2 $Pt_{1.5}Ru_1$

Table B.2.3 Best-fit parameters for fresh, poisoned, and regenerated samples of $Pt_{1.5}Ru_1$ at the Pt L_{III}-edge.

Pt L_{III}-edge											
$Pt_{1.5}Ru_1$ fresh				Pt_1Ru_3 poisoned				Pt_1Ru_3 regenerated			
	R / Å	*N*	σ^2 / Å^2		*R* / Å	*N*	σ^2 / Å^2		*R* / Å	*N*	σ^2 / Å^2
Pt-Pt	2.76	9.9	0.0008	Pt-Pt	2.76	10.1	0.0008_f	Pt-Pt	2.76	7.6	0.0008_f
Pt-Pt	3.91	4.9	0.001	Pt-Pt	3.91	5.1	0.001_f	Pt-Pt	3.92	3.6	0.001_f
Pt-Pt	4.80	16.6	0.001	Pt-Pt	4.80	17.6	0.001_f	Pt-Pt	4.80	12.3	0.001_f
Pt-Pt	5.53	9.9	0.003	Pt-Pt	5.53	10.4	0.003_f	Pt-Pt	5.54	7.6	0.003_f
Pt-Ru	2.72	1.2	0.009	Pt-Ru	2.72	1.0	0.009_f				
R-factor = 4.96%		Chi^2 = 1.45		*R*-factor = 5.44%		Chi^2 = 1.30		*R*-factor = 7.59%		Chi^2 = 4.41	

Table B.2.4 Best-fit parameters for fresh, poisoned, and regenerated samples of $Pt_{1.5}Ru_1$ at the Ru K-edge.

Ru K-edge											
$Pt_{1.5}Ru_1$ fresh				Pt_1Ru_3 poisoned				Pt_1Ru_3 regenerated			
	R / Å	*N*	σ^2 / Å^2		*R* / Å	*N*	σ^2 / Å^2		*R* / Å	*N*	σ^2 / Å^2
Ru-Ru	2.68	7.8	0.003	Ru-Ru	2.68	7.8	0.003_f	Ru-Ru	2.68	5.6	0.003_f
Ru-Ru	3.79	2.4	0.0008	Ru-Ru	3.78	2.3	0.0008_f	Ru-Ru	3.79	2.3	0.0008_f
Ru-Ru	4.26	0.2	0.001	Ru-Ru	4.24	0.4	0.001_f	Ru-Ru	4.27	0.7	0.001_f
Ru-Ru	4.68	7.0	0.002	Ru-Ru	4.68	7.5	0.002_f	Ru-Ru	4.68	7.7	0.002_f
Ru-Ru	5.05	4.1	0.0008	Ru-Ru	5.05	3.8	0.0008_f	Ru-Ru	5.05	4.8	0.0008_f
Ru-Ru	5.34	4.2	0.0006	Ru-Ru	5.34	4.9	0.0006_f	Ru-Ru	5.34	4.7	0.0006_f
Ru-Pt	2.72	2.3	0.005	Ru-Pt	2.72	1.8	0.005_f	Ru-Pt	2.73	3.1	0.005_f
R-factor = 5.84%		Chi^2 = 0.64		*R*-factor = 7.72%		Chi^2 = 0.88		*R*-factor = 7.15%		Chi^2 = 1.12	

B.3 Lists of Restraints: Pt L_{III}-Edge

B.3.1 Pt Foil

s1 > 0.001 {0.001}

s2 > 0.001 {0.001}

s3 > 0.001 {0.001}

s4 > 0.001 {0.001}

s1 < 0.01 {0.001}

s2 < 0.01 {0.001}

s3 < 0.01 {0.001}

s4 < 0.01 {0.001}

S02 ~= 0.85 {0.2}

E0 < -1 {0.5}

|(v1 - v0)| ~= 2.76 {0.01}

|(v2 - v0)| ~= 3.91 {0.01}

|(v3 - v0)| ~= 4.79 {0.01}

|(v4 - v0)| ~= 5.53 {0.01}

s1 ~= s2 {0.015}

s2 ~= s3 {0.015}

s3 ~= s4 {0.015}

|(v2 - v1)| ~= 2.765 {0.05}

|(v3 - v2)| ~= 2.765 {0.05}

|(v4 - v3)| ~= 2.765 {0.05}

|(v3 - v1)| ~= 2.765 {0.05}

|(v1 - v4)| ~= 2.765 {0.05}

B.3.2 Pt catalyst

s1 > 0.001 {0.001}

s2 > 0.001 {0.001}

s3 > 0.001 {0.001}

s4 > 0.001 {0.001}

s1 < 0.01 {0.001}

s2 < 0.01 {0.001}

s3 < 0.01 {0.001}

s4 < 0.01 {0.001}

S02 ~= 0.85 {0.2}

E0 < -1 {0.5}

s1 ~= s2 {0.015}

s2 ~= s3 {0.015}

s3 ~= s4 {0.015}

|(v2 - v1)| ~= 2.765 {0.05}

|(v3 - v2)| ~= 2.765 {0.05}

|(v4 - v3)| ~= 2.765 {0.05}

|(v3 - v1)| ~= 2.765 {0.05}

|(v1 - v0)| ~= 2.76 {0.05}

|(v2 - v0)| ~= 3.91 {0.05}

|(v3 - v0)| ~= 4.79 {0.05}

|(v4 - v0)| ~= 5.53 {0.05}

B.3.3 Pt_1Ru_3 catalyst (fresh, poisoned, regenerated)

s1 > 0.001 {0.001}

s2 > 0.001 {0.001}

s3 > 0.001 {0.001}

s4 > 0.001 {0.001}

s1 < 0.01 {0.001}

s2 < 0.01 {0.001}

s3 < 0.01 {0.001}

s4 < 0.01 {0.001}

S02 ~= 0.85 {0.2}

E0 < -1 {0.5}

|(v1 - v0)| ~= 2.76 {0.01}

|(v2 - v0)| ~= 3.91 {0.01}

|(v3 - v0)| ~= 4.79 {0.01}

|(v4 - v0)| ~= 5.53 {0.01}

s1 ~= s2 {0.015}

s2 ~= s3 {0.015}

s3 ~= s4 {0.015}

|(v2 - v1)| ~= 2.765 {0.05}

|(v3 - v2)| ~= 2.765 {0.05}

|(v4 - v3)| ~= 2.765 {0.05}

|(v3 - v1)| ~= 2.765 {0.05}

|(v1 - v4)| ~= 2.765 {0.05}

s5 ~= s1 {0.015}

s5 > 0.001 {0.001}

s5 < 0.01 {0.001}

|(v6 - v0)| ~= 3.79 {0.01}

|(v6 - v5)| ~= 2.7 {0.05}

|(v5 - v0)| ~= 2.7 {0.01}

s6 > 0.001 {0.001}

s6 < 0.01 {0.001}

|(v7 - v0)| ~= 4.7 {0.01}

|(v7 - v6)| ~= 2.7 {0.05}

|(v7 - v5)| ~= 2.7 {0.05}

s7 > 0.001 {0.001}

s7 < 0.01 {0.001}

|(v8 - v0)| ~= 5.4 {0.01}

s8 > 0.001 {0.001}

s8 < 0.01 {0.001}

s5 ~= s6 {0.015}

s6 ~= s7 {0.015}

s7 ~= s8 {0.015}

|(v8 - v7)| ~= 2.7 {0.05}

|(v8 - v5)| ~= 2.7 {0.05}

B.3.4 $Pt_{1.5}Ru_1$ catalyst (fresh, poisoned, regenerated)

s1 > 0.001 {0.001}

s2 > 0.001 {0.001}

s3 > 0.001 {0.001}

s4 > 0.001 {0.001}

s1 < 0.01 {0.001}

s2 < 0.01 {0.001}

s3 < 0.01 {0.001}

s4 < 0.01 {0.001}

S02 ~= 0.85 {0.2}

E0 < -1 {0.5}

|(v1 - v0)| ~= 2.76 {0.01}

|(v2 - v0)| ~= 3.91 {0.01}

|(v3 - v0)| ~= 4.79 {0.01}

|(v4 - v0)| ~= 5.53 {0.01}

s1 ~= s2 {0.015}

s2 ~= s3 {0.015}

s3 ~= s4 {0.015}

|(v2 - v1)| ~= 2.765 {0.05}

|(v3 - v2)| ~= 2.765 {0.05}

|(v4 - v3)| ~= 2.765 {0.05}

|(v3 - v1)| ~= 2.765 {0.05}

|(v1 - v4)| ~= 2.765 {0.05}

s5 ~= s1 {0.015}

s5 > 0.001 {0.001}

s5 < 0.01 {0.001}

|(v5 - v0)| ~= 2.72 {0.01}

B.3.5 $Pt_1Ru_{1.5}$ catalyst

s1 > 0.001 {0.001}

s2 > 0.001 {0.001}

s3 > 0.001 {0.001}

s4 > 0.001 {0.001}

s1 < 0.01 {0.001}

s2 < 0.01 {0.001}

s3 < 0.01 {0.001}

s4 < 0.01 {0.001}

S02 ~= 0.85 {0.2}

E0 < -1 {0.5}

|(v1 - v0)| ~= 2.76 {0.01}

|(v2 - v0)| ~= 3.91 {0.01}

|(v3 - v0)| ~= 4.79 {0.01}

|(v4 - v0)| ~= 5.53 {0.01}

s1 ~= s2 {0.015}

s2 ~= s3 {0.015}

s3 ~= s4 {0.015}

|(v2 - v1)| ~= 2.765 {0.05}

|(v3 - v2)| ~= 2.765 {0.05}

|(v4 - v3)| ~= 2.765 {0.05}

|(v3 - v1)| ~= 2.765 {0.05}

|(v1 - v4)| ~= 2.765 {0.05}

s1 ~= s5 {0.015}

|(v5 - v0)| ~= 2.7 {0.01}

s5 > 0.001 {0.001}

s5 < 0.01 {0.001}

B.4 List of Restraints: Ru K-Edge

B.4.1 Ru foil

s1 > 0.001 {0.001}

s2 > 0.001 {0.001}

s3 > 0.001 {0.001}

s4 > 0.001 {0.001}

s1 < 0.01 {0.001}

s2 < 0.01 {0.001}

s3 < 0.01 {0.001}

s4 < 0.01 {0.001}

S02 ~= 0.85 {0.2}

E0 < -1 {0.5}

s1 ~= s2 {0.015}

s2 ~= s3 {0.015}

s3 ~= s4 {0.015}

|(v1 - v0)| ~= 2.67 {0.05}

|(v2 - v0)| ~= 3.78 {0.05}

|(v2 - v1)| ~= 2.67 {0.05}

|(v3 - v0)| ~= 4.27 {0.05}

|(v3 - v1)| ~= 2.67 {0.05}

|(v4 - v0)| ~= 4.67 {0.05}

|(v4 - v2)| ~= 2.67 {0.05}

|(v5 - v0)| ~= 5.06 {0.05}

|(v5 - v3)| ~= 2.67 {0.05}

|(v5 - v2)| ~= 2.67 {0.05}

|(v5 - v1)| ~= 2.67 {0.05}

s5 > 0.001 {0.001}

s5 < 0.01 {0.001}

s4 ~= s5 {0.015}

|(v6 - v0)| ~= 5.33 {0.05}

|(v6 - v4)| ~= 2.67 {0.05}

s6 > 0.001 {0.001}

s6 < 0.01 {0.001}

s6 ~= s5 {0.015}

B.4.2 Ru catalyst

s1 > 0.001 {0.001}

s2 > 0.001 {0.001}

s3 > 0.001 {0.001}

s4 > 0.001 {0.001}

s1 < 0.01 {0.001}

s2 < 0.01 {0.001}

s3 < 0.01 {0.001}

s4 < 0.01 {0.001}

S02 ~= 0.85 {0.2}

E0 < -1 {0.5}

s1 ~= s2 {0.015}

s2 ~= s3 {0.015}

s3 ~= s4 {0.015}

|(v1 - v0)| ~= 2.67 {0.05}

|(v2 - v0)| ~= 3.78 {0.05}

|(v2 - v1)| ~= 2.67 {0.05}

|(v3 - v0)| ~= 4.27 {0.05}

|(v3 - v1)| ~= 2.67 {0.05}

|(v4 - v0)| ~= 4.67 {0.05}

|(v4 - v2)| ~= 2.67 {0.05}

|(v5 - v0)| ~= 5.06 {0.05}

|(v5 - v3)| ~= 2.67 {0.05}

|(v5 - v2)| ~= 2.67 {0.05}

|(v5 - v1)| ~= 2.67 {0.05}

s5 > 0.001 {0.001}

s5 < 0.01 {0.001}

s4 ~= s5 {0.015}

|(v6 - v0)| ~= 5.33 {0.05}

|(v6 - v4)| ~= 2.67 {0.05}

s6 > 0.001 {0.001}

s6 < 0.01 {0.001}

s6 ~= s5 {0.015}

N5 < 12 {2}

B.4.3 Pt_1Ru_3 catalyst (fresh, poisoned, regenerated)

s1 > 0.001 {0.001}

s2 > 0.001 {0.001}

s3 > 0.001 {0.001}

s4 > 0.001 {0.001}

s1 < 0.01 {0.001}

s2 < 0.01 {0.001}

s3 < 0.01 {0.001}

s4 < 0.01 {0.001}

S02 ~= 0.85 {0.2}

E0 < -1 {0.5}

s1 ~= s2 {0.015}

s2 ~= s3 {0.015}

s3 ~= s4 {0.015}

|(v1 - v0)| ~= 2.67 {0.05}

|(v2 - v0)| ~= 3.78 {0.05}

|(v2 - v1)| ~= 2.67 {0.05}

|(v3 - v0)| ~= 4.27 {0.05}

|(v3 - v1)| ~= 2.67 {0.05}

|(v4 - v0)| ~= 4.67 {0.05}

|(v4 - v2)| ~= 2.67 {0.05}

|(v5 - v0)| ~= 5.06 {0.05}

|(v5 - v3)| ~= 2.67 {0.05}

|(v5 - v2)| ~= 2.67 {0.05}

|(v5 - v1)| ~= 2.67 {0.05}

s5 > 0.001 {0.001}

s5 < 0.01 {0.001}

s4 ~= s5 {0.015}

|(v6 - v0)| ~= 5.33 {0.05}

|(v6 - v4)| ~= 2.67 {0.05}

s6 > 0.001 {0.001}

s6 < 0.01 {0.001}

s7 > 0.001 {0.001}

s7 < 0.01 {0.001}

|(v7 - v0)| ~= 2.7 {0.05}

N5 < 12 {2}

B.4.4 $Pt_{1.5}Ru_1$ catalyst (fresh, poisoned, regenerated)

s1 > 0.001 {0.001}

s2 > 0.001 {0.001}

s3 > 0.001 {0.001}

s4 > 0.001 {0.001}

s1 < 0.01 {0.001}

s2 < 0.01 {0.001}

s3 < 0.01 {0.001}

s4 < 0.01 {0.001}

S02 ~= 0.85 {0.2}

E0 < -1 {0.5}

s1 ~= s2 {0.015}

s2 ~= s3 {0.015}

s3 ~= s4 {0.015}

|(v1 - v0)| ~= 2.67 {0.05}

|(v2 - v0)| ~= 3.78 {0.05}

|(v2 - v1)| ~= 2.67 {0.05}

|(v3 - v0)| ~= 4.27 {0.05}

|(v3 - v1)| ~= 2.67 {0.05}

|(v4 - v0)| ~= 4.67 {0.05}

|(v4 - v2)| ~= 2.67 {0.05}

|(v5 - v0)| ~= 5.06 {0.05}

|(v5 - v3)| ~= 2.67 {0.05}

|(v5 - v2)| ~= 2.67 {0.05}

|(v5 - v1)| ~= 2.67 {0.05}

s5 > 0.001 {0.001}

s5 < 0.01 {0.001}

s4 ~= s5 {0.015}

|(v6 - v0)| ~= 5.33 {0.05}

|(v6 - v4)| ~= 2.67 {0.05}

s6 > 0.001 {0.001}

s6 < 0.01 {0.001}

|(v7 - v0)| ~= 2.72 {0.01}

s7 > 0.001 {0.001}

s7 < 0.01 {0.001}

B.4.5 $Pt_1Ru_{1.5}$ catalyst

s1 > 0.001 {0.001}

s2 > 0.001 {0.001}

s3 > 0.001 {0.001}

s4 > 0.001 {0.001}

s1 < 0.01 {0.001}

s2 < 0.01 {0.001}

s3 < 0.01 {0.001}

s4 < 0.01 {0.001}

S02 ~= 0.85 {0.2}

E0 < -1 {0.5}

s1 ~= s2 {0.015}

s2 ~= s3 {0.015}

s3 ~= s4 {0.015}

|(v1 - v0)| ~= 2.67 {0.05}

|(v2 - v0)| ~= 3.78 {0.05}

|(v2 - v1)| ~= 2.67 {0.05}

|(v3 - v0)| ~= 4.27 {0.05}

|(v3 - v1)| ~= 2.67 {0.05}

|(v4 - v0)| ~= 4.67 {0.05}

|(v4 - v2)| ~= 2.67 {0.05}

|(v5 - v0)| ~= 5.06 {0.05}

|(v5 - v3)| ~= 2.67 {0.05}

|(v5 - v2)| ~= 2.67 {0.05}

|(v5 - v1)| ~= 2.67 {0.05}

s5 > 0.001 {0.001}

s5 < 0.01 {0.001}

s4 ~= s5 {0.015}

|(v6 - v0)| ~= 5.33 {0.05}

|(v6 - v4)| ~= 2.67 {0.05}

s6 > 0.001 {0.001}

s6 < 0.01 {0.001}

s7 > 0.001 {0.001}

s7 < 0.01 {0.001}

|(v8 - v0)| ~= 2.7 {0.01}

|(v7 - v0)| ~= 2 {0.01}

s7 ~= s8 {0.015}

s8 > 0.001 {0.001}

s8 < 0.01 {0.001}

|(v9 - v0)| ~= 3.91 {0.01}

s8 ~= s9 {0.015}

s9 > 0.001 {0.001}

s9 < 0.01 {0.001}

|(v9 - v0)| ~= 3.79 {0.01}

|(v9 - v8)| ~= 2.7 {0.05}

Appendix C

This appendix contains the Supplementary Information of the published paper, *Robust Bimetallic Pt-Ru Catalysts for the Rapid Hydrogenation of Toluene and Tetralin at Ambient Temperature and Pressure*, found in Chapter 4.

Supplementary Information of Stanley, J.N.G.; Heinroth, F.; Weber, C.C.; Masters, A.F.; Maschmeyer, T., *Appl. Catal., A* **2013**, 454, 46–52.

C.1 Area of a hexagon

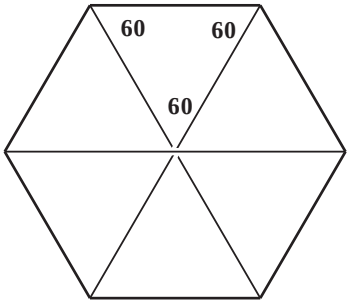

A hexagon of side length, *a*, is made up of six equilateral triangles of sides, *a*.

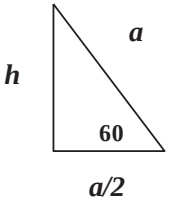

The height, *h*, can be determined from $a^2 = h^2 + (a/2)^2$

So $h^2 = a^2 - (a/2)^2 = a^2 - a^2/4 = 3a^2/4$

Then, $h = (a/2)(\sqrt{3})$

Since the area of a triangle = *(1/2)(base)(height)*

The area of each equilateral triangle = $\left(\frac{1}{2}\right)(a)\left(\frac{a\sqrt{3}}{2}\right) = \frac{a^2\sqrt{3}}{4}$

So the area of the hexagon = $\frac{6a^2\sqrt{3}}{4} = \frac{3a^2\sqrt{3}}{2}$

C.2 Area of the circles contained in a hexagon – hexagon packing density

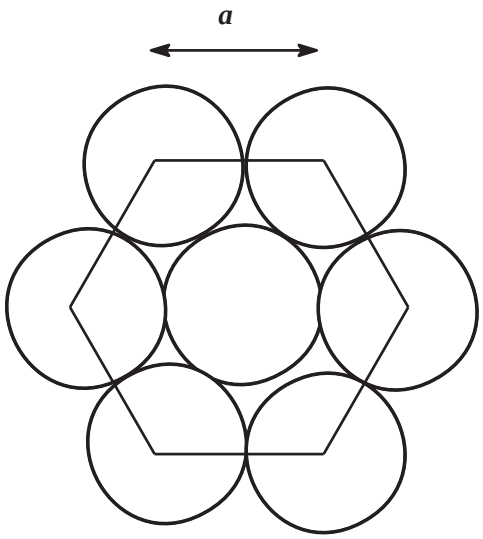

A hexagon of side length, *a*, has 6 circles of radius, *a/2*, one at each vertex, and a circle of radius, *a/2*, at it's centre. One third of each circle is within the hexagon (since the angle subtended by the two radii, each part of a side of the hexagon is 120 °.

So, the number of circles at the corners of the hexagon = 6(1/3) = 2. Since the hexagon also contains a complete circle, the number of circles within the hexagon = 2 + 1 = 3.

Therefore the packed area within the hexagon = $3\pi(a/2)^2 = (3/4)\pi a^2$.

Since the area of a regular hexagon, of side length *a*, is $a^2 \frac{3}{2}\sqrt{3}$

And the area of the circles that can be packed into a hexagon = $\frac{3\pi a^2}{4}$

Then, the packing density of a hexagon = $\left(\frac{3\pi a^2}{4}\right)\left(\frac{2}{a^2 3\sqrt{3}}\right) = \frac{\pi}{2\sqrt{3}}$ (= 90.69%)

That is, $\pi/(2\sqrt{3})$ of the surface of a hcp sphere will be covered by atoms

(The flat-to-flat distance of a regular hexagon, $d = a\sqrt{3}$, so the area = $d^2 \frac{\sqrt{3}}{2} = d^2 \sin 60$)

C.3 The available (covered) surface area of the nanoparticles

For nanoparticles of diameter, d,

Surface area of a sphere of radius *d/2* = $4\pi\left(\frac{d}{2}\right)^2 = \pi d^2$

If the packing efficiency of the hexagons on that surface = $\frac{\pi}{2\sqrt{3}}$

Then, the available surface area of a spherical hcp nanoparticle of diameter, *d*, = $\left(\frac{\pi}{2\sqrt{3}}\right)\pi d^2 = \pi^2 d^2/2\sqrt{3}$

C.4 Number of Ru atoms that can cover this area

The cross section area of a Ru atom of radius, *r*, = πr^2

So, the number of Ru atoms, radius, *r*, on the spherical nanoparticle surface = $\left(\frac{\pi^2 d^2}{2\sqrt{3}}\right)\left(\frac{1}{\pi r^2}\right) = \frac{\pi}{2\sqrt{3}}\left(\frac{d}{r}\right)^2$

C.5 Number of Ru atoms in the spherical nanoparticle

(i) Volume of Ru atom

Volume of Ru atom of atomic radius *r* is $\frac{4}{3}\pi(r)^3$

(ii) Available volume of nanoparticle

Volume of a sphere of radius *d/2* is $\frac{4}{3}\pi\left(\frac{d}{2}\right)^3$

since packing efficiency of hcp is $\frac{\pi}{\sqrt{18}}$

Then available volume of hcp sphere is $\left[\frac{\pi}{\sqrt{18}}\right]\left[\frac{4}{3}\pi\left(\frac{d}{2}\right)^3\right] = \frac{\pi^2}{6\sqrt{18}}d^3$

(iii) Number of Ru atoms in the available volume

So number of Ru atoms in the sphere = $\frac{3\pi^2 d^3}{(6\sqrt{18})(4\pi r^3)} = \frac{\pi}{8\sqrt{18}}\left(\frac{d}{r}\right)^3$

C.6 Fraction of Ru atoms on the surface of the nanoparticle

If number of Ru atoms on the surface $= \left(\frac{\pi}{2\sqrt{3}}\right)\left(\frac{d}{r}\right)^2$

Then fraction of Ru atoms on the surface = $\left(\frac{\pi}{2\sqrt{3}}\right)\left(\frac{d}{r}\right)^2 \frac{8\sqrt{18}}{\pi}\left(\frac{r}{d}\right)^3 = 4\sqrt{6}\left(\frac{r}{d}\right)$

Then, if $d = 10 \times 10^{-9}$ m, and $r = 134 \times 10^{-12}$ m $= 0.134 \times 10^{-9}$ m, then, $r/d = 0.0134$, and fraction of Ru atoms on surface $= 0.0134 \times 4\sqrt{6} = 0.1313$

If only half of these are accessible, then fraction of accessible Ru atoms = 0.0656,

So TOF should be multiplied by 1/0.0656 = 15.3

Appendix D

This appendix contains the Supplementary Information of the published paper, *Reactions of p-Coumaryl Alcohol Model Compounds with Dimethyl Carbonate. Towards the Upgrading of Lignin Building Blocks*, found in Chapter 5.

Supllementary Information of Stanley, J.N.G.; Selva M.; Masters, A.F.; Maschmeyer, T.; Perosa, A., *Green Chem.* **2013**, *15*, 3195–3204.

D.1 ^{1}H NMR and MS spectra of all reported compounds and ^{13}C NMR spectra of new compounds.

cinnamyl methyl carbonate (1a), clear, pale yellow liquid. GC/MS (relative intensity, 70 eV) m/z: 192 (M^{+}, 16%), 133 (19), 103 (67), 102 (68), 91 (26), 79 (11), 78 (10), 77 (27), 50 (12), 43 (19).

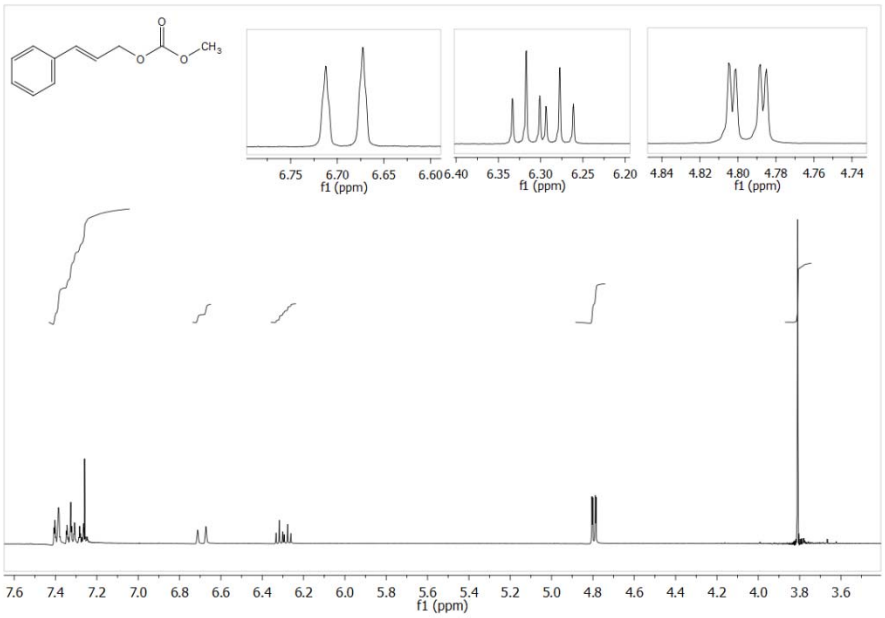

Figure D.1 ^{1}H NMR of cinnamyl methyl carbonate (**1a**).

^{1}H NMR (400 MHz, $CDCl_3$) δ (ppm) 7.42–7.24 (m, 5H), 6.69 (d, *J* = 15.9 Hz, 1H), 6.29 (dt, *J* = 15.9, 6.5 Hz, 1H), 4.80 (dd, *J* = 6.5, 1.3 Hz, 2H), 3.81 (s, 3H).

cinnamyl methyl ether (1b), clear, colourless liquid. GC/MS (relative intensity, 70 eV) m/z: 148 (M^+, 55%), 147 (30), 133 (13), 121 (13), 118 (18), 117 (69), 115 (100), 105 (42), 103 (24), 91 (38), 89 (12), 79 (20), 78 (15), 77 (42), 65 (15), 63 (19), 55 (12), 51 (34), 50 (16), 45 (15), 41 (13).

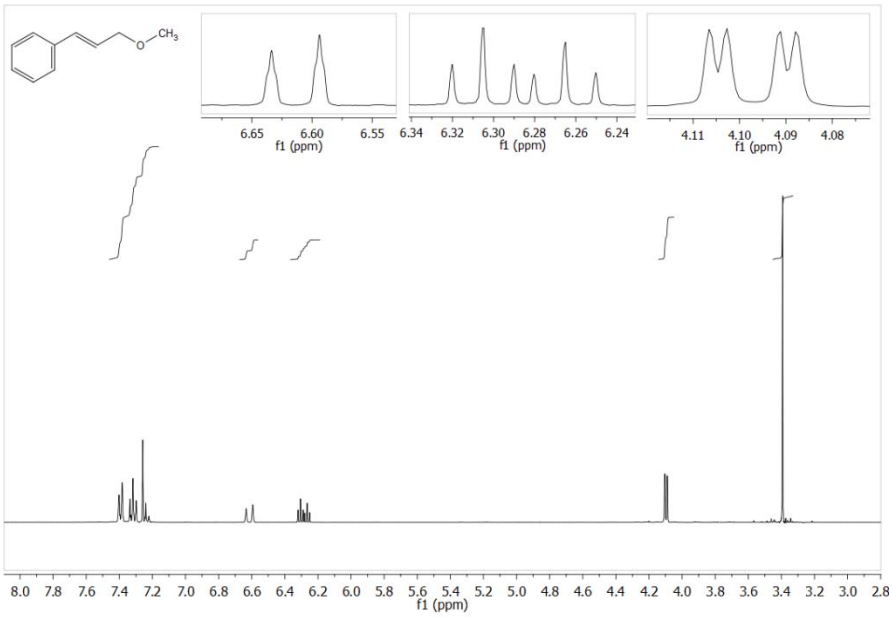

Figure D.2 ^{1}H NMR of cinnamyl methyl ether (**1b**).

^{1}H NMR (400 MHz, $CDCl_3$) δ (ppm) 7.42–7.21 (m, 5H), 6.61 (d, *J* = 16.0 Hz, 1H), 6.29 (dt, *J* = 16.0, 6.0 Hz, 1H), 4.10 (dd, *J* = 6.0, 1.4 Hz, 2H), 3.39 (s, 3H).

3-methoxy-3-phenylpropene (1c), clear, colourless liquid. GC/MS (relative intensity, 70 eV) m/z: 148 (M^+, 55%), 147 (48), 133 (11), 121 (62), 118 (21), 117 (86), 116 (72), 115 (100), 105 (47), 103 (11), 91 (68), 89 (16), 79 (11), 78 (17), 77 (92), 71 (12), 65 (20), 63 (24), 55 (29), 52 (11), 51 (52), 50 (26), 41 (25).

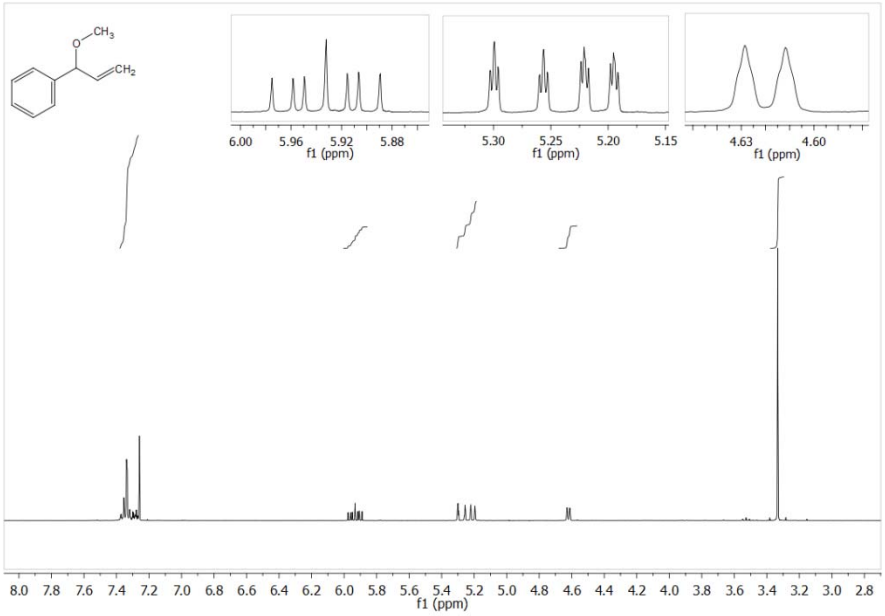

Figure D.3 ^{1}H NMR of 3-methoxy-3-phenylpropene (**1c**).

^{1}H NMR (400 MHz, $CDCl_3$) δ (ppm) 7.38–7.25 (m, 5H), 5.93 (ddd, *J* = 17.1, 10.4, 6.7 Hz, 1H), 5.25 (m, 2H), 4.62 (d, *J* = 6.7 Hz, 1H), 3.33 (s, 3H).

3-(4-methoxyphenyl)-1-propanol (2a), clear, colourless liquid. GC/MS (relative intensity, 70eV) m/z: 166 (M^+, 19%), 122 (11), 121 (100), 91 (13), 78 (10), 77 (17).

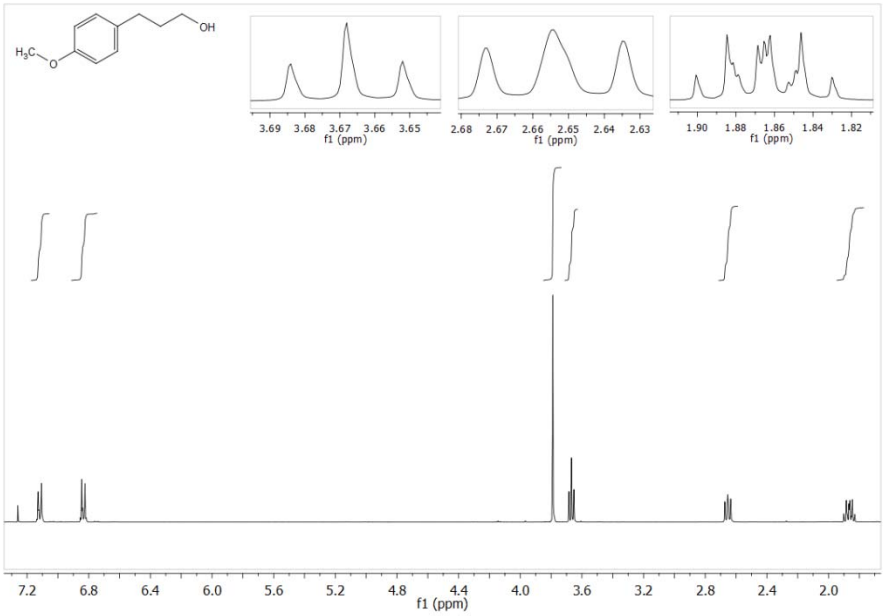

Figure D.4 ^{1}H NMR of 3-(4-methoxyphenyl)-1-propanol (**2a**).

^{1}H NMR (400 MHz, $CDCl_3$) δ (ppm) 7.12 (d, J = 8.5 Hz, 2H), 6.83 (d, J = 8.5 Hz, 2H), 3.79 (s, 3H), 3.67 (t, J = 6.5 Hz, 2H), 2.65 (t, J = 7.5 Hz, 2H), 1.90–1.82 (m, 2H).

4-(3-methoxypropyl)phenol (2b), clear, colourless liquid. GC/MS (relative intensity, 70eV) m/z: 166 (M^+, 19%), 134 (73), 133 (75), 108 (13), 107 (100), 105 (11), 91 (17), 78 (10), 77 (38), 65 (10), 51 (11), 45 (35).

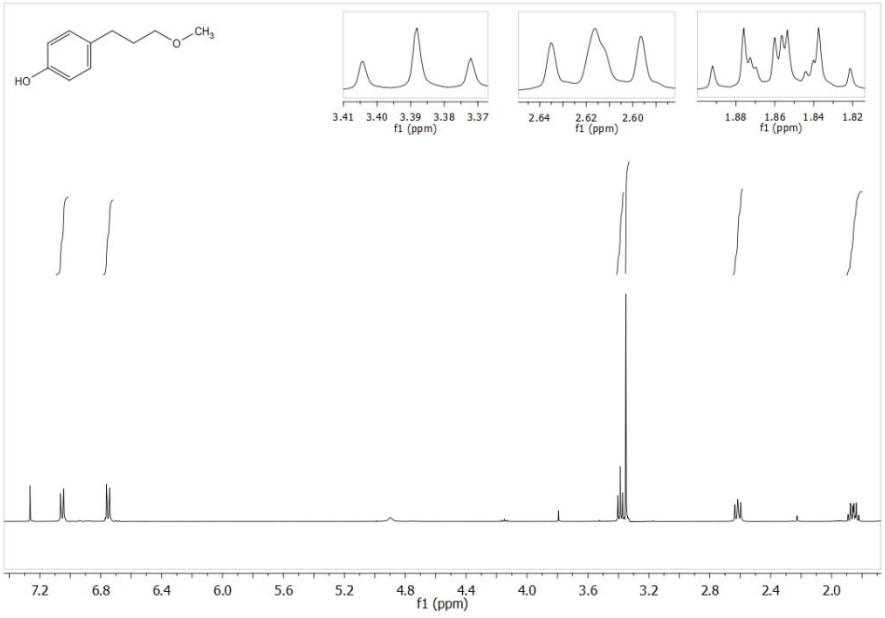

Figure D.5 ^{1}H NMR of 4-(3-methoxypropyl)phenol (**2b**).

^{1}H NMR (400 MHz, $CDCl_3$) δ (ppm) 7.05 (d, *J* = 8.5Hz, 2H), 6.75 (d, *J* = 8.5Hz, 2H), 3.39 (t, *J* = 6.5Hz, 2H), 3.35 (s, 3H), 2.62 (t, *J* = 7.4 Hz, 2H), 1.90–1.81 (m, 2H).

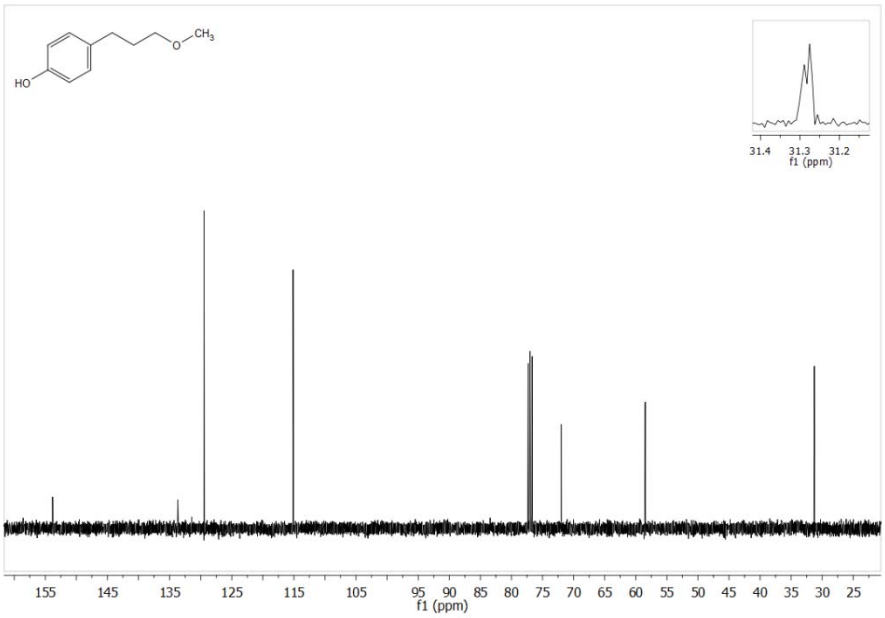

Figure D.6 ^{13}C NMR of 4-(3-methoxypropyl)phenol (**2b**).

^{13}C NMR (100 MHz, $CDCl_3$) δ (ppm) 153.8, 133.7, 129.5, 115.1, 72.0, 58.5, 31.3, 31.3.

3-(4-hydroxyphenyl)propyl methyl carbonate (2c), clear, colourless liquid. GC/MS (relative intensity, 70eV) m/z 210 (M^+, 7%), 135 (15), 134 (90), 133 (87), 119 (10), 107 (100), 91 (16), 78 (11), 77 (35), 59 (13).

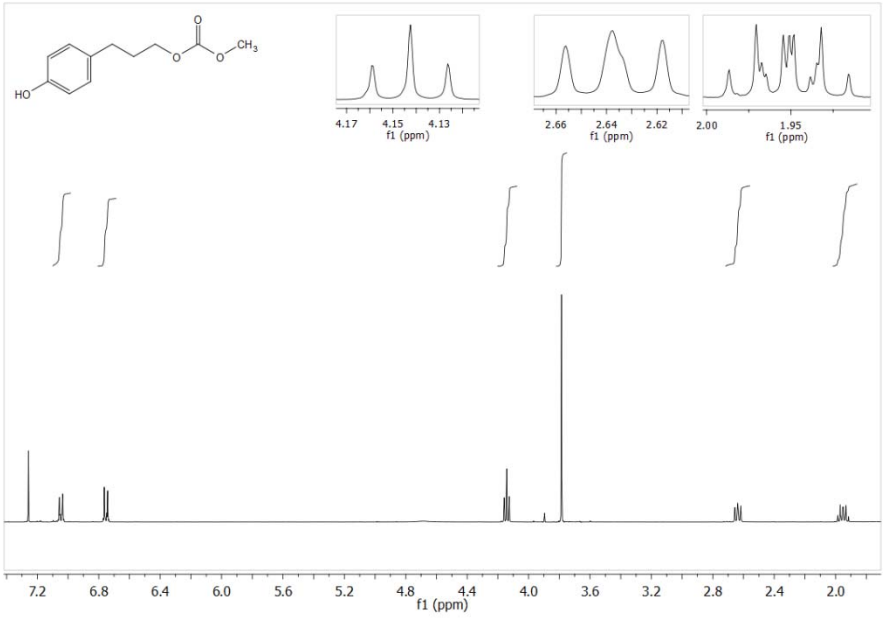

Figure D.7 ^{1}H NMR of 3-(4-hydroxyphenyl)propyl methyl carbonate (**2c**).

^{1}H NMR (400 MHz, $CDCl_3$) δ (ppm) 7.05 (d, *J* = 8.5, 2H), 6.75 (d, *J* = 8.5, 2H), 4.14 (t, *J* = 6.5Hz, 2H), 3.79 (s, 3H), 2.64 (t, *J* = 7.5Hz, 2H), 1.99–1.91 (m, 2H).

3-(4-methoxyphenyl)propyl methyl carbonate (2d), clear, colourless liquid. GC/MS (relative intensity, 70eV) m/z: 224 (M^+, 12%), 149 (14), 148 (72), 147 (47), 133 (14), 121 (100), 117 (21), 105 (11), 91 (23), 78 (18), 77 (24), 65 (10), 59 (12).

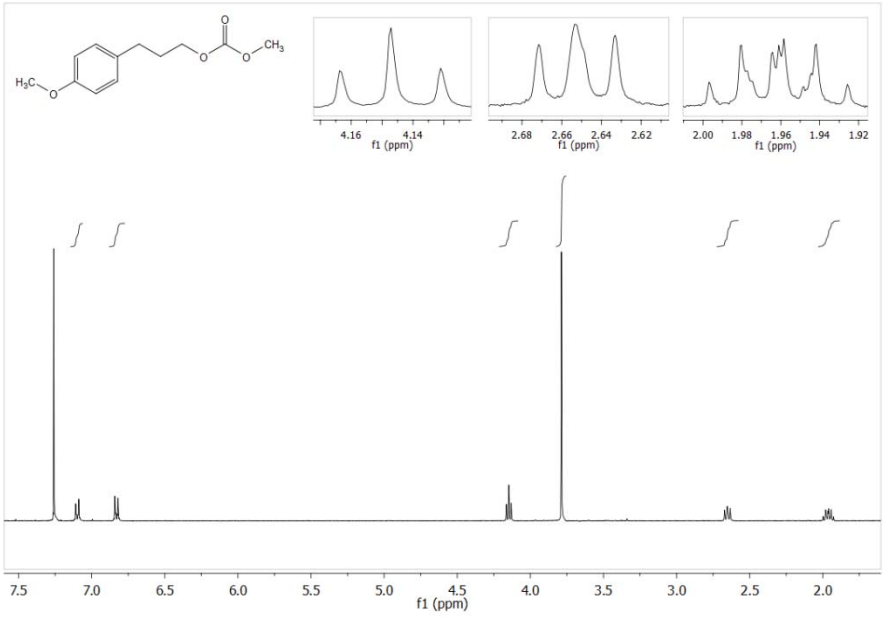

Figure D.8 ^{1}H NMR of 3-(4-methoxyphenyl)propyl methyl carbonate (**2d**).

^{1}H NMR (400 MHz, $CDCl_3$) δ (ppm) 7.10 (d, J = 8.6 Hz, 2H), 6.83 (d, J = 8.6Hz, 2H), 4.15 (t, J = 6.5Hz, 2H), 3.79 (s, 3H), 2.65 (t, J = 7.4Hz, 2H), 2.00–1.92 (m, 2H).

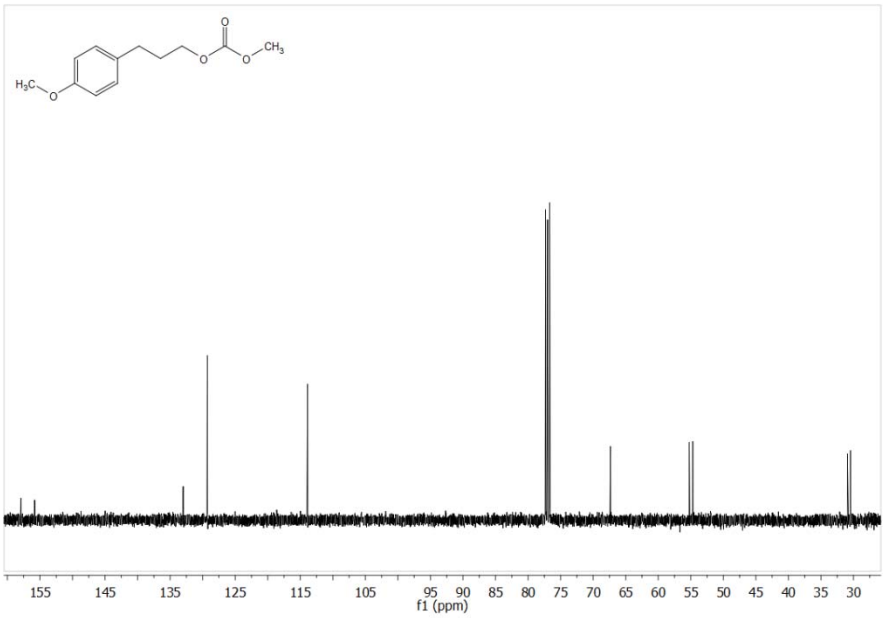

Figure D.9 ^{13}C NMR of 3-(4-methoxyphenyl)propyl methyl carbonate (**2d**).

^{13}C NMR (100 MHz, $CDCl_3$) δ (ppm) 157.9, 155.7, 132.9, 129.2, 113.8, 67.3, 55.1, 54.7, 30.8, 30.3.

1-methoxy-4-(3-methoxypropyl)benzene (2e), clear, colourless liquid. GC/MS (relative intensity, 70 eV) m/z: 180 (M^+, 22%), 122 (14), 121 (100), 117 (16), 94 (11), 91 (24), 77 (25), 78 (19), 65 (11).

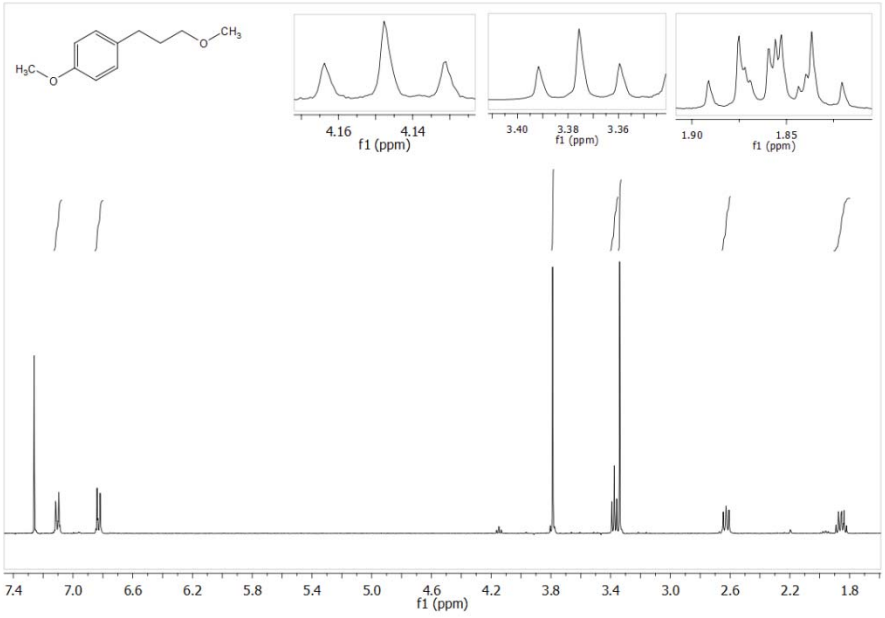

Figure D.10 ^{1}H NMR of 1-methoxy-4-(3-methoxypropyl)benzene (**2e**).

^{1}H NMR (400 MHz, $CDCl_3$) δ (ppm) 7.11 (d, J = 8.6 Hz, 2H), 6.83 (d, J = 8.6Hz, 2H), 3.79 (s, 3H), 3.38 (t, J = 6.4 Hz, 2H), 3.34 (s, 3H), 2.63 (t, J = 7.5 Hz, 2H), 1.90–1.81 (m, 2H).

Estratto per riassunto della tesi di dottorato

Studente: Jessica N. G. Stanley Matricola: 955965

Dottorato: Dottorato di ricerca in Scienze Chimiche

Ciclo: XXVI

Titolo della tesi: **Novel Applications of Catalysis for Green and Sustainable Chemistry**

Estratto:

Questa tesi prende in esame lo studio fondamentale di catalizzatori per processi chimici più sostenibili. In particolare:

(1) Lo sviluppo di un catalizzatore resistente allo zolfo per il trattamento della biomassa per la produzione di carburanti liquidi per mezzi di trasporto.

(2) La riduzione della domanda energetica ed il miglioramento della semplicità di utilizzo di catalizzatori per l'idrogenazione di aromatici, in particolare per il fattibile e sicuro stoccaggio d'idrogeno, mediante la coppia reversible toluene/metilcicloesano.

(3) Lo studio della conversione catalitica mediante l'impiego di dimetilcarbonato, di molecole modello delle componenti della lignina come risorsa di composti aromatici d'origine rinnovabile.

Firma dello studente

Abstract for the summary of the PhD Thesis

Student: Jessica N. G. Stanley Matriculation number: 955965

PhD: PhD in Chemical Sciences

Cycle: XXVI

Title of the thesis: **Novel Applications of Catalysis for Green and Sustainable Chemistry**

Abstract:

This thesis examines fundamental studies of catalysts for more sustainable processes, addressing three particular challenges:

(1) Developing sulfur resistant catalysts that have potential applications in the processing of biomass for the production of liquid transportation fuels.

(2) Reducing energy requirements and increasing the catalyst ease-of-use (especially water tolerance) for the hydrogenation of aromatics, particularly for the safe and feasible storage of hydrogen using the reversible toluene/methylcyclohexane couple.

(3) Catalytically converting models of lignin building blocks as a source for renewable aromatic chemicals.

Signature of the student